The Inertial Properties

of the

German Shepherd

O. Yvette Jones, MSc

University of
Strathclyde
Glasgow

5th October 2015

This thesis is submitted in partial fulfilment of the
requirements of the degree of Doctor of Philosophy

Department of Biomedical Engineering
Wolfson Centre
University of Strathclyde
106 Rottenrow
Glasgow, G4 0NW

Signed:

Date: October 7, 2015

ABSTRACT

The police service dog has a long history stretching as far back as the 1400's. One of the most popular dog breeds deployed by both the police and military has been the German Shepherd yet little is known about the morphology or body segment parameters of this breed. Knowledge of these measures is essential for developing biomechanical models that can guide clinicians in developing surgical interventions, injury treatment and prevention procedures. The aim of this thesis was to provide a complete set of body segment parameters and inertial properties for the German Shepherd. In addition, a canine motion capture suit and marker model was proposed for use with this dog population.

Morphometric measures and 3-dimensional inertial properties, including mass, centre of mass, moment of inertia and volume, were measured from 17 segments from each of 6 German Shepherd police service dog cadavers. Measurements were performed with frozen segments similar to the procedure on primates described by Reynolds (1974), on humans by Chandler et al. (1975) and on horses by Buchner et al. (1997). Using whole body mass and geometric modelling, multiple linear regression equations were developed from the collected data so that they may be used to estimate segment masses and inertial tensors in living dogs. Using a custom Lycra suit and 44-marker full-body marker set, kinematic data were collected to assess the practicality of the model, to observe the dogs' acceptance of the motion capture suit and to ensure fore and hind limb flexion/extension angles were comparable to those of other canine studies.

Using frozen cadavers, tissue loss was minimal at an average loss of 0.49% of total body mass. Hind limbs, at 6.8% of body mass, were 2.3% heavier than the forelimbs. Of the over 100 morphometric measures analysed, 33 were kept for inclusion in the linear regression equations and joint centre estimations. Analyses of body mass alone, found that, except for the abdominal segment ($r = .845$, $p \leq .05$), body mass did not correlate well with segmental masses. Similarly for moments of inertia, only the manus and pes produced predictive results using body mass alone.

11 regression equations were developed for predicting segment masses, and 33 equations were developed for predicting moments of inertia about the three primary axes of each segment. Regression correlation analyses were summarized for each segment and a table of normalised average segment masses, centres of mass, radii of gyration and segment densities was produced.

Five police service dogs took part in the evaluation of the motion capture suit. Overall the marker set and suit performed well and was well-received by dog/handler teams. The markers took very little time to apply, remained in place for the majority of trials and the suit itself did not visibly affect the dog's natural movement. An analysis of the kinematic data produced outputs showing characteristic patterns of flexion/extension similar to those found in other canine research.

With the development of regression equations for predicting segment mass and moments of inertia combined with the proposed marker model and novel method of marker attachment, inverse dynamic analyses may be applied in future investigations of canine mechanics, potentially guiding surgical procedures, rehabilitation and training for the German Shepherd breed.

Key Words: Canine, German Shepherd, morphometry, kinematics, kinetics, inertial properties, body segment parameter, segment model, moment of inertia, mass distribution.

ACKNOWLEDGEMENTS

The completion of this thesis and my PhD has been a long and adventurous journey that could not have been achieved without the invaluable support and encouragement of a great number of individuals.

To begin with I would like to thank my initial educational supervisor, Dr Ben Stansfield, for listening to my proposal and believing it was worth pursuing. His insight and scholarly advice helped build a requisite level of personal expectation that has served well throughout the project.

The role was soon taken by Dr Philip Riches, to whom I express my deepest appreciation and gratitude. Throughout my studies I was keenly aware that, as an external and part-time student, parent and working professional, I did not fit the mould of the traditional graduate student and this produced a great many challenges. His understanding, patience, expert guidance, analytical skills and meticulous scrutiny helped to deliver a thesis of which I can be very proud.

I would like to sincerely thank my colleague and research partner, Dr Silvia Raschke for allowing me to take the reins on what started off as a 'small' research project so that it could be turned into something grand. Without her belief in the idea, her hard work and dedication we could not have been granted the funding and tremendous support required to get this project off the ground.

A very special thank you to my friend and colleague, Dr David Kenyon, who spent countless hours assisting through all aspects of the data collection. Driven by sheer interest and willingness to help he has been an inspiration and I am truly indebted. Available whenever needed, he brought levity to the most unpleasant or mundane of tasks, providing great conversation with recounts of recent books read, television mysteries and family adventures.

I am hugely indebted to my friends and colleagues Johanne Mattie, Christine Flegal, and Angie Wong, who have been there through thick and thin, providing moral support and encouragement every step of the way.

TABLE OF CONTENTS

LIST OF FIGURES

LIST OF TABLES

1   INTRODUCTION

1.1   Background

1.1.1   Police Dog History

Throughout history the dog has been identified as an important partner in security and law enforcement. As far back as Roman times humans have used canines for safety and hunting and it is known that the Romans and the Spanish conquistadors used dogs in times of war. In 14th century France dogs were used to guard dock installations, and at the same time in Scotland bloodhounds were being used as "slough" (sleuth) hounds [Lee, 2014]. In 15th century England dogs were used by parish constables and, in fact, a tax was levied upon the English people for maintaining the hounds used for tracking criminals [Boece et al., 1536]. There was even a law that stated whoever denied entrance to one of the dogs would be treated as an accessory to the crime [Sloane, 1955].

Before 1890 police dogs had no formal training and were used primarily as trackers or as guard dogs. But in 1895, both Belgium and France successfully began training dogs to work with police on foot patrol. Around the same time, German infantryman, Captain Max von Stephanitz took a more scientific approach to working dog development with experiments in breeding, training and utilisation. He started with an Alsatian wolfdog, a yellow and grey wolf-like dog whom he'd observed at a dog show for his intelligence, outstanding strength and performance. This dog became the first registered German Shepherd dog and so began an intense, selective breeding program of sheepherding dogs, focusing on mental strength and work ethic. But as Germany became more mechanised and the need for herding dogs declined, von Stephanitz realized he needed to take the breed in another direction. With the support of police and working dog clubs he developed a set of tests specifically designed to enhance tracking, formal obedience, and protection work. He convinced the government authorities to employ the German Shepherd dog in the various divisions of service. The breed eventually served during the First World War as medical service dogs,

sentinels, trackers, messengers, supply carriers and guard dogs [Sloane, 1955, German Culture, 2012, Nova Scotia German Shepherd Dog Club, 2014].

Today, the German Shepherd is arguably the most popular breed of dog deployed in police work and in the military, with the Belgian Malinois a popular second. In Canada, there are currently 112 teams with the RCMP alone with many others distributed throughout major cities across the country. They are highly intelligent, agile and well-suited to active working environments, including public order enforcement, tracking, locating illicit substances such as drugs or explosives, and/or cadaver detection.

1.1.2   Injury Treatment and Prevention

Considerable expense is placed in the attainment and maintenance of police dog teams. In Canada, the estimated cost to train a member and dog team is $60,000. A healthy police service dog costs less than $1,000 annually to maintain [RCMP Police Dog Services, 2008], however if they become injured those costs substantially increase, not only due to veterinary fees but the department also loses a canine team until the dog is back in the service.

Similar to an athlete, police dogs must maintain top physical condition to obtain success in their job and do so through regular training and conditioning over the course of an average eight-year career. Just like the athlete, they will occasionally sustain an injury while training or on the job, in fact, the very nature of the job exposes these dogs to all manner of danger and potential injury. If you were an elite human athlete you would likely reap the benefits of a biomechanical assessment to aid in treatment or rehabilitation progress. While there has been great developments in the knowledge of veterinary musculoskeletal disease and surgical techniques, evaluation of functional outcome from these techniques are primarily subjective and based on the experience and observational skills of the clinician. For the police dog there is little consistent data to assist veterinarians in determining the correct time to return to work after an injury. In their studies on equine lameness, Keegan et al [1998, 2007] showed that

there can be considerable variation between clinicians, suggesting that a biomechanical analysis has potential as an objective method of determining equine lameness. Clinical experience can significantly affect the ability to correctly identify gait abnormalities and subjective assessments are not reliable when the lameness is only slight [Colborne, 2004]. In a discussion with local veterinary specialists, differences of as much as five months have been found in clinical reports quoting on the same injury [Animal Critical Care Group, 2005]. There is a clear need to develop best practices that include biomechanical assessments for training, rehabilitation and health screening of police dogs.

Before work can begin on examining training techniques, work related physical risk or the effectiveness of treatment and rehabilitation methods, it is necessary to gather baseline information of the physical attributes of the German Shepherd police dog (GSD). Knowledge of morphometric parameters are key to understanding the kinematics and kinetics of this particular working dog and ultimately for the development of injury treatment and prevention procedures. There is very little information that exists to describe the size, mass (M) and centre of mass (CoM) of this specific working dog's body or its segments. There have been numerous studies on horses and some on racing dogs, however, a review of existing canine research found no studies that focused on the biomechanics and rehabilitation of police dogs.

In humans, biomechanical assessments, including full inverse dynamic calculations of joint moments and powers, are often used to guide rehabilitation, treatment and even surgery [Colborne, 2007]. Discussed and reviewed on numerous occasions, locomotor analysis has been a played a considerable role in the treatment of musculoskeletal disorders in humans [Winter, 1976, Winter and Robertson, 1978, Winter, 1981, Cappozzo, 1983, Brand, 1989, Perry et al., 1992, Winter, 1993, Whittle, 1996, Davis, 1997, Baker, 2006]. The most prevalent application has been in the management of cerebral palsy (CP), particularly for directing surgical intervention. The many recognised contributors to this area include Sutherland [1969, 1978], Ounpuu [1991, 1996, 1996], DeLuca [1997, 1998], and Gage [1995, 2001], to name a few. In De

Luca's study [1997] of 91 children with CP who were to undergo surgical intervention, 52% of initial opinions were changed upon review of gait analysis data, leading to a reduction in invasive treatments and overall cost. Other pathologies that have benefited from biomechanical analysis include, but are not limited to, stroke, amputation, arthritis, and multiple sclerosis [Winter and Sienko, 1988, Paul, 1994, Sutherland, 2002, Sutherland, 2005].

Efforts in equine locomotion research are largely propelled by the prevalence of lameness and the drive to succeed in racing and dressage. In a study of equine carpal lameness, Back et al. (1993) performed a comparative study of clinical gait assessment and clinical lameness scores and found that two measures correlated well, suggesting gait analysis may be used to study lameness in greater detail. Shortly after, in a search for lameness indicators, Buchner et al. (1996) evaluated compensatory movements of the equine head and trunk during the walk and the trot. They identified that vertical acceleration of the head was best at quantifying forelimb lameness while vertical displacement of the tuber sacrale performed best at quantifying lameness in the hind limb. In other studies, joint forces, moments and powers have been evaluated in the hopes of understanding the mechanics and energy cost of lameness [Clayton et al., 1998]. A finding of power consistencies at each joint indicated the possibility that changes in work profiles may assist in identifying specific lameness conditions. A study having similar findings was carried out by Nielsen et al. (2003) for the dog forelimb, however this study was limited to 2-dimensions. There are few canine studies which are able to utilize segment inertial properties to report on joint moments and powers. In one of these experiments, Dogan et al. (1991) performed pre and post-operative gait analysis of canine hind limbs after total hip replacement. The results of their study showed that normal walking dynamics (vertical forces, craniocaudal forces and extension moments) may be restored within 4 months of total hip replacement.

In most clinical situations, kinematic and kinetic measures have been used to determine changes in joint angles, contact forces, muscle activation patterns and joint

loads for the process of selecting or excluding treatment options. Brand (1989) has suggested 4 reasons for performing a clinical gait analysis:

1. Diagnosis between diseases.

2. Assessing the nature or severity of a disease or injury.

3. Monitoring progress with or without treatment.

4. Prediction of the treatment outcomes

Although medical diagnosis is included here, gait analysis is rarely used strictly for this purpose. Rather, instead, being used to "quantitate the mobility state of a medical disorder and determine the neuromuscular-skeletal contributions to that state" [Simon, 2004].

Despite its usefulness, clinical gait analysis is not without its limitations. For gait data to be useful there must be limited variability between test subjects and measured trials, all collected data, including anthropometry/morphometry, must be accurate and the results reproducible. The greatest limitation for most potential users is in the expense of the lab itself. Excluding renovations, the space requirements, high speed digital cameras, force plates and analysis software can place a gait lab at an average $400,000 CDN (200,000 GBP). With regard to models employed, segment parameters must be input into the model and kinematic data are then calculated from surface markers positioned relative to bony landmarks. Segment parameter measurement accuracy is dependent on the experience of the researcher or clinician. Additionally, marker accuracy is one of the greatest sources for error in both human and animal evaluations and can be affected by skin vibration, muscle attachment, level of subcutaneous adipose tissue, stability of fixation and by the experience of the researcher/clinician in applying the marker. Joint centres are assumed to be located either directly from surface markers or estimated algorithmically from mathematical formulae. Errors with respect to markers and parameter measures can be limited through experience and training and within-study variability can be further reduced if the same clinician(s) perform (s) all marker applications. Furthermore, advances in technology have

permitted the implementation of algorithms to offset the effects of marker vibration, significantly reducing the effects of marker error [van Weeren et al., 1992, Alexander and Andriacchi, 2001].

To apply clinical gait assessments to GSDs a database of accurate body segment parameters (BSPs) like those generated by Chandler et al. (1975) for humans, are required from which regression equations may be generated to predict segmental moments of inertia (MoI) in living subjects. From these equations, mathematical models can be created with which one can make empirical assumptions for such unknowns as joint moments, shear and compressive forces.

This project supplements the few existing reports of information with data regarding mass distribution characteristics of the GSD as described by the principle moments of inertia and their orientation to the body and segment morphometry [Onar, 1999].

1.2 Project Rationale

Investigation of internal forces and moments experienced by the body cannot be directly measured but can be estimated noninvasively through the use of biomechanical models. The information gleaned from an objective biomechanical analysis can assist in diagnosing pathologies, developing and assessing the effectiveness of surgical procedures, and for monitoring rehabilitation and training programs. For canine biomechanical analyses to be effective, accurate link-segment models that include definitive body segment parameters are required.

Objective: The objective of this project was to create a biomechanical model of the GSD by establishing a complete set of three-dimensional inertial properties of the dog including morphometry, mass, centre of mass, inertial tensors and density of all body segments. Based on these measurements, regression equations were determined for the estimation of inertial properties in living dogs. A full-body link-segment model was developed using a best-fit geometric segment approximation combined with the proportional regression equations developed from cadaveric segments. The mass distribution characteristics obtained were used to establish a reliable means of

estimating these same properties on living dogs from easily measured body parameters.

Rationale: The model of the GSD will be a fundamental tool with which to measure the biomechanics of the dog for purposes of assessment, training and/or rehabilitation.

1.3 Aims

The aims of this thesis are as follows:

- Directly measure and record a complete set of body segment parameters and three dimensional inertial properties of GSDs, including mass, centre of mass, volume and moment of inertia.

- Develop a set of regression equations to estimate segmental masses and moments of inertia in living dogs

- Develop and test a motion capture marker model through kinematic evaluation of German Shepherd police dogs. The regression equations and marker model may then be combined in future for use in a full dynamic kinematic and kinetic assessment of live dogs.

2 LITERATURE REVIEW

The goal of this project was to create a biomechanical model of the GSD with which to describe the locomotor performances of living dogs based on regression equations that estimate inertial properties of each body segment. This objective necessitates that a review be conducted on the following areas: general canine anatomy including specific landmarks associated with this investigation and an overview of some of the musculoskeletal issues known to the German Shepherd breed; methods of measuring body segment parameters; the use of regression equations to extrapolate body segment parameters (BSPs) are also explained, including applications to humans, current methods as applied in the veterinary field and finally a summary of biomechanics in veterinary research.

The limitations of available data and technologies and currently available non-invasive techniques for measuring body segment parameters are detailed providing the rationale for further work in this field. A summary at the end of the chapter evidences and provides a clear rationale for the specific research hypothesis presented.

2.1 Canine Anatomy

The following sections provide directional terminology relevant to the quadruped. Skeletal diagrams of the dog with relevant landmarks are also provided.

2.1.1 Directional Terms

Anatomical directional terms are universal expressions used in vertebrate zoology and human anatomy to avoid confusion when identifying body planes or structures. Regardless of the position of the limbs, each directional term is based on the neuraxis of the animal, is referenced by a standard anatomical position and has an opposing counterpart. The neuraxis of humans in comparison to other animals, particularly quadrupeds, differs such that different anatomical directional terms will customarily be used. The standard position for humans refers to the body standing upright with arms at the side and palms facing forward. In veterinary nomenclature, the notion of a

standard anatomical position was recently abandoned and the terms of direction were related to parts of the body, making the terms applicable to all vertebrates [Nomenclature, 2005]. When using common expressions (behind, above, etc.) however, quadruped standard anatomical position is typically an alert, upright stance with head up and feet square [Dyce et al., 2009].

For the dog, the expressions *cranial* and *caudal* apply to all parts of the body with the exception of the head, forepaw or manus, and hind paw or pes. The terms for the forepaw are *dorsal* and *palmar*; those for the hind paw are *dorsal* and *plantar*. The preferred terms on the head are *rostral*, *caudal*, *dorsal*, and *ventral*. *Anterior*, *posterior*, *superior*, and *inferior* are used only in the inner ear, eye and jaw areas. *Medial* and *lateral* apply to the whole body except on the phalanges, where *axial* refers to the side of the digit toward the axis of the limb and *abaxial* to the side away from the axis of the limb. The axis of the limb passes between the third and the fourth digits [Evans and De Lahunta, 2013].
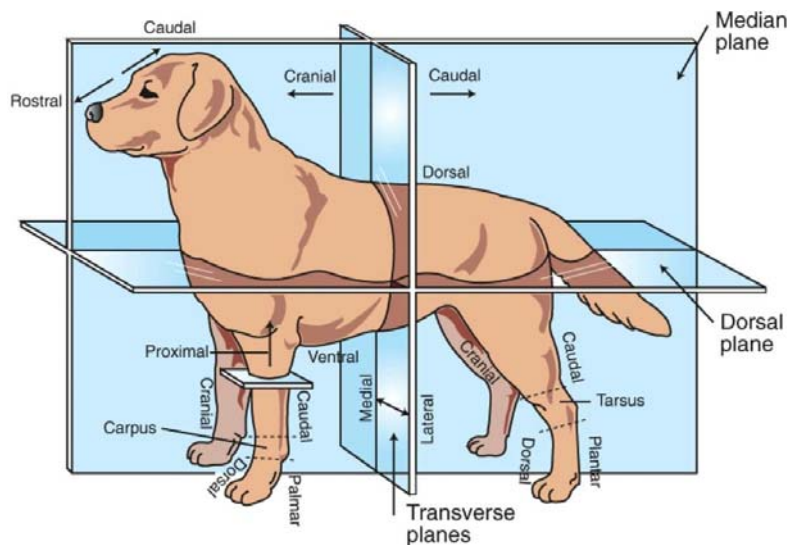
Figure 2.1: Directional terms

(Unknown (2015), adapted from Evans and De Lahunta (2013))

Figure 2.1 shows the standard position and directional terms used for most quadrupeds and for this investigation.

2.1.2 Skeletal System and Landmarks

Anatomical landmarks are used as reference points when collecting any form of biomechanical information. They are palpable bony prominences, such as those found at the proximal and distal ends of a segment, fissures such as the *nasion* or the *menton*, or tissue structures such as the *omphalion* or *tragion*. Their locations are used for indicating segment boundaries, determining joint centres, axes of rotation or virtual points such as centre of mass. They are also used for calculating segment lengths or for locating other nearby landmarks that are not easily found on their own, such as joint lines. Figures 2.2 to 2.4 and Table 2.1 show the canine skeleton with corresponding labels and landmarks that may be used for biomechanical evaluation.
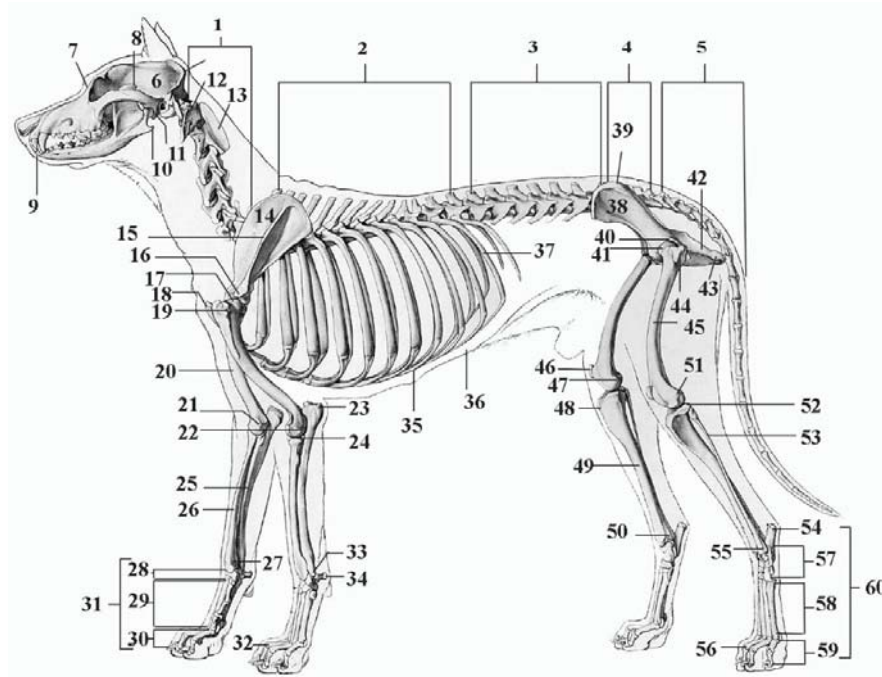
Figure 2.2: Lateral skeleton and landmarks – whole body

It has been customary to measure segments based on joint axis of rotation [Clauser et al., 1969, Reynolds, 1974, Chandler et al., 1975]. Segment boundaries in this investigation are similar to those standardised for horses by Sprigings and Leach (1986) whereby two segments are separated in the transverse plane along the transverse joint rotation between the medial and lateral reference points. Craniometric landmarks and measurements (Figures 2.5 to 2.7) were defined in accordance to established methods for the German Shepherd by Brehm et al. (1985) and Onar (1999). See Section 3.1.2 for detailed methods and measures.

Table 2.1: Skeleton labels

1) 7 cervical vertebrae	21) medial humeral epicondyle	41) femoral head
2) 13 thoracic vertebrae	22) lateral humeral epicondyle	42) ischium
3) 7 lumbar vertebrae	23) olecranon tuber	43) ischiatic tuberosity
4) 3 sacral vertebrae (fused)	24) radiohumeral joint	44) greater trochanter
5) caudal vertebrae	25) ulna	45) femur
6) cranium	26) radius	46) patella
7) nasion	27) radial styloid process	47) medial femoral epicondyle
8) mandibular arch	28) carpus	48) tibial tubercle
9) menton	29) metacarpus	49) tibia
10) angular process	30) phalanges	50) medial malleolus
11) condyloid process	31) manus/forepaw	51) lateral femoral epicondyle
12) atlas	32) distal 3rd phalanx	52) lateral tibial condyle
13) axis	33) ulnar styloid process	53) fibula
14) scapula	34) accessory carpal	54) calcaneus
15) scapular spine	35) xyphoid cartilage	55) lateral malleolus
16) acromion process	36) omphalion	56) distal 3rd phalanx
17) coracoid process	37) 12th rib	57) tarsus
18) sternum: manubrium	38) ilium	58) metatarsus
19) greater tubercle of the humerus	39) cranial dorsal iliac spine	59) phalanges
20) humerus	40) acetabular rim	60) pes/hind paw
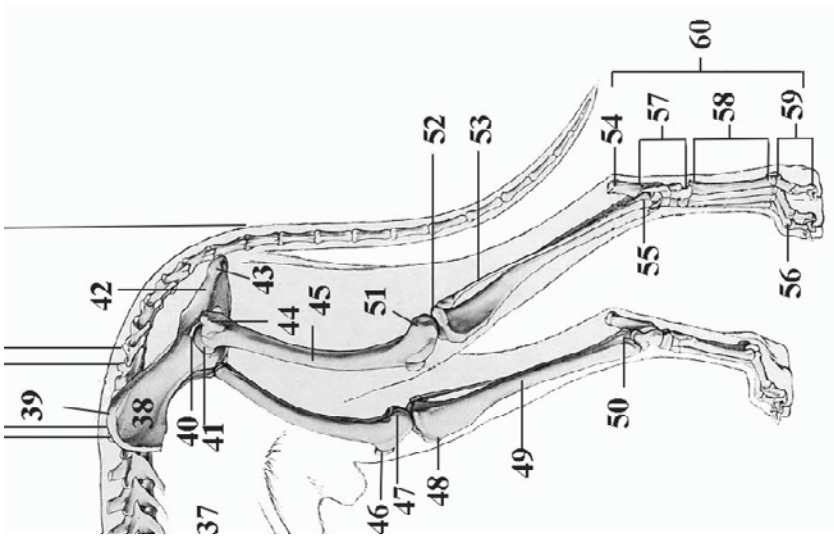
Figure 2.4: Close-up view of hind limb lateral skeleton and landmarks
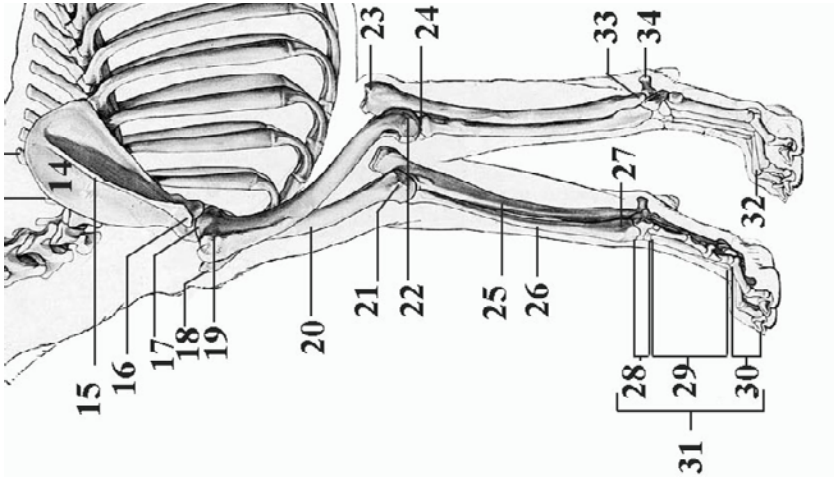
Figure 2.3: Close-up view of forelimb lateral skeleton and landmarks
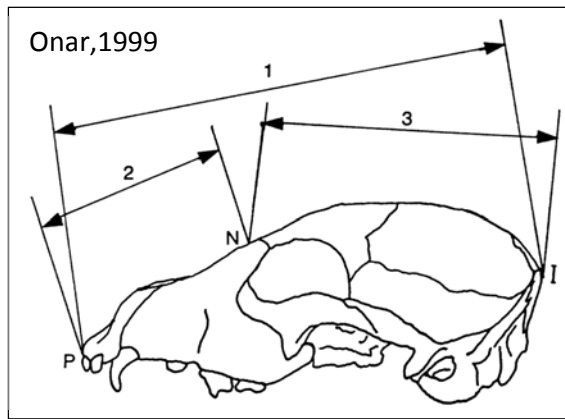
Figure 2.5: Cranium, lateral view

1-skull length,
2-viscerocranial (face) length
3-cranial length
I–inion (external occipital protuberance)
N-nasion
P-prosthion
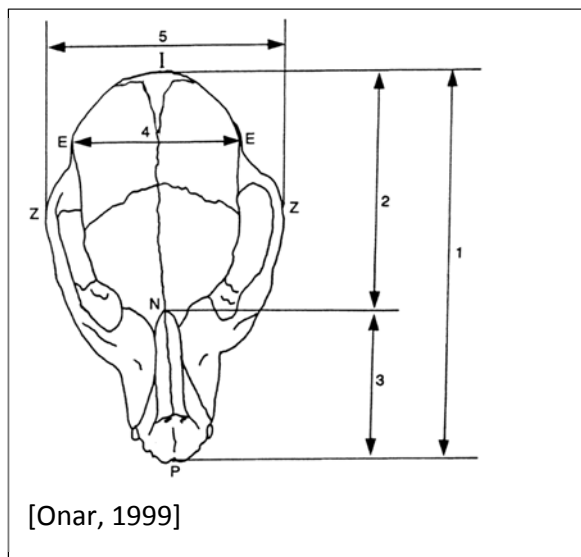
Figure 2.6: Cranium, dorsal view

1-skull length
2-cranial length
3-viscerocranial (face) length
4-neurocranium width
5-zygomatic width
E-eurion
I-inion (external occipital protuberance)
N-nasion
P-prosthion
Z-zygion
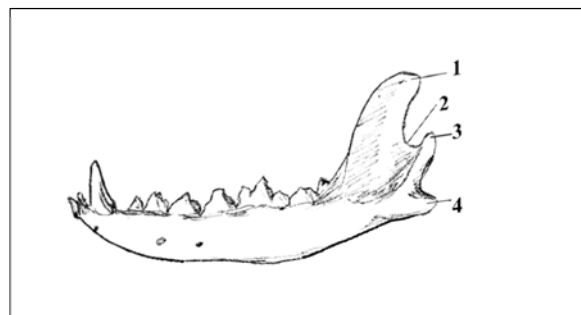
Figure 2.7: Canine mandible

1-coronoid process
2-mandibular notch
3-condylar process
4-angular process

2.2 Pathologies of the German Shepherd

Large dog breeds, including the GSD, are predisposed to a number of musculoskeletal conditions as a result of their body size and/or their rapid growth rate. Some of the more prevalent orthopaedic conditions are hip and elbow dysplasias and cranial cruciate ruptures and degenerative myelopathy [Wahl et al., 2008, Asher et al., 2009]. Since a biomechanical evaluation of the GSD may help in the analyses of these pathologies, they are described in more detail below.

2.2.1 Canine Hip Dysplasia

Canine hip dysplasia (CHD) is a polygenic disorder in which the head of the femur and the acetabulum do not correctly fit together thereby causing abnormal movement of the femoral head and instability of the hip joint. The result is painful, damaging friction, deformation of the acetabulum, progressive loss of cartilage and eventually arthritis [Alexander, 1992, Fries and Remedios, 1995, ACVS, 2015].

Some dogs with CHD will not have obvious symptoms, others may present with varying degrees of lameness, reluctance to rise or jump, frequent shifting of weight to the forelimbs, intolerance to activity, and muscle wasting in the rear limbs. Differential diagnosis is determined through physical examination for joint laxity, pain and limited range of motion, radiographs and gait evaluation [Fries and Remedios, 1995, Asher et al., 2009].

Treatment for this condition can vary greatly and is dependent on the age and size of the dog, the level of discomfort, and how far the condition has progressed. Initial treatment is through conservative management including weight loss, physical therapy, dietary supplements and osteoarthritis medication [ACVS, 2015]. Older dogs with arthritis tend to respond to this approach better than younger dogs without arthritis. Surgical options can include a total hip replacement or, for dogs showing no signs of arthritis, a double or triple pelvic osteotomy, where the pelvic bone is cut in 2 or three places and the segments rotated to improve the contact of the femoral head by the acetabulum [Ginja et al., 2010, ACVS, 2015].

2.2.2 Canine Elbow Dysplasia

Canine elbow dysplasia (CED) is a general term for another polygenic disorder that occurs in the elbow joint of large dog breeds [Wahl et al., 2008, Asher et al., 2009]. It can manifest in one or both joints, alone or in combination, in the form of *ununited anconeal process* (UAP), *fragmented medial coronoid process* (FCP), *osteochondritis dessicans* (OCD) (Figure 2.8), or *elbow incongruency* [Kirberger and Fourie, 1998, Cook and Cook, 2009].
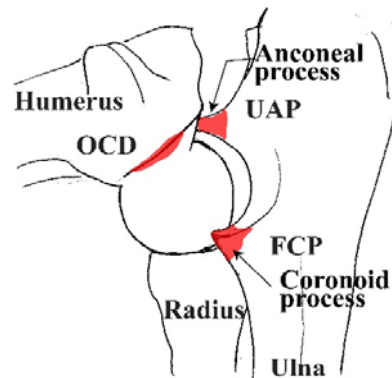
Figure 2.8: Conditional locations for elbow dysplasia

In the case of *UAP*, the anconeal process fails to fuse properly to the ulna during growth. The bony protuberance becomes detached from the ulna causing joint irritation and degeneration [Trostel et al., 2003a, Reuss-Lamky, 2012].

With *FCP*, the coronoid process of the ulna fissures or detaches completely causing joint irritation and degeneration. In some cases this may be the result of a disproportion in length between the radius and ulna causing overload and failure of the medial aspect [Trostel et al., 2003a, Reuss-Lamky, 2012].

OCD is a disruption of bone and cartilage development that causes progressive thickening of the cartilage to the point of separation from the bone. The resulting loose flap of cartilage can move around in place or detach to float freely within the joint causing inflammation, swelling and pain [Trostel et al., 2003a, Reuss-Lamky, 2012].

Elbow incongruency is the asynchronous growth of the radius and ulna due to premature closure of a growth plate or a growth plate injury. The ulnar growth plate is particularly susceptible to injury due to its shape. The result is partial elbow dislocation, radial bowing and external rotation of the either the carpus or elbow joint [Michelsen, 2013].

All conditions of elbow dysplasia are thought to be the result of osteochondrosis of the articular or physeal cartilage that results in incongruent growth of the radius and ulna [Kirberger and Fourie, 1998]. Symptoms can present as lameness, abnormal gait (e.g. flipping their feet when they walk), fatigue, limited willingness to participate in activity and symptoms worsening after exercise. The dog may hold their elbows out or tightly against their body with feet rotated outwards to reduce the load on the affected area of the joint. Diagnosis is made through clinical observation of these and other symptoms, joint palpation, functional tests, and imaging techniques such as radiographs, CT and MRI. As with CHD, initial treatment for CED is conservative management including weight loss, physical therapy, dietary supplements and osteoarthritis medication [Becker, 2012, Reuss-Lamky, 2012].

Arthroscopy is the method of choice for surgical treatment and is used for both diagnosis and treatment of CED as it is minimally invasive thereby reducing the risk of infection and other complications and there is a faster rate of recover. This procedure provides excellent visualization for evaluation of joint surface and incongruences, and permits removal of abnormal or loose tissue in the same process [Reuss-Lamky, 2012]. Other procedures include sliding humeral osteotomy, proximal adducting ulna osteotomy, joint resurfacing, joint replacement, denervation and arthrodesis [Michelsen, 2013].

Many treatment approaches are successful in the short term, however, with time osteoarthritis typically sets in as a secondary condition [Reuss-Lamky, 2012].

2.2.3 Cranial Cruciate Ligament Ruptures

Like the anterior cruciate ligament in humans, the cranial cruciate ligament in the dog is a stabilizing structure within the canine knee or stifle joint (Figure 2.9). The ligament runs from posteriolateral aspect of the head of the femur to the anteriomedial aspect of the head of the tibia and is responsible for keeping the tibia from sliding forward with respect to the femur. *Cranial cruciate ligament (CCL) ruptures* are another common source of chronic lameness in the dog. The ligament may become stretched or torn causing the knee joint to become unstable, leaving the meniscal cartilage vulnerable to tearing [Johnson and Johnson, 1993].
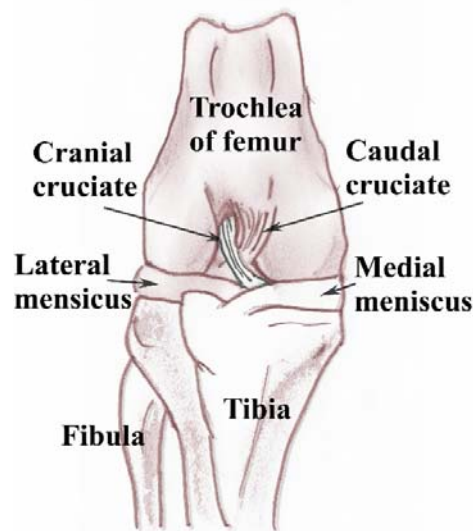
Figure 2.9: Anatomy of the knee joint

Symptoms of damage or rupture include varying degrees of lameness, stiffness, swelling on the medial aspect of the knee, reduced activity, and avoidance on bending the knee or holding the leg to one side when sitting and/or trouble jumping into a vehicle.

Because the damage is soft-tissue based, radiographic diagnosis is not directly possible however it may be useful in ruling out other conditions. Other methods of diagnosis

include qualitative gait assessment and positive functional tests like the cranial drawer and tibial compression tests (in both tests the tibia will slide forward with respect to the femur) [Johnson and Johnson, 1993, Harasen, 2002].

For most dogs with CCL rupture, surgery is the recommended treatment. The more traditional surgical approach and, one that still works well, involves ligament replacement. With this procedure there is the risk of the new stabilizing material failing, leading to a build-up of scar tissue causing reduced range of motion. A current, more favoured method is tibial plateau levelling osteotomy where the tibia is cut and rotated to reduce the downward sloping angle of the tibial plateau, thereby eliminating the tendency of the femur to slide forward on the tibia [ACVS, 2015].

2.2.4   Degenerative Myelopathy

Canine degenerative myelopathy (CDM) is an insidious incurable chronic degenerative disease of the canine spinal cord most commonly reported in the GSD [Coates and Wininger, 2010]. Onset is typically after the age of 7 but can appear between 5 and 14 years of age and is characterised by loss of proprioceptive function, weakness and incoordination of the hind limbs, progressing over time to complete paralysis [Barclay and Haines, 1994, Wahl et al., 2008].

In the initial stages it will seem that the dog is arthritic. In most cases both limbs will be affected but to different extents. Stable walking is difficult on smooth surfaces where an abnormal gait will become more obvious. On changing direction the hind legs may cross over and the hips become unstable, the toes may also knuckle over and scuff on the ground. As the disease progresses, there is muscle atrophy in the hind limbs and pressure sores begin to develop from the dog repeatedly lying down [Barclay and Haines, 1994]. Toileting remains normal until very late in the disease. Eventually their forelimbs also become affected and they can no longer walk. At this time euthanasia is usually recommended [Averill, 1973, Coates et al., 2007, CGD Network, 2009, Coates and Wininger, 2010, Zeiler et al., 2013]. The complete cycle

may take anywhere from 6 months to a year [Averill, 1973]. Through the course of the disease the dog does not experience pain or discomfort.

Diagnosis of the disease is through process of elimination of other disorders. MRI or CT scan, myelography, electrodiagnostic testing and cerebrospinal analysis are all techniques used through this process, however definitive diagnosis is determined post-mortem through histopathic examination of the spinal cord [Coates et al., 2007].

Proper diet and exercise has been shown to extend the survival time. Dogs receiving intensive physiotherapy have been shown to remain ambulatory longer, surviving an average of 255 days compared to 130 days for dogs receiving moderate to no physiotherapy intervention [Kathmann et al., 2006, Wahl et al., 2008].

Cause of the disease is yet unknown. One theory suggests a possible link between vitamin B deficiency and CDM [Clemmons, 1992] however this theory remains unsubstantiated [Wahl et al., 2008]. Vitamin E levels have also been found to be lower in CDM cases. Links to Vitamin E deficiencies and neurological disorders in humans suggest stronger support that CDM may be an immune related disorder [Williams et al., 1985, Fechner et al., 2002], however further study is needed. A recent study into the molecular genetics of the disease suggests that CDM could share similar pathologic mechanisms to human ALS or Lou Gehrig disease [Awano et al., 2009, Coates and Wininger, 2010].

The disorders described in this section are just some of the chronic conditions that may benefit from a gait evaluation which targets specific joints. As with humans, it has been suggested that these, as well as many other acute and chronic conditions, will present with different biomechanical signatures, opening up the possibility that an objective clinical gait evaluation would be a useful diagnostic tool for characterizing gait [Bennett et al., 1996, DeCamp et al., 1996, Poy et al., 2000]. Such a tool would be possible for the GSD with the body segment parameters provided by this investigation.

2.3 Body Segment Parameters

 BSPs are essential to the study of the dynamics of locomotion. To describe the mechanics of any moving body, that body is typically divided into segments and viewed as a linked multi-segmented system with specific geometry and inertial parameters for each segment. BSPs include scalar (mass, length, area, volume, density/specific gravity and moment of inertia/inertial tensor) and vector measures (centre of mass, centre of volume) which may be acquired by a variety of methods. This section provides an overview of the historical progression of BSP research in human and non-human biomechanics research. Common methods and techniques of extracting these measurements are explained including the benefits and limitations with reference to related investigations. While much of the foundation work discussed here has been based on human cadaveric studies, each one may be applicable to finding BSPs for the GSD, or any other animal.

2.3.1   Human Applications

Interest in the anthropometric and inertial parameters of the human body and its segments has been demonstrated by many investigators over the past three centuries [Borelli, 1681, Harless, 1858, Braune and Fischer, 1889, Clauser et al., 1969, Hatze, 1980, Pearsall and Reid, 1994]. In early practical applications, Braune and Fischer (1889) and Fischer (1906) looked at the motion of the centre of gravity of the infantry soldier carrying full field equipment and rifle and at the effectiveness of a new pack for carrying equipment. Dempster (1955) looked at anatomical, geometric and mechanical features of male operators in an effort to understand the movement of the pilot in the cockpit and to define the dimensions of the seated workspace. Two other significant and commonly cited BSP studies were performed by Clauser et al. (1969) and Chandler et al. (1975). Their investigations were designed to gather anthropometric parameters for use in aerospace research, in particular, for the design and testing of impact protection systems and in the design of isomorphic models for use when risk of injury prevents the use of real humans. These first studies make up

the most comprehensive database of direct-measure full-body BSPs. Details of these and other studies follow in 2.3.3 as the various evaluation techniques are explained.

The limited availability of cadavers and specialized equipment in these early studies have led researchers to explore improved methodologies, specific population groups and advances in technology. Throughout these developments a number of systematic reviews have also been conducted. Some have been chronological surveys; Pearsall and Reid (1994) provide an extensive chronological summary, in written and table form, of human BSP research, including sample size, age, gender, parameters measured and methods used. Others have reviewed methodologies [Contini et al., 1963, Drillis et al., 1964, Lephart, 1984, Cappozzo et al., 2005, Plaga et al., 2005, Damavandi et al., 2009], still others have reviewed morphological applications [Jensen, 1993].

2.3.2 Non-Human Application's

Efforts to refine measurement techniques and interest in the development and locomotor dynamics of non-human primates have also generated investigations into the mass distribution properties of chimpanzees [Schoonaert et al., 2007], baboons [Reynolds, 1974, Martin et al., 1989, Raichlen, 2005] and other monkeys [Crompton et al., 1996]. BSP research in the veterinary field began later with racehorses, influenced by the high incidence of lameness and the desire for a better understanding of equine athletic performance [Sprigings and Leach, 1986, Buchner et al., 1997].

Depending on the method used, whole-body evaluations can be extremely time consuming, costly and, in some cases, unnecessary [Amit et al., 2009, Wicke and Dumas, 2014]. For these reasons investigators may instead choose to limit their studies to individual segments. For example, extensive morphometric evaluations have been conducted on the GSD skull [Onar et al., 1997, Onar, 1999, Onar and Gunes, 2003, Alpak et al., 2004]. In one study by Onar (1999), craniometric measures were taken from 33 skulls of GSD puppies according to established methods [Brehm et al., 1985, Yildiz et al., 1993, Simoens et al., 1994, Onar et al., 1997] and studied for relationships

between skull parameters and indices for defects, for example, the shape of the skull and risk for nasal cancer.

In many quadrupeds, lameness is a primary concern so the limbs are also common target segments for limited BSP studies [Nielsen et al., 2003, Shahar and Banks-Sills, 2004, Helms et al., 2009, Nauwelaerts et al., 2011]. Ragetly et al. (2008) looked at non-invasive methods of determining BSPs for the hind limb of Labrador Retrievers through the use of CT scans. The study compared dogs with cranial cruciate deficiencies to those without the disease in an attempt to develop strategies of studying the pathogenesis of this and other joint diseases. In another study quantifying net forces and joint moments in the limbs of pigs, Thorup et al. (2007) measured the fore and hind limbs of 12 pig cadavers to establish joint axes of rotation. An additional 5 cadavers were each dissected into 10 limb segments according to the previously determined rotational axes and then frozen. All measures were limited to the right side and included morphometry, masses, CoM in the sagittal plane and MoI.

Looking for less invasive methods of collecting BSP's, Amit et al. (2009) used MRI scans to collect a complete set of inertial properties for the dog. Scan costs and processing time limited his investigation to just 3 mixed breed, mid-sized dogs. The dogs were divided into 15 segments for which volume was measured directly from the scan images, density was taken from previously reported tissue studies, mass, CoM, and MoI were calculated from these values. CoM and MoI were normalized according to Dumas et al. (2007) and Cheng et al. (2000).

Out of all this research, the greatest challenge has been in developing a BSP model capable of accurately providing a subject-specific dynamic biomechanical analysis. Despite the advances in technology, this is currently not possible without the input of group-specific body segment parameters. This investigation will be the first complete set of BSPs developed specifically for the male working GSD.

2.3.3   Measurement Techniques

Direct measurements of sample populations can be taken via cadaver segmentation or from living subjects through the use of scanning methods (γ-ray, CT, MRI). Since most BSPs are difficult to measure directly from a living individual it has been common practice to indirectly estimate them through models based on values taken from a sample population. There are many methods for extracting these data including water displacement, balance board measures, mathematical modelling, kinematics and photogrammetry [Pearsall and Reid, 1994, Vaughn et al., 1999]. This section reviews commonly used methods for obtaining body segment parameters, including their assumptions, benefits and limitations as presented in various studies. Sections 2.3.3.1 to 2.3.3.7 refer to methods used in this investigation, sections 2.3.3.8 to 2.3.3.9 cover other techniques employed in the literature.

2.3.3.1   *Cadaver Segmentation*

A popular approach, and one of the earliest, to estimating body segment parameters has been based on data collected from cadavers. Cadaver segmentation involves dividing the cadaver into segments based on anatomy or movement mechanics, typically transecting joint centres, and measuring BSPs for each segment.

To simplify the biomechanical model created with the extracted parameters it is usually assumed that the segments are rigid and therefore there is no change in dimensions. Moreover, based on work by Bernstein et al. (1936) on 76 living male and 76 living female subjects aged 12-75, it has been considered acceptable to assume segment density to be uniform throughout the length of the segment and that the density values would be characteristic of a live individual [Drillis et al., 1964, Durkin and Dowling, 2003].

This being a safe assumption, and that mass is a product of density and volume ($m=\rho V$) it has been common practice to use volumetric data to determine mass, which in turn has been used to calculate centre of mass (CoM) and moment of inertia (MoI) when it was not suitable to measure them directly.

A study by Harless [1858, 1860] was the first comprehensive attempt to quantify human BSPs, introducing many methods of acquiring data that are still applicable today. His initial research was based on 2 unembalmed human cadavers, one aged 25, the other of unknown age. He separated them into 18 segments through the pivotal axis of each joint by first severing the tissue in a plane that bisected the joint centre of rotation then disarticulating the joint itself. The segment ends were then sutured together over each end to prevent excessive tissue contracture. He employed several methods to extract his data: whole body mass and centre of mass were measured using the balance method, segment volume was determined using the immersion method for the smaller segments and geometric modelling for the trunk, mass and inertia properties were calculated on the assumption of a uniform density of 1.066. Following the same procedures, Harless (1860) completed an additional study of 6 cadavers (3 men, 3 women, age range 20-68), from these concluding that age and gender are significant factors in segment density [Clauser et al., 1969].

The aforementioned research by Braune and Fischer (1889) utilised 3 male cadavers (aged 18-50) [Pearsall and Reid, 1994], opting to freeze them first to retard fluid loss. This prohibited dissecting out the joints as Harless had done. Instead they were separated through the approximate centres of rotation by way of a straight cut bisecting the joint. Centre of mass was determined by hanging the segment from each of three axes and marking the intersection of the three planes on the segment. In order to add segmental moments of inertia, Fischer (1906) followed up with data from a single cadaver from which mass and centre of mass were also recorded using the same procedures as Braune and Fischer (1889) [Clauser et al., 1969].

Dempster's research aimed to improve the construction of test manikins so they may have more realistic geometric, kinematic and mechanical ranges, similar to that which existed within Air Force flying personnel. Specifications were also drafted to show limb ranges for seated postures. The study was based on 8 cadavers; 7 unpreserved, 1 preserved. Each cadaver was divided into 17 segments: hands, forearms, upper arms, shoulders, abdomen, thorax, head/neck, thighs, shanks, and feet, all of which were

frozen prior to separation. Anthropometric dimensions, mass, centre of mass, volume, density and moment of inertia were determined for each segment. The cadaver data were supplemented by anthropometric and volumetric measures on 39 living Caucasian males (aged 18-30). It was noted, cadaver subjects were older men (aged 52-83), smaller (158.5-186.6 cm; 113-159.5 lbs.) than the group of military personnel they were aiming to represent [Dempster, 1955].

Clauser et al. (1969) desired to learn more about the human mechanical system so that physical and computer models could be used in place of real subjects in materials testing. In a study similar to Dempster (1955) and Braune and Fischer (1889), mass, volume, centre of mass and anthropometric dimensions were gathered from 13 preserved male cadavers having an average height, weight and age of 172.72 cm, 66.52 kg, and 49.31 years, respectively. An important note about the preservation process; despite it being a non-standardised process, the researchers believed that because the preservative had a similar density to the average density of human tissue [Behnke et al., 1995], if one were to add same amount of preservative as lost fluid there should be no change in mass of the cadaver. Mass distribution in the embalmed cadaver should therefore be closely comparable to that of living subjects, however, this assumption has not been yet been verified.

Chandler et al. (1975), interested in finding the inertial properties of the human body, derived regression equations from the segmentation of 6 male cadavers aged 45-65 years. Anthropometry, mass, CoM, volume and MoI were measured on all 14 segments of each cadaver. The resulting data were normalised as a function of body mass and height. By normalizing, the BSPs may be employed in link segment models to estimate the joint kinetics. Their research concluded that a) segment volumes are good predictors for moments of inertia and b) for major limb segments of humans, the principle moments about the mediolateral (I_{xx}) and anteroposterior (I_{yy}) axes are approximately equal in magnitude with moments about the longitudinal axis (I_{zz}) being approximately 20 percent less than I_{xx} and I_{yy} values.

These early studies represent the most commonly cited and comprehensive data base of directly measured BSPs. The majority of follow-up studies aim at refining previous research methods by attempting to simplify the measurement process, find less invasive approaches to extracting data and improve upon the accuracy of the data collected [Clarys and Marfell-Jones, 1986]. For example, Hatze (1980) presented a computational geometric model to calculate BSPs of living subjects. The goal was to generate a model capable of differentiating between male and female subjects, while taking into account the shape variation of each segment and accounting for variable densities. The model consisted of 17 segments for which 242 anthropometric measurements were taken from each of 3 males and 1 female cadaver. The abdomen and thorax were one complete segment, the shoulders were removed from the thorax and presented as separate segments. The Hatze model divides each segment into smaller mass components made up of different geometric structures. This method allowed shape and density fluctuations of the segment to be more accurately modelled, permitting variations in tissue density within segments. Segment rigidity then became the only assumption, there were no assumptions on segment symmetry as is customary in geometric models.

In another study, Huang and Suarez (1983) explored alternate methods of studying children, utilizing CT scans to look at the density and cross-sectional geometry of a 10-month old porcine cadaver and the cadaver of a 3 year old female leukemia patient. A second porcine cadaver was used for dissectional comparison with the CT scanned results. Due to the resemblance of anatomical features, porcine subjects have been used as surrogates for children in translational research [Swindle et al., 2012]. Mass, CoM and MoI were calculated from 1cm cross-sectional scans, with particular interest in comparisons of the head and neck areas for application in biodynamic modelling, computer-based vehicle crash simulation and manikin design. They concluded that there were marked differences between the inertial properties of the two specimens and thereby questioned of the use of porcine subjects as surrogates in biomechanical studies of the head and neck in children.

Due to the limited literature available on dogs, the search for published research on BSPs was extended to other animals including non-human primates, horses and pigs. The studies found are summarised in Table 2.2.

For primates, Reynolds (1974) presented a method of measuring moment of inertia from 4 frozen baboon specimens using a simple pendulum. Segmentation methods followed those of Clauser et al. (1969) and Dempster (1955). Each segment was measured for mass, volume, location of CoM, and MoI about the principal axes. Regression equations were developed for predicting these parameters from either body mass or from segment volume. Vilensky (1979) used similar methods to obtain masses, CoM, and MoI in the Rhesus monkey, providing regression equations for predicting these parameters from body mass. Martin et al. (1989) investigated the feasibility of measuring segment inertial properties using MRI. BSPs determined from cross-sectional images of eight baboon limb segments were compared to the same parameters obtained using standard cadaveric measurement techniques. While results showed MRI to be a promising method of extracting BSPs, the expense and processing time required for this method renders it impractical at this time. Crompton et al. (1996) presented a geometric link-segment model derived from cadaver segments taken from chimpanzees and an orangutan. Rather than the customary circular cross-sections, the segments were modelled to have elliptical cross sections and curved profiles. Inertial properties were derived using a double pendulum technique (see 2.3.3.4) paired with primatometric measurements.

The investigation of BSPs in veterinary research has been limited primarily to horses and there are even fewer studies on dogs. Partial sets include single plane whole body CoM measures [Krüger, 1941, Buchner et al., 2000], CoM and MoI for the forelimb [Geary and Kingsbury, 1975, Nielsen et al., 2003, Nauwelaerts et al., 2011] and for the hind limb [Wentink, 1978, Sprigings and Leach, 1986, Nauwelaerts et al., 2011, Ragetly et al., 2012]. In 1986, using 2 gelded Thoroughbreds and 1 female Thoroughbred cross, researchers began looking at complete sets of sagittal plane parameters including a standardised approach to equine segmentation and mass

distribution measures. Each cadaver was divided into 19 segments and CoM determined for each segment [Sprigings and Leach, 1986]. Inertial properties were not measured. Kubo et al. (1992) followed with breed-specific, 2-dimensional segment data for Thoroughbreds. Volumetric measures were determined using the water displacement method; density was calculated from volume and mass; CoM was determined by suspension.

Buchner et al. (1997) presented the first set of three-dimensional equine inertial properties in a study of 6 horses wherein they developed a 26-segment model, collecting segment mass, CoM, MoI and density, creating regression equations for estimating inertial properties of living subjects. The segmentation model was similar to the one created by Sprigings and Leach (1986) however the shoulders and digits were further bisected and the tail was also included for an additional 7 segments. In the most recent study by Nauwelaerts et al. (2011), segment mass and inertial properties of the fore and hind limbs of 38 horses were measured for the sagittal plane by way of suspension and trifilar pendulum methods. In general, the mass distribution results of this study agree with those of previous researchers for measures within this plane, [Sprigings and Leach, 1986, van den Bogert et al., 1989, Kubo et al., 1992, Buchner et al., 1997, Nauwelaerts et al., 2011] suggesting their segmentation model is consistent across horses of different breeds.

The first study to target canine BSPs was published by Dogan et al. (1991). Their study looked at gait biomechanics of 5 mixed breed dogs pre and post unilateral cemented total hip replacement. At the end of the study the dogs were euthanized and hind limbs disarticulated to extract inertial properties of the segments using balance and pendulum techniques. The parameters gathered were used to determine sagittal plane joint kinetics for the hip, stifle, and talocrural joints. Nielsen et al. (2003) completed a similar study to Dogan, this time looking at 2 dimensional inverse dynamic modelling of the forelimb of 6 mixed breed dogs.

Table 2.2: Summary of non-human body segment parameters

Reference	Year	State		Sample					Segment parameters							Measurement method
		cad	liv	animal	N	gender	age		#	A	V	M	D	CoM	MoI	
Kruger[1]	1941			horse										x[a]		
Reynolds	1974	f		baboon	4	F			14	x	x	x		x	x	geometric model, cadaver segmentation, pendulum (MoI), suspension (CoG)
Grand[2]	1977a	nf		primates								x				
Grand[2]	1977b	nf		macaque								x				
Wentink	1978		x	ponies & horses	8									x[a]	x[a]	cinephotography right hind limb
Vilensky	1979	f		rhesus monkey	15	7M 8F	adult					x		x	x	regression model
Huang & Suarez[3]	1983	nf		pig	1		10 wks			x		x	x			cadaver segmentation, CT scan
Sprigings & Leach	1986	nf		horse	3	2GM, 1F	6,11 ,?		19					x[a]		cadaver segmentation, reaction board[6], suspension method for segments <4.5kg
Ishii et al[1]	1986	nf		horse	1						x	x	x			cadaver segmentation, photographic volume
Wells & De Menthon[2]	1987	nf		lemur	1	M			15			x		x	x	pendulum (torsion bifilar), modified suspension

Table 2.2: Summary of non-human body segment parameters, cont'd

Reference	Year	State		Sample				Segment parameters							Measurement method
		cad	liv	animal	N	gender	age	#	A	V	M	D	CoM	MoI	
Morbeck & Zihlman	1988	nf		orangutan	2	M F					x					
Martin et al.	1989	nf		baboon	5			8 total	x	x				x		cadaver (embalmed), segmentation[7], pendulum[8] & MRI (limbs segments only), reaction board[9]
van den Bogert[4]	1989			pony	5			26		x		x[a]		x[a]		regression model
Dogan[5]	1991	nf		dog	5			8		x		x[a]		x[a]		(hind limb only) - balance, pendulum
Kubo	1992	f		horse (Thorough-bred)	3	1GM 2F	9,4,4	20	x			x				water displacement, photographic suspension
Crompton et al.	1996	1f 3nf		chimpan-zee /orangutan	1-Apr	2M 2F/M		8	x	x				x		cadaver segmentation, water displacement, geometric modelling, balance board[10], pendulum (double)
Onar	1997	nf		dog (GSD)	32		.25-.5	1								head - morphometry only
Buchner	1997	f		horse	6	3GM 3F	2-13	26	x (trunk)	x	x	x		x		cadaver segmentation[11], pendulum[12], reaction board, regression model[11]

Table 2.2: Summary of non-human body segment parameters, cont'd															
Reference	**Year**	**State**		**Sample**				**Segment parameters**							**Measurement method**
		cad	liv	animal	N	gender	age	#	A	V	M	D	CoM	MoI	
Buchner	1997	f		horse	6	3GM 3F	4	26	x	x (trunk)	x	x	x	x	cadaver segmentation[11], pendulum[12], reaction board, regression model[11]
Onar	1999	nf		dog (GSD)	33		.25-.5	1							head - morphometry only
Buchner	2000		x	horse	12	7GM 5F		20					x		Buchner 1997 model
Onar & Gunes	2003	nf		dog (GSD)	32		.25-.6	1							morphometry only
Nielsen et al.[5]	2003	nf		dog	6			4			x	x		x	forelimb only - balance board, pendulum
Shahar & Banks-Sills	2004	nf		dog	1										morphometry only
Raichlen	2005		x	baboon	4		infant								geometric model[13]
Colborne et al.[5]	2005	nf		dog (Lab/Greyhound)	4-Mar			5			x	x			balance
Schoonaert[1]	2007		x	chimpanzee	53	23M 30F		8						x	geometric model[13]

Table 2.2: Summary of non-human body segment parameters, cont'd														
Reference	**Year**	**State**		**Sample**				**Segment parameters**						**Measurement method**
		cad	liv	animal	N	gender	age	#	A	V	M	D	CoM	MoI	
Thorup[1]	2007	f		pig	5			10			x		x	x	balance, quick release (fore/hind limbs)
Ragetly	2008		x	dog (Lab Ret)	24		6+	6	x	x	x		x	x	CT (hind limbs), DEXA (area), regression model, density[14]
Amit	2009	nf		dog	3	2M 1F	3-5	15		x	x	x	x	x	MRI (10mm)
Nauwelaerts	2011	nf		horses	38		10 +/- 9	11			x		x	x	cadaver segmentation (1 fore/1 hind limb), string suspension, pendulum (trifilar)

Abbreviations: cad/f=frozen cadaver, cad/nf=nonfrozen cadaver, liv=living, N=number of subjects, A=area, V=volume, M=mass, D=density, CoM=centre of mass, MoI=moment of inertia, M=male, GM=gelded male, F=female, a=sagittal plane only

Method referenced from: 1=Kubo (1992), 2=from Crompton (1996), 3=from Buchner (1997), 4=from Nauwelaerts (2011), 5=from Ragetly (2008), 6=Hay (1978), 7=Reynolds (1974), 8=Chandler (1975), 9=Drillis (1966), 10=Contini (1972), 11=van den Bogert (1984), 12=Lephart (1984) , 13=Crompton (1986), 14=Zatsiorsky (1983)

In 2005, research on dogs advanced a little further with a breed specific study comparing power distribution in the hind limbs of Labrador Retrievers and Greyhounds. Unfortunately this study was limited in that only CoM was recorded using the balance method, inertial properties were not included in the study [Colborne et al., 2005].

The only complete set of 3 dimensional BSPs collected cadaverically was done through the use of MRI. Amit et al. (2009) extracted canine inertial properties based on 3 cadavers of mixed breed dogs. The dogs were separated into 15 segments and segment mass was determined through multiplying segment tissue volume by its associated density. To enable extrapolation to other dogs, the CoM was normalised to the length of the segment and MoI normalised by the square of the segment length [Cheng et al., 2000, Dumas et al., 2007, Amit et al., 2009]. While this study does not use the common assumption of uniform density, the small sample size, mixed breed and gender may not provide a sample representative enough of the German Shepherd breed.

The greatest benefit to using cadaver segmentation for determining BSPs is that it permits direct measurements of mass, volume, CoM and MoI for individual segments. That being said, as with less invasive means of extracting BSP data, the method has its limitations, the most common being small sample size. Due to a limited supply of sources, most investigations involving cadavers have a small number of specimens and the figures obtained from these populations cannot be used indiscriminately, rather they should be used to examine like groups [Colborne et al., 2005]. It is therefore important that researchers understand how the BSPs were derived and on which populations they may appropriately use them in biomechanical modelling [Clauser et al., 1969, Pearsall and Reid, 1994]. As an example, use of the models of Clauser et al (1969) and Dempster (1955) resulted in poor appendicular estimates of college-aged individuals [Wicke and Dumas, 2014]. In addition, for most cadaver methods, total body mass is used as a predictive variable within the model and therefore may not be precise enough on its own for segment estimations. Some concern has also been

expressed that freezing increases volume, decreases density and somehow affects the measured inertia parameters but there is no supporting documentation [Reid and Jensen, 1990]. Finally, a variety of factors can lead to the possibility of large errors in the comparison of datasets, including embalming vs freezing vs fresh tissue, differing definitions of segment boundaries and varying amounts of tissue lost in the dissection process.

2.3.3.2 *Geometric Modelling*

Geometric modelling simplifies the shape of body segments so that the BSP's of the living, be they human or non-human, may be mathematically derived from a series of measurements taken directly from the segment [Pearsall and Reid, 1994]. Pioneered by Harless (1860), geometric modelling was introduced as an alternative to the immersion method for determining body volume and mass [Drillis et al., 1964]. Segment mass properties are estimated by modelling each segment as a single geometric shape, such as a sphere or frustum of a cone [Hanavan E P, 1964, Vaughn et al., 1999], or as a series of shapes [Hatze, 1980, Wicke et al., 2009] from which mass (Equation 2.1) and inertial properties could be derived from its density and volume. Equations for determining moment of inertia of standard geometric shapes are readily available in technical manuals and online. As an example, if one assumes the upper arm to be in the shape of a *right circular cylinder* then the volume (*V*) and corresponding mass moment of inertia (*I*) about the flexion/extension axis would be defined as:

$$V = \frac{1}{4\pi}c^2 h \qquad \text{(Equation 2.1)}$$

$$I = \frac{M}{12}(.076c^2 + h^2) \qquad \text{(Equation 2.2)}$$

Where M = mass of the segment, c = mid circumference and h= segment length [Oberg, 1992]

Geometric modelling can be simple, where segments are modelled as basic geometric solids. They can also be more complex, where a single segment can be made up of any number of shapes, zones or slices. Simple, single shape geometric modelling often assumes the segment has a linear profile and that cross sections are circular. Fewer morphometric measures are needed, volume is either measured directly or estimated using applicable geometric shape-based equations that incorporate segment length, circumference and/or diameter measures. In most cases density is assumed to be uniform throughout the segment [Behnke et al., 1995, Wicke et al., 2009]. This method is most appropriate where time is a factor in the data collection session or if the subject group is unlikely to withstand handling or numerous measurements, e.g. children or animals. Other investigators who have used this method include Whitsett Jr (1962) who constructed a model based on 14 segments of various shapes. Inertial parameters were calculated for each shape using density parameters provided by Dempster (1955). Similarly, Hanavan E P (1964) created a model made up of 15 geometric shapes; the head was represented as an ellipsoid, the torso as elliptical cylinders, the hands as spheres, the remaining segments were frustums of right circular cones. Segment masses were predicted using 25 anthropometric measures and Barter's regression equations [Barter, 1957, Reid and Jensen, 1990]. Weinbach (1938) assumed in his model that any cross-section of the human body segment is elliptical and that density is uniform and equal to 1000 gr/cm^3. On evaluation, however, when compared to direct measures using his pantograph and planimeter technique, Dempster (1955 - see Chapter II, item 40 for complete description) found this computational method to be accurate for volumes of the human head, neck and trunk but not so for the rest of the body [Drillis et al., 1964].

More advanced geometric models section the segments into more than one shape or zone. In contrast to the simple geometric model, these models require more time to apply, require more detailed segment morphometry and may require additional processing time if scanning methods are involved. Similar to BSP estimation using CT scanning methods, each segment zone is approximated to a geometric shape and

measures of circumference and height, or slice thickness, are gathered to approximate the volume of the zone. Adding up the volumes of the zones that make up the segment will provide the total volume of the segment. The smaller the height of each zone, the closer the geometric estimation will be to the actual segment dimensions [Contini et al., 1963]. The success of this method is in balancing the accuracy, i.e. number of measures required in the model, to the practicality of carrying out all the required measures.

As an example, Hatze (1980) model requires 242 anthropometric measures and several different shapes to represent the various segments, making this the most accurate measure of segment volumes. He revised the study and reduced the required measures to 133, however, despite fewer requirements, this model remains understandably underutilised [Wicke and Dumas, 2014].

In another complex model, Jensen (1993) used a full-body elliptical model to represent each segment as a series of stacked 20 mm zones. The model consisted of 16 segments having the same boundaries and densities as reported by Clauser et al. (1969). With cameras placed orthogonal to each other, each subject was photographed from the frontal and sagittal planes. Width and breadth measurements were recorded from each zone and volume determined from these measurements. Similar to Jensen, Wicke et al. (2009) did a comparative study of a new geometric model. DXA scanning was used for criterion measures to estimate segment mass, centre of mass location, and moment of inertia (frontal plane only). They modified the Jensen model by eliminating the uniform density assumption and used sectioned ellipses to represent the trunk.

With regard to the accuracy of geometric models, Harless (1858) found that the smaller segments produced more accurate estimations. For larger segments like the trunk, differences of 3.7% were found when calculated mass results based on the frustum of a right cone were compared with measured mass. Studies have shown that uniform density assumptions have a minimal effect on estimations of inertial properties and that volume overall accuracy is more greatly affected by volume [Ackland et al., 1988, Wicke et al., 2009, Wicke and Dumas, 2014]. That being said,

geometric models that include a non-uniform density function provide more accurate segment inertial parameter estimates despite being more laborious to utilise [Nigg, 1994]. The accuracy of the geometric model is greatly improved by ensuring more suitable geometric shapes are used to represent the various body segments and inertial parameters.

For purposes of this study, it was assumed that segment density among subjects was constant, determined as an average calculated from measured cadaveric volumes and segment masses. To model segment masses of the living, segments were represented as similarly shaped geometric solids. For example, if the foreleg is similar in shape to a cylinder, to find the mass of the foreleg one would use the mathematical formula for calculating the mass of a cylinder:

$$M = \frac{\rho}{4\pi}(l)(c)^2 \qquad \text{(Equation 2.3)}$$

where l is the length and c the circumference of the foreleg.

2.3.3.3   *Regression Modelling*

The relationship between force and motion may be studied by representing the body and its segments as a simple biomechanical model. BSPs are applied to biomechanical models to make estimates of kinetic data. A caveat of this practice being that the accuracy of the model depends on how closely the population group in question matches the representative sample used in the model. Adding BSP's measured from the individual allows the model to be customized to that individual and the relationship between body segments may then be studied using direct or inverse dynamics. In order for the regression model to work for the individual, regression equations must be developed from representative samples that would permit estimation of body segment masses which cannot be directly measured in the living. Regression coefficients are used in statistics to express the level to which a relationship exists between sets of data. If there is a relationship it can then be modelled with a regression equation that incorporates the corresponding coefficient and its residual, thereby permitting future

predictions based on similar datasets. As an example, using age as variable x and height as variable y, one could predict the height that a child may be at age 10 based on heights measured on their birthdays from ages 2 through 8.

In biomechanics, regression equations are used to estimate segmental inertial properties (mass, CoM, MoI, radius of gyration) in living subjects using selected morphometric measures as predictors. Typical predictor variables are body mass for segment mass and segment length for radius and radius of gyration [Jensen, 1993].

The regression equation takes on the form:

$$y = mx + b \qquad \text{(Equation 2.4)}$$

Where, *x* and *y* are the variables; *m* = the coefficient, or slope of the regression line; *b* = the residual, or intercept point of the regression line and the *y* axis

It is assumed that there are set relationships, in the form of coefficients, between body mass, segment length, and segment parameters. These relations are 1) the ratio of segment mass to total body mass, 2) the ratio of the distance of mass centre from proximal and/or distal joint to total length of segment 3) the ratio of the radius of gyration of the segment about the mediolateral centroidal axis to the total segment length [Drillis and Contini, 1966].

Moment of inertia is defined as a measure of a body's resistance to angular motion. It is typically expressed in units kgm^2 and could be considered to vary with the mass and the square of the length of the segment. Assuming a segment is similar to a geometric shape such as a cylinder, the following linear regression equations could be used for predicting segment MoI about the corresponding principal axes [Vaughn et al., 1999]:

$$I_{xx} = C1(Total\ body\ mass)(Length)^2 + C2 \qquad \text{(Equation 2.5)}$$

$$I_{yy} = C1(Total\ body\ mass)(Length)^2 + C2 \qquad \text{(Equation 2.6)}$$

$$I_{zz} = C1(Total\ body\ mass)(Length)^2 + C2 \qquad \text{(Equation 2.7)}$$

where *C1* and *C2* are regression coefficients determined from those directly measured from corresponding axes of a representative sample (e.g. cadaveric subjects). I_{xx} and I_{yy} could be moments of inertia about the transverse axes, e.g. flexion/extension, abduction/adduction and I_{zz} is the moment of inertia about the polar axis, or internal/external rotation. The three biaxial measurements I_{xy}, I_{xz}, and I_{yz} would be determined in the same way.

This method using coefficients was originally presented by Harless (1860) to be later used by Braune and Fischer (1889), Bernstein et al. (1936) and Dempster (1955) so that whole body mass and segment length would be all that was needed to estimate segment mass, centre of mass and moment of inertia. Fischer (1906) later added a 4th coefficient – ratio of radius of gyration about the longitudinal axis with respect to total segment length [Contini et al., 1963].

Many researchers investigating human body segment parameters have developed and used regression equations to predict BSPs [Whitsett Jr, 1962, Hinrichs, 1985, Zatsiorsky and Seluyanov, 1985, Durkin and Dowling, 2003, Le et al., 2009, Wicke and Dumas, 2014], in many cases using data generated from other studies in an attempt to improve existing predictor equations or to adapt them to desired outcomes. In 1957, Barter assembled all the data collected by Braune and Fischer (1889), Fischer (1906) and Dempster (1955) into a set of regression equations to predict segment masses from whole body mass. Despite the obvious differences between subject groups and methods for extracting data, he felt that the equations would be useful in providing a quick method of estimating segment mass. Using anthropometric measurements reported by Chandler et al. (1975), Yeadon and Morlock (1989) developed regression equations for determining moments of inertia from 3 principle axes and Veeger et al. (1997) used regression equations already developed by Clauser et al. (1969) to estimate mass and CoM.

The majority of regression equations developed thus far have been on humans. There are very few studies on animals that have developed and/or employed regression equations for the purpose of estimating BSPs in living animals [Buchner et al., 2000,

Buchner et al., 2001]. To date, Buchner et al. (1997) has developed the only set of regression equations for estimating the inertial properties of living horses for all three principle axes of each segment. Furthermore, Ragetly et al. (2008) have published the only existing regression model for dogs, unfortunately their study was limited to the hind leg. In their investigation of cranial cruciate ligament disease in the Labrador Retriever, an inverse dynamic model was required to analyse joint mechanics in an effort to gain an understanding of the pathogenesis of this disease. Regression equations were therefore developed from morphometric measurements and body mass to predict the mass, CoM and MoI for the thigh, crus and foot segments.

Another approach to regression equations has been taken by Vaughn et al. (1999). In their book Dynamics of Human Gait, they describe a technique for estimating segmental inertial properties in living bodies based on a process that combines cadaver averages and mathematical modelling. This method relates cadaveric segment averages with the total body mass and segmental mass, volume and anthropometric measures from living subjects. The result can be expressed mathematically in the form of a linear regression equation:

$$Segment\ mass = C1(Total\ body\ mass) + C2(Length)^3 + C3 \quad \text{(Equation 2.8)}$$

where C1, C2 and C3 are regression coefficients derived from the cadavers used in Chandler et al.'s study [1975]. This approach has proved promising, showing greater correlations using body mass and segment volume as predictors rather than by body mass alone[Vaughn et al., 1999]. In addition, the limited number of measures required make it an attractive approach for use with animals.

2.3.3.4 *Pendulum Method*

Locomotion, in fact body movement in general, is achieved by moving body segments about joint rotational axes. From Newton's 2nd Law, inertia is a property of that rotation and can be described as a function of torque (τ) and angular acceleration (α).

$$\tau = I\alpha \qquad \text{(Equation 2.9)}$$

The inertia of a segment (I) is expressed as the product of the mass of the segment (m) and the square of its distance from the rotational axis (R). In order for the body to accelerate in an angular direction, sufficient torque must be generated to overcome the inertia of the segment.

$$I = mR^2 \qquad \text{(Equation 2.10)}$$

where R is the radius of gyration about a specific axis.

The *moment* of inertia (MoI) of a segment expresses the distribution of the segment's mass about a given axis. In a dynamic model we must find these values about each principle axis to calculate the angular momentum of the body and its segments in 3 dimensions. This can be achieved using an oscillation technique in the form of a simple pendulum (Chandler et al., 1975; Dempster, 1955; Lephart, 1984). The simple pendulum is made up of a pivot point a string and a mass. The string is considered to have no mass and to be inelastic, the mass is permitted to swing freely. In this way the pendulum has no effect on the frequency of oscillation. Gravity and string tension are the only forces acting on the mass.

More complex pendulums have also been used to determine MoI: the compound pendulum, the double pendulum and the torsional pendulum. The compound pendulum is similar to the simple pendulum except the pendulum itself has mass, radius of gyration and MoI that must be accounted for [Braune and Fischer, 1889, Dempster, 1955]. The double pendulum (Figure 2.10) is one in which one pendulum is attached to another so the pendulum may oscillate about 2 different axes.
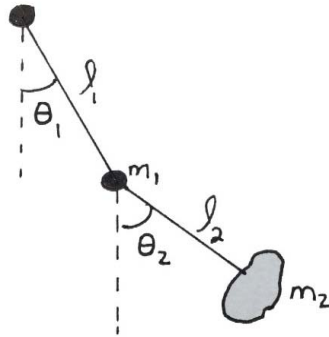
Figure 2.10: Double pendulum

This method offers a more precise timing measure for determining moment of inertia for segments where the periodicity of the oscillations of a single pendulum are very rapid [Wells and DeMenthon, 1987]. The procedure requires finding the associated periods for each pendulum and solving equations of motion for: short pendulum plus segment, long pendulum plus segment, short pendulum only, long pendulum only [Contini et al., 1963, Wells and DeMenthon, 1987]. The torsional pendulum is made up of a platform that is either set upon a spring or torsion bar and attached to the ground at the base or hung from above via a wire attached to a suspension frame. The platform and spring/wire system is of known physical attributes (e.g. platform mass and spring constant or rigidity modulus of the wire). The subject or segment is placed on the platform. When the platform is rotated about the axis of the suspension wire and then released, the wire applies a torque to rotate the platform back to its original position, oscillating back and forth at a specific frequency. MoI is determined by

measuring the mass of the object and the period of rotation of the pendulum [Drillis et al., 1964]. Variations of this method include the bifilar (2-wire) and trifilar (3-wire) torsional pendulum, where the platform is supported by additional wires [Wells and DeMenthon, 1987, Nauwelaerts et al., 2011].

The simple pendulum technique used in this and many other studies was first developed by Winstandley et al. (1968) [Reynolds, 1974].
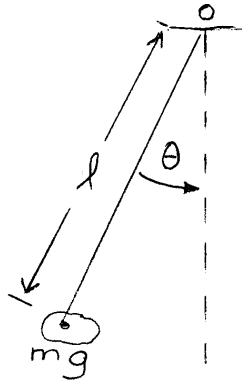
Figure 2.11: Simple pendulum

Shown in Figure 2.11, and referring to the formula for torque (Equation 2.9) the motion of the simple pendulum is defined by the formula:

$$I_{oo} \frac{d^2\theta}{dt^2} = mgl\ sin\theta \qquad \text{(Equation 2.11)}$$

Where I_o is the mass moment of inertia of the pendulum about axis "o"; $\frac{d^2\theta}{dt^2}$ is the angular acceleration; m is the mass of the pendulum; g is the gravitational constant; l is the distance from the axis of rotation to the centre of gravity of the pendulum; and $sin\ \theta$ is the sin function of the half-angle of motion.

Since $Sin\ \theta = \theta$ in radians for small oscillations whose half-angle is less than 5 degrees, (Equation 2.11) can be rewritten in the form:

$$\frac{d^2\theta}{dt^2} + \frac{mgl}{I_{oo}}\theta = 0 \qquad \text{(Equation 2.12)}$$

This is a common expression for the free oscillation of a simple harmonic system. The natural frequency for which is given by [Reynolds, 1974]:

$$I = \frac{mgl}{\omega^2} \qquad \text{(Equation 2.13)}$$

And

$$\text{angular frequency, } \omega = \frac{2\pi}{T} \quad or \quad \omega^2 = \frac{4\pi^2}{T^2} \qquad \text{(Equation 2.14)}$$

where ω is equal to frequency in radians per second and T is the period of oscillation in seconds.

The equation for MoI of a simple pendulum about its axis of rotation (o) then becomes:

$$I_o = \frac{mglT^2}{4\pi^2} \qquad \text{(Equation 2.15)}$$

To determine the moment of inertia of the segment about its CoM, a parallel axis transfer is necessary [Reynolds, 1974, Chandler et al., 1975, Lephart, 1984].

$$I_{CoM} = \frac{mglT^2}{4\pi^2} - ml^2 \qquad \text{(Equation 2.16)}$$

The number of independent variables (*m, l, T*) provide many opportunities for error if care is not taken in the measurement procedures. Dowling et al. (2006) demonstrated that the pendulum method was insensitive to errors in mass measurements but not so for errors in the period of oscillation. He also obtained significantly more accurate results by suspending the segment with the axis located at the radius of gyration rather than at the more favoured proximal suspension [Dempster, 1955, Dowling et al., 2006].

A variation of the pendulum method is the quick release. Based on Newton's 2nd law (Equation 2.9), this technique has been used to determine segmental MoI in the living (for a complete description see Drillis and Contini (1966), Pearsall and Reid (1994)).

The procedure involves the segment being placed so that the proximal joint is fixed. Attached to the distal end at a known distance from the proximal joint is a cord and accelerometer. The other end of the cord is attached to a device of known constant, such as a spring, and a potentiometer to measure the force required to deflect the spring. The torque generated about the proximal joint is proportional to the force applied and the length of the lever arm, i.e. the proximal joint centre and the attachment point of the cord at the distal end of the segment. Instantaneous acceleration of the limb, produced by sharply cutting the taught cord, is measured by the accelerometer. Assuming no friction exists within the proximal joint and there is no antagonistic muscle reaction, all values are used to calculate the MoI about the proximal joint [Bouisset and Pertuzon, 1968, Reid and Jensen, 1990].

2.3.3.5 *Balance Technique*

The balance technique is used for determining the location of the CoM for the whole body, in whole or in part, in 2- or 3- dimensions. The first documented use of the balance method was in a study by Borelli (1681) to evaluate whole body centre of mass. In his experiment, a cadaver was first placed on a board balanced on a single edged fulcrum and then the board moved until it appeared to be balanced. Unfortunately Borelli's method did not take into account the mass of the plank [Harless, 1860, Pearsall and Reid, 1994]. In an effort to improve upon this method, the Weber brothers [1836] repeated the procedure with a live subject, this time balancing the plank at its centre of mass and keeping one end supported. The subject lay supine on the board and moved until the platform began to tilt. The subject then reversed position so the head was in the previous position occupied by the feet and the procedure was repeated. The position of the top of the head was noted for each procedure and the centre of mass in the coronal plane determined to be half the distance between the two points.

Variations of this technique have been demonstrated by other researchers [Harless, 1860, Bernstein et al., 1936, Dempster, 1955, Clauser et al., 1969, Reynolds, 1974,

Vilensky, 1979] for both whole body CoM and for individual segment CoM. In either case, the body/segment is placed on a board that is supported on one fulcrum, or "knife edge" as is often stated in the literature. The segment is moved on the board until it is in balance, at which point the fulcrum and CoM would coincide for that axis [Contini et al., 1963, Reid and Jensen, 1990, Pearsall and Reid, 1994, Crompton et al., 1996, Dowling et al., 2006, Ragetly et al., 2012]. For 2-dimensions, the measures are taken from the sagittal plane and the distance measured from the proximal point. The location of CoM is then expressed as a ratio of total segment length. For 3 dimensions the measures are taken along each of the primary axes and the distance measured from an established origin.

Because this investigation was completed in 3 dimensions an origin was required. To achieve this each segment was placed in a box with established origin, similar to those use by Reynolds (1974), Chandler et al. (1975) and Lephart (1984). The above procedure was carried out for each box/segment combination as described in 3.1.2.5.

Introduced by Du Bois-Reymond (1900), the reaction board method (Figure 2.12) is related to the balance technique and is used to locate CoM in living subjects.

a,b,c=horizontal distances
W=body weight
w=segment weight
F_r=resultant force reading from scale.
M=Fulcrum
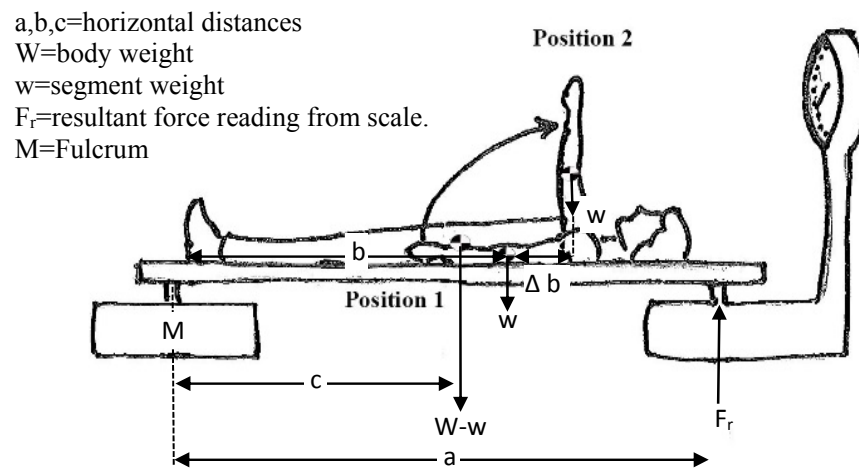
Figure 2.12: Reaction board method for determining weight of a segment, from Hay (1973)

Moments about M in Position 1:

$$F_{r1}a = wb + c(W - w)$$

<div align="right">(Equation 2.17)</div>

Moments about M in Position 2:

$$F_{r2}a = w\,(b + \Delta b) + c(W - w)$$

<div align="right">(Equation 2.18)</div>

Weight of the arm segment:

$$a(F_{r2} - F_{r1}) = w\Delta b$$

<div align="right">(Equation 2.19)</div>

$$therefore,\ \ w = \frac{a(F_{r2} - F_{r1})}{\Delta b}$$

<div align="right">(Equation 2.20)</div>

The method can be used for both whole body and segmental evaluations [Drillis et al., 1964, Bernstein, 1967, McKinon et al., 2004] and involves placing a plank of known mass horizontally supported at two points, one of which is a force plate or scale. Depending on the desired measure, CoM (when determining segment mass) or relative segment mass are assumed to be known. Using the principles of static equilibrium and a net torque of zero one may determine the CoM of the subject or segment [Winter, 1990, Pearsall and Reid, 1994]. Reaction forces are determined while the subject lies supine on the board, then raises the target segment from horizontal to vertical with its CoM directly above the joint axis. The change in reaction moment (taken from the scale) is used to estimate segment mass. While this method is considered to produce very precise measurements [Drillis and Contini, 1966, de Leva, 1996], it can be time consuming and is difficult to apply to all body segments [Reid and Jensen, 1990].

2.3.3.6 *Suspension Method*

Another variation of the balance technique is the suspension method [Braune and Fischer, 1889, Dempster, 1955, McConville and Clauser, 1976, Kubo et al., 1992, Nauwelaerts et al., 2011]. There are many approaches, however, in short, the segment is suspended within the desired plane by a string, wire or rod. On equilibrium, a vertical line can be made through the point location of the CoM within that plane.

In one version of this method, Braune and Fischer (1889) drove 3 thin metal rods through the segment at right angles to the 3 cardinal planes. The segment was suspended from each rod and the CoM determined as the point of intersection between the 3 planes when in vertical equilibrium. This method is somewhat questionable as it is unclear if the rods were placed all at once. If so one would expect the mass of the rods to have some effect on the results.

Wells and DeMenthon (1987) presented another version of this method, creating a device which contained a tray suspended between two support stands. A segment is placed on the tray and, when balanced, a line on the tray surface and a vertical pointer underneath the tray would coincide. That location would then be marked on the segment.

Using a wire, Kubo et al. (1992) suspended each of their segments from 2 different locations, taking photographs from the sagittal plane view. CoM was determined as the intersection point between 2 plumb lines drawn from the suspension points.

2.3.3.7 *Immersion*

Immersion is a method of determining the volume of body segments by measuring how much water is displaced by the immersed segment. The volume of displaced water then becomes the volume of the segment being studied. This technique is useful such that it can be applied to living subjects as well as cadavers and can be used to determine total segment volume or in any proportion that is required.

As stated in 2.3.3.1 it is generally assumed that the density of the segment remains homogenous, therefore the mass of the segment can be determined by multiplying the density by its volume. That being said, this method cannot be used for measuring the body as a whole. According to Ivanitzkiy (1956), the trunk has a lower density than the rest of the body so the centre of mass will not coincide with the centre of volume. It is also necessary to take into account any air that may be contained in the lungs and stomach.

The method was first described by [Harless, 1858] in his textbook of Plastic Anatomy. For his procedure, a device large enough to contain the segment in question is constructed and filled with water. The segment was then inserted and the resulting overflow caught in a surrounding container. The overflow volume was measured, providing the volume of the immersed limb. A number of other studies, including the one described here, have employed this method of determining volume [Bernstein et al., 1936, Dempster, 1955, Ivanitzkiy, 1956, Plagenhoef, 1979]. [Crompton et al., 1996] used it in his study of BSPs of primates; defining parameters for the development of a musculoskeletal model of the upper extremity, Veeger et al. (1997), used the method to determine muscle volume, achieving an accuracy of 1 ml; and in the latest, Piovesan et al. (2011) used the method for estimating arm segment parameters.

2.3.3.8 *Medical Imaging Techniques*

Today's medical imaging techniques have provided an accurate, non-invasive means for researchers to determine BSPs from the living. Scanning methods include gamma mass scanning [Brooks and Jacobs, 1975, Zatsiorsky and Seluyanov, 1983], computerized tomography (CT) [Huang and Suarez, 1983, Pearsall et al., 1996], magnetic resonance imaging (MRI) [Martin et al., 1989, Cheng et al., 2000], and dual energy X-ray absorptiometry (DEXA) [Durkin and Dowling, 2003, Dowling et al., 2006, Durkin and Dowling, 2006].

The principle of gamma mass scanning is that when a gamma radiation beam passes through the various segment tissues, the strength of the beam is reduced. By measuring the beam's intensity one can measure the density of the object in question [Zatsiorsky and Seluyanov, 1983]. Using this method, Zatsiorsky and Seluyanov (1985) generated multiple regression equations from a large group of college aged males and females to estimate segment mass, CoM and radii of gyration measures.

Computed tomography (CT) was introduced in 1976 as a method of measuring the density of tissues. Cross-sectional images of the segment are taken at set intervals

permitting the volumetric calculations and providing the added advantage of measuring the various tissue distributions so that densities may also be calculated. Similar to gamma mass scanning, CT scans can provide accurate measures of tissue density, making it a useful tool for BSP research. In estimations of forearm density from cadavers, Rodrigue and Gagnon (1983) demonstrated density calculations within 4.81% of criterion values taken by direct measurement. Furthermore, in a comparison study looking at the BSP's of leg segments, Ackland et al. (1988) found strong relationships between photogrammetry and CT measures of cadavers and living people [Pearsall and Reid, 1994]. In addition, CT scans do not have geometric distortion and can provide a minimal spatial resolution of 1.0 x 1.0 mm^2 for slices between 2 and 13 mm [Huang and Suarez, 1983].

Magnetic resonance imaging (MRI), like the CT scan, also obtains cross-sectional images of the body, however there is no exposure to radiation. When the body is placed in a magnetic field, the magnetic moment of the hydrogen nuclei of a particular tissue take on a specific orientation. That moment generates an electromagnetic force that is received through a computer interface to create pictures. Tissues will appear at different resolutions or brightness levels depending on the magnetic dipole orientation as the magnetic field passes through it [Martin et al., 1989]. A number of researchers have employed this method for determining BSPs [Ackland et al., 1988, Martin et al., 1989, Cheng et al., 2000, Amit et al., 2009, Helms et al., 2009]. Favourable agreements have been found in comparison studies of MRI, water displacement and reaction board measures for whole body mass and CoM [Pearsall and Reid, 1994]. Mungiole and Martin (1990) also determined mass, CoM and MoI for the lower leg of 12 males, concluding that the results were comparable to the criterion cadaver studies.

Another medical imaging technique, dual energy x-ray absorptiometry uses low energy x-rays from two different sources to measure bone density. Depending on the tissue, a certain amount of the x-rays will be blocked, permitting tissue mapping. In a recent study on cranial cruciate lameness, Ragetly et al. (2008) utilised this method to determined morphometry, density, total mass of the hind foot of Labrador Retrievers.

In a comparison study, Wicke and Dumas (2014) used DXA as criterion method to his geometric based model. While results appeared favourable, differences in dissection boundaries make it difficult to compare them to data already in existence. In addition, using a human cadaver leg and a homogenous plastic cylinder, it has been demonstrated that DEXA could measure mass, length, CoM and MoI to within 3.2% [Durkin and Dowling, 2006]. Unfortunately the DXA machine is limited to scans in the frontal plane.

Medical imaging methods are not only costly and time consuming, each piece of equipment requires specially trained operators. In addition, for gamma, CT and DEXA scans, subjects are exposed to small levels or radiation, making these methods less favourable.

2.3.3.9 *Photogrammetry*

Typically used with live subjects, photogrammetry is another method researchers have used to determine body and segment volume [McConville and US Air Force AMRL, 1981, Young et al., 1983, Jensen, 1989, Jensen, 1993, Page et al., 2007]. It is a form of contour mapping, similar to the aerial photography used to create terrain contour maps, using photos of the subject or segment in order to find its volume. There are two versions of this method: mono- and stereo photogrammetry, also known as stereoscopy. The former utilises one camera, the latter two; for both methods a constant elevation, a straight line for example, is projected onto the specimen. The procedures are the same for each, except that for the stereo- method two cameras are used side-by-side to create a three dimensional image when the two photographs are juxtaposed. The segment of interest is photographed and the resulting picture is treated as an aerial photograph upon which contour levels are applied. The portions of the body part between successive contour levels form segments whose volumes can be found by use of a polar planimeter on the photograph as described in detail by Wild (1954) [Contini et al., 1963]. In short, based on the intersection of two projections

created from the juxtaposed images it is possible to calculate the appropriate height values for the overlapping image area.

Pierson (1963) demonstrated the accuracy of the photogrammetric method by measuring the volume of a basketball using water displacement as the criterion. Upon comparing the two methods, his results showed a difference of only 1.2%, making it a promising alternative. In addition, Tanner (1951) demonstrated the repeatability of the method using 70 subjects, concluding that photogrammetry is a reliable method of determining anthropometry [Drillis et al., 1964]. Note, to maintain accuracy on the depth measure, the field of view of the area in question must be visible in the field of view of both cameras. It has also been stated that photogrammetric methods have a tendency to underestimate the MoI values in obese individuals [Damavandi et al., 2009], possibly due to the uniform mass distribution assumption in cadaver criterion studies, however this is not confirmed [Hatze, 1980].

Unfortunately this method is limited by a lengthy analysis time and the need for costly specialised equipment to record and analyse surface shape [Reid and Jensen, 1990].

2.4 Applications in Veterinary Biomechanics

Forces, moments and powers experienced within the musculoskeletal structure can be estimated non-invasively using BSP data. Regardless of the animal, knowledge of the inertial properties of any body is a prerequisite to understanding the kinetic factors that affect performance. Such information is useful for scientific exploration of motor skill coordination in agility tasks, gait, identification of aetiologies for conditions such as arthritis or lameness, and evaluation of surgical or rehabilitation interventions such as joint replacements. As described in sections 2.3.1 and 2.3.2, BSPs are available for humans and hence numerous studies exist describing human gait dynamics. Next to humans, the horse is arguably the most studied animal, generating considerable biomechanical interest in recent years. Most works have been largely static [Colborne, 2004], however the recent availability of BSPs for some breeds [Buchner et al., 1997] have generated opportunities to better understand the finer details of equine gait

dynamics, such as movement of whole body centre of mass in both the sound [Buchner et al., 2000] and lame horse [Buchner et al., 2001] based on 3 dimensional locations of segmental centres of mass. With studies of equine inverse dynamics being approximately 10 years behind human studies, canine biomechanics is a further 10 years behind horses [Colborne, 2007]. Despite the many mechanical differences [Wentink, 1979], Buchner's [1997], procedures for biomechanical assessment vary little across animals. Furthermore, there are many similarities: in addition to being pets, both are popular racing, agility and show animals, lameness is a common musculoskeletal ailment, even the BSP model, landmarks and marker placements are similar. It therefore makes sense to include here a look at the progress made in equine research as a potential guidelines to future canine research.

2.4.1 Equine Biomechanics

Probably the most famous gait study in biomechanics is one that took place in 1878 in which Eadweard Muybridge photographed a horse 'in flight', proving that all 4 of a horse's hooves do, indeed, leave the ground at some point in their stride. Muybridge, a photographer renowned for his spectacular images of Yosemite and Alaska, was hired by Leland Stanford, founder of Stanford University, to photograph his horses. He used a series of 12 cameras installed with tripwires set to trigger the shutter of each camera as one of Stanford's prize trotting horses went by. The brief filmstrip captured the horse's movement along the track, including minute details that were difficult to detect by the naked eye, such as the position of the legs and the angle of the tail. And so, the study of animal locomotion had begun and the invention of the motion picture was soon to follow [Leslie, 2001]. Since that time, due to the horse racing industry and riding activities there has been extensive research on equine gait [Clayton et al., 1998, Barrey, 1999, Keegan, 2007, Robilliard et al., 2007, Oosterlinck et al., 2010]. Race outcomes can be greatly affected by shoe, harness and racetrack design [Seder and Vickery, 2003]. In addition, the high incidence of lameness in race horses caused by training and competition explains the extensive biomechanical analyses of equine locomotion [Jeffcott et al., 1982].

Objective equine biomechanics research began in the early 1970's with Fredricson's [1971] use of high speed film and specially designed hoof markers system to evaluate gait kinematics. Wentink [1979] soon followed up using film and electromyography to study the normal locomotor pattern of the right hind limb of the horse during walking. Results of the study demonstrated the relationship between kinetics, muscle activity and periods within the stride cycle. Also using film analysis, Sprigings and Leach (1986) presented a mathematical algorithm for determining total body centre of gravity from three equine cadavers. Sixteen millimetre film was used to study racehorses in order to establish motion-based segmentation methods for use in their cadaver research. Each horse was dissected into nineteen segments and the centre of gravity located for each segment. Gerhardt and Ripstein (1990) added to this in their book, Measuring and Recording of Joint Motion: Instrumentation and Techniques. They presented a method for measuring equine morphometry, identifying landmarks and suggesting a neutral position based on the Anatomical Neutral-Zero Measuring Method. Clayton and Schamhardt (2000) took this further, suggesting data collection methods, marker locations and normalization patterns.

Gait mechanics studies have included mapping of gait characteristics, both normal [Wentink, 1978, Wentink, 1979, Lanovaz et al., 1999, Seder and Vickery, 2003, Robilliard et al., 2007] and pathological [Merkens and Schamhardt, 1988, Gustås et al., 2006, Keegan, 2007, Goff et al., 2008, Wennerstrand et al., 2009, Goff et al., 2010, Moore, 2010] , energy efficiency measures [Griffin et al., 2004, Harrison et al., 2010] and performance strategies [Powers and Harrison, 1999, Unt et al., 2010]. Recent studies have demonstrated low agreement between clinicians for lameness scores, suggesting a need for more objective methods of evaluating lameness [Keegan et al., 1998, Colborne, 2004]; and a study by Buchner [2001] suggests that horses with forelimb lameness show a typical and well described locomotor pattern. It is assumed that, similar to humans, specific joint motions at various phases of gait may be efforts to distribute body weight away from the affected limb [Weishaupt et al., 2004, Weishaupt et al., 2006]. The kinematic and kinetic patterns associated with these

compensatory movements could be used as pathological indicators, which, when combined with subjective evaluations would assist clinicians with diagnosis and treatment methods.

2.4.2   Canine Biomechanics

As is the case with horses, canine research has largely been completed on racing dogs however not to the same extent. Numerous kinematic studies have been completed (Hottinger et al. 1996, DeCamp et al. 1993, DeCamp et al. 1996, Bennett et al. 1996, Poy et al. 2000), most of which are descriptive studies displaying normal and/or pathological gait patterns. In a 2-dimensional comparison study of clinically normal and hip dysplastic GSDs, Miqueleto et al. (2013) found greater maximum angle and maximum angular velocity in the hip and lesser maximum angular velocity in the carpal joint in dysplastic dogs. Agostinho et al. (2011) showed that dogs of different breeds demonstrate similar kinematic patterns but with significantly different magnitudes.

Kinetic analysis in dogs has been limited primarily to studies of ground reaction forces [Strasser et al., 2014]. Using force plates, Riggs et al. (1993) observed the effects of 3 different velocities on the gait of 7 Greyhounds, concluding that velocity significantly affected impulse and ground reaction force measures and must therefore be controlled in the experimental design. In another study using 5 Greyhounds and 5 handlers, variances in peak vertical force were observed to determine if they were an effect of the dog, the handler or trial repetition. Based on the low variance it was determined that multiple handlers may be used in experiments without affecting outcomes. With the GSD, occasionally another handler may step in to guide the dog. A study such as this could provide valuable information about the dog's effectiveness in a similar situation. An investigation of jump landing in agility dogs presented extremely high peak vertical force for the forelimbs [Pfau et al., 2011]. For the GSD, jumping into vehicles, over fences and other obstacles is a routine part of their job. An investigation such as this, including inverse dynamics, would provide information about internal

joint loads, providing objective data about injury risk to soft tissues of the shoulder and back.

Recent trends in canine research have moved toward evaluations of treatment methods and success of surgical interventions [Trostel et al., 2003b, Michelsen, 2013]. Gillette and Angle (2008) have shown that a kinematic and kinetic analysis is useful for indicating the status and function of the neuromusculoskeletal system. Hicks and Millis (2014) completed a recent study of canine lameness, looking at compensatory movements of the head, pelvis and thoracolumbar spine associated with asymmetric weight bearing in the hind legs of dogs at a trot. It was found that dogs having only subtle asymmetric weight bearing demonstrated greater total motion of the pelvis on the non-affected side and greater thoraco-lumbar lateral angular displacement on the affected side.

Foss et al. [2013a, 2013b] looked at ways to evaluate cervical spondylomyelopathy in Doberman Pinschers using a digital motion capture system. Current outcome measures are purely subjective, being based on the owner's and the clinician's perception. The dogs were fit with a lycra suit, similar to the one used in this study, to which 32 reflective markers were applied. Kinematic data gathered included: stride duration, length, and height; maximal and minimal spinal angles; elbow and stifle flexion and extension; and maximum and minimum distances between the thoracic and pelvic limbs. Their results show that an objective gait analysis reveals more consistent kinematic differences in the thoracic limbs.

In summary, an objective gait analysis including detailed joint mechanics could augment as a clinical diagnostic tool for identifying pathologies associated with gait anomalies such as this, impacting future evaluations of musculoskeletal disorders and therapeutics [DeCamp, 1997]. It is important to note that, when performing an objective gait analysis on dogs, for quantitative gait analysis to be comparable between dogs, within dogs, between sides (i.e. left and right) and between fore and hind limbs, they must be traveling at a constant velocity in a symmetrical gait such as the trot [Allen et al., 1994, Schaefer et al., 1998, Gillette and Zebas, 1999]. Even within the

trot there is some speed-related variation in kinematic pattern [Riggs et al., 1993] therefore it's possible that a treadmill-based design may afford greater control over the stride velocity than that of over-ground trotting. Furthermore, as previously mentioned, for the biomechanical model to work, the input data must be specific to a population (i.e. breed, gender, morphology) [Durkin and Dowling, 2003].

In Canada, there is great interest on the part of municipal and national police organisations in improving best practices when it comes to injury treatment and prevention within their canine teams. Any of the aforementioned pathologies or an acute or overuse injury can afflict the police dog, keeping both the dog and the handler from performing their duties. The ability to quantify functional changes in gait would greatly assist the clinician in the diagnosis, treatment and prevention of injuries in this breed. To accomplish this using the traditional inverse dynamic approach, knowledge of the segment mass distribution properties of the German Shepherd are required so that they may be combined with the measureable ground reaction forces and morphometric data to solve for intersegmental forces, net joint moments and powers. To our knowledge, only one other study has provided a full set of body segment parameters [Amit et al., 2009]. This study was limited to 3 dogs of mixed breed. Other studies have provided limited data specific to the Greyhound (n=4) and Golden Retriever (n=3,14) hind limbs [Colborne et al., 2005, Ragetly et al., 2008] and the forelimb (n=6) of mixed breed dogs. [Nielsen et al., 2003]. To date there have been no complete sets of body segment parameters specific to the German Shepherd.

This thesis aims to directly measure and provide a complete set of body segment parameters and three dimensional inertial properties of GSDs, including mass, centre of mass, volume and moment of inertia. With the data collected, a set of regression equations will be developed with which to estimate segmental masses and moments of inertia in living dogs. The final equations will be evaluated using live German Shepherds.

To successfully achieve these objectives, a variety of methods have been employed for this study. Cost, availability of equipment and proof of a method's successful use

in past studies all were significant factors in the process of method selection. Based on these criteria, cadaveric segmentation was selected over medical imaging as the best overall method of achieving the goals of the study. Directly measured parameters include mass, volume, CoM, principle and biaxial MoI's. Volume is measured using the immersion method, CoM using the balance technique, and MoI's measured using the pendulum method, the timing for which is determined using a Vicon motion capture system. Density and products of inertia are calculated from the measured data. Anatomical landmarks for this study are palpable as reference points located just beneath the skin. This is important for their use in calculating segment lengths and determining segment joint centres. As employed by Vaughn et al. (1999), a combined geometric-regression model is being explored for use in estimating segment masses and moments of inertia.

3   DEVELOPMENT OF THE INERTIAL MODEL

This investigation is a cadaveric study examining the morphometric and inertial properties of the GSD. The data extracted are used to construct a biomechanical model with which to evaluate whole body dynamics in living dogs.

Methods used in this study were selected primarily due to their low cost and practicality for use on working GSDs. Police dogs can have varying temperament therefore the goal is to create a model sufficiently accurate but that also requires limited input of BSP measures.

3.1   Materials and Methods

The methods and techniques used were similar to those used for humans and primates by Clauser et al. (1969), Reynolds (1974) and Chandler et al. (1975). With limited established methodologies from canine BSP studies utilizing cadaver segmentation and the obvious canine to human anatomical differences, a detailed protocol on selection and treatment of the cadavers, in whole and in part, was established. Each subject was segmented and the mass, centre of mass, moments of inertia, and volume were measured for each segment. Standard (e.g. lengths, widths, circumferences) and three-dimensional (orthogonal x, y, z coordinates) morphometry of the body and segments were also determined. Through donated services, whole body CT scans and x-rays of limbs were also included for some dogs. With respect to this study the data were primarily used for confirmation of direct-measured morphometry and landmark locations. See Discussion for future directions for these additional data.

3.1.1   Specimen Selection

The Canadian Police Dog Service Training Centre and dog handlers from the British Columbia Lower Mainland region police services (which includes national and municipal police forces) were provided information about the research and given the opportunity to volunteer the remains of their dog to the research project upon death

(see Appendix A). Subject preparations began immediately following euthanasia (see laboratory procedures outlined in Appendix B. Using similar measures and techniques as those of Reynolds (1974), Gerhardt and Ripstein (1990) and Onar (1999) morphometric dimensions listed in Appendix C were measured. All dogs were euthanized by the handler's preferred veterinarian. No dogs were euthanized strictly for the purpose of this study.

In an effort to maintain uniform specimen size and shape, the guiding criteria in cadaver selection was physical condition. No limitations were placed on height or weight, however specimens exhibiting congenital abnormalities, structural atrophy, excessive weight loss or obesity were not considered. All dogs were required to be at least 2 years of age (to ensure muscle maturity), intact (no amputees or severe trauma), disease-free and either on active duty at time of death or retired but still physically fit.

Following these criteria, 6 male GSD cadavers were donated to the study by the Royal Canadian Mounted Police (RCMP). The dogs had a mean age of 4.75 years (range 2 to 8.5 years) and a mean body mass of 36.8 kg (range 34.29 to 39.41 kg).

3.1.2 Procedure

Subject preparations began immediately following euthanasia. Dogs 1 to 3 were transported immediately to the laboratory to begin collecting conventional morphometrics (i.e. lengths, breadths, circumferences) on the intact cadaver. Two local diagnostic clinics donated their scanning services for the remaining 3 dogs so dogs 4 to 6 were first taken for x-rays and full-body CT scans before they, too, were taken to the lab to begin measurements. The following sections detail the steps of the data collection process as outlined in Appendix B, including dissections and BSP measurements.

3.1.2.1 *CT Scans*

Dogs 4 and 5 were imaged at 2mm slices using a Picker PQS CT system located at Canada West Veterinary Specialists (Burnaby, BC CA). Dog 6 was imaged at 1mm

slices using a Toshiba Aquilion helical CT system located at Canada Diagnostic (Vancouver, BC CA). Dogs were positioned in sternal recumbency with fore and hind legs extended. Images were used to verify measured segment dimensions and will be used for further investigation comparing measured and calculated segment volumes and tissue densities.

3.1.2.2 *Preliminary Measures & Freezing*

Using similar measures and techniques as those of Reynolds (1974), Gerhardt and Ripstein (1990) and Onar (1999), morphometric dimensions (Appendix C) were recorded for use in the model for estimating moments of inertia. To prepare for dissection and morphometric measures, selected landmarks were identified with an oil pencil on the skin prior to freezing, including: the left and right acromion processes, xyphoid process, umbilicus, T13, left and right cranial dorsal iliac spine, S1, and left and right femoral head. This simplified finding these landmarks when the cadaver was frozen. Unlike the procedures of Reynolds (1974) and Chandler (1975), the dogs were not shaved so as not to affect segment mass. The subject was also placed in a suspension frame in a neutral stance position (Figure 3.1) via a custom harness and frame designed to fit within the dimensions of a 700 litre chest freezer (Sears Kenmore®).

Figure 3.1: Suspension frame for neutral stance positioning

This kept the subject correctly posed for freezing in case early rigor mortise made it difficult to position. Since no standard anatomical neutral position has been established for the dog, the selection of "neutral position" was loosely based on the relaxed four footed stance with tail down (Figure 3.2) but with mouth closed and right and left sides placed symmetrical. While an extended and abducted position would be ideal for purposes of segmentation, a relaxed stance position retains a more natural mass distribution within each segment.

Figure 3.2: Neutral stance position

Subjects were frozen at -18°C conditions for a minimum of 48 hours, a necessary step not only to extend the handling time but it also formed a rigid body for the inertia measurements, limited fluid loss during dissection and handling, and kept tissues static thereby maintaining the position of the centre of mass for each segment. Potential fluid loss by sublimation [Hower, 1970] was monitored at each stage of experimentation through periodic weighing. After conventional morphometric dimensions were collected the subject was placed in a similar frame and positioned inside the freezer (Figure 3.3).

Figure 3.3: Suspension frame configured for deep freeze

3.1.2.3 *Segmentation*

Segmentation occurred over 1-2 days. The body was divided into seventeen segments (Figure 3.4): head, neck, torso, abdomen, tail, right and left brachium, right and left antebrachium, right and left manus, right and left thigh, right and left crus, and right and left pes. All cuts passed through the estimated instantaneous joint centre of rotation, as located by Dempster and demonstrated by Clauser et al. (1969) for humans and for horses by Sprigings and Leach (1986) and Buchner et al. (1997).
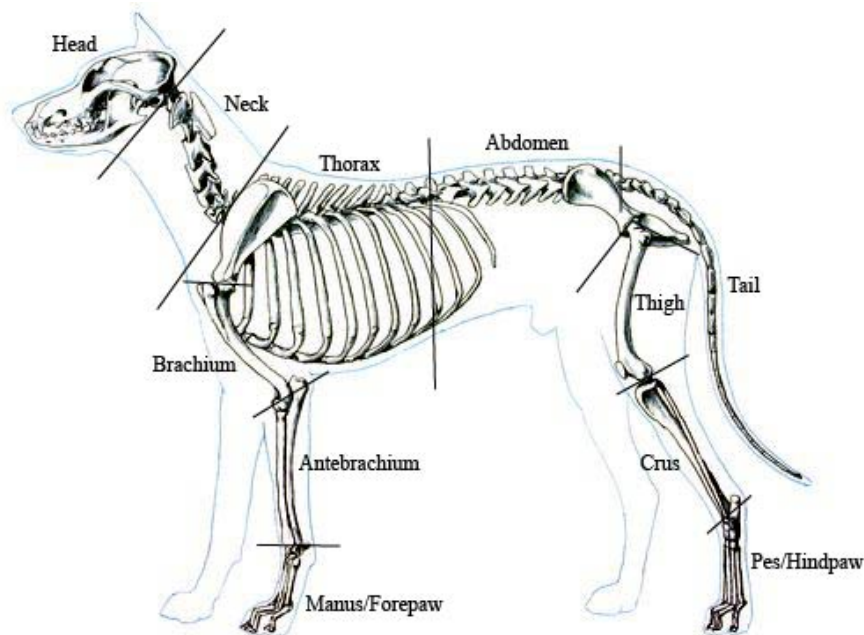
Figure 3.4: Seventeen-segment model of the dog showing segmentation lines

Due to the difficulty in achieving a clean separation it was necessary to include the scapula as part of the torso. Cuts were made using a battery powered reciprocating saw, a hand-held stainless steel butcher saw and an electric Stryker saw. Any lost tissue was weighed for inclusion in the summation of segment masses for comparison of pre and post segmentation. Upon dissection, segments were weighed and photographed to document cuts and location of primary points and landmarks. They

were then placed in freezer bags, tightly sealed to control dehydration, carefully labelled and returned to the freezer.

3.1.2.3.1 Head/Neck
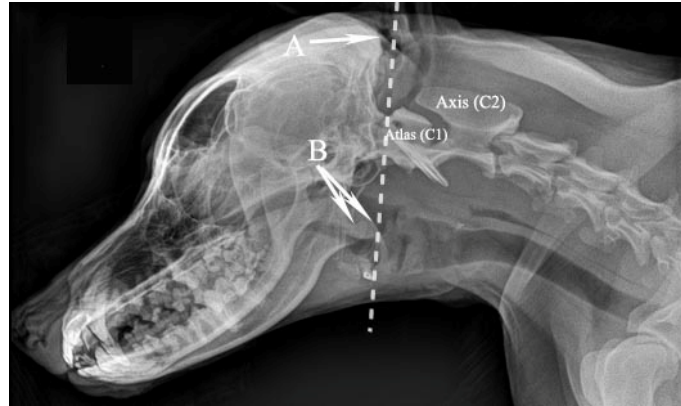
Figure 3.5: Radiograph of head/neck showing A) the external occipital protuberance and B) the right and left paracondylar processes. Dashed line indicates the location of plane of separation created by these landmarks.

With the head at approximately 125 degrees to the cervical spine, separation of the head from the neck passed along a plane tangent to the midpoint between the external occipital protuberance and the cranial point of the spinous process of the axis (keeping the ears intact) and the right and left paracondylar processes (Figure 3.5).

3.1.2.3.2 Neck/Thorax

With the cervical spine at approximately 150 degrees to the thoracic spine, separation of the neck from the thorax passed along a plane tangent to the greater tubercle of the humerus and the cranial border of the shoulder blade (Figure 3.6) on the right and left sides.
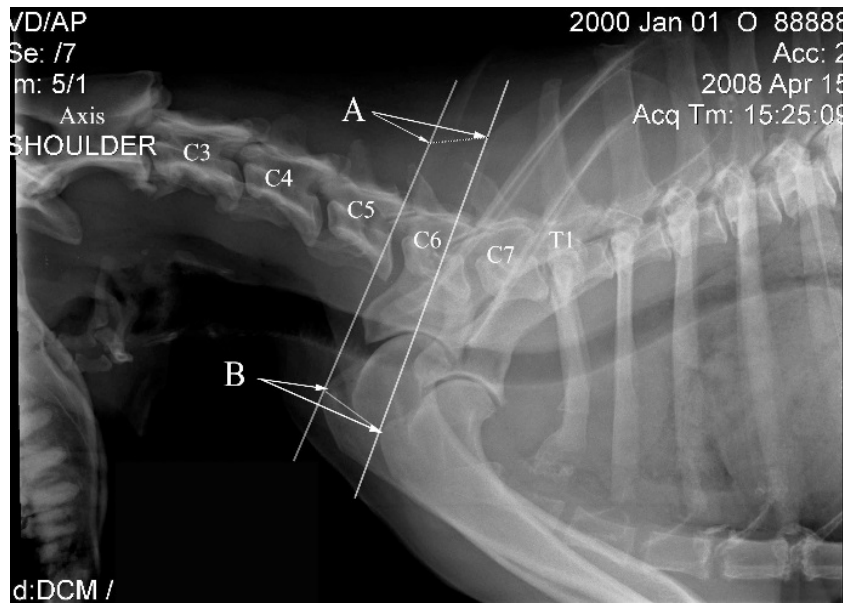
Figure 3.6: Radiograph of neck/torso showing plane of separation marked by lines tangent to A) the right and left cranial border of the scapula and B) right and left greater tubercle of the humerus.

3.1.2.3.3 Brachium/Thorax

Separation of the upper arm from the torso required a compound cut; the first was on the underside of the brachium following the axial crease upward along the body to the humeral head, the second ran across from the greater tubercle of the humerus, tangent to the midline between the acromion and humeral head to the apex of the axial crease (Figure 3.7).
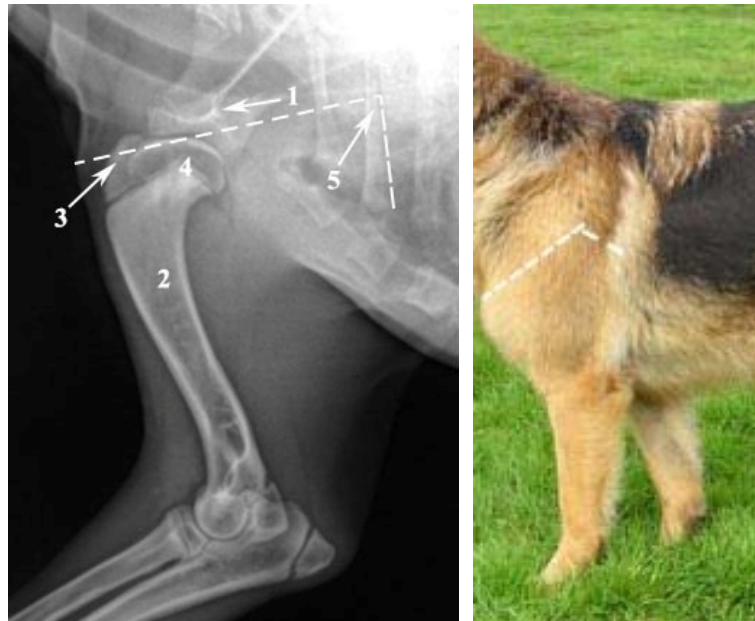
Figure 3.7: Lateral view of left brachium showing segmentation lines. Note landmarks: 1) acromion, 2) humerus, 3) greater tubercle of the humerus, 4) humeral head, 5) apex of the axial crease

3.1.2.3.4 Brachium/Antebrachium

The brachium was separated from the antebrachium along a plane passing through the medial and lateral humeral epicondyles and a point at the crease of the elbow (Figure 3.8, line A). Note that, in stance, the flexure surface of the brachium is approximately 145 degrees relative to the antebrachium, causing the olecranon tuber to be partially bisected within the brachial segment.

Figure 3.8: Lateral view of left forelimb showing cut lines at elbow and wrist as well as key landmarks used in bisection

1) ulna	4) ulnar styloid process (hidden, see Figure 3.9)	7) olecranon tuber
2) radius	5) accessory carpal	8) crease of the elbow
3) radial styloid process	6) lateral epicondyle	9) humerus

3.1.2.3.5 Antebrachium/Manus

The antebrachium was separated from the manus along a plane tangent to the radial and ulnar styloid processes and the accessory carpal bone, keeping it intact (Figure 3.8, line B; Figure 3.9). The extensor surface of the antebrachium is approximately 170 degrees relative to the manus.

Figure 3.9: Dorsal aspect of right manus showing dashed bisection line, radius (1), ulna (2), radial syloid process (3), and ulnar styloid process (4).

3.1.2.3.6 Thorax/Abdomen

On observation, the canine torso can rotate separately from the abdomen, particularly if changing direction while running however there are no studies documenting the specific movement of the thoracic spine in relation to the lumbar spine. It was decided that the torso and abdomen would be measured separately in order to provide an opportunity for future investigation in this area.
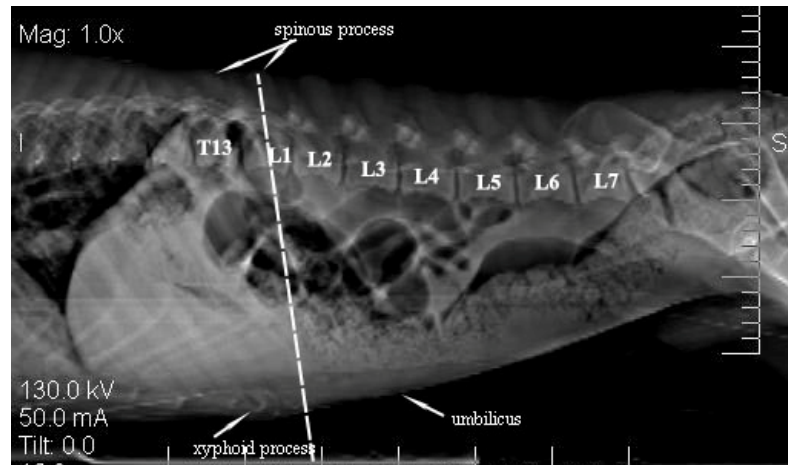
Figure 3.10: Left lateral view of thorax/abdomen showing dashed bisection

The plane of separation of the torso from the abdomen was made tangent to the midpoint between T13 and L1 spinous processes and the midpoint between the xyphoid process and the umbilicus (Figure 3.10).

3.1.2.3.7 Abdomen/Thigh

The separation of the thigh from the abdomen required a compound cut. The inferior plane passed from the point of the ischial tuberosity to the femoral head at the inferior edge of the acetabulum. The superior plane passed diagonally from the apex of the thigh crease to the most superior projection of the greater trochanter, through the femoral head to the acetabulum to meet the first cut (Figure 3.11).
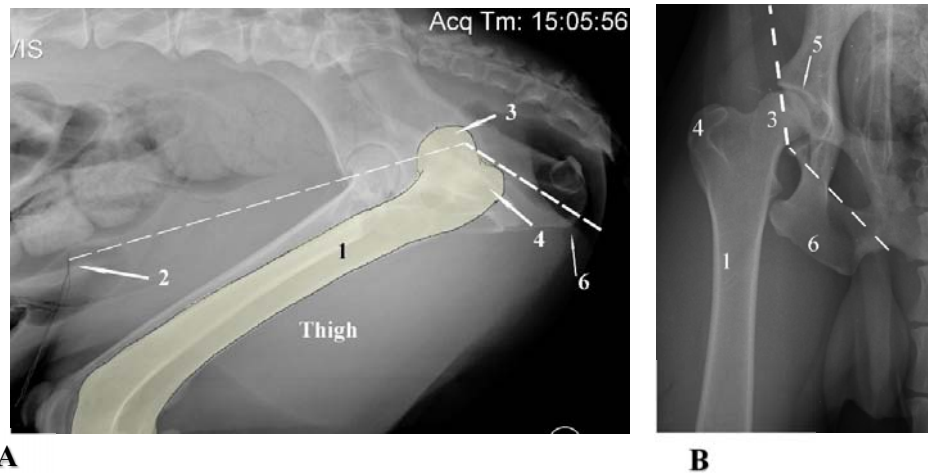
Figure 3.11: A & B: Lateral and ventral radiographic views of hip separation, shown by dashed line. Note key features: 1) femur 2) thigh crease apex 3) femoral head 4) greater trochanter 5) acetabulum 6) ischial tuberosity

3.1.2.3.8 Thigh/Crus

Similar to brachium/antebrachium, the separation of the crus from the thigh passed along a plane bisecting the medial and lateral femoral epicondyles and a point at the crease at the back of the knee with the knee flexed at approximately 100 degrees (Figure 3.12).

Figure 3.12: Ventral view of left knee showing separation of the thigh from the crus as indicated by the dashed line. 1) femur 2) tibia 3) fibula 4) lateral femoral condyle 5) medial femoral condyle

3.1.2.3.9 Crus/Pes

Separation of the pes from the crus (Figure 3.13) was made with the pes flexed at 95 degrees to the crus. The cut plane passed just distal to the lateral and medial malleoli and tangent to the dorso-caudal edge of the calcaneus.

Figure 3.13: Right lateral view of the ankle separation indicated by the dashed line. Note key landmarks 1) calcaneus 2) medial and lateral malleoli 3) tibia and fibula

3.1.2.3.10 Abdomen/Tail

The tail was removed along a plane separating the sacrum from the first caudal vertebra.

3.1.2.4 *Mass*

Whole body mass was measured prior to dissection using a Bertec® 4060-10 strain-gauge-based force plate (Bertec Corporation, Columbus, OH, USA). All other mass measures were completed directly using a Mettler SB32001DR Dual Range Precision Balance. The balance has a capacity of 32100g and is accurate to 0.1g for measures below 6400g, 1.0g for measures over 6400g. (Mettler Toledo® Canada, Mississauga, ON, CA). To monitor any loss of mass due to sublimation, segment masses were taken immediately upon dissection, again approximately 1-2 days later at the same time

inertial properties were taken, and a third time approximately 1 week later when volumetric measures were completed.

3.1.2.5 *Creating the 3-D Coordinate System and Pendulum for Moment of Inertia*

After morphometric dimensions and segmentation cuts were complete, it was necessary to determine landmark coordinates, CoMs and MoIs for each segment relative to a 3-D orthogonal, Cartesian coordinate axis system. The irregular shape of the segments prompted the creation of a segment holder similar to those used in previous studies [Dempster, 1955, Chandler et al., 1975, Reynolds et al., 1975, Lephart, 1984] that would also act as the required coordinate system. With marked primary (xx, yy, and zz) and secondary (xy, xz, and yz) axes, the segment holder created an external axis with set origin, as shown in Figure 3.14, that could then be used to locate segment landmark coordinates (see Appendix D: 3D point location form) and CoM of the segment using the balance method (section 0) and to determine the swing period about all 6 axes for MoI calculations using the simple pendulum method section 2.3.3.4). These 3 sets of measurements have a close positional relationship thus it was imperative that the segment remain frozen to control internal movement and solidly fixed in place to control external movement throughout this series of measurements.
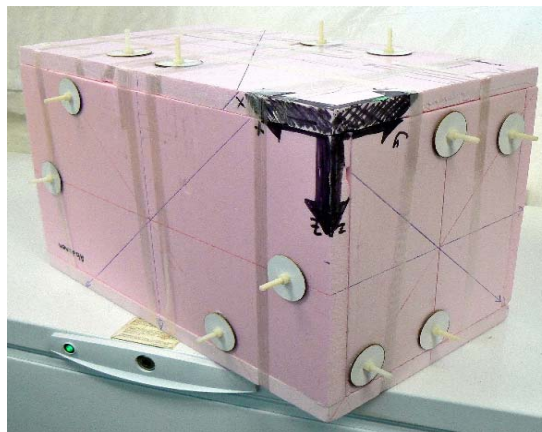
Figure 3.14: Segment holder for the abdominal segment showing origin, primary and secondary axes, and bolts for attaching pendulum string

The segment holders were 4-sided boxes constructed of rigid Styrofoam (2.5cm thickness for the heavier abdomen and thorax; 1.3cm thickness for all other segments) glued together for rigidity. The boxes were optimally sized to fit each segment as closely as possible to limit the effect of its mechanical properties relative to the segment. Each segment was aligned as closely as possible with the longitudinal axis of the segment box as defined by its proximal and distal joint centres.

The segment was fixed securely on foam saddles attached to the base inside the box, held in place using strong adhesive tape which wrapped around and attached to the outside of the base, similar the demonstration below in Figure 3.15.
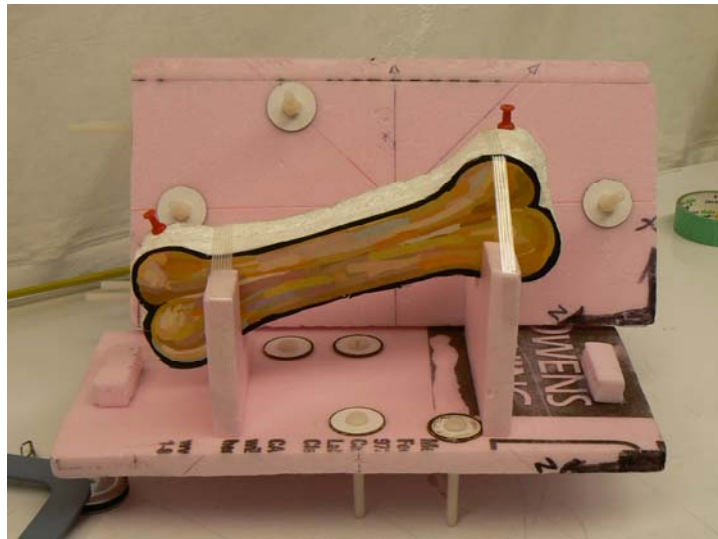
Figure 3.15: Segment holder demonstration with segment secured inside

When placed on the base, the lid would clamp down on the tape, further securing the segment. The lid was then taped down firmly to the box, which also afforded thermal isolation to the frozen segment. To remove the segment, the tape was cut and left in place so that it could be included in the mass and inertial measurements of the empty box.

For the 15 smaller segments, the boxes were suspended by 2 strings attached to the box wall using nylon bolt fasteners as shown in Figure 3.16.
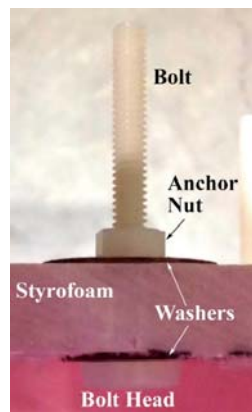
Figure 3.16: Small box string attachment used for 15 of 17 segments, side view

There were 2 string connectors per swing axis for a total of 12 connections per segment box. For each connection, a 6cm nylon bolt, with melamine washer for force dispersement, was fed through a carefully placed hole in the Styrofoam box followed by another washer, and a single nylon nut to anchor it all in place.

To attach the string, a hole was drilled into the head of a nylon acorn nut fitting the dimensions of the bolt. The string was fed through the hole from the top and tied off. The strings were then attached to the box by screwing the acorn nut tightly onto the bolt as shown in Figure 3.17.
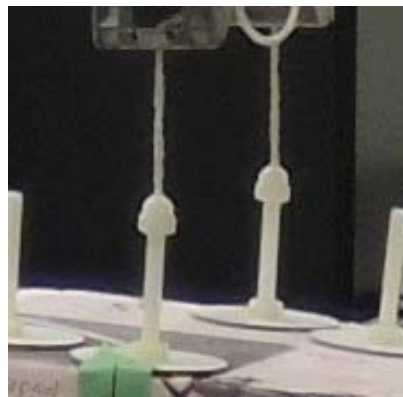
Figure 3.17: Pendulum strings connected to box

The larger abdomen and thorax segments were too heavy to be suspended from the segment box wall. Instead, the box was used as a spacer with nylon reinforced holes instead of bolts and the segment was suspended directly using 27 kg rated stainless steel wire. The wire was fed from the outside of the box through one of the two holes in the suspension axis, wrapped around the segment and back out of the box through the second hole in the suspension axis (Figure 3.18).
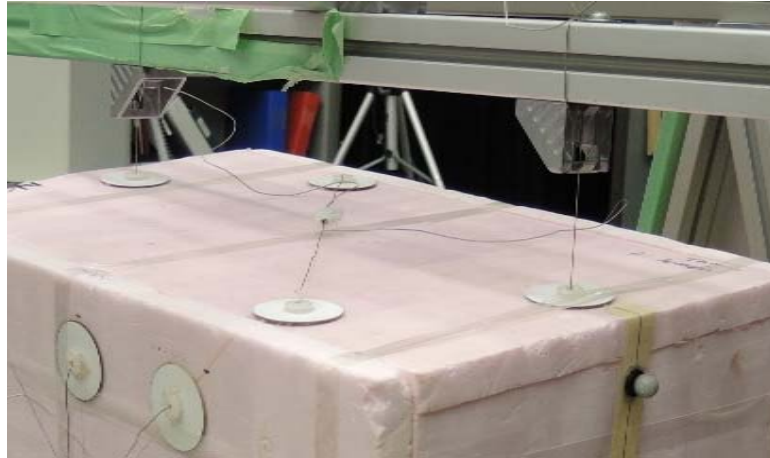
Figure 3.18: Pendulum wires and segment box configured for abdomen and thorax

This was repeated for all axes prior to any measures being taken so that the segment inside was secured in place. Axes that were not being measured had their wires tightly clamped to prevent any possible movement of the heavy segment inside (Figure 3.19).
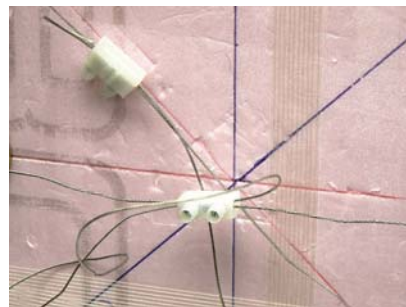
Figure 3.19: Wire clamps for abdomen and thorax

Finally, all segment boxes were suspended from a rigid frame and each string or wire passed through a sliding guide that could be moved to fit each axis and segment box and then securely clamped in place to form the pivot about which the pendulum was swung (Figure 3.20).

Figure 3.20: Pendulum frame

3.1.2.6   *Moment of Inertia (MoI)*

Moment of inertia for each segment was measured using the simple pendulum method developed by Winstandley et al. (1968) and described in detail by Reynolds (1974). The segment holder was swung in the vertical plane with the period of oscillation, length of pendulum and mass of the segment being the three basic measurements. Subtracting the known mechanical properties of each box (mass, CoM, MoI) from the composite (box plus segment) measures it was possible to determine the inertial properties of the segment alone.

As derived in 2.3.3.4, when the segment is hung vertically and swung in small oscillations with a half angle of less than 5 degrees, the MoI about its axis of rotation

can be calculated using (Equation 2.15). Furthermore, to find the MoI about an axis passing through the CoM of the segment it was necessary to perform a parallel axis transfer (Equation 2.16).

To extract the MoI of the segment about its CoM from the composite measures, Equation 2.15 can be expanded to the following form:

$$l_{CoM} = \frac{mg_c l_c T_c^2 - mg_b l_b T_b^2}{4\pi^2} - m_s l_s^2 \qquad \text{(Equation 3.1)}$$

Where the subscript c refers to the composite box, subscript b refers to the empty box and subscript s refers to the segment. This formula may be used to determine MoI for all 6 axes (xx, yy, zz, xy, xz, yz).

According to gravitational station 9061-68 based at Vancouver International Airport, gravity (g) was equal to 9.8091567 m/sec². Masses (m) were measured as described in section 3.1.2.4. The length of the pendulum (l) was determined by 2 components: the combined length of the string and bolt configuration (for the small boxes) or the wire (for the 2 larger boxes) from the pivot point to the box surface; and the vertical distance from the outer surface to the CoM of the empty box and the CoM of the composite box (with segment in place). Based on the valued obtained, the following formula was used to determine the length to the CoM of the segment:

$$m_c l_c = m_b l_b + m_s l_s \qquad \text{(Equation 3.2)}$$

Therefore,

$$l_s = \frac{m_c l_c - m_b l_b}{m_s} \qquad \text{(Equation 3.3)}$$

Where l_s equals the length to the CoM of the segment, m_s equals the mass of the segment, similarly $m_c l_c$ equal the corresponding measures of the composite box and $m_b l_b$ equals the corresponding measures of the empty box.

A Vicon Optical Capture System recorded the period of oscillation (T) over 3 successive trials. The mean of these three values was used to calculate MoI for each

segment. To achieve this, 2 markers were positioned vertically on the segment box and 2 more were placed on a plumb bob hanging from the pendulum frame directly in front of the segment box. Reference frames were first collected with the pendulum stationary so that the initial angle of the box with respect to the plumb bob was recorded. The pendulum box was then set in motion and the swing angle and period of oscillation were recorded.

3.1.2.7 *Centre of Mass (CoM)*

The CoM for each segment was determined using the balance technique described in section 2.3.3.5. Segment boxes were balanced on a knife edge (Figure 3.21). Once equilibrium was found the location at the balance point was measured from the origin of the box. Measures were taken from both the right and left sides of the box and an average taken to determine the midpoint. This procedure was repeated for the primary axis of each segment a minimum of 3 times each and averaged across measures.

Figure 3.21: Balance technique for finding CoM of the forepaw

3.1.2.8 *Determination of Swing Period*

Swing period was determined using the pendulum method as shown in Figure 3.20 and described in 3.1.2.6. A plumb bob hung from the pendulum frame with string marked with reflective markers created a stationary reference line. Reflective markers

placed on the segment box created a second vertical line which, when observed with the stationary reference line, permitted observation of swing angle. A Vicon motion capture system recorded marker oscillation at a frame rate of 120 Hz, an example of which is shown in Figure 3.22. Three swing trials were completed and peak to peak timing data recorded for all 6 axes of each segment. To avoid the possibility of errors, the first and last maximum and minimum peaks were discarded. The remaining peak to peak data was averaged within trials for those with multiple peaks and then averaged again across all three trials. The final average oscillation time was used in calculating moment of inertia for the corresponding segment and axis.

Abdomen
Swing period about Y (flex/ext) axis
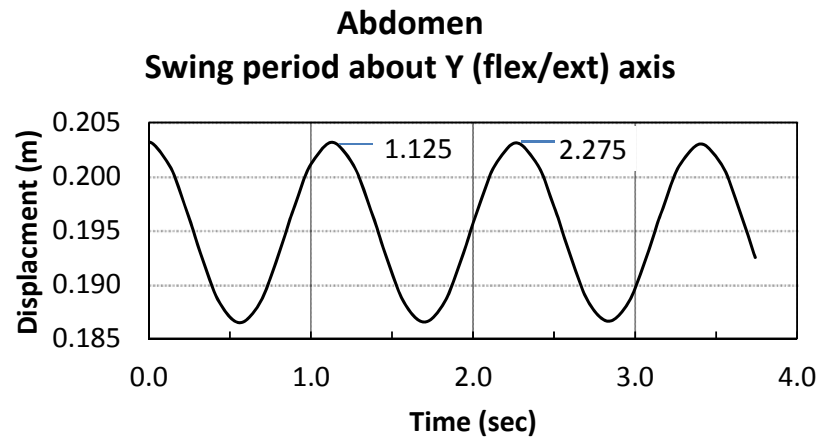
Figure 3.22: Pendulum swing period for the abdomen flexion/extension axis

3.1.2.9 *3-Dimensional Landmark Coordinates*

After completing CoM and pendulum measures, key landmarks were identified with pins and coordinates measured and recorded from the origin of the segment box.

3.1.2.10 *Volume*

The last step in the data collection process was to measure the volume of each segment using the immersion method (section 2.3.3.7). It is important to leave this step last so

the water will not affect the other measures. For this study a series of clear containers sized according to segment were used to measure the amount of water displaced. The main premise was to have the container sufficiently narrow enough to just fit the segment so that error created by the excess surface area was reduced. The container was first filled to a height equivalent to the length of the segment and a mark was then made on the side of the container to indicate the height of the meniscus without the segment. The segment was then introduced to the container of water with care being taken to release any air trapped in the hair. Once submerged another mark was made on the outside of the container to indicate the height of the meniscus with the segment (Figure 3.23).

The segment was then removed and any lost water was replaced to fill the container to the first meniscus line. Water was then measured to fill the container to the second meniscus line. The amount of water required to fill the container from the first line to the second was considered to be the volume of the segment.
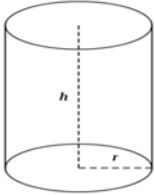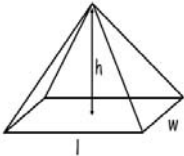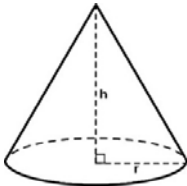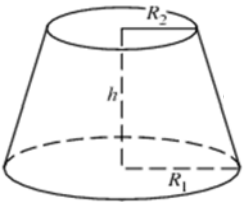
Figure 3.23: Volume measure, hind paw

3.1.2.11 *Regression Analysis*

Segment inertial data of living subjects can be estimated by geometric shape of the segments or measured directly through cadaveric studies. Based on methods used for humans by Vaughn et al. (1999), the methods used in this investigation exploit the relationship between mass, density and volume, i.e. segment mass should be related to segment volume, or the volume of some shape that is representative of the segment. Regression equations were created from whole body mass and simple geometric modelling using morphometric dimensions to predict mass and MoIs for 17 segments of the GSD. To work with GSDs, in particular, police dogs, it is necessary to create a model that is not only accurate but that can also be personalized to the dog, is relatively inexpensive, requires little time and handling to gather measurements and must be safe for the dog, the handler and the clinician collecting the data. With these aspects in mind, a number of morphometric dimensions and geometric shapes were tested through the course of analysis to find those which best correlated to the segment in question.

The shapes tested include: a cylinder, a rectangular pyramid, a cone, a conical frustum, and an ellipsoid. The following tables illustrate the geometric shapes, their corresponding formulas for volume (Table 3.1) and MoI (Table 3.2) about each axis and the regression equations derived for estimating segmental mass and MoI based on whole body mass and segment morphometry. Note: Formulas have been adjusted to permit the use of circumference (*c*) measures rather than radius (*r*).

As shown in section 2.3.3.3, since volume is made up of 3 dimensions, the multiple linear regression equation for predicting segment mass will include body mass and up to 3 morphometric dimensions (Equation 2.8). In a similar equation, MoI predictors include body mass and up to 2 morphometric dimensions (Equation 2.5).

Table 3.1: Segment mass based on regression equations derived from shape geometry

Cylinder:	mass (m) = density (ρ)*volume (v), therefore, if:
	$Volume\ (v) = \pi r^2 h = \left(\frac{1}{4\pi}\right) c^2 h$,
	$Mass\ of\ a\ cylinder = \frac{\rho}{4\pi} l_s c_s^2$
	Based on whole body mass and segment volume, the multiple regression equation to predict mass of a cylinder-shaped segment is :
	$m = (C1 * M) + (C2 * l_s c_s^2) + C3$
Pyramid, rectangular base:	$v = \left(\frac{1}{3}\right)(l)(w)(h)$
	$Mass\ of\ a\ pyramid = \frac{1}{3}(\rho)(l)(w)(h)$
	so the regression equation to predict mass of a pyramid – shaped segment is:
	$m = (C1 * M) + (C2 * l_s w_s h_s) + C3$
Cone:	$v = 1/3(\pi)(r^2)(h) = \frac{1}{12\pi} c^2 h$
	$Mass\ of\ a\ cone = \frac{\rho}{12\pi} c^2 h$
	so the regression equation to predict mass of a cone – shaped segment is:
	$m = (C1 * M) + (C2 * c_s^2 l_s) + C3$
Conical frustum (truncated cone):	$v = \left(\frac{1}{3}\right)(\pi)(h)(R_1^2 + R_1 R_2 + R_2^2)$
	$= (\frac{h}{12\pi}) c_1^2 + c_1 c_2 + c_2^2$
	$Mass\ of\ conical\ frustum = \frac{\rho}{12\pi}(h)(c_1^2 + c_1 c_2 + c_2^2)$
	so the regression equation to predict mass of a segment shaped like a conical frustum is:
	$m = (C1 * M) + (C2 * (l_s)(c_{s1}^2 + c_{s1} c_{s2} + c_{s2}^2)) + C3$
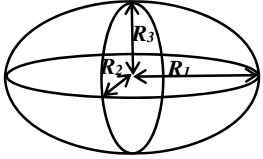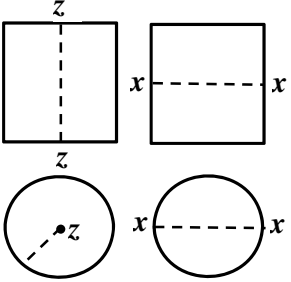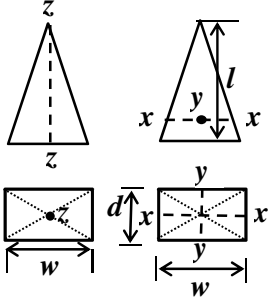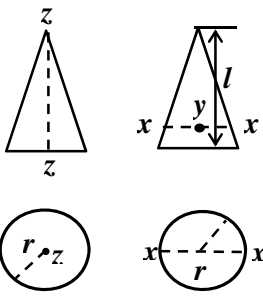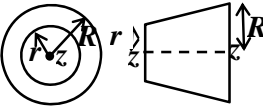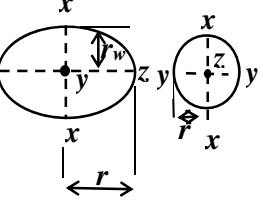
Ellipsoid:	$v = \left(\dfrac{4}{3}\right)(\pi)(R_1)(R_2)(R_3)$
	$v = \left(\dfrac{4}{3}\right)(\pi)\left(\dfrac{l_1}{2}\right)\left(\dfrac{c}{2\pi}\right)^2 = \dfrac{lc^2}{6\pi}$
	$Mass\ of\ ellipsoid = \dfrac{1}{6\pi}(\rho)(lc^2)$
	so the regression equation to predict mass of an ellipsoid-shaped segment is: $m = (C1 * M) + (C2 * l_s c_s^2) + C3$

M = whole body mass, m = mass of the segment, v = volume, ρ = density, r = radius, l = length of cylinder, l_s = length of segment, c = circumference, c_s = circumference of the segment, C_1 = coefficient with respect to whole body mass, C_2 = coefficient with respect to volume, C_3 = residual coefficient

Table 3.2: Moments of inertia about the CoM of a segment - regression equations derived from shape geometry (from Oberg (, Machinery's Handbook). All formulas are referenced through the centre of mass.

Cylinder:	referring to z-z axis: $I_z = \frac{1}{2}mr^2$ if , $r = \frac{c}{2\pi}$ $I_z = \frac{1}{8\pi^2}mc^2$	referring to x-x axis: $I_x = \frac{1}{12}m(3r^2 + l^2)$ Therefore, using c $I_x = I_y = \frac{1}{12}m(.076c^2 + l^2)$
	so regression equations to predict MoI for a cylinder are: $I_z = \left(C_1 * \frac{1}{8\pi^2}Mc_s^2\right) + C_2$ $I_x = I_y = (C_1 M)(.076c_s^2 + l_s^2) + C_2$	
Pyramid, rectangular base:	referring to z-z axis: $I_z = \frac{m}{20}(w^2 + d^2)$ referring to x-x axis: $I_x = m(\frac{3}{80}l^2 + \frac{d^2}{20})$ $= \frac{m}{80}(3l^2 + 4d^2)$	referring to y-y axis: $I_y = m\frac{3}{80}(l^2 + \frac{w^2}{20})$ $= \frac{m}{80}(3l^2 + 4w^2)$
	so regression equations to predict MoI for a pyramid are: $I_z = \left[\frac{C_1 M}{20}(w^2 + d^2)\right] + C_2$ $I_x = [(C_1 M)(3l^2 + 4d^2)] + C_2$ $I_y = [(C_1 M)(3l^2 + 4w^2)] + C_2$	

Cone:	referring to z-z axis:	referring to x-x axis:
	$I_z = \dfrac{3m}{10}r^2$ if , $r = \dfrac{c}{2\pi}$ $I_z = \dfrac{3}{40\pi^2}mc^2$	$I_x = \dfrac{3m}{20}(r^2 + \dfrac{l^2}{4})$ Therefore, $I_x = I_y = \dfrac{3}{80}m\left[\left(\dfrac{c}{\pi}\right)^2 + l^2\right]$
	so regression equations to predict MoI for a cone are: $I_z = \left[C_1 * M * \dfrac{3}{40\pi^2}c_s^2\right] + C_2$ $I_x = I_y = C_1 * \dfrac{3M}{80}\left[\left(\dfrac{c_s}{\pi}\right)^2 + l^2\right] + C_2$ Note: cs refers to the circum	
Frustum of a cone: 	referring to z-z axis: $I_z = \dfrac{3m(R^5 - r^5)}{10(R^3 - r^3)}$ if , $r = \dfrac{c}{2\pi}$ $I_z = \dfrac{3m[(\frac{C}{2\pi})^5 - (\frac{c}{2\pi})^5]}{10[(\frac{C}{2\pi})^3 - (\frac{c}{2\pi})^3]}$ $I_z = .0076m\dfrac{(C^5 - c^5)}{(C^3 - c^3)}$	with reference to axis x-x, see I_x and I_y equations for cone (above)
	so regression equations to predict MoI for a frustum of a cone are: $I_z = \left[C_1 * M * .0076\dfrac{(C_s^5 - c_s^5)}{(C_s^3 - c_s^3)}\right] + C_2$ For I_x and I_y see equations for cone (above)	
Ellipsoid: 	referring to z-z axis: $I_z = \dfrac{m}{5}(r_w^2 + r_d^2)$ using c, $r = \dfrac{c}{2\pi}$ and the formula becomes: $I_z = 0.01013mc^2$ using d, $r = \dfrac{d}{2}$ and the formula becomes: $I_z = 0.1md^2$	referring to x-x axis: $I_x = \dfrac{m}{5}(r_l^2 + r_d^2)$ referring to y-y axis: $I_y = \dfrac{m}{5}(r_l^2 + r_w^2)$ If using l and c, or l and d these formulas become: $I_x = I_y = \dfrac{m}{20}[l^2 + (\dfrac{c}{\pi})^2]$ $I_x = I_y = \dfrac{m}{20}[l^2 + d^2]$

so regression equations to predict MoI for an ellipsoid are:

$$I_z = (C_1 * Md^2) + C_2$$

$$I_x = I_y = \left[C_1 M[l^2 + (\frac{c_s}{\pi})^2]\right] + C_2$$

Or

$$I_z = (C_1 * Mc_s^2) + C_2$$

$$I_x = I_y = (C_1 M[l^2 + d^2]) + C_2$$

I = polar mass moments of inertia; M = whole body mass, m = mass of the segment, r = radius, l = length of cylinder, l_s = length of segment, d = diameter, c = circumference, c_s = circumference of the segment or the smaller circumference in the case of the frustum, C_s = larger circumference of the segment (frustum) C_1 = coefficient with respect to whole body mass, C_2 = residual coefficient

3.2 Results

The results presented here include summaries of select morphometric dimensions and body segment parameters (mass, volume, density and moments of inertia) gathered from 6 male pure-bred German Shepherd cadavers. All segments had been frozen for the segmentation process therefore tissue loss was minimal at an average loss of 182g or 0.49% of total body mass per dog.

Regression equations were developed from the collected data so that they may be used to predict segment masses and moments of inertia for the living German Shepherd working dog. Timing methods for determining moment of inertia are also described, as well as a synopsis of regression correlation analyses, dimensional summaries and finally, a table of normalised average segment masses, CoMs, radii of gyration and average segment densities.

3.2.1 Morphometry and Body Segment Parameters

At the start of the research it was unknown which data would provide the best regression correlations therefore a variety of dimensions were evaluated based on currently used human models, such as the Helen Hayes model [Vaughn et al., 1999, Buczek et al., 2010], and animal studies [Reynolds, 1974] as well as on geometric

shapes. Dimensional data selected for use in developing the model are presented along with additional measures that may prove useful in future studies. A complete list of dimensions and their corresponding definitions can be found in Appendix C.

The hind limbs, at 6.8% body mass were 2.3% heavier than the forelimbs at 4.5% body mass. The thorax presented the greatest density at 1083 kgm^{-3} while the thigh and manus had similar densities at 940 and 934 kgm^{-3}, respectively.

In addition to mass, volume and moment of inertia, a total of 100 morphometric dimensions were gathered from each dog, including: total body mass, 23 separate measures for the forelimbs, 33 for the hind limbs, and 43 for the rest of the body. Due to the large number of measurements it was not possible to confirm all measures for accuracy by remeasuring each one. Dogs 4 and 5 were first scanned using the Picker PQS CT system. Since this system was slow, rigor mortise began before all dimensional data could be collected. The 2 dogs required freezing before all morphometric measures could be collected thereby making it more difficult to palpate key landmarks for determining segment length. For those dogs, landmarks were identified with grease pencil markings on the skin prior to freezing.

Dog number 4 had noticeably more subcutaneous adipose tissue than the other dogs. To determine if this would have any effect on results, select parameters were tested for outliers using Mahalanobis' Distance, Cook's Distance and Centred Leverage Value. While some data points were identified as outliers, they were not consistently from dog 4. Of those that were identified, on graphical review of predictors and residuals it was not clear in many cases that they indeed should be excluded (see graphs for selected models of each segment in Figure 3.24 and Figure 3.25). Additional tests using the Outlier Labelling Rule with 2.2 as the multiplier did not identify any outliers. It was decided that due to the small sample size it was difficult to conclusively exclude any data points so no individual data were excluded from any of the analyses.

To complete data collection and confirm repeatability, multiple sets of measures were conducted on select dimensions. An initial (i) set was collected upon receipt of the dog, prior to segmentation; a second (s) set was collected approximately one week later after segmentation was complete; segment lengths could also be checked for accuracy using a third set of measures calculated from the 3-dimensional (3d) coordinates of the proximal and distal joint centres. *Note: The dimension was calculated by first determining the difference between the proximal and distal joint locations for each of x, y and z then calculating the sum of squares for the combined differences. The square root of this sum of squares value becomes the calculated length.*

Paired-sample t-tests were conducted on these multiple measures to confirm no significant differences existed between measurement sets taken at the different times of the study. A finding of significant differences ($p<.05$) between a compared pair indicated that the measure in question is not reliably repeatable and was excluded from the model. Statistical non-significance ($p>.05$) indicated that multiple measures of the parameter in question produced repeatable results and could be used in the development of geometric-based regression equations. Paired samples correlations provide a further gauge of the relationship between the 2 sets of measures. Summary results of the paired samples t-tests are provided in Table 3.3.

In the following subsections, body segment parameters and summary descriptives are presented for each segment along with observations noted during the analyses. Unless otherwise stated, to reduce processing time, correlated pairs were not averaged for this study, therefore the dimensions displayed include only one of the paired samples. Measures were selected based on performance in the correlation analyses described in sections 3.2.2 and 3.2.3. Complete morphometry, body segment parameters and repeated measures analyses for each subject and segment can be found in Appendix E.

Table 3.3: Summary of paired sample t-tests on repeated measures

Pair	Dimension (m)	Paired Differences			t	df	Sig. (2-tailed)	Paired Sample Correlations	
		$\overline{x}$	SD	$\sigma_{\overline{x}}$				Corr	Sig.
1	Manus length (3D-s)	.0005	.0034	.0010	.560	11	.587	.093	.773
2	Paw length (s-i)	.0015	.0022	.0006	2.349	11	.039	.894	<.001
3	Wrist circumference (s-	.0015	.0031	.0009	1.698	11	.118	.861	<.001
4	Manus circumference (i-s)	.0002	.0060	.0017	.143	11	.889	.905	<.001
5	Manus breadth (i-s)	-.0052	.0067	.0019	-2.651	11	.023	.410	.185
6	Wrist breadth (s-i)	-.0040	.0042	.0012	-3.249	11	.008	.336	.286
1	Antebrachium proximal to distal length (s-3d)	.0021	.0074	.0021	.975	11	.351	.869	<.001
1	Brachium proximal to distal length (3d-s)	.0030	.0084	.0024	1.220	11	.248	.717	.009
2	Acromion to lateral epicondyle length (i-s)	.0037	.0254	.0073	.508	11	.622	-.234	.464
3	Humerus to lateral epicondyle length (s-i)	-.0131	.0232	.0067	-1.962	11	.076	-.151	.641
1	Pes: heel to tip of 3rd phalanx length (s-i)	-.0007	.0039	.0011	-.626	11	.544	.854	<.001
2	Pes breadth (s-i)	.0007	.0031	.0009	.800	11	.441	.427	.166
1	Crus: proximal to distal it ctr length (3d-s)	.0047	.0146	.0042	1.109	11	.291	.639	.025
2	stifle circ (s-i)	-.0055	.0158	.0046	-1.215	11	.250	.729	.007
3	calf circ (s-i)	.0252	.0220	.0063	3.970	11	.002	.676	.016
1	Head: bizygomatic breadth (3d-i)	.0095	.0194	.0079	1.198	5	.284	.354	.492
1	Neck: caudal to cranial it ctr length (s-i)	.0048	.0098	.0040	1.195	5	.286	.935	.006
2	Mid circ (s-i)	-.0133	.0271	.0111	-1.203	5	.283	-.517	.293
1	T13/L1 length7S1 @ spinous process vs @ segment ctr length	-.0041	.0204	.0077	-0.531	6	.614	.960	.001
2	Waist @ omphalion circ (s-i)	-.0865	.0704	.0287	-3.009	5	.030	.345	.503
3	Waist crease circ (s-i)	-.0412	.0529	.0216	-1.906	5	.115	.626	.184
1	Thorax : xyphoid process circ (s-i)	-.0122	.0458	.0187	-.651	5	.544	.003	.995
2	Mid thorax circ (s-i)	-.0135	.0159	.0065	-2.084	5	.092	.831	.040
3	Mid-segment breadth (s-i)	-.0121	.0257	.0105	-1.155	5	.300	-.093	.861
1	Tail: sacrum to tail tip length (3d-i)	.0055	.0252	.0103	.536	5	.615	.035	.948
2	Midtail circ (s-i)	-.0122	.0143	.0058	-2.082	5	.092	.564	.244

3.2.1.1 *Manus*

For the combined values of the left and right manus, repeated measures comparisons were made on manus length from the proximal joint centre to the tip of the third digit, paw length (metacarpal phalangeal joint to tip of third digit), wrist circumference around radial and ulnar styloid processes, carpus/metacarpus circumference, manus circumference (around pads, 2nd to 5th mcpj), manus breadth and wrist breadth.

Significant differences were found between paw lengths, manus breadths and wrist breadths, indicating that these measurements are not repeatable and would likely not be ideal for inclusion in geometric-based regression equations. This is not unexpected since the paw digits can be easily splayed and dimensions can vary with stance position and wrist angle. If using the paw circumference, it is recommended measures be taken with the paw unweighted and the wrist angle at 180 degrees. Similarly, wrist breadth relies on ulnar and radial styloid landmarks, which can be quite broad with no defining centroid and are slightly offset, thereby increasing the likelihood of variability between measurements.

Of the remaining 3 pairs of measures showing no significant differences, manus circumference and wrist circumference paired measures showed strong correlations (p<.001), while the 2 sets of manus length measurements did not (p=.773). These results indicate that:

- Both sets of the manus circumferences could be averaged and included in the model as one set. The same could be said for the wrist circumference.

- If not averaging the data, either the pre or post segmentation measures may be used to determine correlation coefficients within the model. This would be acceptable for both the wrist and the manus. For the purposes of this study and to reduce data processing time, only the post-segmentation wrist and pre-segmentation manus circumferences will be used.

- For the manus length, either the 3d measures or the post segmentation measures could be used for the development of the model but it is not

recommended they be combined and averaged as it could reduce the strength of the correlation and, therefore, the accuracy of the regression coefficients.

Table 3.4 summarises the morphometry and body segment parameters selected for further analysis of the manus. Length data shown are from the calculated 3D measures (3d), which produced slightly better correlations than the post-segmentation (s) measures for determining segment mass. Wrist (s) and manus (i) circumferences are also shown. Principle moments of inertia, (I_x, I_y & I_z), biaxial moments of inertia (I_{xz}, I_{yz} & I_{xy}) and products of inertia ("I_{xz}", "I_{yz}", "I_{xy}") are also presented.

Table 3.4: Manus - body segment parameters and summary descriptives

Parameter	Min	Max	$\bar{x}$	$\sigma_{\bar{x}}$
Mass (kg)	0.230	0.312	0.267	9.96E-03
Volume (cm^3)	240	340	287	12.9
Density (kg/cm^3)	8.14E-04	1.04E-03	9.34E-04	2.56E-05
Manus l (cm)	16.1	17	16.5	0.108
Wrist c (cm)	14.8	16.8	15.9	0.24
Manus c (cm)	15.1	19.3	17.2	0.579
$I_{int/ext\ (x)}$ (kg*cm^2)	4.32	6.37	6.37	0.787
$I_{abd/add\ (z)}$ (kg*cm^2)	4.87	14.2	10.3	1.25
$I_{flx/ext\ (y)}$ (kg*cm^2)	5.08	14.2	9.83	1.17
I_{xy} (kg*cm^2)	1.31	13.8	9.41	1.41
I_{xz} (kg*cm^2)	7.45	14.4	10.1	0.87
I_{yz} (kg*cm^2)	6.29	13.5	10.2	0.944
"I_{xy}" (kg*cm^2)	-0.425	9.04	2.64	1.11
"I_{xz}" (kg*cm^2)	0.149	7.52	4.02	1.01
"I_{yz}" (kg*cm^2)	-1.95	4.48	1.68	0.741

3.2.1.2 *Antebrachium*

For the antebrachium, left and right measures were combined and a paired samples t-test comparison was performed on the proximal to distal segment lengths taken post-segmentation (antebrachium l p-d_s) and calculated from 3-d joint centre locations

(antebrachium l p-d_3d). There were no significant differences found, $t(11) = .975$, $p = .351$, two-tailed as well as strong paired sample correlations. Two other possible length measures, the length from the olecranon process to the ulnar stylus, and from the lateral epicondyle to the ulnar stylus, were also investigated but their measures presented with a large mean variability so were not included in the final correlational analysis. Repeated measures were not completed on these dimensions.

Table 3.5: Antebrachium - body segment parameters and summary descriptives

Parameter	Min	Max	$\bar{x}$	$\sigma_{\bar{x}}$
Mass (kg)	0.418	0.598	0.506	0.024
Volume (cm^3)	390	618	521	30.7
Density (kg/cm^3)	9.14E-04	1.09E-03	9.78E-04	2.42E-05
Antebrachium l p-d (cm)	19.2	23.8	21.4	0.611
Olecranon-stylion (cm)	18.6	24.3	21.7	0.846
Radiale-stylion (cm)	16.3	22.7	19.7	0.789
Elbow c (cm)	23.1	27.5	25.2	0.558
Mid c (cm)	17.0	20.0	18.3	0.405
Elbow b (cm)	5.00	6.90	5.64	0.279
$I_{int/ext\ (z)}$ ($kg*cm^2$)	4.40	13.2	9.82	1.23
$I_{abd/add\ (x)}$ ($kg*cm^2$)	24.7	45.6	32.7	2.64
$I_{flx/ext\ (y)}$ ($kg*cm^2$)	20.3	33.1	26.9	1.85
I_{xy} ($kg*cm^2$)	27.6	46.8	37.2	1.96
I_{xz} ($kg*cm^2$)	16.7	27.4	23.1	1.3
I_{yz} ($kg*cm^2$)	12.5	28	18.8	2.16
"I_{xy}" ($kg*cm^2$)	2.24	11.2	6.84	1.12
"I_{xz}" ($kg*cm^2$)	5.18	37.7	24.3	4.67
"I_{yz}" ($kg*cm^2$)	-28.4	19.1	-5.33	5.57

Since it was unknown how well elbow circumference would perform in the regression correlations, elbow breadth was also measured. In addition to the pre (i) and post (s) segmentation measures, a third elbow breadth measure was taken during the analysis of the brachium segment. To evaluate the three elbow breadth datasets for consistency, one-way repeated measures ANOVA was completed, $F(2,22) = 3.63$, $p<.05$.

Significant differences were found however Mauchly's test indicated that the assumptions of sphericity had been violated, $\chi^2(2) = 11.2$, p = .004 therefore degrees of freedom were corrected using Greenhouse-Geisser estimates of sphericity ($\varepsilon = 0.6$). The results show there was no significant variation in elbow breadth, $F(1.195,13.15)$ = 3.63, p =.073, suggesting that elbow breadth measures are repeatable and that any of the sets of dimensions may be used for developing geometric-based regression equations. Table 3.5 summarises the morphometry and body segment parameters selected for the antebrachium. For purposes of this study only the 3d antebrachium length data will be used. In addition to the dimensions already discussed, mid-segment circumference was also selected for analysis. Note: wrist circumference is shared for the manus and antebrachium, refer to the manus for dimensional summaries.

3.2.1.3 *Brachium*

For the brachium, three different approaches to segment length were explored. The first was the proximal to distal joint centre length, measured at post segmentation (s) and compared with the length calculated from 3d coordinates. For the second approach, the acromion process and lateral epicondyle were chosen as palpable landmarks. Pre (i) and post (s) segmentation measurements were taken and compared for consistency. Similarly (s vs i), the third approach again used the lateral epicondyle for the distal end landmark but used the head of the humerus as the palpable proximal landmark.

There were no significant differences found in any of the three paired comparisons so all three measures were kept for further analysis. The paired sample correlations however, show only the measures of proximal to distal joint centre producing a significant correlation (p=.009), indicating that either of the proximal to distal brachium length measures were strong enough to use in the regression model or they could be combined and averaged. The non-significant correlations for length measures using the acromion and the humerus landmarks suggest that these measures are not adequately repeatable and may not produce significant regression correlations. For

purposes of this study only the post-segmentation measures (s) of all 3 segment lengths will be used for further analyses. Table 3.6 summarizes the morphometry and segment parameters recorded for the brachium.

Table 3.6: Brachium - body segment parameters and summary descriptives

Parameter	Min	Max	$\bar{x}$	$\sigma_{\bar{x}}$
Mass (kg)	0.631	1.14	0.880	0.077
Volume (cm^3)	640	1220	908	86.2
Density (kg/cm^3)	8.99E-04	1.08E-03	9.74E-04	1.80E-05
Prox-Dist l (cm)	14.7	17.9	16.2	0.411
Acromion-radiale l (cm)	16.4	20.6	18.5	0.604
Humerus-radiale l (cm)	14.4	17.2	15.5	0.455
Axillary c (cm)	34.5	42.8	39.7	0.956
Mid-brachium c (cm)	27.0	35.5	31.2	1.03
$I_{int/ext\,(x)}$ ($kg*cm^2$)	13.0	49.4	29.9	4.06
$I_{abd/add\,(z)}$ ($kg*cm^2$)	18.9	78.3	51.5	8.07
$I_{flx/ext\,(y)}$ ($kg*cm^2$)	21.6	88.8	43.7	7.16
I_{xy} ($kg*cm^2$)	20.1	56.1	36	4.74
I_{xz} ($kg*cm^2$)	14.6	63.4	29.2	5.39
I_{yz} ($kg*cm^2$)	26.4	83.5	51.7	8.23
"I_{xy}" ($kg*cm^2$)	1.13	32.6	8.85	3.27
"I_{xz}" ($kg*cm^2$)	4.56	28.2	17.2	2.96
"I_{yz}" ($kg*cm^2$)	-0.38	89.2	19.1	9.80

3.2.1.4 *Pes*

For the pes (right and left sides combined and averaged), comparisons were made on measures of the length of the heel to tip of the third phalanx just at the base of the nail. The first set of data was taken post segmentation, the 2nd set of data was calculated from the 3d point locations of the proximal and distal joint centres. Pes breadth, taken across the 2nd to 5th metatarsal heads, was measured twice at pre- and post-segmentation.

Table 3.7: Pes - body segment parameters and summary descriptives

Parameter	Min	Max	$\bar{x}$	$\sigma_{\bar{x}}$
Mass (kg)	0.277	0.334	0.303	9.28E-03
Volume (cm^3)	260	343	305	12.6
Density (kg/cm^3)	9.75E-04	1.06E-03	9.97E-04	1.41E-05
Proxt jt ctr-tip of met III l (cm)	18.4	20.9	20.1	0.358
Heel-tip of met III l (cm)	22.6	24.7	23.8	0.326
Heel-mtpj III l (cm)	15.8	17.5	16.6	0.243
Ankle c (cm)	18.5	21.4	20.1	0.391
Mid-pes c (cm)	11.7	13.5	12.9	0.278
Pes c (cm)	14.1	16.8	15.6	0.413
Pes b (cm)	5.2	5.5	5.35	0.0428
Pes d (cm)	4.19	4.3	4.22	0.0171
$I_{int/ext\ (z)}$ (kg*cm^2)	13.5	23.2	18.9	1.59
$I_{abd/add\ (x)}$ (kg*cm^2)	6.12	12.0	8.93	0.797
$I_{flx/ext\ (y)}$ (kg*cm^2)	15.7	18.6	17.3	0.511
I_{xy} (kg*cm^2)	9.58	26.3	13.4	2.66
I_{xz} (kg*cm^2)	7.68	15.4	10.1	1.22
I_{yz} (kg*cm^2)	13.9	24.3	17.2	1.60
"I_{xy}" (kg*cm^2)	1.86	7.12	5.36	0.823
"I_{xz}" (kg*cm^2)	5.71	10.7	7.29	0.763
"I_{yz}" (kg*cm^2)	-2.04	4.75	2.40	0.984

No significant differences were found for either of the 2 sets of dimensions however the heel to tip of 3rd phalanx produced a significant correlation, p=.000. Both sets of pes lengths and the post-segmentation breadth were kept for further analyses. These and additional measures included for regression analyses are summarized in

Table 3.7.

3.2.1.5 *Crus*

Three sets of comparisons were made for measures of the crus; calf circumference, proximal to distal length, and stifle circumference. In comparing the two sets of calf circumferences, there were significant differences between measures, t(11)=3.97,

p=.002. On observation, it was difficult to get a consistent measure of calf circumference because the muscle belly is not defined in some dogs so there was some reliance on a measure of proportion of the segment length to find a consistent landmark. This would add another dimension to the list of required measures so this dimension was removed from further analysis.

Table 3.8: Crus - body segment parameters and summary descriptives

Parameter	Min	Max	$\overline{x}$	$\sigma_{\overline{x}}$
Mass (kg)	0.451	0.64	0.559	0.027
Volume (cm^3)	410	630	548	33.3
Density (kg/cm^3)	9.14E-04	1.12E-03	1.03E-03	3.33E-05
Prox-dist jt ctr l (cm)	19.1	21.7	20.7	0.355
Tibiale med-sphyrion (cm)	19.3	23.8	21.5	0.606
stifle (knee) c (cm)	29.0	33.0	31.6	0.564
stifle (knee) b (cm)	4.00	7.03	5.57	0.402
$I_{int/ext\,(z)}$ (kg*cm^2)	10.3	23.9	15.5	1.95
$I_{abd/add\,(x)}$ (kg*cm^2)	24.0	37.0	28.5	1.98
$I_{flx/ext\,(y)}$ (kg*cm^2)	23.3	34.9	28.0	1.69
I_{xy} (kg*cm^2)	21.0	62.9	39.7	7.27
I_{xz} (kg*cm^2)	7.82	25.1	15.3	2.77
I_{yz} (kg*cm^2)	19.1	23.0	21.6	0.556
"I_{xy}" (kg*cm^2)	-7.60	12.6	3.77	3.18
"I_{xz}" (kg*cm^2)	23.1	38.3	29.3	2.49
"I_{yz}" (kg*cm^2)	-11.2	33.1	3.14	6.80

Measures of length taken from the proximal to distal joint centre of the segment just after segmentation were compared with those calculated from the 3D coordinate data of the same joint centres. Also compared were measures of stifle and calf circumferences taken pre (i) and post (s) segmentation. No significant differences were found in segment length or stifle circumference, making them both good candidates for further analysis.

Table 3.8 summarizes dimensions gathered for the crus. Proximal to distal (3d) and stifle (s) dimensions are shown. An additional length defined by the medial condyle of the tibia (because it is a pronounced landmark) and the medial malleolus was also included for regression analysis.

3.2.1.6 *Thigh*

No repeated measures were completed for the thigh. Dimensions (Table 3.9) included lengths from proximal to distal joint centre, which can be measured from the lower edge of the femoral head to the midpoint of a line transecting the lateral and medial femoral condyles, and also from the middle of the greater trochanter to the lateral femoral epicondyle. Upper thigh circumference was measured from the angle where the thigh meets the abdomen at the flank fold, on an angle across the greater trochanter to the ischial tuberosity. Mid-thigh was taken at the half-length between the greater trochanter and the tibial condyle.

Table 3.9: Thigh - body segment parameters and summary descriptives

Parameter	Min	Max	$\overline{x}$	$\sigma_{\overline{x}}$
Mass (kg)	0.920	1.99	1.62	0.150
Volume (cm^3)	1000	2400	1760	183
Density (kg/cm^3)	8.29E-04	9.86E-04	9.26E-04	2.34E-05
Prox-dist jt ctr l (cm)	14.0	18.7	16.1	0.801
Trochanter-fem condyle l (cm)	15.3	19.0	17.1	0.616
Upper thigh c (cm)	45.0	50.0	47.4	0.768
Mid thigh c (cm)	39.0	43.6	41.9	0.637
$I_{int/ext\,(z)}$ (kg*cm^2)	63.7	132	101	9.24
$I_{abd/add\,(x)}$ (kg*cm^2)	33.0	117	79.7	12.2
$I_{flx/ext\,(y)}$ (kg*cm^2)	64.7	155	110	11.7
I_{xy} (kg*cm^2)	55.1	144	95.5	11.8
I_{xz} (kg*cm^2)	39.8	115	76.4	10.5
I_{yz} (kg*cm^2)	60.6	156	109	12.5
"I_{xy}" (kg*cm^2)	6.17	28.4	19.0	3.27
"I_{xz}" (kg*cm^2)	13.2	41.8	28.0	3.71
"I_{yz}" (kg*cm^2)	24.0	47.5	38.8	3.51

3.2.1.7 *Head*

For the head, bizygomatic breadth measurements were taken twice: once prior to segmentation and the second calculated from 3-dimensional coordinate measures.

Table 3.10: Head - body segment parameters and summary descriptives

Parameter	Min	Max	$\bar{x}$	$\sigma_{\bar{x}}$
Mass (kg)	2.43	3.11	2.83	0.115
Volume (cm^3)	2.24E-03	3.15E-03	2.82E-03	1.40E-04
Density (kg/cm^3)	956	1080	1000	20.3
Head jt ctr-tip of nose l (cm)	23.2	25.5	24.6	0.324
Inion-prosthion l (cm)	25.2	27.6	26.5	0.413
Head base c (cm)	47.0	53.0	49.7	0.908
Base of nose @ incisors c (cm)	23.0	28.5	25.6	0.835
Mid-head c (cm)	46.0	53.5	49.5	1.04
Biorbital b (cm)	10.9	12.9	11.9	0.266
Bizygomatic b (cm)	13.1	18.4	15.0	0.846
$I_{int/ext\ (z)}$ (kg*cm^2)	232	274	254	5.53
$I_{abd/add\ (x)}$ (kg*cm^2)	131	248	192	16.2
$I_{flx/ext\ (y)}$ (kg*cm^2)	216	279	249	10.2
I_{xy} (kg*cm^2)	162	279	229	17.3
I_{xz} (kg*cm^2)	128	215	169	11.9
I_{yz} (kg*cm^2)	206	313	261	14.5
"I_{xy}" (kg*cm^2)	37.4	72.3	51.8	5.16
"I_{xz}" (kg*cm^2)	49.3	97.9	78.2	6.94
"I_{yz}" (kg*cm^2)	65.8	109	82.2	7.29

No significant differences were found, however correlations were non-significant as well. Dimensions determined from 3D measures were selected for further investigation. A number of other dimensions were also recorded based on previous work [Onar, 1999] however only those listed in Table 3.10 were used in the regression analyses. See Appendix C for dimensional definitions.

3.2.1.8 *Neck*

For the neck, caudal to cranial length was measured twice: once prior to segmentation and the second calculated from 3-dimensional coordinate measures with no significant differences found and excellent paired sample correlations (p=.006). A second comparison was completed on the mid circumference of the neck from pre (i) and post (s) segmentation measures. Again, there were no significant differences between these measures, however paired sample correlations were non-significant. For both neck length and mid-neck circumference the post segmentation (s) measures were selected for further evaluation. See Table 3.11 for body segment parameters and dimensional summaries.

Table 3.11: Neck - body segment parameters and summary descriptives

Parameter	Min	Max	$\bar{x}$	$\sigma_{\bar{x}}$
Mass (kg)	1.88	3.27	2.41	0.244
Volume (cm^3)	1820	3680	2550	292
Density (kg/cm^3)	8.39E-04	1.04E-03	9.57E-04	3.23E-05
Caud-cran jt ctr l (cm)	13.7	18.8	16.2	0.997
Caudal end @ shoulders c (cm)	48.0	51.2	49.9	0.491
Mid c (cm)	46.8	48.5	47.5	0.274
Cranial end @ axis c (cm)	44.5	47.5	45.9	0.397
$I_{int/ext\ (z)}$ (kg*cm^2)	105	213	155	15.9
$I_{abd/add\ (x)}$ (kg*cm^2)	126	200	160	11.2
$I_{flx/ext\ (y)}$ (kg*cm^2)	84.6	192	143	19.6
I_{xy} (kg*cm^2)	79.2	205	132	18.8
I_{xz} (kg*cm^2)	112	231	175	20.9
I_{yz} (kg*cm^2)	64.9	242	151	24.1
"I_{xy}" (kg*cm^2)	31.4	80.8	50.0	7.23
"I_{xz}" (kg*cm^2)	23.2	51.3	34.7	3.88
"I_{yz}" (kg*cm^2)	21.9	71.0	46.2	9.04

3.2.1.9 *Abdomen*

For the abdomen, caudal to cranial length was measured from T13L1 to L7S1 spinous processes and again from the 3D locations of the polar centres (not the joint centres) of each end of the segment.

Table 3.12: Abdomen - body segment parameters and summary descriptives

Parameter	Min	Max	$\bar{x}$	$\sigma_{\bar{x}}$
Mass (kg)	6.52	11.7	8.94	0.702
Volume (cm^3)	6940	12300	9260	714
Density (kg/cm^3)	9.41E-04	9.87E-04	9.64E-04	7.71E-06
LT13/L1-L7S1 spin proc l (cm)	29.5	41.1	36.8	1.94
waist at crease c (cm)	51.0	64.0	55.9	2.42
$I_{int/ext\ (z)}$ (kg*cm^2)	400	1640	1160	186
$I_{abd/add\ (x)}$ (kg*cm^2)	455	1210	738	106
$I_{flx/ext\ (y)}$ (kg*cm^2)	851	2340	1460	213
I_{xy} (kg*cm^2)	612	1670	1050	166
I_{xz} (kg*cm^2)	707	1520	993	131
I_{yz} (kg*cm^2)	1110	2450	1590	210
"I_{xy}" (kg*cm^2)	108	247	163	20.1
"I_{xz}" (kg*cm^2)	-20.1	375	246	58.0
"I_{yz}" (kg*cm^2)	-1350	415	70.2	283

There were no significant differences between the measures, indicating that the spinous processes may be used to determine segment length. Paired sample correlations were significant, p=.001.

Two different measures of waist circumference were taken at pre (i) and post (s) segmentation times, one was at the level of the omphalion (umbilicus) and the other was at the waist crease where the thigh meets the abdomen. No significant differences were found for the waist crease measures, although the paired sample was not correlated, p=.184. Despite the low correlation, the post segmentation measure was kept for use in the regression analyses. Omphalion circumferences

showed significant differences between measures and therefore was excluded from the study, $t(5)=-3.009$, $p=.03$. A summary of abdominal dimensions is presented in Table 3.12.

3.2.1.10 *Thorax*

For the thorax, paired sample t-tests were run on 3 separate dimensions taken at pre and post segmentation: circumference at the xyphoid processes, circumference at the mid-thorax, and breadth at the mid-thorax. No significant differences were found in any of the 3 comparisons, however only the measures taken at the mid-thorax (the halfway point between C7/T1 and T13/L1) were found to be significantly correlated, $p=.04$. The data collected for this dimension at post segmentation was kept for further analysis, all others were removed from further inclusion in the study. Body segment parameters and summary statistics for relevant dimensions are shown in Table 3.13.

Table 3.13: Thorax - body segment parameters and summary descriptives

Parameter	Min	Max	$\overline{x}$	$\sigma_{\overline{x}}$
Mass (kg)	12.1	15.3	14	0.444
Volume (cm^3)	10400	16700	13300	1070
Density (kg/cm^3)	9.19E-04	1.35E-03	1.08E-03	8.34E-05
C7T1-T13/L1 jt ctrs l (cm)	32.4	41.7	37.1	1.29
C7T1-T13/L1 spin proc l (cm)	29	36.8	33.4	1.27
mid thorax c (cm)	71.8	78.2	75.0	1.16
largest c (cm)	69.0	81.0	75.0	1.71
base of neck c (cm)	40.5	66.5	56.7	3.73
$I_{int/ext\ (z)}$ (kg*cm^2)	2120	3230	2810	160
$I_{abd/add\ (x)}$ (kg*cm^2)	1240	1460	1350	35.7
$I_{flx/ext\ (y)}$ (kg*cm^2)	2130	3300	2830	171
I_{xy} (kg*cm^2)	1810	2460	2220	97.9
I_{xz} (kg*cm^2)	1460	2220	1970	124
I_{yz} (kg*cm^2)	2480	3170	2890	110
"I_{xy}" (kg*cm^2)	296	362	319	10.1
"I_{xz}" (kg*cm^2)	573	869	702	43.5
"I_{yz}" (kg*cm^2)	560	1670	1000	154

3.2.1.11 *Tail*

For the tail, paired sample t-tests were run on 2 sets of tail lengths to test for repeatability. The first was a set of repeated measures for the length defined as sacrum to tail tip, on dimensions recorded at pre-segmentation vs. a length calculated from 3d landmarks. A second analysis was run on the same 3d length from sacrum to tail tip but compared to a length measured from the 1st caudal vertebra to tail tip. Since the tail curved in this location, this was designed to test if either of the two landmarks could be used.

Table 3.14: Tail - body segment parameters and summary descriptives

Parameter	Min	Max	$\bar{x}$	$\sigma_{\bar{x}}$
Mass (kg)	0.23	0.374	0.296	0.0213
Volume (cm^3)	220	540	345	45.1
Density (kg/cm^3)	6.93E-04	1.08E-03	8.95E-04	6.85E-05
Sacrum to tip of tail l (cm)	41.9	46.5	43.8	0.762
1st caudal vert to tip of tail l (cm)	39.6	48.3	43.5	1.27
Base of tail at sacrum c (cm)	13.4	16	14.9	0.399
Base of tail at 1st caudal vert c (cm)	12.9	16.4	14.4	0.61
$I_{int/ext\,(z)}$ ($kg*cm^2$)	4.40	13.4	8.21	1.41
$I_{abd/add\,(x)}$ ($kg*cm^2$)	50.5	78.6	60.7	4.37
$I_{flx/ext\,(y)}$ ($kg*cm^2$)	38.0	63.6	48.5	4.27
I_{xy} ($kg*cm^2$)	32.8	60	44.2	4.37
I_{xz} ($kg*cm^2$)	29.7	226	71.0	31.2
I_{yz} ($kg*cm^2$)	31.9	42.3	36.1	1.63
"I_{xy}" ($kg*cm^2$)	12.6	29.5	21.2	2.41
"I_{xz}" ($kg*cm^2$)	-9970	2100	-435	1920
"I_{yz}" ($kg*cm^2$)	-4940	-658	-2040	628

A third t-test compared mid-tail circumferences taken at pre and post segmentation. No significant difference was found between any of the three pairs. Paired sample correlations of the first test, however, showed no correlation. This was not unexpected since the initial measures follow the contours of the tail while the 3d measures are a

straight line between the tail tip to the sacrum, bypassing the curve at the top of the tail. Consequently, it is also not surprising that the comparison between the 3-d length and the caudal length were highly correlated (p=.004). Mid-tail circumferences did not show significant correlation and were not included for further analysis. See Table 3.14 for summaries of dimensions and body segment parameters.

3.2.2   Correlations for Predicting Segment Mass

Single and multiple linear regression analyses were carried out to find coefficients that may be used to develop a regression model for estimating segmental mass and MoI for living German Shepherd police dogs. Independent (predictor) variables were whole body mass and segmental morphometric dimensions. The limbs were assumed symmetrical so the best fit combined average (n=12) of both sides is presented for most segments. Where this was not possible (e.g. Manus MoI), the best fit left or right side results (n=6) are presented instead. In these cases, explanation can be found under the associated segment headings that follow. Note: the term 'best fit' refers not only to the model presenting with the best correlation but also favoured the least number of measures required for the model, repeatability, and ease of collection of the required morphometric measures from live dogs. For example, it is common for the dogs to have sensitive feet, to not appreciate arms wrapped around them or to have anyone near their hind quarters. Therefore, where possible, it is best to use measurements that require little handling in these areas.

After collecting morphometric dimensions and body segment parameters, the next step was to develop regression equations that could closely predict segment mass. Since body mass for living subjects is relatively easy to obtain, the first approach was to investigate how closely body mass alone would correlate to each of the segment masses. Upon evaluation very little correlation was found, in fact, the abdominal segment produced the only significant correlation when compared to body mass alone, r = .845, p≤.05, with a R^2 = .715 (see Appendix H for full results).

As previously stated, another approach is to model the segment after some geometric form. For purposes of this study, density is presumed uniform throughout each segment and can be determined from the directly measured segment volumes and masses. Using the methods described in 3.1.2.11, select morphometric dimensions were applied to a variety of geometric models for each segment. The regression coefficients produced by the models having the best fit were selected for inclusion in regression equations for predicting segment masses.

Parameters relevant to the regression equations are shown in Table 3.15. In all cases, dimensions are expressed in centimetres, masses are in kilograms and moments of inertia in kg*cm^2.

Simple linear regression correlations of geometric volumes (predictor) compared with segment masses (actual) produced acceptable results for some segments however, a multiple regression analysis including body mass as a second predictor considerably improved some of the correlations. As a result it has been kept as an input parameter for all segment mass predictions. The final multiple linear regression equations for determining segment mass can be found in Table 3.16. Table 3.17 summarizes the results of the multiple regression analysis for the models selected for inclusion in the linear regression equations (refer to Table 3.1 and Table 3.2 for regression equations derived from shape geometry). For the mass correlations, the manus, antebrachium, crus, thigh, and neck were modelled as right rectangular cylinders; the brachium, abdomen and thorax were each modelled as the frustum of a right circular cone; the hind paw was modelled as a right rectangular pyramid; the head was modelled as an ellipse; and the tail was modelled as a cone. Because we are working with more than one predictor it is necessary to use the adjusted coefficient to compensate for the added variable. Results of the correlations can also be seen graphically in Figure 3.24. As previously stated, right and left sides were assumed symmetrical so the same formula is assumed for both right and left. On application, the dimensions from each limb will be input into the model.

Table 3.15: Parameter labels and definitions for regression equations

Parameter	Name			Definition
A		Total body mass		
B1	Left	carpal jt	circum-	Bistyloid circumference
B2	Right	(wrist)	ference	
C1	Left	ante-	length	proximal to distal joint centre
C2	Right	brachium		
D1	Left	brachium	length	proximal to distal joint centre
D2	Right			
E1	Left	axillary	circum-	Circumference @ highest point in the axilla,
E1	Right		ference	perpendicular to long axis of the brachium
F1	Left	elbow	circum-	olecranon process-crease across epicondyles
F2	Right		ference	
G1	Left	pes	length	Prox jt ctr to podactylion III (base of nail)
G2	Right			
H1	Left	pes	breadth	width across metatarsal phalangeal joints
H2	Right			
J1	Left	pes	depth	depth from midpoint between malleoli and and base
J2	Right			of the pes
K1	Left	crus	length	proximal to distal joiont centre
K2	Right			
L1	Left	hock	circum-	bimalleolar circumference
L2	Right	(ankle)	ference	
M1	Left	thigh	length	mid centroid of femoral head
M2	Right			
N1	Left	stifle	circum-	circumference at mid-patella
N2	Right	(knee)	ference	
P		head	length	atlas/axis jt ctr to end of nose
Q		head	breadth	ecto-orbitale width
R		neck	length	Base of the head (Axis) to C7
S		atlas/axis j	circum-	Circumference at Axis
T		neck	mid-	mid length, halfway between the Axis and C7
U		C7/T1 jt	circum-	Circumference at the base of neck at the shoulders
V		thorax	length	C7/T1 jt ctr to T13/L1 jt ctr
W		T13/L1 jt	circum-	largest circumference at base of ribs
X		abdomen	length	T13/L1 to L7/S1 (spinous processes
Y		waist	circum-	at level of waist crease (narrowest)
Z		tail	length	sacrum to tip of tail
ZA		tail	circum-	at sacrum
ZB1	Left	manus	length	caudal edge of met pad to podactylion III
ZB2	Right			
ZC1	Left	carpus	breadth	bistyloid breadth
ZC1	Right	(wrist)		
ZD1	Left	hock	breadth	bimalleolar breadth
ZD1	Right	(ankle)		

Table 3.16 Regression equations for predicting segment mass

Segment	Regression Equation
Manus =	$(-0.003)*(A) + (69.762)*ZB*B^2 + 0.077$
Antebrachium =	$(0.012)*(A) + (101.084)*C*B^2 - 0.463$
Brachium =	$(0.092)*(A) + (25.062) D*(E^2+E*F+F^2) - 3.811$
Pes =	$(-0.009)*(A) + (633.875)*G*H*J + 0.357$
Crus =	$(0.075)*(A) + (139.127)*K*L^2 - 3.393$
Thigh =	$(0.018)*(A) + (105.849)*M*N^2 - 0.711$
Head =	$(0.243)*(A) + (1602.163)*P*Q^2 - 11.739$
Neck =	$(0.063)*(A) + (98.915)*R*T^2 - 3.527$
Abdomen =	$(0.030)*(A) + (16.692)*X*(W^2+W*Y+Y^2) + 0.106$
Thorax =	$(0.094)*(A) + (11.135)*V*(W^2+W*U+U^2) + 4.966$
Tail =	$(0.020)*(A) + (22.123)*Z*ZA^2 - 0.667$

Table 3.17: Mass correlation summaries

Segment	R^2	Adj'd R^2	Model Shape	Dimension 1	Dimension 2	Dimension 3
Manus	0.891	0.867	Cylinder	Prox to Dist jt ctr length (3d)	Wrist circ (s)	
Ante-brachium	0.920	0.903	Cylinder	Prox to Dist jt ctr length (Ave 3d+s)	Wrist circ (s)	
Brachium	0.711	0.646	Frustum	Prox to Dist jt ctr length (s)	Axillary circ	Elbow circ
Pes	0.914	0.895	Pyramid	Prox jt ctr to tip of 3rd phalanx (s)	Pes breadth	Pes depth
Crus	0.653	0.576	Cylinder	Prox to Dist jt ctr length (3d)	Ankle circ (s)	
Thigh	0.762	0.709	Cylinder	Prox to Dist jt ctr length (3d)	Knee circ	
Head	0.867	0.778	Ellipse	Jt ctr to nose (3d)	Biorbital breadth	
Neck	0.970	0.952	Cylinder	Prox to Dist jt ctr length (s)	Mid circ	
Abdomen	0.974	0.957	Frustum	Prox to Dist jt ctr length (s)	circ @T13/L1	circ @ waist crease
Thorax	0.988	0.978	Frustum	Prox to Dist jt ctr length (3d)	Base of ribs circ	base of neck circ
Tail	0.960	0.934	Cone	Prox to Dist jt ctr length (3d)	base of tail circ	

Figure 3.24: Correlations for predicting segment mass from body mass and segment morphometry

*Note: R^2 correlations presented in the graphs are the unadjusted coefficient of determination
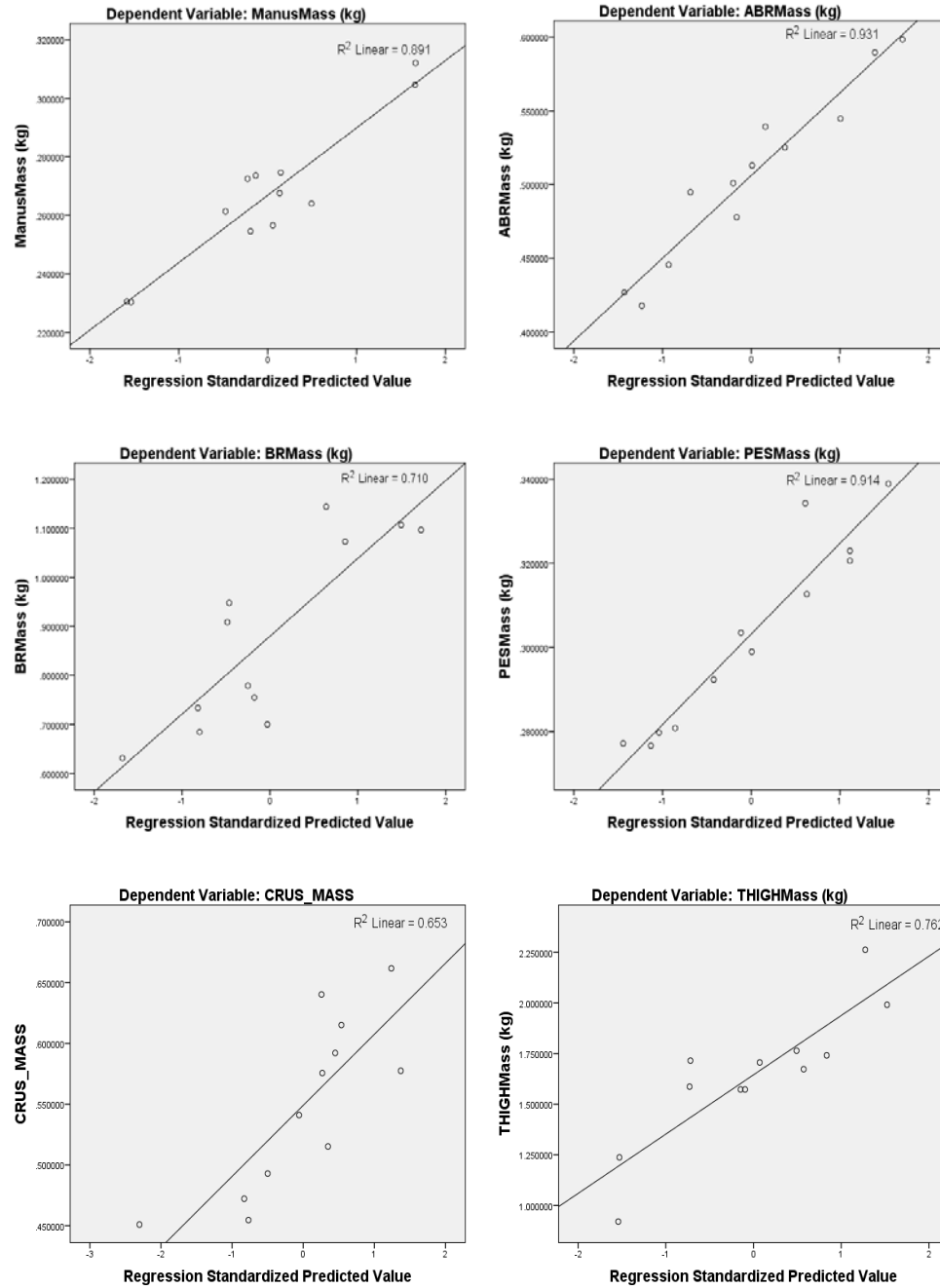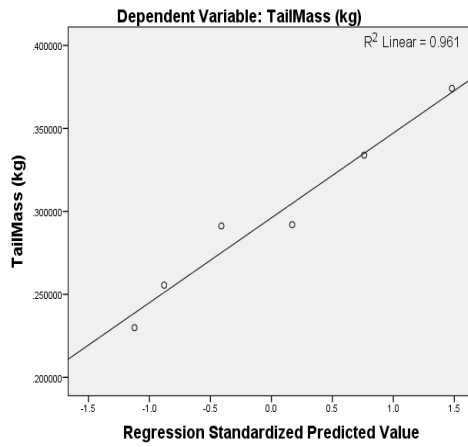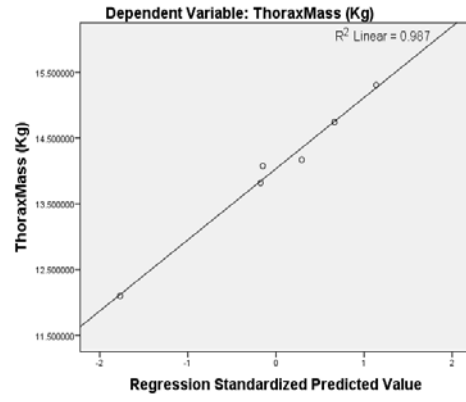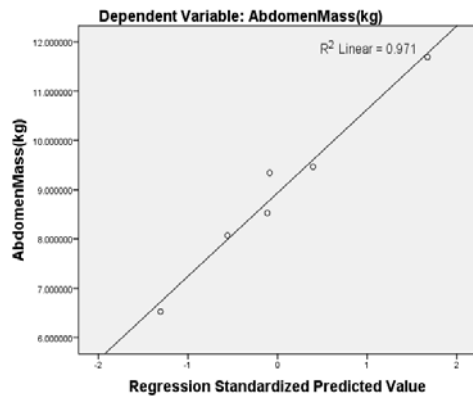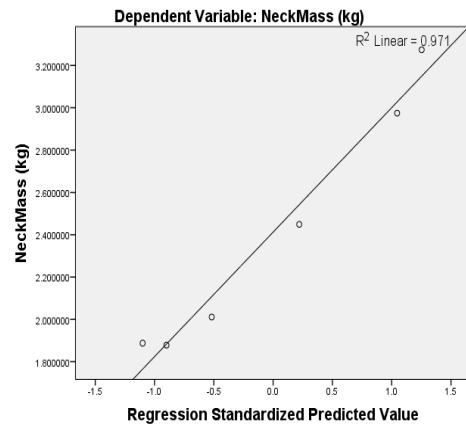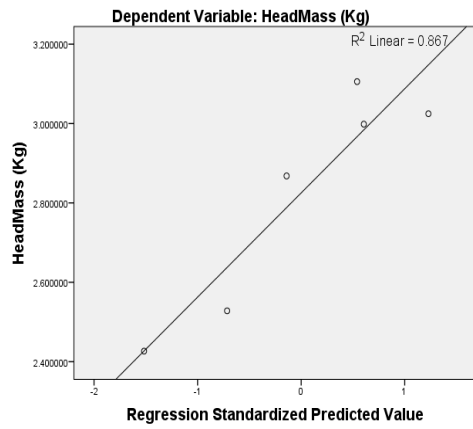
3.2.3 Correlations for Predicting Moment of Inertia

A number of regression models were tested for predicting mass moment of inertia (MoI) for each segment and axis. These included:

- simple correlations of *body mass* to *segment MoI*

- simple correlations of *calculated MoI* for geometric shape (cylinder, frustum, ellipse, pyramid, and cone) to *measured MoI*

- multiple correlations of *body mass* and *calculated MoI* for geometric shape (cylinder, frustum, ellipse, pyramid, and cone) to *measured MoI*

- right and left segments separate and combined for all of the above

Simple correlations of MoI to body mass produced satisfactory results for the limbs when combining right and left sides. Only the *Pes* segment produced significant correlations ($p<.05$) for all three X, Y and Z axes. When right and left sides were tested separately there were significant improvements with 55% of the measured axes producing significant results at $p<.05$ and 77% of those measured significant at $p<.10$. For the remainder of the segments less than half of the correlations were significant. Results of these correlations can be found in Appendix I.

Correlations to geometric shape were applied using a variety of combinations of the dimension. When tested separately, results for the right and left limbs were significant for many of the applied combinations. The number of significant correlations were drastically reduced when the combined right and left MoI data were compared with the models.

Multiple regression correlations of body mass *and* geometric model produced much better results and so it was this approach that was used for the majority of the correlations. A comparison of these results may be seen in Appendix G. The final multiple linear regression equations for determining moments of inertia can be found in Table 3.18.

Table 3.18: Regression equations for predicting segment moment of inertia

Segment	Axis	Equation
Manus	i/e (x)=	$(-.00012)*A + .0052$
	f/e (y)=	$(-.00015)*A + .00654$
	ab/ad (z)=	$(.00018)*A - .00558$
Antebrachium	ab/ad (x)=	$(-.00032)*A + (.00066)*A*(.076*B^2+C^2) + .01406$
	f/e (y)=	$(-0.00005)*A + (.00160)*A*(.076*B^2+C^2) + .00168$
	i/e (z)=	$(0.0001)*A + (.00173)*A*C^2 - .00496$
Brachium	ab/ad (x)=	$(.00053)*A + (.00223)*A*(E/\pi)2+D2 - .1990$
	f/e (y)=	$(0.00082)*A + (.00465)*A*(E/\pi)2+D2 - .03308$
	i/e (z)=	$(.00015)*A + (.003)*A*((E5-F5)/(E3-F3)) - 0.02139$
Pes	ab/ad (x)=	$(.00009)*A - .00256$
	f/e (y)=	$(-.00007)*A + .00417$
	i/e (z)=	$(-.00016)*A + .00786$
Crus	ab/ad (x)=	$(.00023)*A + (.00137)*A*(.076*L2+K2) - .00785$
	f/e (y)=	$(0.00021)*A + (.00108)*A*(.076*L2+K2) - .00659$
	i/e (z)=	$(0.00009)*A - (.00423)*A*L2 + .00454$
Thigh	ab/ad (x)=	$(-.00091)*A + (.00258)*A*(.076*N2+M2) + .03813$
	f/e (y)=	$(-0.0006)*A + (.00536)*A*(.076*N2+M2) + .02502$
	i/e (z)=	$(-.00067)*A + (.00001)*A*N2 + .03467$
Head	i/e (x)=	$(.0008)*A + (.15568)*A*Q2 - .09160$
	f/e (y)=	$(-0.00112)*A - (.00283)*A*(P2+Q2) + .07403$
	ab/ad (z)=	$(-.00007)*A - (.00613)*A*(P2+Q2) + .04484$
Neck	i/e (x)=	$(-.00154)*A - (.00313)*A*((U5-S5)/(U3-S3)) + .11749$
	f/e (y)=	$(-0.0007)*A + (.01245)*A*(U/\pi)2+R2 + .01634$
	ab/ad (z)=	$(-.00129)*A + (.00719)*A*(U/\pi)2+R2 + .04938$
Abdomen	i/e (x)=	$(.00814)*A + (.00471)*A*((W5-Y5)/(W3-Y3)) - .28462$
	f/e (y)=	$(0.01457)*A + (.01824)*A*(W/\pi)2+X2 - .50031$
	ab/ad (z)=	$(-.02726)*A + (.00616)*A*(W/\pi)2+X2 + 1.08268$
Thorax	i/e (x)=	$(.00384)*A + (.00183)*A*((W5-U5)/(W3-U3)) - .05972$
	f/e (y)=	$(-0.00514)*A + (.04659)*A*(W/\pi)2+V2 + .12633$
	ab/ad (z)=	$(-.00566)*A + (.04428)*A*(W/\pi)2+V2 + .16146$
Tail	ab/ad (x)=	$(.00015)*A + (.00198)*A*(AZ/\pi)2+Z2 - .01353$
	f/e (y)=	$(-0.00042)*A + (.00148)*A*(AZ/\pi)2+Z2 + .00989$
	i/e (z)=	$(.0001)*A + (.00173)*A*AZ2 - .00410$

Note: i/e=internal/external rotation; f/e = flexion/extension; ab/ad = abduction/adduction

The models for generating the regression equations were selected based on the level of correlation as well as the number of required measures and ease of application to a live dog, in particular, a police dog, since these dogs are less likely to appreciate excessive handling nor do they like to stand still while the measurements are collected.

Single and multiple linear regression analyses were carried out for MoI about 6 axes. Results of the correlations selected for inclusion in the study can be found in Table 3.19 and graphically in Figure 3.25. As with segment mass, independent (predictor) variables were whole body mass and segmental morphometric dimensions in the form of formulas for calculating geometric moment of inertia (for predicting segment moment of inertia). Right and left sides were assumed symmetrical so the same formula is assumed for both right and left. On application, the dimensions from each limb will be input into the model.

The same geometric models applied to segment mass estimation were applied for MoI except the manus and pes were modelled by body mass alone, and the neck was modelled as a frustum. Low correlations were observed for the manus and crus when right and left segment data were combined so, instead, the right limb was used for creating the regression equations for these two segments.

Table 3.19: MoI Correlation Summaries

Segment	Axis	R^2	Adjst'd R^2	Model Shape	Length	Dimension 2	Dimension 3
Manus*	x	0.721		Mass			
	y	0.689		alone			
	z	0.870					
Ante-brachium	x	0.669	0.595	Cylinder	Prox to Dist jt ctr (ave 3D + s)	Mid Circ	
	y	0.558	0.459				
	z	0.906	0.886				
Brachium	x	0.904	0.883	Frustum	Prox to Dist jt ctr (s)	Axillary Circ	Elbow circ
	y	0.778	0.728				
	z	0.516	0.408				
Pes	x	0.870		Mass			
	y	0.687		alone			
	z	0.594					
Crus*	x	0.941	0.903	Cylinder	Prox to Dist jt ctr (3d)	Ankle circ	
	y	0.992	0.985				
	z	0.964	0.941				
Thigh	x	0.780	0.732	Cylinder	Prox to Dist jt ctr (3d)	Knee circ	
	y	0.830	0.792				
	z	0.564	0.466				
Head	x	0.990	0.984	Ellipse	Atlas joint ctr to tip of nose	Biorbital breadth	
	y	0.832	0.720				
	z	0.824	0.708				
Neck	x	0.889	0.816	Frustum	atlas/axis jt ctr to c7/t1 jt ctr	Circ @ C7/T1	Circ @ Atlas/Axis
	y	0.922	0.871				
	z	0.986	0.976				
Abdomen	x	0.956	0.929	Frustum	Prox to Dist jt ctr (s)	Circ at T13/L1	Circ @ waist crease
	y	0.792	0.653				
	z	0.812	0.687				
Thorax	x	0.960	0.935	Frustum	T13/L1 to C7/T1 jt ctr_3d	Circ at T13/L1	Circ @ C7/T1
	y	0.843	0.739				
	z	0.857	0.763				
Tail	x	0.966	0.944	Cone	sacrum to tip of tail	Tail circ at base of sacrum	
	y	0.976	0.960				
	z	0.949	0.913				

* - used data from right side only (n=6)

Figure 3.25: Correlations for predicting segment moment of inertia from body mass and segment morphometry

*Note: R^2 correlations presented in the graphs are the unadjusted coefficient of determination
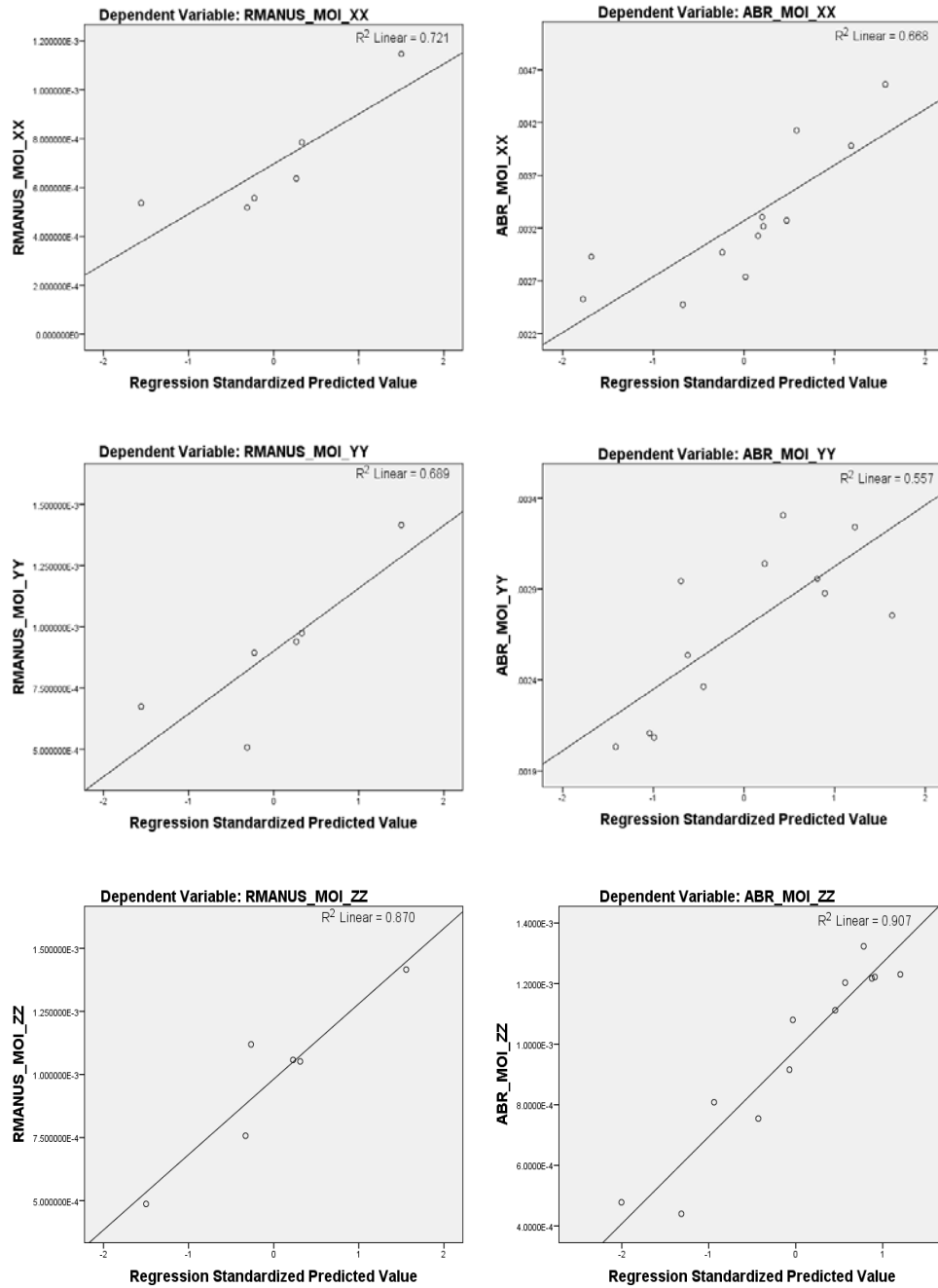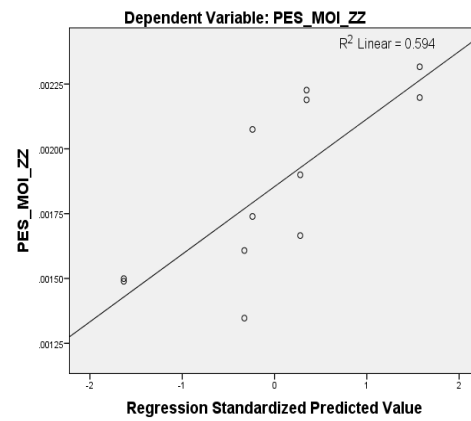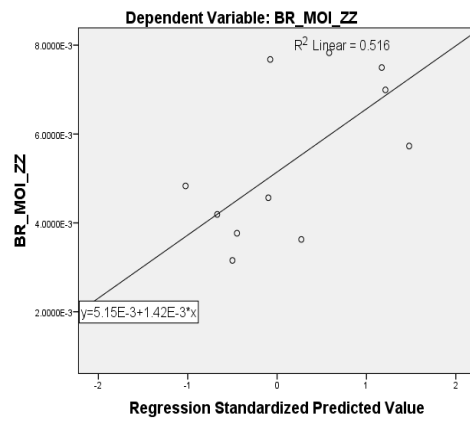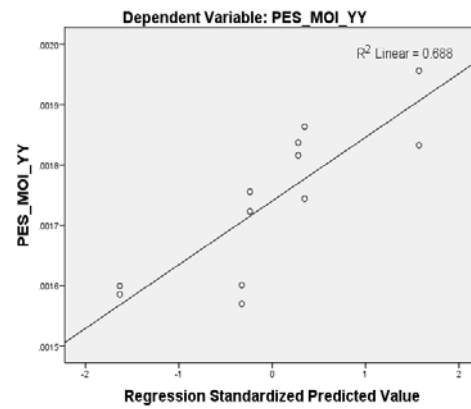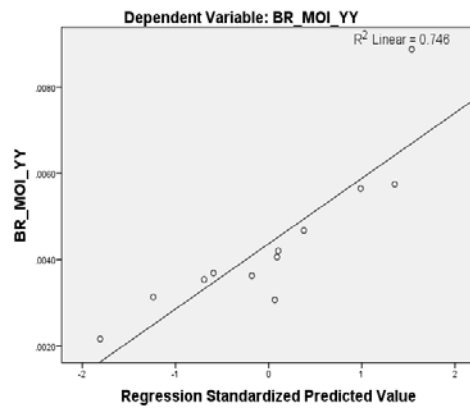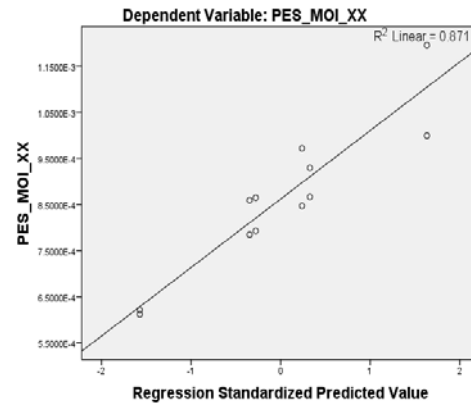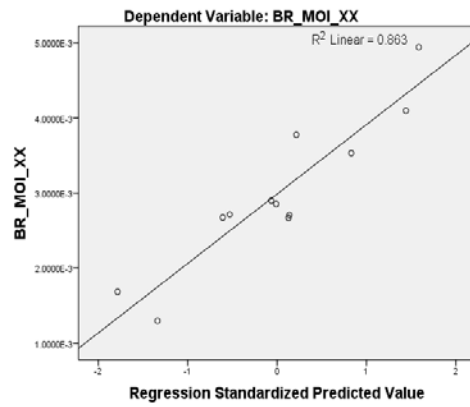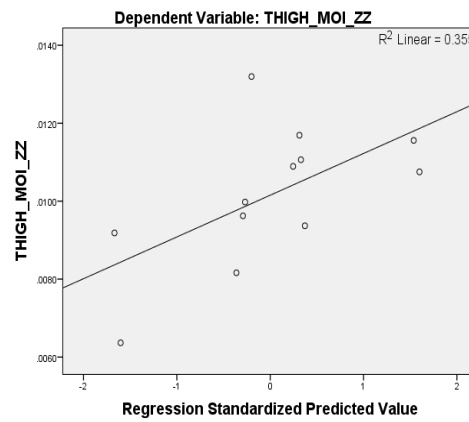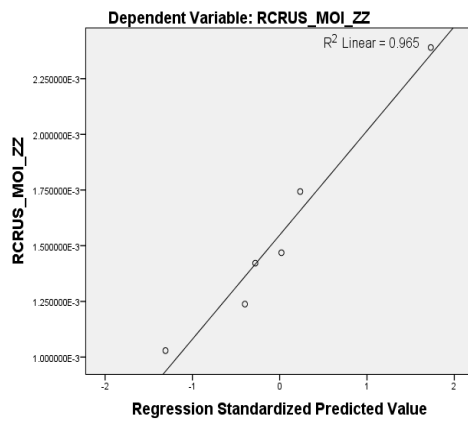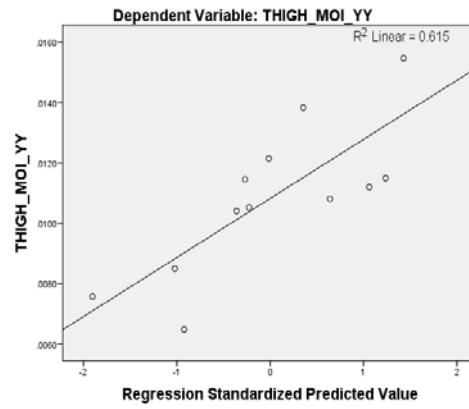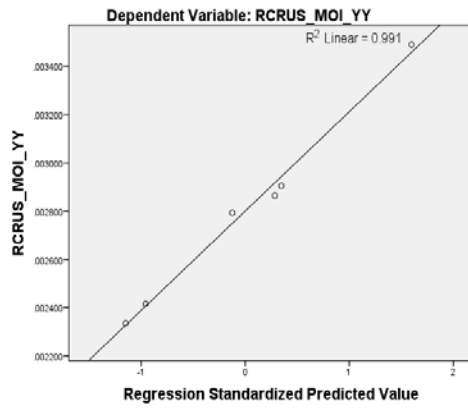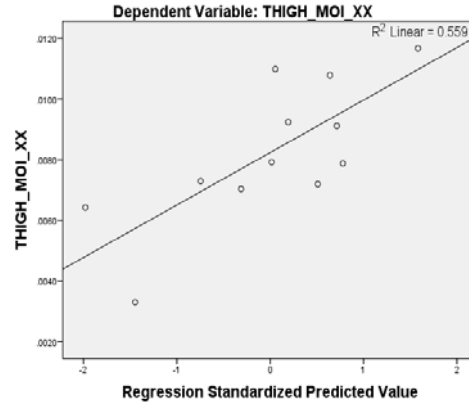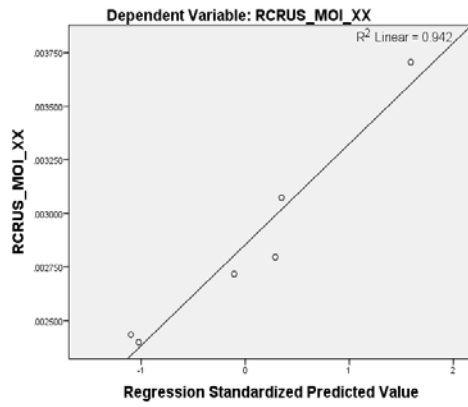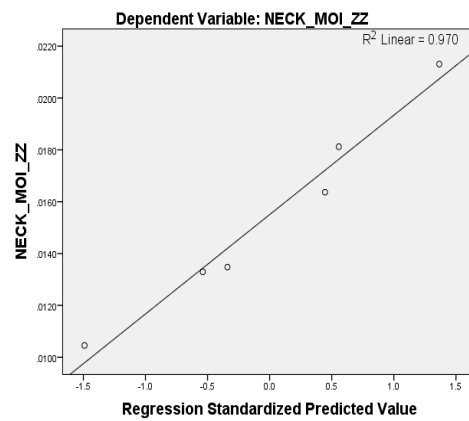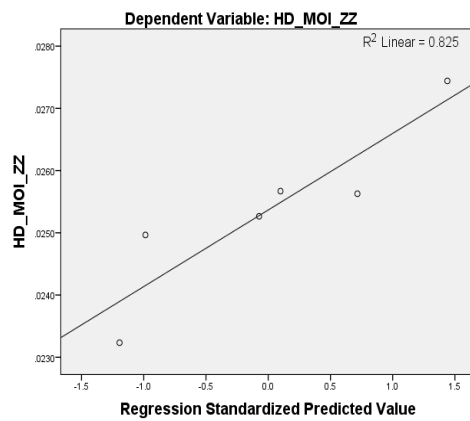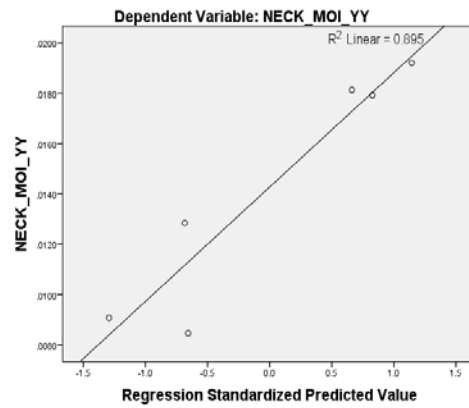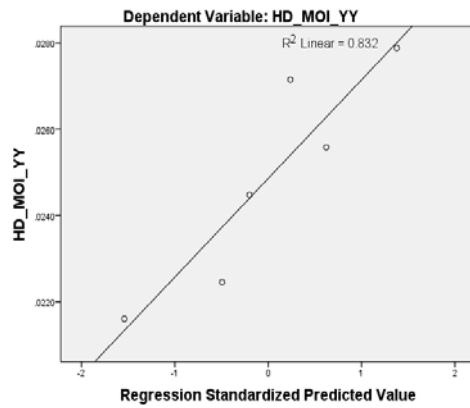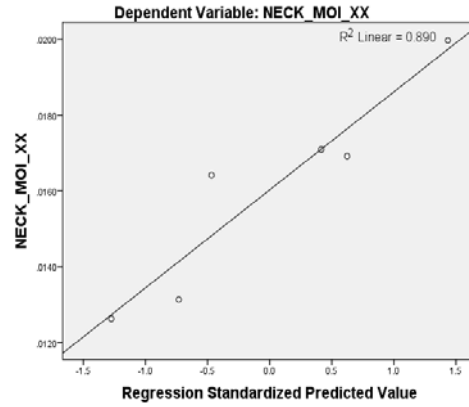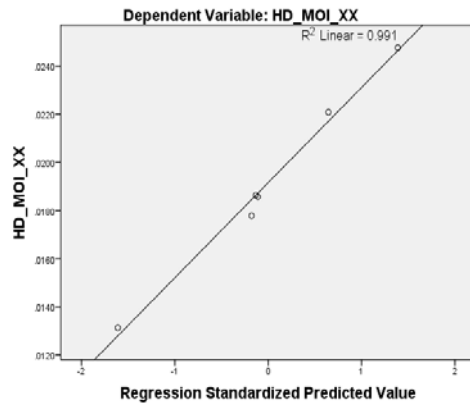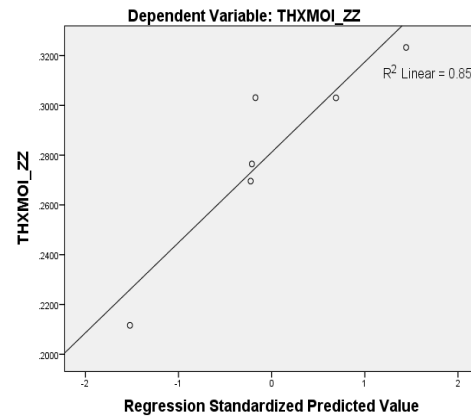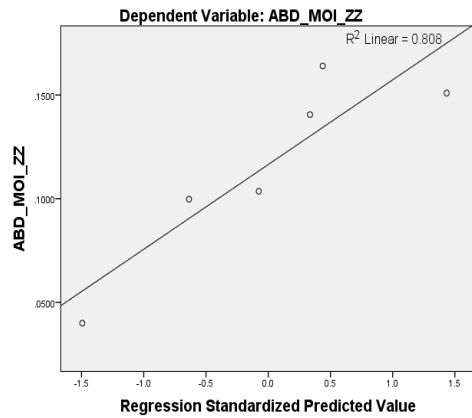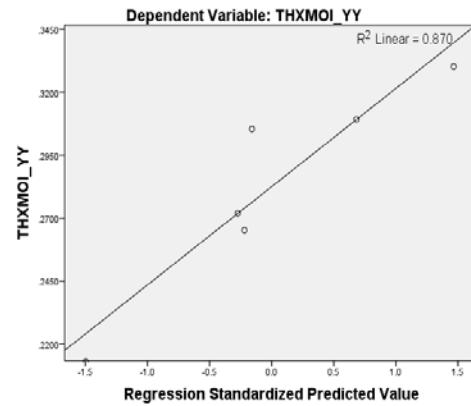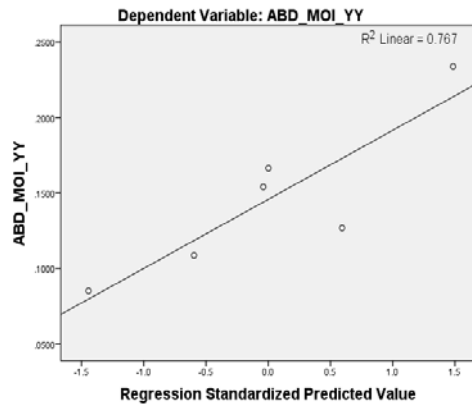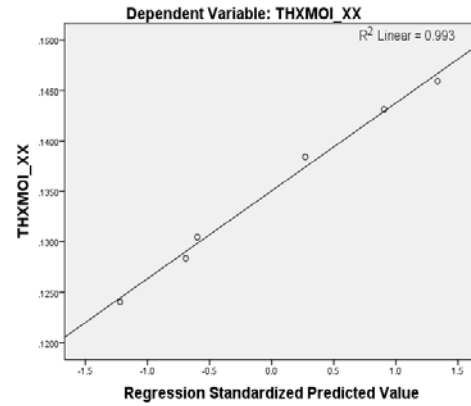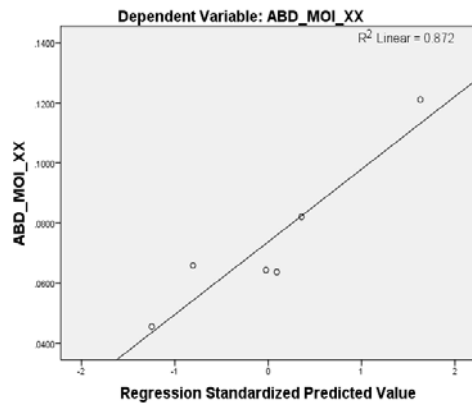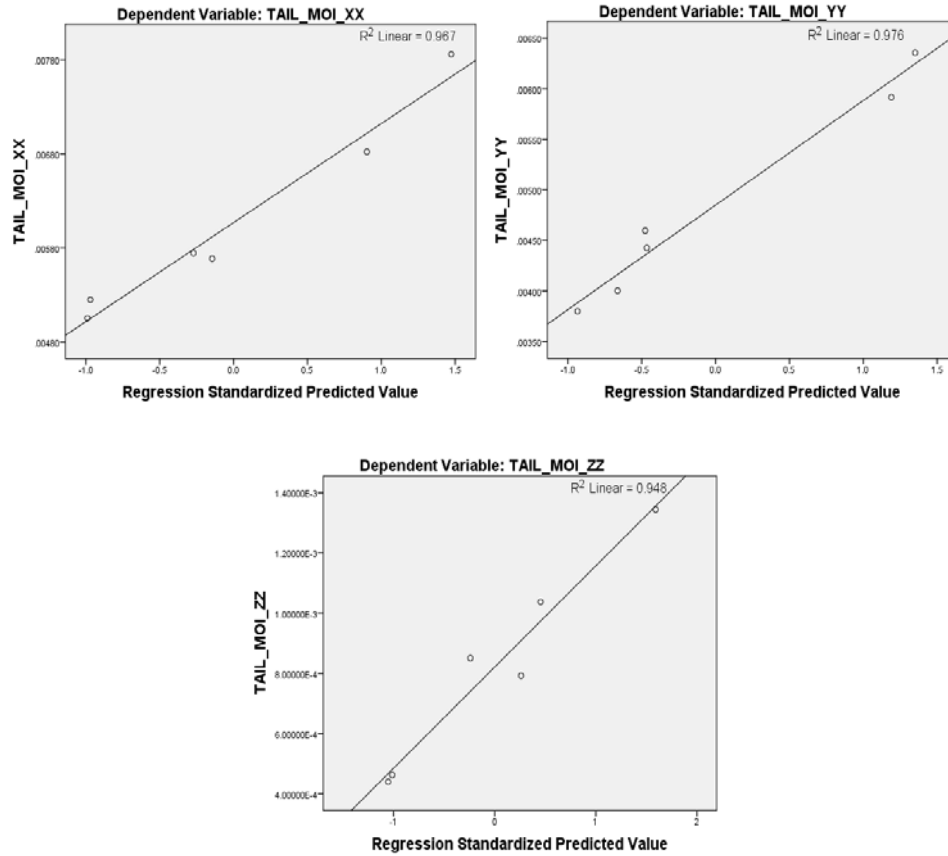
A summary of normalized segment masses, centres of mass, radii of gyration and densities can be found in Table 3.20. Segment masses have been normalized to total body mass, centre of mass and radius of gyration (about the long axis) has been normalized to segment length.

Table 3.20: Normalized segment masses, centres of mass, radii of gyration and densities

Segment	Endpoints (cran-caud or prox-dist)	Segment Mass/ Total Mass		Centre of Mass / Segment Length				Radius of Gyration (about long axis) / Segment Length						Density (kg/m³)	
		$\bar{x}$	$\sigma_{\bar{x}}$	$R_{prox/cran}$	$\sigma_{\bar{x}}$	$R_{dist/caud}$	$\sigma_{\bar{x}}$	k_{cg}	$\sigma_{\bar{x}}$	k_{prox}	$\sigma_{\bar{x}}$	k_{dist}	$\sigma_{\bar{x}}$	$\bar{x}$	$\sigma_{\bar{x}}$
Manus	Mid wrist to distal 3rd phalanx	.0072 ± .0002		.4848 ± .0089		.5185 ± .0091		.0993 ± .0023		.495 ± .0085		.5279 ± .0092		934.02 ± 18.10	
Ante-brachium	Lateral epicondyle to carpal jt	.0138 ± .0005		.3941 ± .0055		.6076 ± .0053		.1171 ± .0019		.4112 ± .0052		.6188 ± .0053		977.54 ± 17.10	
Brachium	Glenohumeral jt to lat epicondyle	.024 ± .0013		.4183 ± .0183		.5869 ± .0197		.1181 ± .0033		.4352 ± .0172		.5988 ± .0197		974.37 ± 12.71	
Pes	Heel to distal 3rd phalanx	.0082 ± .0002		.514 ± .0044		.4881 ± .0042		.1214 ± .0018		.5282 ± .0043		.503 ± .0041		1013.58 ± 12.45	
Crus	Femoral condyle to lateral maleolus	.015 ± .0006		.3659 ± .0113		.6364 ± .0111		.1098 ± .0029		.3823 ± .0107		.6459 ± .011		1010.60 ± 19.38	
Thigh	Greater trochanter to femoral condyle	.0451 ± .0028		.4463 ± .0115		.5601 ± .0124		.1332 ± .0019		.4659 ± .0112		.5759 ± .0119		939.78 ± 13.40	
Head	Inion to prosthion	.077 ± .0039		.3165 ± .0081		.6842 ± .0082		.1569 ± .0035		.3535 ± .0069		.702 ± .0083		1004.18 ± 20.29	
Neck	Atlas/axis to C7/T1	.0661 ± .0068		.5627 ± .0122		.4431 ± .0128		.1383 ± .0054		.5797 ± .0113		.4643 ± .0127		970.01 ± 25.53	
Abdomen	T13/L1 to tail base	.2415 ± .0153		.4677 ± .0047		.5343 ± .005		.1944 ± .0046		.5066 ± .0038		.5686 ± .0057		963.89 ± 7.71	
Thorax	C7/T1 to T13/L1	.3806 ± .0101		.5368 ± .011		.467 ± .0109		.2213 ± .0038		.5807 ± .011		.517 ± .0092		1083.39 ± 83.44	
Tail	Base of tail to tip	.008 ± .0005		.3128 ± .0158		.6892 ± .0162		.1998 ± .0063		.3719 ± .0134		.7177 ± .0161		900.63 ± 63.73	

3.3 Discussion

Adapting methods previously described by Reynolds (1974) for baboons and Chandler et al. (1975) for humans, this study provides a complete set of body segment parameters and three dimensional inertial properties for the German Shepherd dog. From the collected data, regression equations have been developed that will estimate segment masses and moments of inertia so that they may be used to create a dynamic link segment model for living dogs of this particular breed.

The techniques used in this investigation are varied and extensive and include:

- cadaver segmentation

- collection of dimensional morphometry for each segment

- collection of three dimensional landmark locations using a right handed Cartesian coordinate system

- use of the immersion method for volumetric measures of each segment

- use of the balance technique for determining segment centre of mass in 3 dimensions

- measures of moments of inertia in 6 axes using the simple pendulum method

- geometric, single and multiple linear regression modelling to estimate segmental mass and moment of inertia in living subjects

Linkage and hinge points are defined at anatomical joint centres of each segment, which are located through the use of surface landmarks identified and defined within the model. These external points assist in providing segment dimensions, the accuracy of which are determined through regression analysis.

The selection of morphometric measures utilized in the regression equations varied with parameter and body segment. As an example, elbow circumference worked well as a factor for estimating the mass of the brachium segment, however the wrist

circumference correlated better for estimating the mass of antebrachium segment. In the same way, models for estimating segment mass did not always work for estimating moment of inertia for the same segment, e.g. of the models tested, the neck is best modelled as a cylinder for estimating segment mass, and as a frustum for estimating its moment of inertia.

In evaluating regression models of moment of inertia, this study combined the right and left sides, increasing the sample size from 6 to 12, however models using either the right or left could be used where one side presented better regression correlations than the other. One could even choose the best fit model for each axis, e.g. for the abdomen, the x-axis may have produced the best results modelled as the frustum of a cone, while the y- and z- axes may be best modelled as a cylinder using the circumference at the base of the ribs.

A number of morphometric measures and model variations were analysed in an attempt to create regression equations that were best able to estimate segment masses and moments of inertia (MoI). While many combinations were found to be non-significant, there were also many others that performed well. Which method to use came down to a combination of accuracy of the correlation and practicality, such as number of measures required, ease of accessing landmarks and ease of acquiring the data from living dogs. For this study, analogous solid geometric models are used to estimate all segment masses, and for moments of inertia for all but the smallest segments, the pes and the manus. Inertial tensors were estimated for these segments using body mass alone. Model selection favoured those with the highest R values, however other models tested presented with lower R values but were still statistically significant. As an example, in correlations of segment mass, the frustum has been selected as the geometric model shape for the abdominal segment using segment length and 2 circumference measurements, at the waist and at the base of the ribs, as input dimensions. This model presented with an adjusted R = .975. Cylindrical models using segment length and only one of the circumference measures also produced significant R values of .959 for the waist and .931 for the base of the ribs (p<.05).

Correlations to body mass alone were significant for this segment as well at R=.845. While estimations of segment masses using body mass on its own for other segments exhibited low correlations, estimations of moment of inertia using this model would produce significant results, particularly for the limb segments when right and left sides are not averaged.

This investigation offers for the first time a complete set of experimental data on the mass and inertial properties of the male German Shepherd. To date, there has been only one other study that has provided a complete set such as this, using MRI to extract data for 3 dogs of mixed breeds [Amit et al., 2009]. The segmentation methods used in this investigation are similar to those used in the Amit study except here the tail has been removed and presented as a separate segment and, due to the flexibility of the spine, the torso has been divided into abdomen and thorax segments so that they may better represent torso movement. No other investigations have offered data on these additional segments.

The comparison of relative mass distribution produced similar findings to Amit et al. (2009) for % body mass and location of centre of mass (CoM). The major difference was in the CoM of the head, which was found to be located 10% more rostral than that of German Shepherds. While the study does not state what breed the dogs were, it was noted that the head of the smallest dog was slightly brachycephalic (flat, wide skull shape) which may have been the source of the variation. Excluding the skull, CoM locations varied between 1.5 and 4.4%, with an average variation of 3.5%. In comparing segment masses normalized to % body mass, again, results were comparable with the greatest variation occurring at the head. Amit et al found the head to be an average of 9.2% of body mass, while the heads of the German Shepherds were found to be an average of 7.7% of body mass. Of the remaining segments, corresponding segment masses within the 2 studies varied between 0.08 and 0.39% with an average variation of 0.11%. One other study by Ragetly et al. (2008) used CT scans to determine inertial properties for the hind limb of 14 clinically normal Labrador retrievers. Average segment masses were within .1% of those recorded here

for the pes and crus segments, however the thigh of the Labrador Retriever was found to be 1.5 % heavier than that of the German Shepherd. Location of CoM was found to be 4.4, 5.6.and 2.6 % more proximal for the pes, crus and thigh, respectively for the Retriever. These differences are relatively slight but show potential differences that could be attributed to breed.

One problem considered in using frozen cadavers was the angle of extension in the limbs. Care was taken to ensure each cadaver was sufficiently suspended in stance in the freezer with paws planted. Excessive flexion would have a dramatic effect on segmentation, causing variation in segment mass and circumference. As noted by Reynolds (1974), moment of inertia is not significantly affected by small errors in mass, however dimensional errors could contribute inaccuracy to the system. A tall dog that has reached the height capacity of the freezer, one who has reached rigor mortise early or any slippage in the suspension mechanism during freezing could introduce such errors. As a result, left and right sided segments were not averaged for each subject but instead were treated as additional segments. In this way an outlying limb segment could be removed from the analysis without losing an entire subject. Errors in length, in particular the length from the pivot of the pendulum system to the CoM of the box/specimen could also render inaccuracies. To minimize these errors, the length of the pendulum from the frame pivot to the box was measured by a set spacer of known length. The length from the exterior of the box to the CoM of the segment was calculated from 3-dimensional measures taken from the box origin. To avoid possibility of error due to settling, the pendulum length was remeasured after each successive trial. Care was also taken to ensure the simple pendulum was maintained, i.e. the composite (box+segment) and the box alone swung from the top of the pivot and not from the box/string juncture.

Another potential source for error lay in the dissection of the thigh and brachium, the anatomy of which made it necessary to complete both with compound cuts. The limited abduction range at the shoulder made it difficult to manoeuvre the cut blade in

the axial area, while thick muscle mass of the inner thigh and the proximity of the ischium provided limited access to the joint, increasing the opportunity for error.

A major limitation of the study is the small number of subjects, making it difficult to remove outliers. A more rigorous statistical method could be run including assumptions tests for independent residuals (e.g. Durbin-Watson), but this would require significant time. With a sample size of 6 and little knowledge of the variation within the breed any conclusions with respect to the population would be tenuous, however one can safely assume that geometric models can be used to represent body segments for purposes of calculating segment mass and moment of inertia, bearing in mind that these models are sensitive to errors in mass and dimensional measures.

3.4   Conclusions

The physical properties of humans for most biomechanics gait research came from data generated more than 4 decades ago. Body segment parameters were extracted from an array of sources using a variety of methodologies. At present, limited data on the German Shepherd dog has prompted an exploration of these proven methods, permitting the development of regression equations that may be used to evaluate the gait mechanics of this particular breed of dog. In the next chapter, equations to determine joint centre locations have been applied to a newly developed marker model and are tested for practicality during a real kinematic evaluation using live dogs from within the policing community. A combination of the results found here and in the next chapter may be applied to future canine biomechanics research.

4 EVALUATION OF A MARKER MODEL FOR CANINE GAIT

Having developed the regression equations needed to determine joint centre locations and the required body parameters for each segment of the German Shepherd, a biomechanical model may be created from which one may generate linear kinematics, centres of gravity and angular kinematics for future use in evaluations of joint dynamics. To demonstrate this, a marker-based model was developed and tested for practical use in the German Shepherd. Hair removal is not an option therefore the challenge was in finding a method to firmly attach the markers over the required landmarks while still keeping them visible and permitting the dog to maintain a natural gait. An evaluation of the resulting marker set is presented here and includes subjective observations as well as a kinematic analysis to describe flexion and extension movements of the limb joints of healthy German Shepherds.

This part of the study was conducted in the Motion Capture Lab at the British Columbia Institute of Technology. The goal was to collect a sample of canine gait using the proposed marker set while at the same time observing the dog's acceptance of a new method of marker attachment, as well as evaluate for practicality the number and positioning of the markers.

4.1 Materials and Methods

As shown previously in Figure 3.4, the canine model is made up of 17 segments: the manus, antebrachium, brachium, pes, crus, and thigh of the right and left limbs, as well as the head, neck, thorax, abdomen and tail. The following sections describe the marker set and define how their positions on each segment may be used to determine joint centres and create the reference systems required for calculating linear and angular kinematics.

4.1.1 Marker Model

To describe the movement of the segment in 3 dimensions a marker system must be defined that will permit calculation of 3 Cartesian coordinates (x,y,z) and 3 angles of

rotation (Euler angles) for each segment. Through the use of an optical motion capture system (Vicon Motion Systems Ltd, UK) the segments were modelled as a series of interconnected links, with each link having its own independent, or local, Cartesian coordinate system that describes its unique 3D position relative to an external, or global, coordinate system.

A segmental local coordinate system is created through the use of at least three non-collinear markers precisely located on anatomical landmarks. In total, 44 marker positions, shown below in Figure 4.1 and defined in Table 2.2, have been selected to create the whole-body model: 17 for the hind limb (including the pelvis), 15 for the forelimb (including the shoulder complex), the remaining 12 define the head, neck, abdomen, thorax, and tail.
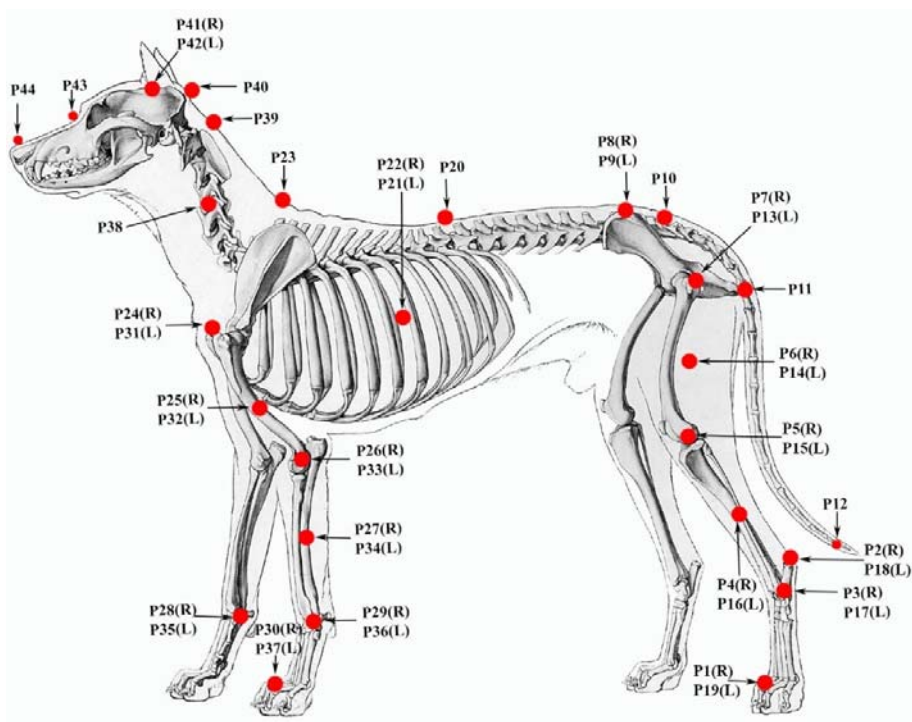
Figure 4.1: Canine marker set, side view

Table 4.1: External marker definitions

Point #	Marker Label	Definition	Marker Placement
P_1	RMTPJ	Right 3rd Metatarsus	On the dorsal aspect of the foot just over the base of the 3rd proximal phalanx of the right hind foot
P_2	RHEEL	Right heel	On the caudal aspect of calcaneous in line with the MTPJ
P_3	RHOCK	Right lateral maleolus	On the lateral malleolus along the joint line and passing through the medial malleolus
P_4	RTIB	Right tibia	Placed on the lower lateral crus to determine the alignment of the ankle flexion axis
P_5	RSTIFLE	Right femoral epicondyle	On the lateral epicondyle along the flexion-extension axis of the knee
P_6	RTHIGH	Right thigh	On the lower lateral 1/3 surface of the thigh
P_7	RHIP	Right greater trochanter	Placed over the lateral aspect of the greater tochanter
P_8	RCDIS	Right cranial dorsal iliac spine	Placed directly over the right caudal dorsal iliac spine
P_9	LCDIS	Left cranial dorsal iliac spine	Placed directly over the left cranial dorsal iliac spine
P_{10}	SACRUM	Base of tail	On the midpoint between the caudal dorsal iliac spines
P_{11}	TAIL_MID	Mid tail	
P_{12}	TAIL_END	End Tail	
P_{13}	LHIP	Left greater trochanter	Se RHIP
P_{14}	LTHIGH	Left thigh	See RTHIGH
P_{15}	LSTIFLE	Left femoral epicondyle	See RSTIFLE
P_{16}	LTIB	Left tibia	See RTIB
P_{17}	LHOCK	Left lateral maleolus	See RHOCK
P_{18}	LHEEL	Left heel	See RHEEL
P_{19}	LMTPJ	Left 3rd Metatarsus	See RMTPJ
P_{20}	T13	13th thoracic vertebra	On the spinous process of the 13th thoracic vertebra
P_{21}	L_RIBS	L Mid Thorax	At widest most lateral aspect of thorax
P_{22}	R_RIBS	R Mid Thorax	At widest most lateral aspect of thorax

Table 4.1 cont'd

Point #	Marker Label	Definition	Marker Placement
P_{23}	C7	7th cervical vertebra	On the spinous process of the 7th cervical vertebra
P_{24}	RACJ	Right shoulder	On the acromio-clavicular joint
P_{25}	RHUM	Right humerus	On the lateralmost aspect of the brachium (upper arm)
P_{26}	RELB	Right elbow	On the lateral epicondyle approximating the elbow flex/ext axis
P_{27}	RULNA	Right ulna	On the lateral aspect of the antebrachium (forearm)
P_{28}	RMEDWRIST	Right medial wrist marker	Inside of the foreleg at the radial styloid along the flexion/extension axis
P_{29}	RLATWRIST	Right lateral wrist marker	Outside of the foreleg at the ulnar styloid along the flexion/extension axis
P_{30}	RMCPJ	Right 3rd Metacarpus	On the dorsum of the manus (paw), just over the head of the third metacarpus
P_{31}	LACJ	Left shoulder	See RACJ
P_{32}	LHUM	Left upper arm marker	See RHUM
P_{33}	LELB	Left elbow	See RELB
P_{34}	LULNA	Left forearm	See RULNA
P_{35}	LMEDWRIST	Right medial wrist marker	See RMEDWRIST
P_{36}	LLATWRIST	Right lateral wrist	See RLATWRIST
P_{37}	LMCPJ	Left 3rd Metacarpus	See RMCPJ
P_{38}	LATNECK	Left lateral neck	Mid lateral aspect of neck
P_{39}	AXIS	Axis	Dorsocaudal aspect
P_{40}	INION	Caudal end of head	Tip of external occipital protuberance
P_{41}	R_EAR	Right Tragion	a cephalometric landmark located at the superior margin of the tragus of the ear
P_{42}	L_EAR	Left Tragion	See R_EAR
P_{43}	NASION	Base of Nose	the depression at the root of the nose that indicates the junction of the intranasal and the frontonasal sutures
P_{44}	NOSE	End of Nose	cleft under the nose

TIBIA, FEMUR, HUM and ULNA markers are used to define reference planes in the process of determining joint centres. They may be attached to the skin or suit directly or via a short wand to extend the marker out from the legs. While the height of the marker is not critical, it is important the marker be placed on the lateral aspect of the segment in line with the proximal and distal markers when viewed from the sagittal plane Due to the small size of the segments, wand extensions in these locations do assist in creating a sufficiently large plane made by the 3 marker points. Unfortunately the wand also has potential to introduce skin/wand movement artefacts therefore it is important they be placed where there is minimal skin/tissue vibration during the movement.

4.1.2   Linear Kinematics

The external markers were used along with morphometric measurements (refer to Table 3.15 for definitions) to calculate internal joint centre positions through an orthogonal UVW reference system that was created for each segment. Following methods and conventions used by Vaughn et al. (1999) for the Helen Hayes Hospital marker set, segment reference systems, corresponding vectors and equations for predicting joint centres are defined and illustrated below.

4.1.2.1   *UVW coordinate system and Joint Centre locations*

In creating the UVW coordinate system for each limb segment, effort was made to keep the U-axis directed caudal to cranial, the V-axis dorsal to ventral and the W-axis running medial to lateral for the right side and lateral to medial for the left. For the pelvis segment, following the convention for the Helen Hayes marker set, the V axis runs right to left and W axis is ventral to dorsal. For right and left sides, descriptions are provided for the right with the corresponding left shown in brackets, e.g. P1(P19) refers to marker 1 on the right MTPJ and corresponding marker 19 on the left MTPJ. For all cases, the right hand rule was maintained.

With regard to joint centres, there are currently no existing data which define joint centre locations for the German Shepherd. As a result, for the tarsal, stifle, carpal and

elbow joints, joint centre was assumed to be located directly on the flexion extension axis defined by associated markers located on the joint line at the midpoint of the measured diameter of the joint. For the hip, T13/S1 and sacrum/tail joints, joint centre locations were based on proportional depth measures (see Table 4.2) taken from CT scans of subjects 4, 5 and 6 described in Section 3 of this thesis. While this method was not ideal due to the limited number of subjects, it was acceptable for the purpose of the investigation and provides a baseline for future study.

Table 4.2: Morphometrics for calculating hip, T13/S1 and sacrum/tail joint centres

Dimension (cm)	Subj 4	Subj 5	Subj 6	Mean	SE
A. CDIS Width	9.2	8.9	9.8	9.29	0.267
B. Femoral neck length	5.0	5.0	4.8	4.93	0.067
C. Depth of T13 marker location to jt ctr	3.9	3.5	3.1	3.50	0.231
D. Depth of sacrum marker location to jt ctr	1.7	1.6	1.7	1.67	0.033
E. Abdomen depth @ T13	27.6	23.4	23.2	24.73	1.434

Location of hip joint centre, calculated as a direct proportion of femoral neck length/CDIS width (B/A), was 0.531; T13/L1 joint centre, calculated as a proportion of abdominal depth (C/E), was 0.142; and Sacrum/Tail joint centre, calculated as a proportion of abdominal depth (D/E), was 0.067. These are further explained in the following descriptions for individual segments and joints.

4.1.2.1.1 Pes

Referring to the proposed canine set from Figure 4.1, markers for the Pes segment are numbered P1(P19) - MTPJ, P2(P18) - HEEL and P3(P17) - HOCK. In creating the UVW for the Pes, shown in Figure 4.2, the origin is located at the HOCK with the W axis running perpendicular to a plane formed by MTPJ, HEEL and HOCK; the U axis running parallel to a line drawn between the MTPJ and HEEL markers; the V axis is at right angles to U and W.
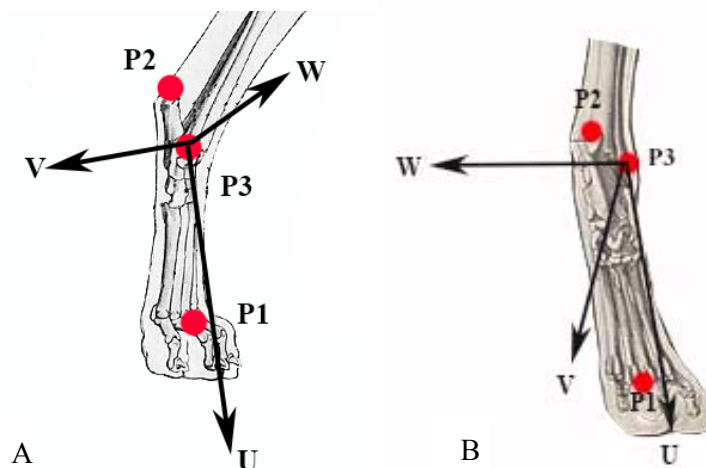
Figure 4.2: Right Pes UVW axes. A. sagittal view, B posterior view

The axes are determined by the following equations:

$$U_{R\&L\ Pes} = \frac{(mtpj - heel)}{|mtpj - heel|} \qquad \text{(Equation 24)}$$

$$W_{R\&L\ Pes} = \frac{(mtpj - hock) \times (heel - hock)}{|(mtpj - hock) \times (heel - hock)|} \qquad \text{(Equation 25)}$$

$$V_{R\&LPes} = W_{R\&LPes} \times U_{R\&LPes} \qquad \text{(Equation 26)}$$

Axis vectors are then used to estimate tarsal joint centres in the following equations:

$$J_{Rhock} = P_3 + 0.5(hock\ breadth)W_{Rpes} \qquad \text{(Equation 27)}$$

$$J_{Lhock} = P_{17} - 0.5(hock\ breadth)W_{Lpes} \qquad \text{(Equation 28)}$$

Similarly, the joint centres of the MTPJs may also be estimated:

$$J_{Rmtpj} = P_1 + 0.5(pes\ depth)V_{mtpj} \qquad \text{(Equation 29)}$$

$$J_{Lmtpj} = P_{19} + 0.5(pes\ depth)V_{Rpes} \qquad \text{(Equation 30)}$$

4.1.2.1.2 Crus

The Crus segment is defined by markers P3(P17) - HOCK, P4(P16) - TIB and P5(P15) – STIFLE (Figure 4.3). The origin of the UVW unit vector triad is located at the STIFLE marker. Similar to the Pes segment, the 3 markers form a plane whose perpendicular axis is identified as U, the V Axis runs parallel to a line between the STIFLE and HOCK markers and the W axis is at right angles to U and V.
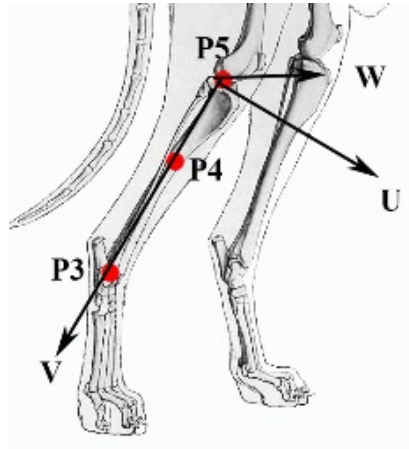
Figure 4.3: Right Crus UVW axes

These axes are calculated from the following equations:

$$V_{R\&L\ Crus} = \frac{(hock-stifle)}{|hock-stifle|}$$ (Equation 31)

$$U_{R\ Crus} = \frac{(tib-stifle)\times(hock-stifle)}{|(tib-stifle)\times(hock-stifle)|}$$ (Equation 32)

$$U_{LCrus} = \frac{(hock-stifle)\times(tib-stifle)}{|(tib-stifle)\times(hock-stifle)|}$$
(Equation 33)

$$W_{R\&L\ Crus} = V_{RCrus} \times U_{RCrus}$$ (Equation 34)

Axis vectors are then used to estimate stifle joint centres in the following equations:

$$J_{RStifle} = P_5 + 0.5(stifle\ diameter)W_{RCrus}$$ (Equation 35)

$$J_{LStifle} = P_{15} - 0.5(stifle\ diameter)W_{LCrus}$$ (Equation 36)

4.1.2.1.3 Pelvis

The location of the hip joint centre is determined from the pelvis markers therefore a UVW reference system is not required for the thigh. The pelvis segment is defined by markers P8 - LCDIS, P9 - RCDIS and P10 – SACRUM, as shown in Figure 4.4. The origin of the UVW unit vector triad is located at the SACRUM marker and the 3 markers form a plane whose perpendicular axis is identified as W, the V Axis runs
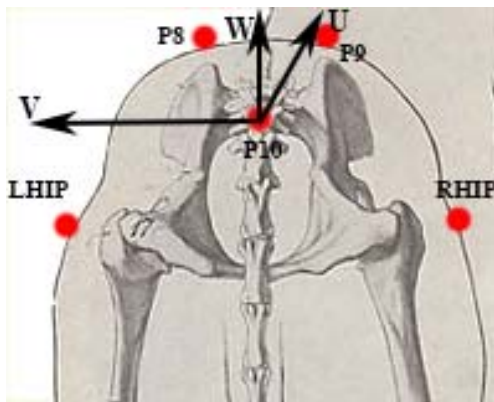
Figure 4.4: Pelvis UVW axes

parallel to a line between the LCDIS and RCDIS markers and the U axis is at right angles to W and V.

These axes are calculated by the following equations:

$$V_{Pelvis} = \frac{(LCDIS - RCDIS)}{|LCDIS - RCDIS|}$$ (Equation 37)

$$W_{Pelvis} = \frac{(RCDIS - sacrum) \times (LCDIS - sacrum)}{|(RCDIS - sacrum) \times (LCDIS - sacrum)|}$$ (Equation 38)

$$U_{Pelvis} = V_{Pelvis} \times W_{Pelvis}$$ (Equation 39)

Currently, no information exists to provide information on the location of hip joint centre for the German Shepherd. As a result, for this model it was assumed that the origin of the hip would remain at the location of the HIP markers for the U (cranial/caudal) and W (dorsal/ventral) axes, and some proportional distance along the V axis. Using the measures from Table 4.2 Table and methods explained at the start of this section, hip joint centres may be estimated using the following equations:

$$J_{RHip} = P\_7 + 0.531(CDIS\ width)\ V_{Pelvis}$$ (Equation 40)

$$J_{LHip} = P_{13} - 0.531(CDIS\ width)V_{Pelvis}$$ (Equation 41)

Similarly, the CT scans were used to determine the average depth of the joint at T13/L1 and at the Sacrum/Tail:

$$J_{T13/S1} = P_{20} + 0.142(abdomen\ depth)W_{Pelvis}$$ (Equation 42)

$$J_{Sacr/Tail} = P_{10} + 0.067(abdomen\ depth)W_{Pelvis}$$ (Equation 43)

4.1.2.1.4 Manus

The manus segment is defined by markers P28(35) - MEDWRIST, P29(36) - LATWRIST and P30(37) - MCPJ. The origin of the UVW unit vector triad is located at the LATWRIST marker and the 3 markers form a plane whose perpendicular axis is identified as U, the W Axis runs parallel to a line between the LATWRIST and MEDWRIST markers and the V axis is at right angles to U and W (Figure 4.5).
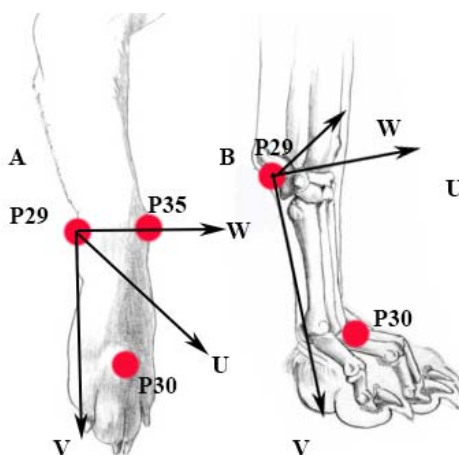
Figure 4.5: Right Manus axes, A. Anterior view, B Sagittal view

These axes are calculated by the following equations:

$$W_{R\&LManus} = \frac{(medwrist - latwrist)}{|medwrist - latwrist|} \qquad \text{(Equation 44)}$$

$$U_{RManus} = \frac{(medwrist - mcpj) \times (latwrist - mcpj)}{|(medwrist - mcpj) \times (latwrist - mcpj)|} \qquad \text{(Equation 45)}$$

$$U_{LManus} = \frac{(latwrist - mcpj) \times (medwrist - mcpj)}{|(medwrist - mcpj) \times (latwrist - mcpj)|} \qquad \text{(Equation 46)}$$

$$V_{R\&LManus} = W_{R\&LManus} \times U_{R\&LManus} \qquad \text{(Equation 47)}$$

These vectors are applied to estimate carpal (wrist) and 3rd MCP (front toe) joint centres using the following equations:

$$J_{RCarpalJ} = P_{29} + 0.5(carpal\ jt\ breadth)W_{RCarpalJ} \qquad \text{(Equation 48)}$$

$$J_{LCarpalJ} = P_{36} - 0.5(carpal\ jt\ breadth)W_{LCarpalJ} \qquad \text{(Equation 49)}$$

$$J_{Rmcpj} = P_{30} - 0.5(manus\ depth)U_{Rmcpj} \qquad \text{(Equation 50)}$$

$$J_{Lmtpj} = P_{37} - 0.5(manus\ depth)U_{Rpes} \qquad \text{(Equation 51)}$$

4.1.2.1.5 Antebrachium

The antebrachium segment is defined by markers P29(36) - LATWRIST, P27(32) - ULNA and P26(33) – ELBOW. The origin of the UVW unit vector triad is located at the ELBOW marker and the 3 markers form a plane whose perpendicular axis is identified as U, the V Axis runs parallel to a line between the ELBOW and LATWRIST and the W axis is at right angles to U and V (Figure 4.6).
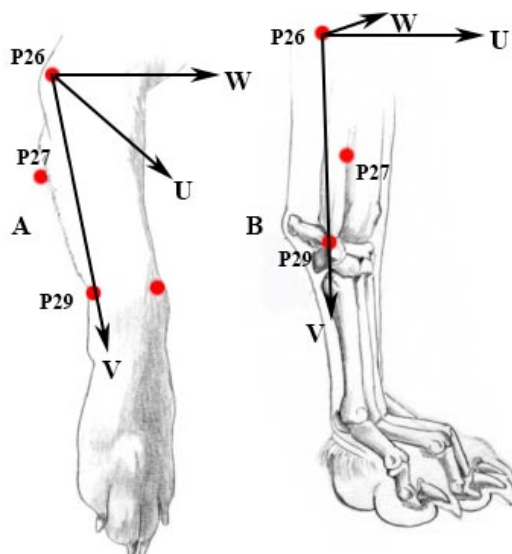
Figure 4.6: Right Antebrachium UVW axes,
A. Anterior view, B Sagittal view

UVW axes are calculated by the following equations:

$$V_{R\&LAbr} = \frac{(latwrist - elbow)}{|latwrist - elbow|} \qquad \text{(Equation 52)}$$

$$U_{R\&LAbr} = \frac{(ulna - elbow) \times (latwrist - elbow)}{|(ulna - elbow) \times (latwrist - elbow)|} \qquad \text{(Equation 53)}$$

$$W_{R\&LAbr} = U_{RAbr} \times V_{RAbr}$$
(Equation 54)

Applying the vectors as before, elbow joint centres are determined using the following equations:

$$J_{Relbow} = P_{26} + 0.5(elbow\ width)W_{RAbr} \qquad \text{(Equation 55)}$$

$$J_{Lelbow} = P_{33} - 0.5(elbow\ width)W_{LAbr} \qquad \text{(Equation 56)}$$

4.1.2.1.6 Shoulder Girdle

The location of the shoulder joint centre is determined from the shoulder girdle markers P23 – C7, P24 - RACJ and P31 - LACJ. The UVW triad origin is located at the C7 marker and the 3 markers form a plane whose perpendicular axis is identified as U, the V Axis runs parallel to a line between the LCDIS and RCDIS markers and the U axis is at right angles to W and V (Figure 4.7).
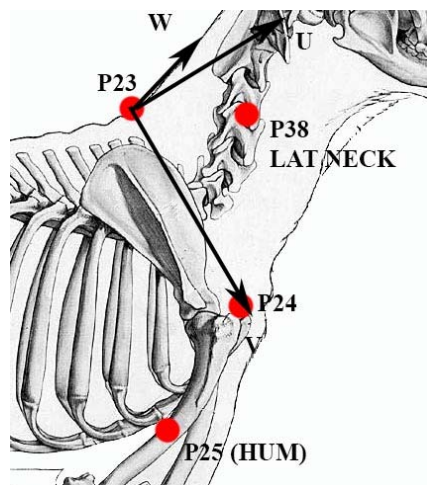
Figure 4.7: Shoulder Girdle UVW axes

138

These axes are calculated by the following equations:

$$W_{Shoulders} = \frac{(Lacj - Racj)}{|Lacj - Racj|}$$ (Equation 57)

$$U_{Shoulders} = \frac{(Racj - C7) \times (Lacj - C7)}{|(Racj - C7) \times (Lacj - C7)|}$$ (Equation 58)

$$V_{Shoulders} = W_{Shoulders} \times U_{Shoulders}$$ (Equation 59)

Applying the vectors as before, acromioclavicular (shoulder) joint centres are determined using the following equations:

$$J_{Rshoulder} = P_3 + 0.344(shoulder\ breadth)W_{RShoulder}$$ (Equation 60)

$$J_{LShoulder} = P_3 - 0.344(shoulder\ breadth)W_{LShoulder}$$ (Equation 61)

4.1.3   Angular Kinematics

Dynamic flexion/extension angles for the tarsal, stifle, hip, carpal, elbow and shoulder were calculated through the use of vector algebra along with specialized computer software (Vicon Bodybuilder) and custom programming (see Appendix K for code). To determine a joint angle, 2 vectors are established in the calibrated 3-D space using the joint centres calculated from the retro-reflective markers as described the previous section. For example, the stifle joint angle is calculated from a vector created by the stifle joint centre and the hip joint centre, and a vector created by the stifle joint centre and the tarsal joint centre. The angle between the two vectors is calculated using the scalar product:

$$\frac{A \bullet B}{|A \bullet B|} = \cos\theta$$ (Equation 62)

Where A and B represent the 2 vectors, |A*B| represents the scalar magnitude of the vectors and θ is the angle of the selected joint in degrees. Joint angles are calculated for 1 stride or gait cycle from toe strike to toe strike for both the fore and hind limbs. To accommodate variances in stride time, data were normalized as a percentage of the gait cycle.

As a check to ensure the output angles were correct (i.e. producing anatomical flexion/extension angles), segment angles for one stride from one trial were analysed by hand using an on-screen protractor over stick figures created by the Vicon software, as demonstrated in Figure 4.8.
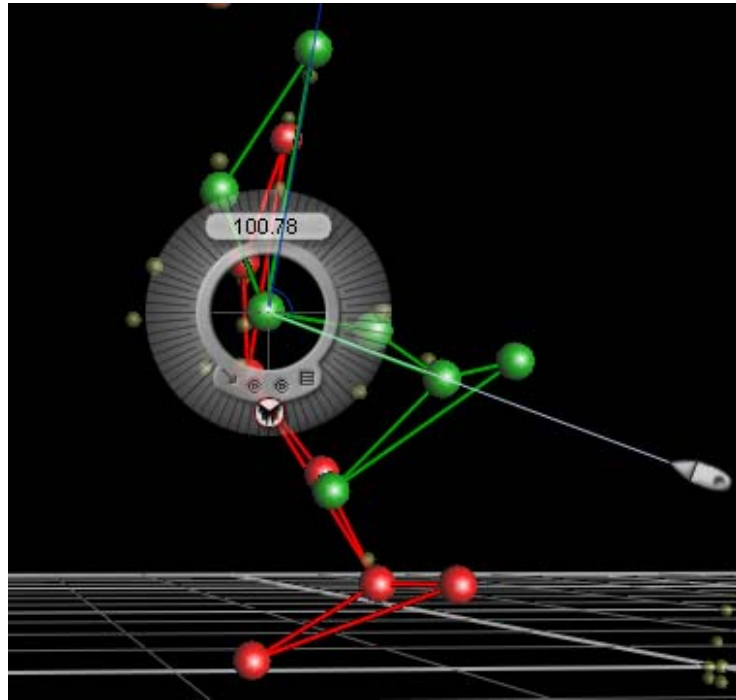
Figure 4.8: Manual verification of model angle outputs using an on-screen protractor. The angle shown is for the left stifle (in green).

The manually measured angles, which were taken from external markers from a 2-dimensional image, provided an estimated range and pattern of movement that could be compared with those generated from the computer model. Note that the computer model outputs were determined from 3-dimensional joint centre calculations so exact comparisons were not expected, but the two methods should present similar movement patterns (graphical shape) and be within a range of approximately 15 degrees. Results of the comparison, shown in Figure 4.9, verified the computer model was producing the correct relative angle outputs.

Figure 4.9: Manual vs calculated joint angles - proofing of angle outputs
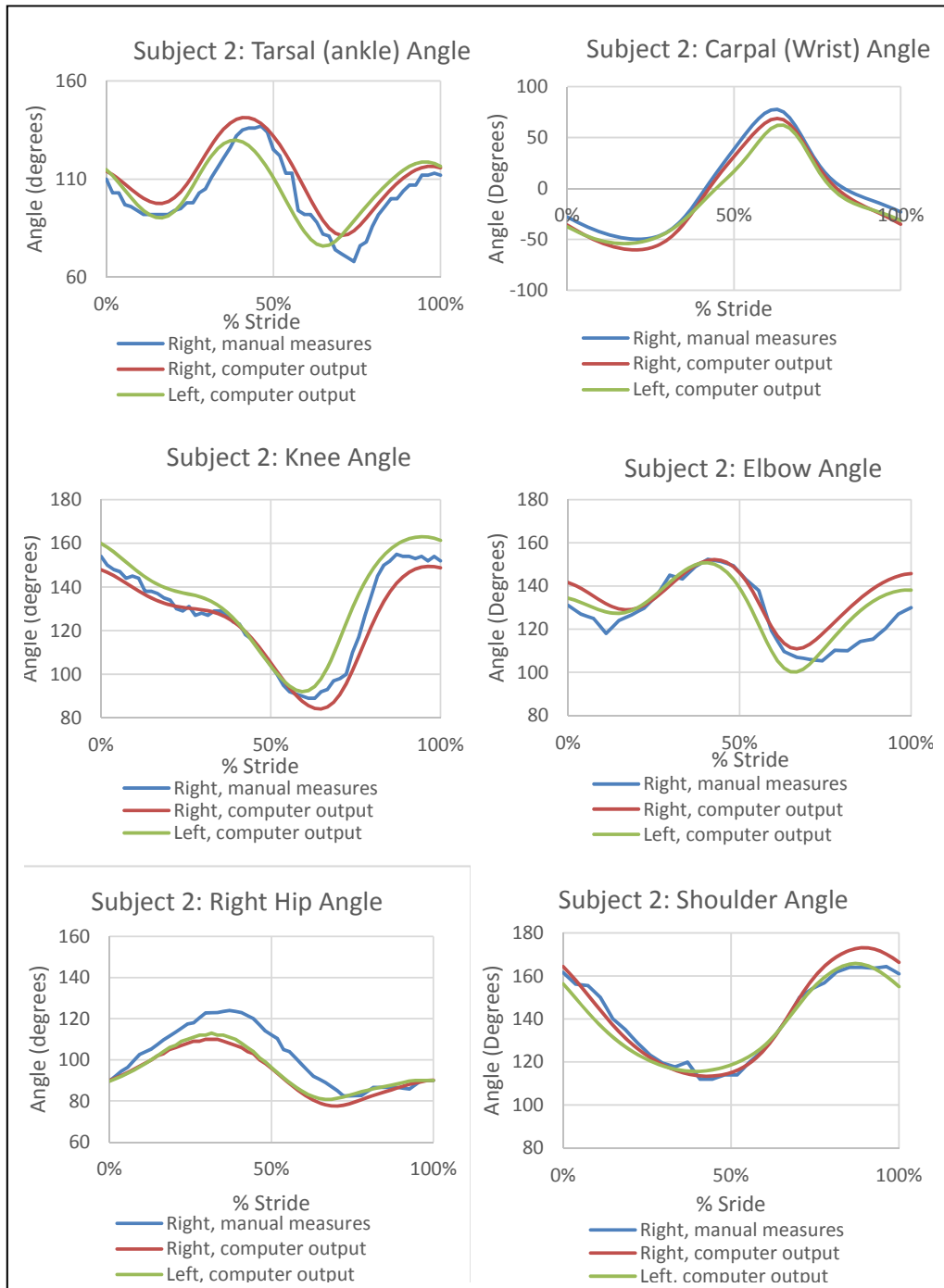
4.1.4   Participants

Five healthy, clinically normal adult German Shepherd police service dogs were recruited from the Vancouver Police Department Canine Unit. There were 4 males and 1 female with a mean age of 5 years ($^+$/- 2.7) and a mean weight of 36.2 kg ($^+$/- 3.7).

4.1.5   Protocol

The complete model is made up of 44 passive reflective markers affixed over anatomical landmarks described in section 4.1.1. All but the 2 facial markers were 14 mm in diameter, nose and nasion markers were 4 mm. To firmly affix the markers in place the dogs were fitted with a custom designed Lycra suit (K9 Topcoat), shown in Figure 4.10, to which all but the foot and head markers could be attached. Face, ears and toe markers were attached with toupee tape. A 7-camera Vicon motion capture system (Vicon Motion Systems Ltd, UK) was used to measure the position of the markers in 3 dimensions at a sampling frequency of 120 Hz. Marker trajectories were filtered with a fourth-order zero-lag Butterworth filter at a cut-off frequency of 6 Hz.

Figure 4.10: Markers applied to dog using lycra bodysuit

Dog/handler teams were typically available at the start of their shift and could be called away at any time during data collection. To reduce the possibility of an interrupted session, data collection was divided into two 1-hour sessions carried out on successive days. The first session was dedicated to collection of morphometric measurements, fitting of the motion capture suit and walking practice along the 12m walkway within the motion capture space. Motion capture data were collected on the second day with teams permitted as much practice as they required to become familiar with the suit, markers and surroundings.

4.1.6 Data Collection and Analysis

Due to dog/handler time constraints actual data collection time was limited to 30 minutes, during which as many useful trials as possible were collected. The researcher and handler monitored each dog closely for any signs of overheating (excessive panting, changes in behaviour). To reduce any possibility of this occurring, data collection times were kept to 15 minute sessions, after which the dogs were provided a break and taken outdoors. Water was available as needed throughout the session.

Of the 5 dogs, all passed through the calibrated space at self-selected velocity: 2 of the dogs were led by their handlers, 3 were commanded to do so on their own. For the latter 3, the handler would command the dog to stay at one end of the walkway while he/she returned to opposite end. The dog would then complete the walking trial on a signal from the handler. A minimum of 3 valid trials (stance/swing phase over one gait cycle for both right and left sides, fore and hind limbs) were preferred, however 2 of the dogs were only able to provide 1 valid trial each. Trials confounded by unnatural or inconsistent movement were discarded, for example, a trial was considered invalid if the dog braked to look up at the handler, a common 'checking in' behaviour for these working dogs.

Spatiotemporal parameters were measured separately for the fore and hind limbs and included:

- Cadence (strides/sec) - determined as the average of the right and left sides

- Walking velocity (cm/s) - calculated as stride length divided by stride time.

- Stride length (cm) - the distance between ipsilateral foot strikes.

- Stride time (s) - time between successive ipsilateral foot strikes.

Distance parameters are based on the HOCK (ankle) marker; foot contact/off events are all expressed as a percentage relative to the ipsilateral gait cycle. A single gait cycle extends from foot strike to foot strike of one leg and includes stance and swing
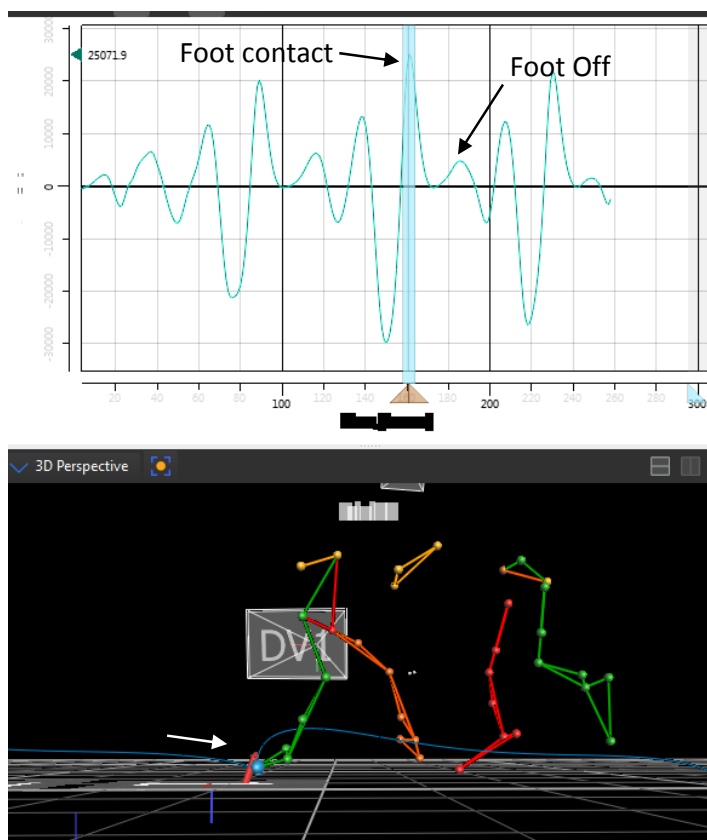
Figure 4.11: Foot contact indicated by max peak vertical acceleration of the MCPJ marker

phases. As shown in Figure 4.11, *foot contact* coincided to within 2 frames of the maximum peak vertical acceleration of the MTPJ and MCPJ markers for the stride cycle, while *foot off* coincided within 2 frames of the following smaller peak, hence these peaks were used as guidelines in defining these timing parameters.

Kinematic data include tarsal, stifle, hip, carpal, elbow and shoulder joint angles, expressed anatomically as relative angles as shown in Figure 4.12.
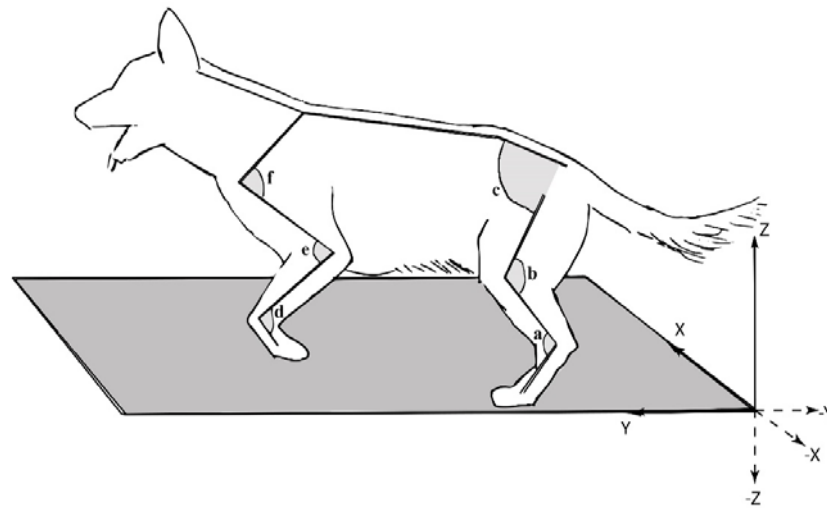
Figure 4.12: Right-handed orthogonal axis used for collecting kinematic data on the German Shepherd. Relative joint angles were calculated and presented as shown, a) tarsal joint, b) stifle joint, c) hip joint, d) carpal joint, e) elbow joint, and f) shoulder joint

All data were collected, processed and analysed using Vicon software: marker trajectories were recorded and produced relative to a global coordinate system that was created during calibration of the testing space (Nexus); trajectory data were input into a custom model to extract joint centre locations and angles (BodyBuilder – see Appendix J and K for model code); joint angles were averaged and visualized for each subject.

4.1.7 Statistical Methods

As this part of the study is an exploratory investigation with limited subjects, controls and trials, any results would be observational and would not have statistical significance, therefore statistical analysis has not been included.

4.2 Results

This part of the investigation serves as a test for usability of a canine motion capture marker suit and marker set, based on the conventional Helen Hayes model for humans, for use with German Shepherd police dogs. The method was assessed according to the dogs' acceptance of the motion capture suit and by a comparison of output angles to other studies for pattern consistency. Because there is limited data on German Shepherds, and none existing for police dogs or for measures from joint centre, less emphasis is placed on the values of the output angles, rather the flexion/extension patterns and ranges should be consistent to those observed in other studies for dogs of similar size.

4.2.1 Acceptance of the Motion Capture Suit

The suit was quick to put on the dogs and snug but not tight. Once donning the suit, the dogs went for a 10-20 minute walk outdoors to get use to the sensation of wearing it. Back in the gait lab, the dogs were able to move freely and naturally while wearing the suit with limited signs of irritation. This was gauged primarily by observing subject behaviour for unnatural/inconsistent gait patterns (e.g. exaggerated lifting of the legs, scratching, biting) of which there was the occasional shaking of the coat but nothing remarkable, as confirmed by the handler.

4.2.2 Placement of the Markers

On average, the markers took 10 minutes to apply. Markers on the suit required the least amount of time to place, while the ones on the head took longer because the dogs did not like to be touched for any length of time in this area. The skin over the nose also required cleaning prior to application of the adhesive and markers. Once applied,

the dogs did not show any irritation toward the markers, likely because they were very small (4mm in diameter).

4.2.3 Spatiotemporal Parameters

Average cadence, walking velocity, stride time and stride lengths for each dog are presented in Table 4.3. Based on velocity classifications selected for large breed dogs (greyhounds) [Riggs et al., 1993], all dogs exhibited trotting velocities. Velocities within the range of 1.5-1.8 m/s were considered slow, medium trots fell within the range of 2.1 to 2.4 m/s and fast trots were classified within the range of 2.7-3.0 m/s. Based on these criteria, Dog 3 demonstrated a slow trot, Dog 4 and 5 exhibited a medium trot, and Dogs 1 and 2 were at a fast trot. Mean fore and hind foot stride lengths and cadences were uniformly consistent.

Table 4.3: Spatiotemporal parameters for German Shepherds at self-selected pace

	Cadence strides/s				Trotting Speed cm/s				Stride Time s				Stride Length cm			
	Fore	+/-	Hind	+/-	Fore	+/-	Hind	+/-	Fore	+/-	Hind	+/-	Fore	+/-	Hind	+/-
Dog 1	2.28	0.095	2.26	0.012	351.1	17	349.3	23	0.439	0.019	0.443	0.071	153.8	2.90	154.4	7.1
Dog 2	2.15	0.045	2.26	0.190	329.1	16	327.3	16	0.465	0.010	0.446	0.036	153.1	8.20	145.8	13.0
Dog 3	1.55	0.130	1.52	0.110	168.2	21	155.2	12	0.647	0.053	0.661	0.049	108.0	5.30	102.2	2.9
Dog 4	1.89	2.530	1.81	6.910	203.7	10	182.7	5	0.529	0.006	0.554	0.029	107.8	6.50	101.3	6.0
Dog 5	1.71	4.160	1.67	7.860	228.1	3	223.4	2	0.583	0.012	0.600	0.024	131.1	0.61	134.0	6.3
Mean	1.92		1.90		256.0		247.6		0.533		0.541		130.8		127.5	
SD	0.30		0.34		80.0		86.6		0.085		0.096		22.8		24.7	

Table 4.4 compares the velocities from the above table in relation to the initiation of swing phase at foot off. In general, with increased velocities, foot off appears to occur earlier in the stride cycle for both the fore and hind foot, with the forefoot off occurring earlier than the hind foot for their respective cycles.

Table 4.4: A comparison of foot off time as a percentage of the gait cycle relative to trotting velocity

| | Hindfoot | | | | Forefoot | | | |
| | Speed (cm/s) | | Foot Off (%) | | Speed (cm/s) | | Foot Off (%) | |
	$\overline{x}$	σ	$\overline{x}$	σ	$\overline{x}$	σ	$\overline{x}$	σ
Dog 1	349	23	28.8	2.41	351	17	37.3	2.09
Dog 2	327	16	31.4	3.28	329	16	39.1	1.47
Dog 3	155	12	49.0	2.39	168	21	48.5	6.60
Dog 4	183	5	50.4	1.58	204	10	50.4	1.67
Dog 5	223	2	38.9	1.53	228	3	37.1	1.27

4.2.4   Dynamic Joint Angles

Since all dogs completed the trial at a trot, all trials were first averaged to observe characteristic patterns for this gait. Patterns and ranges of flexion/extension angles calculated from the marker set and averaged across all dogs and all trials for the hind limb (Figure 4.13) and forelimb (Figure 4.14) are in agreement with other studies [Decamp et al., 1993, Hottinger et al., 1996]. For the hind limb, the dogs were in stance for 38% (+/- 10.4%) of the gait cycle. The tarsal joint had two peaks of extension: a maximal extension occurring just after at foot off at 42% and a slightly smaller peak occurring just prior to foot strike (98%) with maximal flexion occurring at mid swing (70%). The stifle joint movement was characterized by a maximal extension peak at foot strike (98%), with only a slight extension at just prior to foot off (30%); maximal flexion occurred during swing phase at 65% of the gait cycle. The hip joint exhibited a single peak of extension at foot off and a single peak of flexion during swing at 85% of the gait cycle. For the forelimb, the dogs were in stance for 42% (+/- 6.47%) of the gait cycle. The carpal joint movement was characterized by a single gradual peak of maximal extension during stance (20%) progressing sharply to maximal flexion occurring during the swing phase at 65% of the gait cycle. Similar to the movement pattern observed for the tarsal joint, the cubital joint movement exhibited 2 peaks of extension: maximal extension at foot off and a second slightly smaller peak at foot strike. Maximal flexion occurred during swing phase (68%) with a small flexion peak also occurring during stance at approximately 15% of the gait cycle. Scapulohumeral

joint movement presented with a single peak of extension during swing phase (90%) progressing gradually into peak flexion at foot off.

Despite all gait falling in the 'trot' classification, there were distinct differences in the subcategories of slow, medium and fast to which large variations may be attributed. In view of the trace standard deviations, the greatest inter-subject variability was observed in the hind limb relative to the forelimb, particularly for the tarsal joint. For the tarsal, stifle, hip, carpal and cubital joints, most variation was observed around the timing and degree of flexion taking place during the swing phase. For the scapulohumeral joint, there was greater variation during extension at the end of the swing phase.

The greatest consistency of general patterns for all joints across all dogs occurred during the stance phase of the gait cycle, with the stifle and scapulohumeral joints having the least variation of all joints.

Figure 4.13: Hind limb average flexion/extension angle for one stride
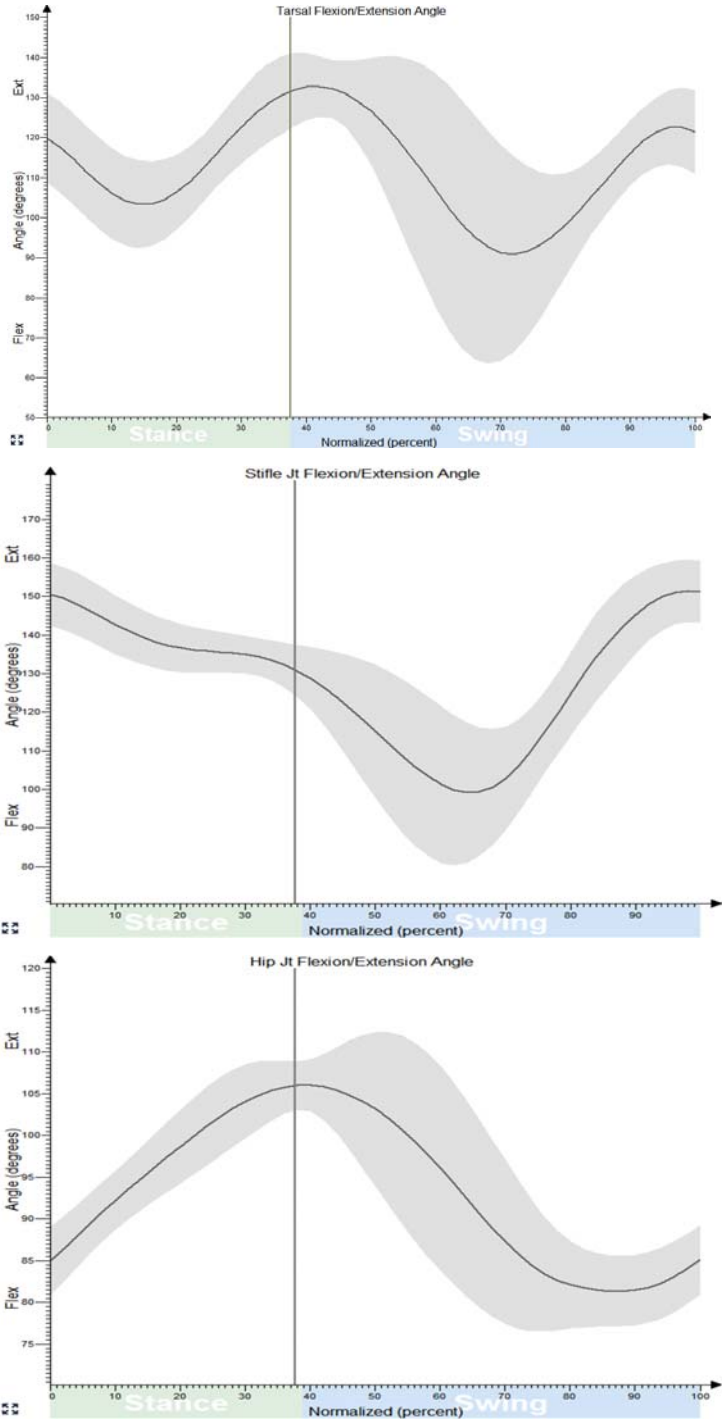
Figure 4.14: Fore limb average flexion/extension angle for one stride
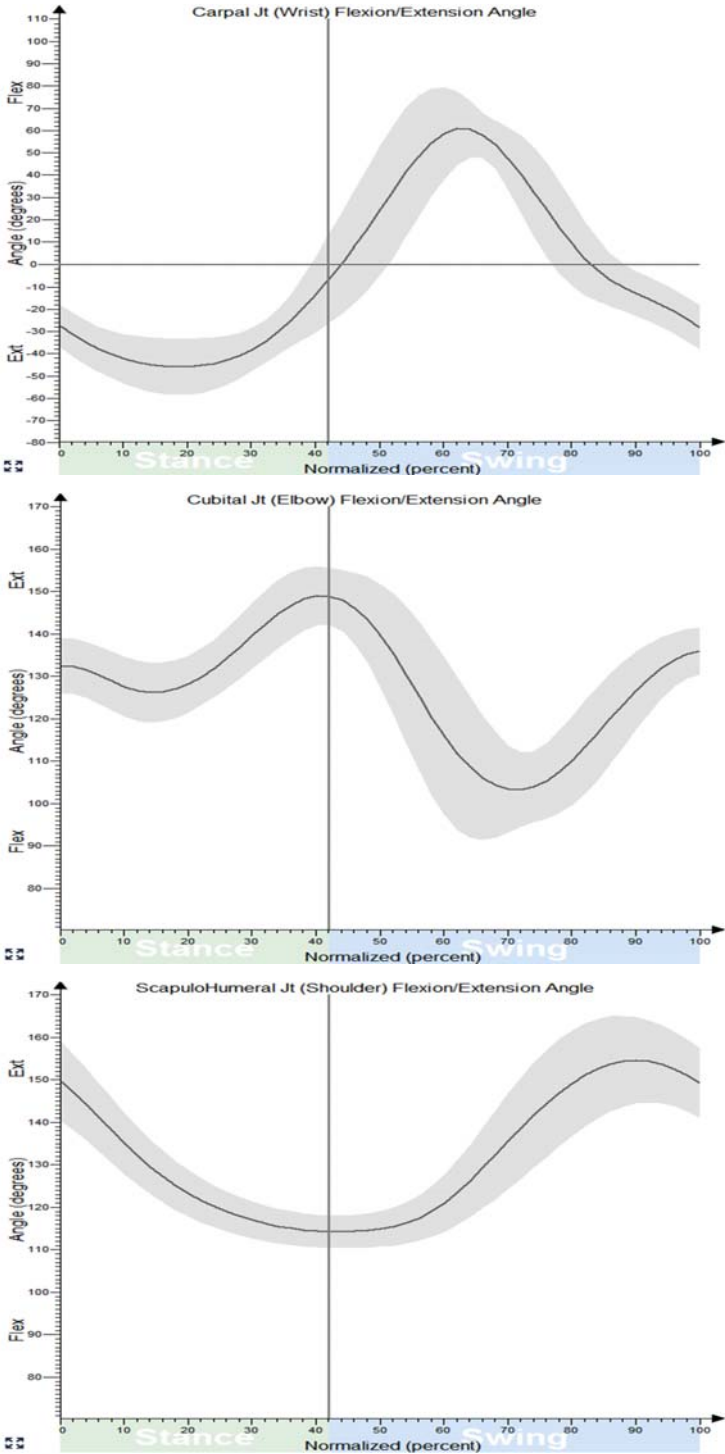
Range of motion descriptives were determined from average traces and are shown in Table 4.5. Tarsal, elbow, shoulder and stifle joints travelled through similar total ranges at an average of 45 degrees. The carpal joint moved through the greatest range of the gait cycle at 106 degrees total range while the hip had the lowest range at 25 degrees.

Table 4.5: Mean range of motion (degrees) for each joint across all dogs

Joint	Max	Min	Total Range	Mean	SD
Tarsal Jt	133	90.8	42.2	113	12.6
Stifle Jt	151	99.0	52.0	129	16.6
Hip Jt	106	81.3	24.7	93.4	8.92
Carpal Jt	60.8	-46.0	106	-4.67	35.8
Elbow Jt	149	103	46.0	128	13.6
Shoulder Jt	155	114	41.0	132	15

Average gait patterns for each dog are shown in Figure 4.15 and Figure 4.16. In general, dogs 3 and 4 present with similar gait patterns, dogs 1 and 2 are also similar and results for dog 5 are somewhere in between the two groups. At slower velocities (dogs 3 and 4), an overall decrease in total range of motion was seen across all joints except the hip, and peak flexion and extension angles were observed later in the gait cycle for all but the shoulder joint. For the tarsal joint this was characterized primarily by a decrease in overall flexion combined with an increase in peak extension at foot strike when compared with the faster velocities. The stifle joint presented with a much smaller peak flexion angle at the slower velocities and little change in extension across all velocities. The hip joint presented with greater peak extension angles with little change in flexion at the slower velocities. There were few differences in magnitude observed for flexion/extension angles in the joints of the forelimb. Only the carpal joint presented with slightly greater peak flexion angles at mid swing.

Figure 4.15: Hind limb flexion/extension angles by dog for one stride
Trace colour code: Dog 1=grey; Dog 2=navy blue; Dog 3=purple; Dog
4=red; Dog 5=green/yellow
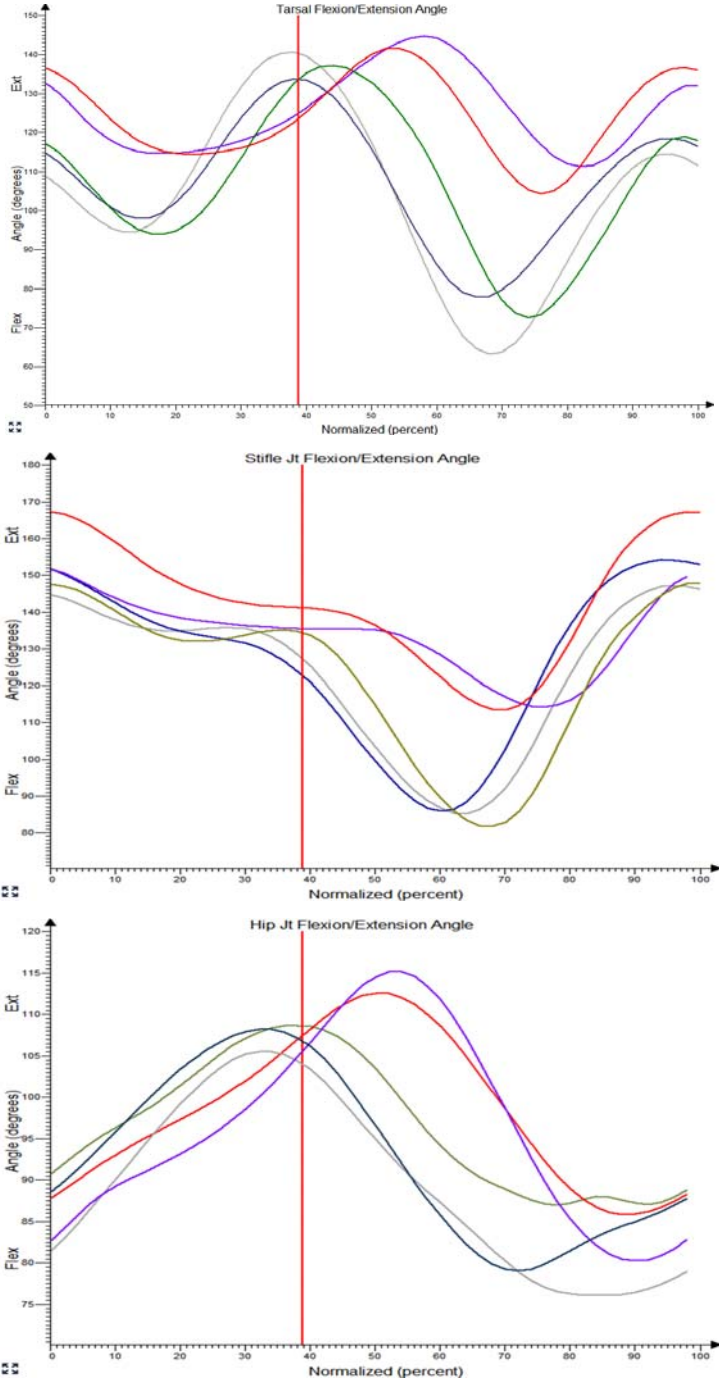
Figure 4.16: Fore limb flexion/extension angles by dog for one stride
Trace colour code: Dog 1=grey; Dog 2=navy blue; Dog 3=purple; Dog 4=red; Dog 5=green/yellow
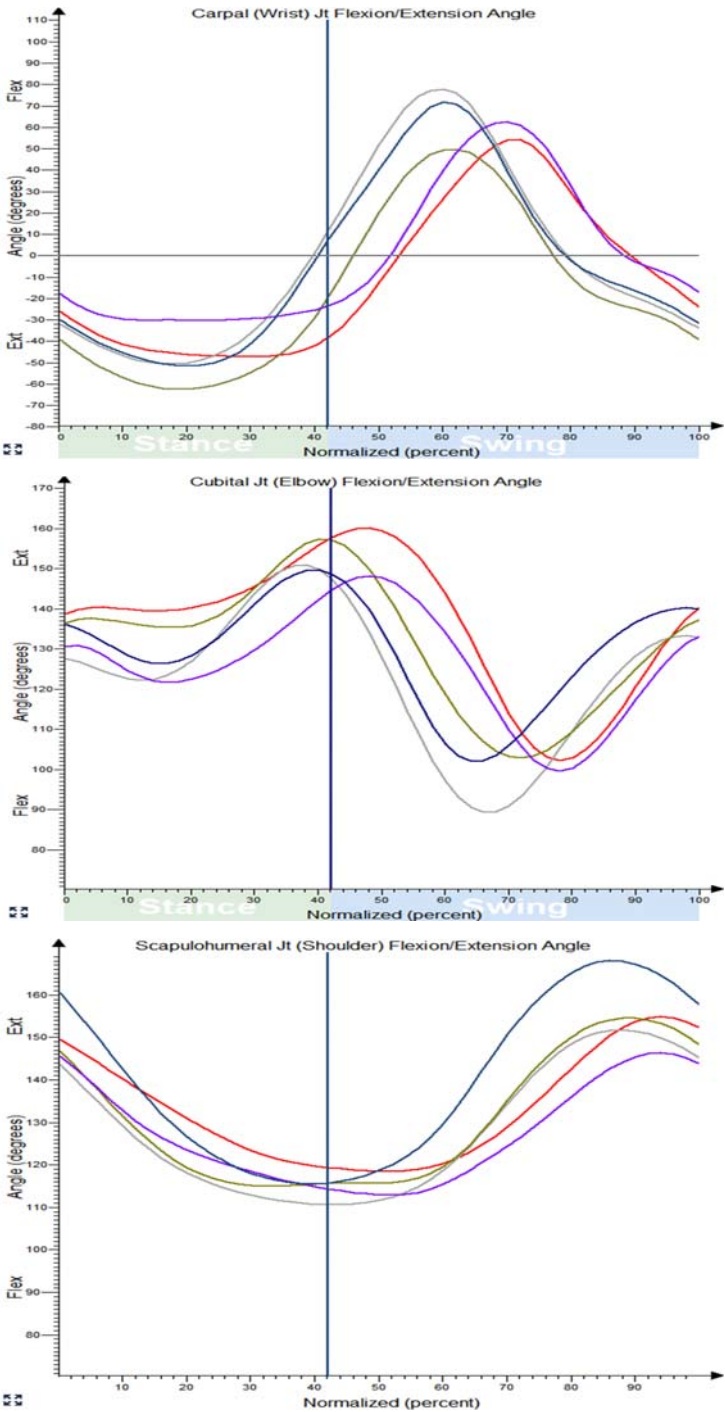
4.3 Discussion

There is little research available on German Shepherd gait [Tian et al., 2011] [Miqueleto et al., 2013] and none specifically on police dogs. With so little information currently available, limitations were not placed on walking velocity so that efforts may be concentrated on evaluating the efficacy of using a motion capture suit, to determine if the marker set was feasible if used to its full capacity of 44 markers, and to observe gait preferences and related performance for use in future evaluations.

4.3.1 The Motion Capture Suit

The German Shepherd has a long, thick coat and loose skin. To reduce difficulty in attaching markers, limitations in marker visibility and skin artefacts, a motion capture suit was created specifically for canine gait research. Police dogs in Canada frequently work and train in body harnesses or ballistic vests so although it was unknown if the suit would affect the dogs' gait, it was expected that they would quickly adapt and resume natural movement. The base suit was an inexpensive (60 USD) lightweight Lycra bodysuit (K9 Topcoat) that was originally created for protection from allergies, wounds and snow. Velcro loop patches were added in areas where markers may be placed. The suit was applied by the handler and required only a few moments to put on. Upon initially donning the suit and occasionally during data collection the dogs would shake themselves to settle their coat and the suit but no other gait limiting behaviour was observed.

A slight increase in panting was noted in the first dog after 20 minutes of data collection, indicating that the dog was getting warm. At that point it was decided that sessions would be limited to a maximum of 15 minutes, after which time the dog would be taken outside, with the suit and markers still attached, for a walk around the facility to cool off. When ready, the dog returned to the lab, markers were checked and data collection resumed. Regardless of whether all required trials were collected, a maximum of 2 15-minute sessions were included in the protocol. With the addition

of the cool-down break no other issues with the suit were noted. Overall the motion capture suit did not visibly affect the dog's natural movement and was well-received by all dog/handler teams.

4.3.2   Subject Trials

With data collection time limits, 3 good trials were collected from Dogs 1, 2 and 3 and one good trial was collected from Dogs 4 and 5. Dogs 1 (a female) and 2 (a male) were able to complete each trial consistently on a simple command from the handler who was posted at the end of the walkway out of view of the camera. Dogs 3 and 4 could not complete the gait task at a controlled walk or trot without the handlers walking along beside them, rather they would complete each trial at a run. This method was not ideal as not only did the presence of the handler block markers from some camera views, it also caused the dog to continually look up at the handler for commands. These dogs required more time for data collection, so much so that only one good trial could be collected from Dog 4. All of this was useful feedback for designing testing protocols in future investigations. Many canine gait studies to date have had success recording 3 to 5 good trials [Dogan et al., 1991, Torres et al., 2013, Hicks and Millis, 2014, Silva et al., 2014, Strasser et al., 2014]. Based on these studies it is recommended that at least 5 good trials be collected. To do so an additional test session may be required. Note that, in studies of humans, it has been suggested that as the number of gait trials increase, gait parameter variability decreases [Maynard et al., 2003, Monaghan et al., 2007] and that 10 trials have been recommended [Diss, 2001, Monaghan et al., 2007].

Despite the label, Dog 5 was the first dog to test the motion capture suit and trials were completed prior to Dogs 1 through 4. Data from this dog were initially not included in the investigation because he was primarily used for perfecting marker placement and use of the marker suit. Head and tail markers were not yet in place and little time was spent on trial completion. This dog, however, was similar to dogs 1 and 2, completing each trial consistently on his own. Upon examination, it was decided that data from one trial should be included for comparison.

4.3.3 Marker Model Performance

The 44 marker model may be used in whole or in part for canine gait. For this evaluation all markers were put in place to monitor application time, effort required to apply, visibility, strength of adhesion and dog acceptance.

Markers took 2 researchers an average of 10 minutes to apply. Initially, face and ear markers were placed on a muzzle (supplied by the handler) however this method was not ideal in that the dog could not drink freely when needed and it was unknown if the addition would cause perturbations in performance so the muzzle was discarded. Instead, markers were attached using a strong double-sided adhesive tape. After a few missed trials due to markers falling off of the feet or head, combined surface cleaning and tape application were perfected and there were limited mishaps.

Markers on the ears were placed low on the tragion so that they could be as attached close to the skin. Markers on the tail were attached with a special elastic non-adhering tape that could be wrapped around the tail. Body markers were strongly attached and none were lost during trials. Using these methods, marker migration was not an issue and all markers were visible within the calibrated space. The dogs did not exhibit any behaviours indicating irritation from marker placement. Graphical output from all markers were clear, particularly for those on the head, neck, body and tail.

4.3.4 Model Outputs

This investigation has been limited to limb kinematics as these have been the primary focus of research in canine biomechanics to date and data are available to which findings here may be compared. The head, neck, torso and tail have been included in the marker model for observation and for estimations of joint centres.

Gait patterns in dogs are known to vary with velocity and analysis typically involves a symmetric gait such as the walk or the trot, characterized by limb movements on one side of the body being repeated on the other. Walking gait includes 2- and 3-limb stance phases and excludes single limb stance; the trot includes a 2-limb stance phase in which the forefoot and hind foot of opposite sides of the body strike the ground

close together; i.e., right hind with left front and left hind with right front [DeCamp, 1997, American Kennel Club, 2015]. With this gait, contact with the ground may be slightly longer in duration for the hindlegs than the forelegs [Nunamaker and Blauner, 1985]. As stated in the results, gait patterns for all dogs in this investigation have been classified as a trot, however variations in timing and magnitude of dynamic joint angles were observed that require further definition to account for variations in this gait classification. In addition, the sub-classifications applied here have been based on movement patterns of the Greyhound, it may be that German Shepherd trotting velocities differ and this is an area that requires further investigation. Furthermore, it has been shown that, compared to the trot, walking gait has more inflections in the dynamic joint angle curves, indicating a more complex joint movement [Hottinger et al., 1996]. The walk also has a prolonged stance phase at approximately 66% compared to the trot at 33% [Decamp et al., 1993, Allen et al., 1994]. It will therefore be important to control this parameter in future investigations if one is to glean desired information and accurately compare gait patterns across dogs. Methods of control may include timing gates for over ground walking or use of a treadmill, both methods have their limitations. As was observed in this investigation, control of over ground walking velocity typically involves the handler walking with the dog, which presents issues with marker visibility and consistency of gait pattern. And although a treadmill is an ideal method of controlling gait velocity, Clements et al. (2005) found that when using this method to study trotting gait in Labrador Retrievers, patterns were not repeatable either within or between dogs over 5 two-minute sessions at 2.0 m/s. It is therefore unknown how long dogs may need to habituate to the treadmill before the technique may be applicable to natural gait. In another study on Greyhounds, however, a statistically consistent pattern was obtained at a velocity of 2.4 m/s [Owen et al., 2004]. There is no clear choice between methods and it may simply be dependent on availability of equipment.

Despite the variations in velocity, all limb joints had characteristic patterns and joint ranges of flexion and extension similar to those found in other canine research

[Decamp et al., 1993, DeCamp et al., 1996, Hottinger et al., 1996]. These results provide evidence that the marker and computational models presented here are working as they should and will prove to be useful tools in furthering canine gait research. Future developments to the computational model will include the addition of abduction/adduction, internal/external rotation angles, joint velocities and accelerations. With the addition of force plate data, as well as the body segment parameters and regression correlation equations developed in Section 3 we may now be able to provide a full objective gait analysis of the German Shepherd police dog.

5 OVERALL DISCUSSION AND FURTHER WORK

Biomechanical models provide a means of quantitatively observing movement mechanics, assisting trainers and clinicians in selecting approaches to training or treatment methods. Equations within these models require the input of body segment parameters and inertial properties so that the data received may be specific to the patient. This information exists for humans [Dempster, 1955, Clauser et al., 1969, Chandler et al., 1975], primates [Reynolds, 1974, Martin et al., 1989, Crompton et al., 1996, Raichlen, 2005, Schoonaert et al., 2007], and horses [Sprigings and Leach, 1986, Buchner et al., 1997]. To date there is only one full-body dataset based on 3 mixed-breed dogs [Amit et al., 2009] and a partial set on the hind limb of the Labrador Retriever [Ragetly et al., 2008]. Such information is not yet available for the German Shepherd. This investigation provides a comprehensive set of body segment parameters, inertial properties and regression equations for estimating segment masses and moments of inertia for the German Shepherd Police Dog. In addition, a full-body marker set was developed and tested on the dogs for usability. All results have been designed to be combined within a biomechanical model to provide feedback to trainers and clinicians about the health of the dog. The following discussion reviews some of the processes that were selected in achieving the research objectives and makes recommendations for areas of improvement and future investigation.

5.1 Development of the Inertial Model

The initial aim of this thesis was to directly measure and record a complete set of body segment parameters and 3-dimensional inertial properties of the German Shepherd Police Dog. The first step in the process was to select an approach to measuring these parameters. Cost for equipment and procedures were limiting factors in the approach however it was also desirable to directly measure as many parameters as possible.

In comparison to medical imaging, cadaveric segmentation permitted the most direct, cost effective method of measuring moments of inertia, volume and mass, the

drawback being that density must be assumed uniform for each segment. Knowledge of the location of various tissue components gained through use of imaging techniques would likely increase the predictive ability of the regression model. For example, a segment may be modelled as a hollow cylinder of bone surrounded by soft tissue, each having a known density. Unexpectedly, the project received donations of full-body CT scans for dogs 4 to 6 which permitted a method of double-checking manually measured length dimensions and presents an opportunity for future study in comparing results drawn from the conventional cadaver segmentation method with those from the more recent imaging methods. If the methods are comparable, CT scans of additional live dogs may be added to the results found here, adding strength to the regression relationship.

The segmentation method can be time consuming and labour intensive and this was especially the case for dogs 1 to 3 as all cuts were made by hand. The greater time required to complete the cuts afforded a decrease in overall time available to perform morphometric measures due to onset of tissue thawing. The steel blades on the hand saws were also somewhat flexible so extra care was required to avoid migration from desired cut lines. An electric reciprocating saw came available for use with Dog 4 and was tested on a smaller segment to determine if it would be beneficial to use this method over the hand saw. The concern with the reciprocating saw was that there would be less control of the cut and more 'sawdust', or waste material. In fact the opposite was found. The stronger blade and faster saw speed made for cleaner, straighter cuts, significantly less time was required to complete each cut and, even though there was very little waste with the hand saw, there was even less with the electric saw. In similar investigations on horses van den Bogert (1989) reported losses between 7 and 13% and Buchner et al. (1997) reported an average loss of 2.4%. Average tissue loss in this investigation was considerably less at 0.49% per dog.

The pendulum method, used to determine direct measures of moments of inertia in 3 dimensions, required extensive planning before it could be implemented. For this method an external coordinate system in the form of a lightweight box was created to

house the segment being measured. The coordinate system was made out of strong but lightweight foam material so that the box would have limited inertial properties on its own. Reasons for this are best explained in the following statement:

> "The inertial properties of the segment may be measured within a 5% tolerance as long as the moment of inertia of the specimen is relatively large compared to the moment of inertia in the same axis of the measuring device. Errors in measuring the two systems which have large moments of inertia are increased when 2 large numbers are subtracted to yield a relatively small number..." - Reynolds (1974).

The inertial tensor of the combined box/segment system was subtracted from that of the box alone to extract the inertial tensor of the segment being measured. The same box coordinate system was used to locate the centre of mass of the segment.

In carrying out the procedures, a number of factors were considered. First, to ensure correlational accuracy across dogs the segment in question must be placed in the box in exactly the same way for each dog. It must be secured firmly in place in the saddles inside the box, ensuring there is no risk of movement for the duration of the procedure. Any movement rendered the landmark coordinates, segment centre of mass locations and all inertial tensor measures for the segment in question inaccurate. After all measures were complete the segment was cut free of the holding tape so that only the segment was removed and the holding tape left in place to be included in measures of the empty box. The larger abdomen and thorax segments presented even greater risk of error due to the greater mass. While the box provided an external axis and held the segment in correct orientation, the segment itself was supported directly with thin wires fed through the box for all 6 axes. It was essential that the segment remained solidly frozen so that the wires didn't cut into the tissue during swing. These wires were held in tension at all times using strong, lightweight wire clamps as described in Section 3.1.2.5.

While freezing the cadaver limits loss of tissue and fluids, it's important to keep in mind that the inertial properties for each segment are only accurate for the position in which it was frozen. Changes in muscle diameter and position through movement would cause variations in the inertial properties, however since a dynamic moment of inertia measure is not yet possible, the static measure is an acceptable representation.

Another potential pitfall noted with the pendulum method was that the box could occasionally swing as a double, or compound, pendulum, i.e. from the fulcrum of the pendulum as well as at the bolt attachment on the box (refer to Figure 3.14). As explained in section 2.3.3.4, time, or period of oscillation, is the most sensitive of all measures, and oversights such as this could introduce significant error. This was rarely an issue at the small swing angle of <5 degrees, however, this condition was observed to occur on occasion and therefore required continual monitoring. The bolts used in this investigation were longer than required, it's possible a shorter bolt may have eliminated this issue.

Morphometric dimensions are required for input into regression equations and inverse dynamic models to estimate segment mass, centre of mass, moments of inertia and joint dynamics for each segment. As stated in section 3.2.1, upon initiating this research it was unknown which morphometric dimensions would be most appropriate, i.e. provide significant correlation and relatively easy to collect. To ensure all possible avenues of exploration were covered a total of 156 measures were included in the initial list of data to be collected on each dog (Appendix C). As the project moved forward it became apparent for a variety of reasons that some of these measures would either not be useful, were too cumbersome to collect, or lacked repeatability, e.g. chest circumference at rib 5, chest breadth, and waist circumference at the omphalion, to name a few, and the list was gradually reduced to 100 to be included for evaluation in the regression analyses. The final list of required measures was reduced to 33 (Table 3.15), a far more manageable number than had been initially identified.

A second aim of the study was to develop regression equations to predict segment mass and moments of inertia for all 3 primary axes. This was achieved through

numerous correlation combinations of subject mass and some geometric shape. In his investigation of the inertial properties of humans, Chandler et al. (1975) found high correlations of segment mass to body mass alone. For all segments but the head (r = 0.873) and feet (r = 0.784 and 0.831) correlations had an r >.917. It was interesting to find that this was not the case for dogs in this study. Here, only the abdominal segment produced significant correlations at r = 0.845 when compared only to body mass. A multiple regression method likening segments to geometric shapes produced better results as was shown in Table 3.17. Regression analyses for predicting masses and moment of inertia were extensive and produced many significant results. The combinations used to create the regression equations in this investigation here are presented in section 3.2.3, however results of other combinations that were evaluated may be seen in Appendix F for mass and Appendix G for moments of inertia. While the ones chosen for use here were taken from the complete test combinations (single method, x,y and z axis results taken from the same test), it would be interesting to mix best results rather than staying with the best fit triad. For example, for moments of inertia for the manus, the best correlations were found when left and right sides were not averaged. In looking at the x axis, the best predictor results came from the left side as it was modelled as a frustum (r = 0.995), for the y axis the best result also came from the left side, modelled as a frustum (r = 0.986), and for the z axis the best result came from the left side modelling the paw as a cylinder using paw circumference (r = 0.991). A similar approach may be taken for mass prediction for all segments. This method introduces a greater number of required morphometric measures but the results may be worth the extra effort.

Overall, despite the challenges faced in using the cadaveric segmentation method, done carefully, it is the criterion method of measuring segmental inertial properties in 3 dimensions, the greatest benefit being that it permits direct measurement of mass, volume, centre of mass and moment of inertia for individual segments. The ability to freeze the cadaver in the desired neutral stance position also ensures that segment mass is aptly distributed for gait analysis in living dogs. Alternative methods such as

medical imaging, although accurate and significantly less invasive, are costly, the equipment requires specially trained operators, analyses are no less time consuming and the dogs must be scanned with legs extended caudally for the hind legs and cranially for the forelegs. For some methods, like the DEXA, scans may also be limited to single planes.

5.2   Canine Marker Model and Kinematic Analysis

A third aim of this study was develop and test a motion capture marker model through kinematic evaluations. The first step in the process was to develop a marker set that could be used in conjunction with the regression equations and parameters developed in the previous sections of this thesis. One of the greatest challenges in gait analysis with this dog population is accurate marker placement. Removal of hair and use of cyano acrylate for adhesion is not permitted, markers fall regularly and length of the coat tends to obscure markers. The motion capture suit was developed in 3 sizes over a series of visits and then tested using 5 dogs from the municipal police force. The dogs and handlers adjusted well to the use of the suit, markers were easy to apply and it performed well without losing a single marker throughout the data collection process.

Upon completion of the motion capture suit, a marker model was developed so that it could be used to calculate virtual limb joint centres, with joint angle measures being calculated from these virtual locations. Although this is a full-body marker set there have been few studies with which to compare head/neck, torso, or tail angles [Hicks and Millis, 2014]. Since the majority of investigations have been limited to analysis of flexion/extension angles within the limbs, and since the primary objective was to evaluate marker and suit performance, this evaluation was limited to limb flexion extension angles for comparison with other studies

With the development of the marker set and suit, the next step was to evaluate the output generated from the markers. With a sample size of 5, limited trials and no limitations on gait velocity, any inferences with respect to population are tenuous.

However, the goal of the investigation was reached in that gait patterns observed in the present study were similar in pattern and range to those found in previous studies of canine gait, thus proving the marker set was working as it should. In hindsight it may have been preferable to limit gait velocity to a specific range, however, without prior knowledge of the dogs' gait, how the suit would perform or what velocity would be ideal for testing it is felt that this was the best approach. The knowledge gained regarding the speed selection, gait patterns and ranges in joint angle with respect to speed will be invaluable for developing future investigations.

This investigation did not include abduction/adduction or internal/external rotation angles, nor did it include velocity or acceleration traces. These data would be natural additions to the current model. Furthermore, inverse dynamic analyses provide useful insight into locomotion, allowing assessment of joint forces moment and powers. In humans such information is invaluable, permitting clinical intervention that may be tailored to the individual needs of the patient. Today, the clinical gait analysis is a commonly used tool that assists in clinicians in diagnosing diseases, injury assessment, providing treatment options and predicting prognosis.

Similarly applied, the information presented in this thesis opens doors to many possible areas of research, and will greatly improve our understanding of the German Shepherd. The model will contribute to the development of a normative and pathological gait database where gait patterns from dogs may regularly be monitored for changes invisible or unclear to the naked eye. Such changes may indicate injury or disease, providing an opportunity for further examination and possible early intervention. For the police dog, early intervention could reduce or eliminate down time for both the handler and the dog, thereby reducing overall costs to the department. This information could also greatly assist in identifying dogs that are predisposed to musculoskeletal disease. With regard to surgical treatments, clinicians will be able to access more detailed objective information about the condition than is provided by the current subjective methods, thereby assisting in decisions around surgical intervention. Indeed, as demonstrated by Dogan et al. (1991) in their evaluation of

canine total hip replacement, if a gait analysis is completed pre and post intervention the effects of any treatment, surgical or otherwise, may be quantitatively evaluated. Surgical treatments require increased healing time compared to non-surgical treatments. DeLuca et al. (1997) have shown that gait analysis can have a significant effect on surgical decision-making in humans. For the police dog, if a surgical procedure can be deemed unnecessary the cost to the department is greatly reduced and recovery time for the dog will can be decreased or even eliminated. Training programs may also be developed or modified based on information gleaned from this model. A recent study by Martin et al. (2016) utilized gait analysis to evaluate the effect of the rider on the spine of the horse, finding that the presence of the rider in the seated position induced and increase in vertical force on the back, decreased the range of motion at T12-L2, and increased the range of motion at T6-T12 and L2-L5. This suggested a compensatory reaction to the pressure applied by the rider; that perhaps basic strength training exercises could be added to the training regimen to reduce the effect of the rider; and modifications to the saddle may aid in redistributing the load. Studies such as this could contribute to the understanding of back pain in the horse. Comparatively, police dogs undergo rigorous training exercises, including bite work, obstacle courses and jumping in and out of vehicles. During these activities they may be wearing a collar, harness or ballistic vest. Combined kinematic and intersegmental analysis would be possible with this model thus providing insight into range of motion and joint loads during such activities and augmenting the development of safe training practices and/or equipment, ultimately keeping the dog (and handler) on the job.

Although the data gathered to produce the regression equations came from male dogs, the kinematic analysis also presented here included one female (Dog 1), with no observable difference when compared to Dog 2, a male. With this in mind, since no other such complete data exists, it is anticipated that the data presented here will expand research for a variety of dogs and dog breeds.

5.3 Conclusion

This thesis provides the first ever complete set of body segment inertial properties developed specifically for the German Shepherd Police Dog. Regression equations were proposed to estimate body segment parameters based on morphometric measures. A full body marker set was also developed, tested and verified for use on living German Shepherd Police dogs. Such knowledge is essential in the creation of locomotor biomechanical models. These new developments provide a basis for future kinematic and inverse dynamic studies of the German Shepherd. The combined results may then be applied in future investigations of canine mechanics, providing feedback that will guide surgical procedures, rehabilitation and training for these dogs.

APPENDICES

APPENDIX A: RESEARCH CONSENT FORM

RESEARCH CONSENT FORM

Development of a Link-Segment Model of the German Shepherd Police Dog

Date:

Principal Investigator: Yvette Jones, BCIT Technology Centre, (604) 456-1123

Purpose:

The purpose of this project is to build a mathematical (link-segment) model an 'average' police dog using measurements taken from the bodies of a minimum of 5 (five) police dogs. Such models are essential in all research that measures the movement and gait of living beings, including dogs, since they provide the researcher or clinician with important details that would assist them in making decisions about treatment or rehabilitation procedures. This will be particularly important after injury and during rehabilitation as it will then be possible to measure changes that cannot be assessed by the eye alone.

Study Procedures:

How will the model be developed?

The euthanized body will carefully be dissected into functional segments (e.g. for hind limb: paw, lower leg, thigh and pelvis). Using special tools, each segment will be measured for weight, length, circumferences, volume and the location of the centre of mass. The measurements will be collected and averaged across dogs. Finally, the resulting data will be used to develop the model of an average German Shepherd police dog so that it may be used for evaluating the movement of living dogs.

What happens after the dissection is completed?

After dissection, the dog's remains will be taken to a crematorium for cremation and the dog's ashes will be returned to you. The researchers will, at all times, treat your dog's body with respect.

Eligibility:

Which dogs are eligible?

1. German Shepherd Police Dogs that have died of natural causes, illness or minor trauma.
2. Both active duty and retired dogs
3. Dogs over 2 (two) years of age

Exclusions*:

Which dogs are not eligible?

- Dogs with diseases or conditions that are communicable to other dogs or humans
- Dogs that have had amputations
- Dogs that are being euthanized due to major traumatic injuries
- Dogs under 2 (two) years of age

*Note: As the protocol is developed it may be necessary to add to the exclusion list.

Risks:

There are no known risks to this study.

Benefits:

Donating your dog's body to the project will allow the first ever mathematical model of the German Shepherd to be developed. This model will help veterinarians, dog handlers and their dogs improve performance on the job and lead safer and healthier lives. Applications will include:

Rehabilitation: the model will be used to set standards of practice for the rehabilitation of injured police dogs. Just as Olympic athletes benefit from specialized research into athletic performance, police dogs will be able to benefit from treatments and related research into their specific performance and medical needs.

Performance: the model will provide insight on training and handling methods. Research in this area will be police service driven and will evaluate various training and handling methods. The goal will be to reduce injury and to better quantify the contribution these dogs make to the community. The results will be incorporated into the professional environment of both the Vancouver Police Department and the RCMP.

Confidentiality:

Information on individual dogs and their handlers will be kept strictly confidential. Copies of this consent form will be kept in a locked cabinet that is only accessible to researchers at the BCIT Technology Centre. It will be the only identifying document and neither you nor your dog will be identified by name in the database or in any reports on the completed study. Your dog will only be identified by numeric code.

Remuneration/Compensation:

Donating your dog to the study will not cost you anything. On euthanization, you will leave your dog's body with your veterinarian, where it will be picked up either by a BCIT researcher or by a representative of the RCMP. There will be no cost to you for cremation.

If you have any questions or desire further information with respect to this study please contact Yvette Jones at (604) 456-1123.

New Findings:

If you choose to register your dog for this study you will be advised of any new information that may affect your willingness to make that donation at the time that your dog passes away, as soon as that information is available to researchers.

Note: Detach this page and return in self-addressed envelope supplied. Keep the remainder of the document for your files.

Subject Consent:

I understand that my donation my dog's remains to be used in this study is entirely voluntary on my part and that I may change my decision to make that donation at any time in the future or at the time of the dog's death, without any consequences. I have received a copy of this consent form for my own records.

I wish to donate my dog's remains to this study, at the time of his or her death.

Owner Signature   Date _____

Witness Signature   Date_____

Investigator's Signature   Date_____

Dog's Name: _____

Dog's Age: _____

Dog's Gender: male / female   (circle one)

Handler's Contact Information:	**Veterinary Contact Information:**
Name: _____	Name: _____
Preferred Mailing Address:	Clinic Name: _____
_____	Mailing Address:
_____	_____
_____	_____
_____	_____
Preferred Telephone: _____	_____
e-mail: _____	Telephone: _____
	Fax: _____
	e-mail: _____

APPENDIX B: OUTLINE OF LABORATORY PROCEDURES

Outline of Laboratory Procedures

1 Sacrifice Dog (done at clinic by the dog's regular veterinarian)

2 Complete CT scan (for dogs 4, 5 & 6)

3 Transport cadaver to laboratory

4 Measure specimen morphometry while intact

5 Weigh whole body

6 Identify key anatomical landmarks and mark prior to freezing

7 Measure necessary segment morphometry prior to freezing

8 Freeze specimen

   a) suspended in standing position

   b) minimum of 24 hrs at -20 F

9 Separate primary segments

10 Weigh each segment and return to freezer, repeat with next segment until finished

11 Place segment in a specimen holder and secure

12 Weigh composite (Specimen in speciment holder)

13 Measure Moments of Inertia using pendulum method

   a) XX axis

   b) XY axis

   c) YY axis

   d) YZ axis

   e) ZZ axis

   f) XZ axis

14 Balance for centre of gravity measurement in 3 positions:

   a) XX axis

   b) YY axis

   c) ZZ axis

15 Locate segment in speciment holder with 3-D point indicator

   a) 0,0,0 point of specimen holder

   b) Tick marks at each cut surface

   c) Joint

   d) Anatomical landmarks, label with colored pins

16 Photograph each segment with marks/pins indicating key landmarks

17 Remove segment specimen from holder and return to freezer

18 Repeat steps 10-16 for all segments

APPENDIX C: LANDMARKS AND DIMENSIONS

Proposed landmarks and dimensions for determining canine morphometry (as adapted from previous studies)		
Measurement	**Landmark(s)**	**Defined by/ Derived from**
General		
age		
weight (gm)		
Trunk & Stem		
neck l	Base of the head (Axis) to C7	
neck c (1)	Circumference at the base of neck at the shoulders	
neck c (2)	mid length, halfway between the Axis and C7	
neck c (3)	Circumference at Axis	
thorax l (1)	C7/T1 jt ctr to T13/L1 jt ctr	
thorax l (2)	a line parallel to C7/T1 jt ctr to T13/L1 that extends down the central axis of the segment	
thorax l (3)	C7/T1 to T13/L1 spinous process	Chandler '75
chest c (1)	mid thorax @ tip of xyphoid cartilage	Chandler '75
chest c (2)	Mid length of C7T1 to T13L1	
chest c (3)	largest circumference at base of ribs	
chest c (4)	@ mesosternale (5th rib jt @ sternum)	Chandler '75
biacromial b	acromion process, r & l	Chandler '75
chest b (1)	in the transverse plane, the most lateral aspect of the thorax at the level of the mesosternale, r & l	Chandler '75
chest b (2)	@ mid segment	
chest b (3)	@ base of ribs	
chest d	in the median plane, the most lateral aspect of the thorax at the level of the mesosternale, r & l	Chandler '75
abdomen l (1)	T13/L1 jt ctr to L7/S1 jt ctr (estimated)	
abdomen l (2)	T13/L1 to L7/S1 (spinous processes)	Chandler '75
pelvis (sacral) l	L7/S1 to ischial tuberosity	Chandler '75
pelvic l	iliocristale to ischiatic tuberosity	Reynolds '74
waist c	at level of omphalion	Chandler '75
waist c2	at level of waist crease (narrowest)	Chandler '75
waist b	at level of omphalion	Chandler '75
waist b2	at level of waist crease (narrowest)	Chandler '75

bispinous b	iliocristale, r & l	Chandler '75
bitrochanteric b	trochanterion laterale, r & l	Chandler '75
ischial b	ischial tuberosity, r & l	Chandler '75
waist d (1)	at level of omphalion	Chandler '75
waist d (2)	at level of waist crease (narrowest)	Chandler '75
Tail l	With the tail hanging down, a straight line from the tip of the tail to the base of the sacrum.	
Tail c	Circumference at base of sacrum	

Left and Right Appendages

brachium l (2)	acromiale to radiale	Chandler '75
brachium l (3)	greater tubercle of humerus - lateral epicondyle of elbow	Chandler '75
brachium l (1)	Prox jt ctr to dist jt ctr	
mid brachium c (1)	Triceps (mid acromiale to radiale)	Chandler '75
axillary c	Circ @ highest point in the axilla, perpendicular to long axis of the brachium	
antebrachium l (ulnar)	olecronale-stylion	Chandler '75
antebrachium l (radial)	radiale-stylion	Chandler '75
antebrachium l (p-d)	Prox-dist jt ctr	
antebrachium max c	maximum circumference	Chandler '75
antebrachium mid c	circ @ mid length between wrist and elbow joint centres	
elbow b	medial-lateral epicondyles	Chandler '75
elbow c	olecranon process-crease across epicondyles	Chandler '75
wrist b	bistyloid diameter	Chandler '75
wrist c	bistyloid circumference	Chandler '75
carpus/metacarpus l	styloid process to base of 5th	Chandler '75
carpus/metacarpus c	just caudal to carpal pad	Chandler '75
carpus/metacarpus b	just caudal to carpal pad	Chandler '75
carpus/metacarpus d	just caudal to carpal pad	Chandler '75
manus l (1)	caudal edge of met pad-ant. 3rd nail base	Chandler '75
manus b	2nd to 5th met @ metacarpal pad	Reynolds '74
manus d	apex of met pad to top of 3rd mcpj	Reynolds '74
manus c	metacarpus II –V@ metacarpal pad	Chandler '75
mid-manus c	half length of wrist jt ctr to tip of IIIrd pad	
manus l (2) to jt ctr	wrist jt ctr to anterior IIIrd nail base	Chandler '75
mc III-dactylion l	mc III-dactylion l	Chandler '75
upper thigh c	at lowest point of the gluteal furrow	Chandler '75

	thigh c	maximum circumference	Chandler '75
	thigh l (1)	prox-dist jt ctr	
	thigh l (2)	trochanterion h - tibiale h	Chandler '75
	mid thigh c	halfway <> trochanterion & tibiale	Chandler '75
	stifle (knee) c	mid patella	Chandler '75
	stifle (knee) b	medial – lateral femoral epicondyles	Chandler '75
	crus l (1)	prox–dist jt ctr	
	crus l (2)	tibiale-sphyrion	Chandler '75
	crus c	maximum circumference	Chandler '75
	ankle b	bimalleolar diameter	Chandler '75
	ankle c	bimalleolar circumference	Chandler '75
	hind paw c	widest part @ pads	
	pes b	metatarsale (laterale-mediale)	Reynolds '74
	pes d	metatarsale III	Reynolds '74
	mid hind foot c	@ half length of pes (1)	Chandler '75
	pes c	@ tarsus/metatarsus across mt pad	Chandler '75
	pes l (1)	prox jt ctr to podactylion III	Chandler '75
	pes l (2)	dorsocaudal tip of calcaneous - pododactylion III	Reynolds '74
	pes l (3)	dorsocaudal tip of calcaneous to IIIrd mtpj	Reynolds '74
	mt III-dactylion l	mt III-dactylion l	Chandler '75
	tarsus/metatarsus l	calcaneus to base of 5th	Chandler '75
	tarsus/metatarsus d	at cuboid	Chandler '75
	tarsus/metatarsus b	at cuboid	Chandler '75
	tarsus/metatarsus c	at cuboid	Chandler '75
	Head (see diag below)		
	total head l (1)	joint ctr to end of nose	
1	total head l (2)	inion-prosthion	Onar '99
	total head l (3)	greatest length	
3	cranial l	inion-nasion	Onar '99
4	cranial b	maximum transverse vault (euryon)	Onar '99
	face l	nose to tragion	Onar '99
	skull case l	tragion to external occipital protuberance	Onar '99
	cranial c	max @ plane of glabella-opisthocranion	Onar '99
	head base c	circumference of plane made up of inion/caudal edge of ear cartilage. throat	
	mid-head c	@ zygion	
	total face h	nasion-gnathion	Onar '99

2	upper face h	nasion-prosthion	Onar '99
	biorbital b	ecto-orbitale	Onar '99
5	bizygomatic b	zygion	Onar '99
	bigonial b	gonion	Onar '99
	snout b	maximum transverse distance	Onar '99
	nose c	circ @ base of nose encompassing upper and lower jaws, mouth closed	
	neck l (1)	caudal - cranial jt ctr	
	neck l (2)	C7/T1 to most craniodorsal point of axis (C2)	Chandler '75
	neck c (1)	maximum circumference	Onar '99
	neck c (2)	just cranial to shoulder blades	
	neck c (3)	just cranial to axis vertebra	
	neck b	maximum	Onar '99
	neck d	perp to long axis	Onar '99

Landmark Definitions:

Acromiale: The acromiale is the point located at the dorsocranial and external border of the acromion process when the dog is standing in neutral position.

Radiale: The superior head of the radius using your right thumb nail; located by palpating downward in the lower portion of the lateral dimple of the elbow.

Stylion: The most distal point on the styloid process of the radius

Olecronale: The most distal point on the olecranon process of the ulna

Mesosternale: A point mid-sternum at the level of the junction of the fifth ribs. Can be located by using a two-handed palpation.

Omphalion: Belly button/umbilicus

Trochanterion laterale: most lateral point of the greater trochanter of the femur

Iliocrystale: most cranial point of the ischium

Dactylion: tip of 3rd phalanx
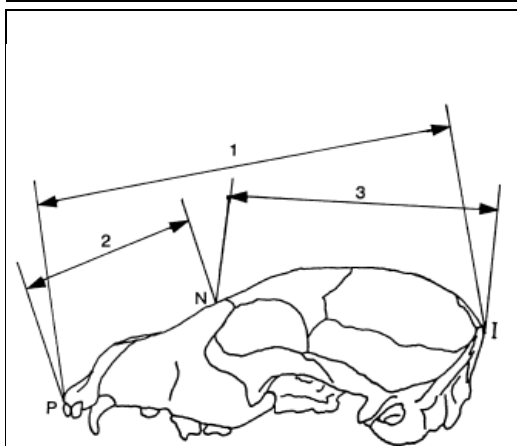
Fig. 2. Measurements of the cranium (lateral view): inion (i), prosthion (p), skull length (1), viscerocranial length (2), and cranial length (3).
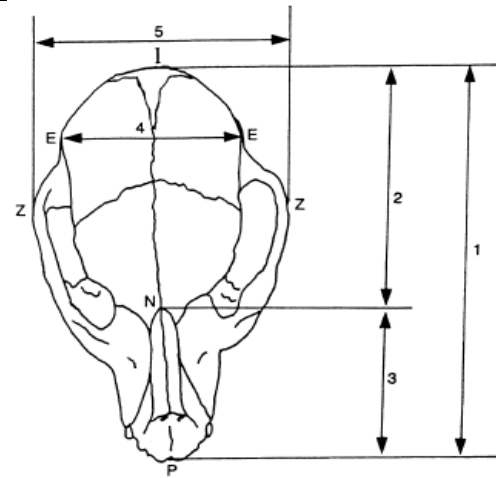
Fig. 1. Measurements of the cranium (dorsal view): inion (I), nasion (N), prosthion (P), euryon (E), zygion (Z), skull length (1), cranial length (2), viscerocranial length (3), maximum width of neurocranium (4), and maximum zygomatic width (5).

Definitions of measuring points on the cranium (Figs 1 and 2)

Inion (I): central surface point on the external occipital pro-
tuberance.
Nasion (N): junction on the median plane of the right and left
nasofrontal sutures.
Prosthion (P): anterior end of the interincisive suture, located
between the roots of the upper central incisor teeth.
Euryon (E): the most lateral point of the brain case.
Zygion (Z): the most lateral point of the zygomatic arch.

APPENDIX D: 3D POINT LOCATION FORM

Three Dimensional Point Location of All Landmarks and Segmentation (cm)				
Date:			Subject #:	
		Distance from box origin (m)		
Segment	Landmark	X	Y	Z
Left Manus (Forepaw)	COG (empty box)			
	COG (full box)			
	Prox jt ctr			
	3rd mcpj			
	Distal 3rd mcpj			
	Dist. 3rd mc @ pad tip			
Right Manus (Forepaw)	COG (empty box)			
	COG (full box)			
	Prox jt ctr			
	3rd mcpj			
	Distal 3rd mcpj			
	Dist. 3rd mc @ pad tip			
Right Antebrachium (Foreleg)	COG (empty box)			
	COG (full box)			
	proximal jt ctr			
	lateral epicondyle			
	distal jt ctr			
Left Antebrachium (Foreleg)	COG (empty box)			
	COG (full box)			
	proximal jt ctr			
	lateral epicondyle			
	distal jt ctr			
Right Brachium (Upper Arm)	COG (empty box)			
	COG (full box)			
	proximal jt ctr			
	ball of humerus			
	acromion			
	distal jt ctr			
Left Brachium (Upper Arm)	COG (empty box)			
	COG (full box)			
	proximal jt ctr			
	ball of humerus			
	acromion			
	distal jt ctr			
Right Pes (Hind Paw)	COG (empty box)			
	COG (full box			
	Heel Point			

	ankle jt ctr			
	3rd mtpj			
	dist 3rd mt (toe tip)			
Left Pes (Hind Paw)	COG (empty box)			
	COG (full box)			
	heel Point			
	ankle jt ctr			
	3rd mtpj			
	dist 3rd mt			
Right Crus (Shank)	COG (empty box)			
	COG (full box)			
	proximal jt ctr			
	lateral maleolus			
	distal jt ctr			
Left Crus (Shank)	COG (empty box)			
	COG (full box)			
	proximal jt ctr			
	lateral maleolus			
	distal jt ctr			
Right Thigh	COG (empty box)			
	COG (full box)			
	proximal jt ctr			
	ischium			
	trochanterion			
	distal jt ctr			
Left Thigh	COG (empty box)			
	COG (full box)			
	proximal jt ctr			
	ischium			
	trochanterion			
	distal jt ctr			
Head	COG (empty box)			
	COG (full box)			
	proximal jt ctr			
	tip of nose			
	Nasion			
	R tragion			
	L tragion			
Neck	COG (empty box)			
	COG (full box)			
	cranial sgmt ctr (@ head)			

	caudal sgmt ctr (@ shldr)			
	cranial jt ctr @ spine (@ head)			
	caudal jt ctr @ spine (@ shldr)			
Tail	COG (empty box)			
	COG (full box)			
	cranial segment ctr			
	tip of tail			
	cranial jt ctr			
Thorax	COG (empty box)			
	COG (full box)			
	caudal jt ctr @ spine			
	cranial jt ctr @ spine			
	caudal segment ctr			
	cranial segment ctr			
	T1 (btwn shoulder blades)			
	T13 spinous process			
Abdomen	COG (empty box)			
	COG (full box)			
	caudal jt ctr			
	cranial jt ctr			
	caudal segment ctr			
	cranial segment ctr			
	l crest of ilium			
	l hip jt ctr			
	l top of hip			
	r crest of ilium			
	r hip jt ctr			
	r top of hip			

APPENDIX E: MORPHOMETRY AND BODY SEGMENT PARAMETERS

Subject/Parameter	segmented / intact/3D	1	2	3	4	5	6	Min	Max	Mean	SE Mean
Left Manus/Forepaw											
Mass (kg)		0.2676	0.2640	0.2306	0.2614	0.2736	0.3046	0.2306	0.3046	0.2670	0.0097
Volume (m^3)		0.00029	0.00027	0.00026	0.00030	0.00026	0.00033	0.00026	0.00033	0.00029	0.00001
Density (kg/m^3)		916.438	977.901	886.795	871.222	1036.237	920.342	871.222	1036.237	934.823	25.193
Manus l (m)	3D*	0.1652	0.1611	0.1609	0.1668	0.1656	0.1663	0.1609	0.1668	0.1643	0.0011
	segmented	0.1639	0.1650	0.1618	0.1650	0.1667	0.1640	0.1618	0.1667	0.1644	0.0007
Paw only l (m)	segmented	0.0780	0.0835	0.0800	0.0850	0.0760	0.0750	0.0750	0.0850	0.0796	0.0016
	intact	0.0800	0.0815	0.0800	0.0830	0.0760	0.0680	0.0680	0.0830	0.0781	0.0022
Wrist jt ctr to mcpj III l (m)	segmented	0.1039	0.0920	0.0854	0.1000	0.1057	0.0830	0.0830	0.1057	0.0950	0.0039
Mcpj - dactylion III l (m)	intact	0.0610	0.0700	0.0690	0.0670	0.0640	0.0530	0.0530	0.0700	0.0640	0.0026
Wrist c (m)	segmented*	0.1600	0.1620	0.1500	0.1570	0.1580	0.1680	0.1500	0.1680	0.1592	0.0024
	intact	0.1550	0.1600	0.1500	0.1600	0.1600	0.1630	0.1500	0.1630	0.1580	0.0019
Carp/Metacarp c (m)	segmented*	0.1610	0.1550	0.1450	0.1400	0.1360	0.1620	0.1360	0.1620	0.1498	0.0045
Manus c (m)	intact*	0.1840	0.1690	0.1510	0.1650	0.1680	0.1930	0.1510	0.1930	0.1717	0.0061
	segmented	0.1800	0.1620	0.1600	0.1630	0.1680	0.1930	0.1600	0.1930	0.1710	0.0053
Carp/Metacarp b (m)	intact	0.0470	0.0460	0.0390	0.0460	0.0480	0.0480	0.0390	0.0480	0.0457	0.0014
Manus b (m)	intact*	0.0630	0.0570	0.0570	0.0620	0.0571	0.0680	0.0570	0.0680	0.0607	0.0018
	segmented	0.0670	0.0685	0.0690	0.0650	0.0610	0.0740	0.0610	0.0740	0.0674	0.0018
Wrist b (m)	segmented*	0.0450	0.0460	0.0404	0.0419	0.0408	0.0440	0.0404	0.0460	0.0430	0.0009
	intact	0.0440	0.0500	0.0460	0.0420	0.0430	0.0530	0.0420	0.0530	0.0463	0.0018
Manus d (m)	intact	0.0380	0.0330	0.0340	0.0460	0.0430	0.0480	0.0330	0.0480	0.0403	0.0026
Carp/Metacarp d (m)	intact	0.0320	0.0360	0.0280	0.0320	0.0270	0.0350	0.0270	0.0360	0.0317	0.0015
$I_{int/ext}$ (kg*m^2)		0.00062	0.00069	0.00046	0.00043	0.00053	0.00073	0.00043	0.00073	0.00058	0.00005
$I_{abd/add}$ (kg*m^2)		0.00128	0.00082	0.00055	0.00134	0.00120	0.00124	0.00055	0.00134	0.00107	0.00013
$I_{flx/ext}$ (kg*m^2)		0.00122	0.00084	0.00066	0.00136	0.00122	0.00109	0.00066	0.00136	0.00107	0.00011

Left manus/forepaw		Paired Differences								Paired Sample Correlations	
					95% Confidence Interval of the Difference						
		Mean	Std. Deviation	Std. Error Mean	Lower	Upper	t	df	Sig. (2-tailed)	Correlation	Sig.
Pair 1	Left_Manus l (m)_3D - Left_Manus l (m)_s	-.00008	.00233	.00095	-.00252	.00236	-.082	5	.938	.484	.331
Pair 2	pawonly_l_s - pawonly_l_i	.00150	.00308	.00126	-.00173	.00473	1.192	5	.287	.831	.040
Pair 3	wrist_c_s - wrist_c_i	.00117	.00343	.00140	-.00243	.00477	.833	5	.443	.817	.047
Pair 4	carp/meta_c_s - carp/meta_c_i	-.02183	.01011	.00413	-.03244	-.01123	-5.291	5	.003	.732	.098
Pair 5	manus_c_s - manus_c_i	-.12533	.01140	.00465	-.13729	-.11337	-26.940	5	.000	.565	.243
Pair 6	manus_b_s - manus_b_i	-.02440	.00394	.00161	-.02854	-.02026	-15.161	5	.000	.431	.394
Pair 7	wrist_b_s - wrist_b_i	.00600	.00767	.00313	-.00205	.01405	1.917	5	.113	-.012	.982

Right Manus/Forepaw											
Subject/Parameter		1	2	3	4	5	6	Min	Max	Mean	SE Mean
Mass (kg)		0.2746	0.2725	0.2304	0.2546	0.2566	0.3121	0.2304	0.3121	0.2668	0.0111
Volume (m^3)		0.00030	0.00028	0.00024	0.00025	0.00032	0.00034	0.00024	0.00034	0.00029	0.00002
Density (kg/m^3)		915.333	973.262	960.000	1018.267	814.497	917.941	814.497	1018.267	933.217	28.403
Manus l (m)	segmented*	0.1655	0.1640	0.1659	0.1640	0.1614	0.1700	0.1614	0.1700	0.1651	0.0012
	3D	0.1654	0.1579	0.1660	0.1642	0.1640	0.1664	0.1579	0.1664	0.1640	0.0013
Paw only l (m)	segmented	0.0819	0.0820	0.0820	0.0830	0.0783	0.0730	0.0730	0.0830	0.0800	0.0016
	intact	0.0800	0.0815	0.0800	0.0830	0.0760	0.0710	0.0710	0.0830	0.0786	0.0018
Wrist jt ctr to mcpj III l (m	segmented*	0.1040	0.0800	0.0735	0.0950	0.0994	0.0990	0.0735	0.1040	0.0918	0.0050
Mcpj - dactylion III l (m)	intact	0.0520	0.1370	0.0700	0.0670	0.0640	0.0580	0.0520	0.1370	0.0747	0.0127
Wrist c (m)	segmented*	0.1600	0.1590	0.1480	0.1600	0.1600	0.1680	0.1480	0.1680	0.1592	0.0026
	intact	0.1550	0.1560	0.1500	0.1600	0.1600	0.1630	0.1500	0.1630	0.1573	0.0019
Carp/Metacarp c (m)	segmented*	0.1610	0.1550	0.1480	0.1400	0.1360	0.1600	0.1360	0.1610	0.1500	0.0043
Manus c (m)	intact*	0.1840	0.1690	0.1510	0.1630	0.1810	0.1910	0.1510	0.1910	0.1732	0.0061
	segmented	0.1870	0.1570	0.1610	0.1630	0.1810	0.1910	0.1570	0.1910	0.1733	0.0060
Carp/Metacarp b (m)	intact	0.0470	0.0460	0.0380	0.0460	0.0480	0.0460	0.0380	0.0480	0.0452	0.0015
Manus b (m)	intact*	0.0659	0.0510	0.0580	0.0660	0.0532	0.0670	0.0510	0.0670	0.0602	0.0029
	segmented	0.0660	0.0675	0.0490	0.0650	0.0610	0.0740	0.0490	0.0740	0.0638	0.0034
Wrist b (m)	segmented*	0.0384	0.0420	0.0373	0.0419	0.0459	0.0440	0.0373	0.0459	0.0416	0.0013
	intact	0.0440	0.0490	0.0450	0.0420	0.0430	0.0540	0.0420	0.0540	0.0462	0.0019
Manus d (m)	intact	0.0370	0.0345	0.0330	0.0460	0.0430	0.0510	0.0330	0.0510	0.0408	0.0029
Carp/Metacarp d (m)	intact	0.0540	0.0370	0.0280	0.0320	0.0270	0.0350	0.0270	0.0540	0.0355	0.0040
$I_{int/ext}$ ($kg*m^2$)		0.00052	0.00115	0.00078	0.00054	0.00056	0.00064	0.00052	0.00115	0.00070	0.00010
$I_{abd/add}$ ($kg*m^2$)		0.00105	0.00049	0.00076	0.00142	0.00106	0.00112	0.00049	0.00142	0.00098	0.00013
$I_{flx/ext}$ ($kg*m^2$)		0.00051	0.00142	0.00098	0.00067	0.00089	0.00094	0.00051	0.00142	0.00090	0.00013

Right manus/forepaw		Paired Differences								Paired Sample Correlations	
					95% Confidence Interval of the Difference						
		Mean	Std. Deviation	Std. Error Mean	Lower	Upper	t	df	Sig. (2-tailed)	Correlation	Sig.
Pair 1	manus_l_3D-manus l_s	-.00118	.00314	.00128	-.00447	.00212	-.919	5	.400	.454	.365
Pair 2	pawonly_l_s - pawonly_l_i	.00145	.00095	.00039	.00045	.00245	3.729	5	.014	.983	.000
Pair 3	wrist_c_s - wrist_c_i	.00183	.00293	.00119	-.00124	.00490	1.534	5	.186	.908	.012
Pair 4	carpusmeta_c_s - carpusmeta_c_i	-.02317	.01434	.00586	-.03822	-.00811	-3.956	5	.011	.402	.429
Pair 5	manus_c_s - manus_c_i	-.12817	.01336	.00546	-.14219	-.11414	-23.494	5	.000	.482	.333
Pair 6	manus_b_s - manus_b_i	-.02217	.00724	.00296	-.02977	-.01456	-7.496	5	.001	.519	.292
Pair 7	wrist_b_s - wrist_b_i	.00542	.00710	.00290	-.00204	.01287	1.868	5	.121	.316	.542

Subject/Parameter	Combined	1	2	3	4	5	6	1	2	3	4	5	6	Min	Max	x̄	σx̄
		Left Manus						Right Manus									
Mass (kg)		0.2676	0.2640	0.2306	0.2614	0.2736	0.3046	0.2746	0.2725	0.2304	0.2546	0.2566	0.3121	0.2304	0.3121	0.2669	0.0100
Volume (m^3)		0.00029	0.00027	0.00026	0.00030	0.00026	0.00033	0.00030	0.00028	0.00024	0.00025	0.00032	0.00034	0.000240	0.000340	0.000287	0.000013
Density (kg/m^3)		916.44	977.90	886.79	871.22	1036.24	920.34	915.33	973.26	960.00	1018.27	814.50	917.94	814.50	1036.24	934.02	25.60
Manus l (m)	segmented*	0.165	0.161	0.161	0.167	0.166	0.166	0.166	0.164	0.166	0.164	0.161	0.170	0.161	0.170	0.165	0.001
	3D	0.1639	0.165	0.1618	0.165	0.16665	0.164	0.1654	0.1579	0.1660	0.1642	0.1640	0.1664	0.1579	0.1667	0.1642	0.0010
Paw only l (m)	segmented	0.078	0.0835	0.08	0.085	0.076	0.075	0.0819	0.0820	0.0820	0.0830	0.0783	0.0730	0.0730	0.0850	0.0798	0.0015
	intact	0.08	0.0815	0.08	0.083	0.076	0.068	0.0800	0.0815	0.0800	0.0830	0.0760	0.0710	0.0680	0.0830	0.0783	0.0019
Wrist jt ctr to mcpj III l (m)	segmented*	0.1039	0.092	0.0854	0.1	0.1057	0.083	0.1040	0.0800	0.0735	0.0950	0.0994	0.0990	0.0735	0.1057	0.0934	0.0043
Mcpj - dactylion III l (m)	intact	0.061	0.07	0.069	0.067	0.064	0.053	0.0520	0.1370	0.0700	0.0670	0.0640	0.0580	0.0520	0.1370	0.0693	0.0091
Wrist c (m)	segmented*	0.16	0.162	0.15	0.157	0.158	0.168	0.1600	0.1590	0.1480	0.1600	0.1600	0.1680	0.1480	0.1680	0.1592	0.0024
	intact	0.155	0.16	0.15	0.16	0.16	0.163	0.1550	0.1560	0.1500	0.1600	0.1600	0.1630	0.1500	0.1630	0.1577	0.0018
Carp/Metacarp c (m)	segmented*	0.161	0.155	0.145	0.14	0.136	0.162	0.1610	0.1550	0.1480	0.1400	0.1360	0.1600	0.1360	0.1620	0.1499	0.0042
Manus c (m)	intact*	0.184	0.169	0.151	0.165	0.168	0.193	0.1840	0.1690	0.1510	0.1630	0.1810	0.1910	0.1510	0.1930	0.1724	0.0058
	segmented	0.18	0.162	0.16	0.163	0.168	0.193	0.1870	0.1570	0.1610	0.1630	0.1810	0.1910	0.1570	0.1930	0.1722	0.0054
Carp/Metacarp b (m)	intact	0.047	0.046	0.039	0.046	0.048	0.048	0.0470	0.0460	0.0380	0.0460	0.0480	0.0460	0.0380	0.0480	0.0454	0.0014
Manus b (m)	intact*	0.063	0.057	0.057	0.062	0.0571	0.068	0.0659	0.0510	0.0580	0.0660	0.0532	0.0670	0.0510	0.0680	0.0604	0.0023
	segmented	0.067	0.0685	0.069	0.065	0.061	0.074	0.0660	0.0675	0.0490	0.0650	0.0610	0.0740	0.0490	0.0740	0.0656	0.0027
Wrist b (m)	segmented*	0.045	0.046	0.0404	0.0419	0.0408	0.044	0.0384	0.0420	0.0373	0.0419	0.0459	0.0440	0.0373	0.0460	0.0423	0.0011
	intact	0.044	0.05	0.046	0.042	0.043	0.053	0.0440	0.0490	0.0450	0.0420	0.0430	0.0540	0.0420	0.0540	0.0463	0.0017
Manus d (m)	intact	0.038	0.033	0.034	0.046	0.043	0.048	0.0370	0.0345	0.0330	0.0460	0.0430	0.0510	0.0330	0.0510	0.0405	0.0026
Carp/Metacarp d (m)	intact	0.032	0.036	0.028	0.032	0.027	0.035	0.0540	0.0370	0.0280	0.0320	0.0270	0.0350	0.0270	0.0540	0.0336	0.0030
$I_{int/ext}$ ($kg*m^2$)		0.00062	0.00069	0.00046	0.00043	0.00053	0.00073	0.00052	0.00115	0.00078	0.00054	0.00056	0.00064	0.00043	0.00115	0.00064	0.00008
$I_{abd/add}$ ($kg*m^2$)		0.00128	0.00082	0.00055	0.00134	0.00120	0.00124	0.00105	0.00049	0.00076	0.00142	0.00106	0.00112	0.00049	0.00142	0.00103	0.00013
$I_{flx/ext}$ ($kg*m^2$)		0.00122	0.00084	0.00066	0.00136	0.00122	0.00109	0.00051	0.00142	0.00098	0.00067	0.00089	0.00094	0.00051	0.00142	0.00098	0.00012

		Paired Differences								Paired Sample Correlations	
		Mean	Std. Deviation	Std. Error Mean	95% Confidence Interval of the Difference		t	df	Sig. (2-tailed)	Corr	Sig.
					Lower	Upper					
Pair 1	Manus_l_m_3D - Manus_l_m_s	.00055	.00340	.00098	-.00161	.00271	.560	11	.587	.093	.773
Pair 2	Paw_l_m_s - Paw_l_m_i	.00148	.00218	.00063	.00009	.00286	2.349	11	.039	.894	.000
Pair 3	Wrist_c_m_s - Wrist_c_m_i	.00150	.00306	.00088	-.00044	.00344	1.698	11	.118	.861	.000
Pair 4	Manus_c_m_i - Manus_c_m_s	.00025	.00605	.00175	-.00359	.00409	0.143	11	.889	.905	.000
Pair 5	Manus_b_m_i - Manus_b_m_s	-.00515	.00673	.00194	-.00943	-.00087	-2.651	11	.023	.410	.185
Pair 6	Wrist_b_m_s - Wrist_b_m_i	-.00395	.00421	.00122	-.00663	-.00127	-3.249	11	.008	.336	.286

Left Antebrachium/Forearm											
Subject/Parameter		1	2	3	4	5	6	Min	Max	Mean	SE Mean
Mass (kg)		0.5393	0.4455	0.4178	0.5010	0.5252	0.5897	0.4178	0.5897	0.5031	0.0257
Volume (m^3)		0.00059	0.00046	0.00039	0.00051	0.00054	0.00061	0.00039	0.00061	0.00052	0.00003
Density (kg/m^3)		914.068	968.551	1071.368	982.288	972.593	963.562	914.068	1071.368	978.738	20.934
Antebrachium l prox-dist(m)	segmented*	0.2200	0.2080	0.2050	0.2020	0.2272	0.2280	0.2020	0.2280	0.2150	0.0047
	3D	0.2114	0.1964	0.2117	0.2018	0.2223	0.2200	0.1964	0.2223	0.2106	0.0041
Olecranon-stylion	intact	0.2340	0.1860	0.2120	0.2190	0.2030	0.2430	0.1860	0.2430	0.2162	0.0085
Radiale-stylion	intact	0.1950	0.1640	0.2070	0.1980	0.1900	0.2230	0.1640	0.2230	0.1962	0.0080
Elbow c (m)	segmented*	0.2420	0.2620	0.2380	0.2750	0.2500	0.2500	0.2380	0.2750	0.2528	0.0056
Mid c (m)	segmented*	0.1850	0.1750	0.1750	0.1800	0.1800	0.1930	0.1750	0.1930	0.1813	0.0028
Elbow b (m)	intact*	0.0510	0.0690	0.0500	0.0530	0.0620	0.0540	0.0500	0.0690	0.0565	0.0030
	segmented	0.0530	0.0650	0.0520	0.0540	0.0496	0.0540	0.0496	0.0650	0.0546	0.0022
	brach	0.0527	0.0600	0.0510	0.0530	0.0496	0.0510	0.0496	0.0600	0.0529	0.0015
$I_{int/ext}$ ($kg*m^2$)		0.00111	0.00048	0.00081	0.00123	0.00108	0.00120	0.00048	0.00123	0.00099	0.00012
$I_{abd/add}$ ($kg*m^2$)		0.00297	0.00398	0.00330	0.00293	0.00274	0.00327	0.00274	0.00398	0.00320	0.00018
$I_{flx/ext}$ ($kg*m^2$)		0.00304	0.00208	0.00236	0.00294	0.00288	0.00296	0.00208	0.00304	0.00271	0.00016

			Paired Differences							Paired Sample Correlations	
		Mean	Std. Deviation	Std. Error Mean	95% Confidence		t	df	Sig. (2-tailed)	Corr	Sig.
					Lower	Upper					
Pair 1	Antebrachium_l_prox_dist_3D - Antebrachium_l_prox_dist_cut	-.004440	.006672	.002724	-.011442	.002562	-1.630	5	.164	0.81657	0.04739

Within-Subjects Factors			Mauchly's Test of Sphericity[a]								
elbow_b	Dependent Variable							Epsilon[b]			
1	Elbow_b_i		Within Subjects Effect	Mauchly's W	Approx. Chi-Square	df	Sig.	Greenhouse-Geisser	Huynh-Feldt	Lower-bound	
2	Elbow_b_s		elbow_b	.291	4.938	2	.085	.585	.656	.500	
3	Elbow_b_brach		Tests the null hypothesis that the error covariance matrix of the orthonormalized								
			a. Design: Intercept								
			b. May be used to adjust the degrees of freedom for the averaged tests of significance.								

Tests of Within-Subjects Effects						
Source		Type III Sum of Squares	df	Mean Square	F	Sig.
elbow_b	Sphericity Assumed	3.942E-05	2	1.971E-05	1.717	.228
Error(elbow_b)	Sphericity Assumed	.000	10	1.148E-05		

Right Antebrachium/Forearm											
Subject/Parameter		1	2	3	4	5	6	Min	Max	Mean	SE Mean
Mass (kg)		0.4949	0.5129	0.4268	0.4777	0.5446	0.5985	0.4268	0.5985	0.5092	0.0240
Volume (m^3)		0.00054	0.00055	0.00039	0.00052	0.00053	0.00062	0.00039	0.00062	0.00052	0.00003
Density (kg/m^3)		916.481	932.606	1094.274	918.718	1027.610	968.393	916.481	1094.274	976.347	29.107
Antebrachium l prox-dist(m)	segmented*	0.1920	0.2180	0.2000	0.2000	0.2381	0.2320	0.1920	0.2381	0.2134	0.0077
	3D	0.1931	0.2245	0.2124	0.1951	0.2304	0.2261	0.1931	0.2304	0.2136	0.0066
Olecranon-stylion	intact	0.2430	0.1860	0.2090	0.2190	0.2030	0.2430	0.1860	0.2430	0.2172	0.0093
Radiale-stylion	intact	0.1980	0.1630	0.2060	0.1980	0.1900	0.2270	0.1630	0.2270	0.1970	0.0085
Elbow c (m)	segmented*	0.2400	0.2540	0.2310	0.2750	0.2500	0.2520	0.2310	0.2750	0.2503	0.0061
Mid c (m)	segmented*	0.1900	0.2000	0.1700	0.1750	0.1750	0.1970	0.1700	0.2000	0.1845	0.0052
Elbow b (m)	intact*	0.0500	0.0670	0.0500	0.0530	0.0620	0.0560	0.0500	0.0670	0.0563	0.0028
	segmented	0.0500	0.0650	0.0520	0.0530	0.0527	0.0560	0.0500	0.0650	0.0548	0.0022
	brach	0.0521	0.0630	0.0505	0.0527	0.0465	0.0530	0.0465	0.0630	0.0530	0.0022
$I_{int/ext}$ ($kg*m^2$)		0.00122	0.00092	0.00044	0.00132	0.00075	0.00122	0.00044	0.00132	0.00098	0.00014
$I_{abd/add}$ ($kg*m^2$)		0.00247	0.00456	0.00313	0.00252	0.00322	0.00413	0.00247	0.00456	0.00334	0.00035
$I_{flx/ext}$ ($kg*m^2$)		0.00203	0.00331	0.00254	0.00211	0.00275	0.00324	0.00203	0.00331	0.00266	0.00022

		Paired Differences							Sig. (2-tailed)	Paired Sample Correlations	
		Mean	Std. Deviation	Std. Error Mean	95% Confidence		t	df		Corr	Sig.
					Lower	Upper					
Pair 1	Antebrachium_l_prox_dist_3D - Antebrachium_l_prox_dist_cut	.000268	.007942	.003242	-.008067	.008603	.083	5	.937	.909	.012

Within-Subjects Factors			Mauchly's Test of Sphericity[a]								
elbow_b	Dependent Variable								Epsilon[b]		
1	Elbow_b_i		Within Subjects Effect	Mauchly's W	Approx. Chi-Square	df	Sig.	Greenhouse-Geisser	Huynh-Feldt	Lower-bound	
2	Elbow_b_s		elbow_b	.156	7.427	2	.024	.542	.576	.500	
3	Elbow_b_brach		Tests the null hypothesis that the error covariance matrix of the orthonormalized								
			a. Design: Intercept								
			b. May be used to adjust the degrees of freedom for the averaged tests of significance. Corrected tests are displayed in the Tests of Within-Subjects Effects table.								

Tests of Within-Subjects Effects							
Source		Type III Sum of Squares	df	Mean Square	F	Sig.	
elbow_b	Greenhouse-Geisser	3.401E-05	1	3.135E-05	1.590	.228	
Error(elbow_b)	Greenhouse-Geisser	.000	5	1.972E-05			

Combined		Left Antebrachium						Right Antebrachium									
Subject/Param		1	2	3	4	5	6	1	2	3	4	5	6	Min	Max	$\bar{x}$	$\sigma\bar{x}$
Mass (kg)		0.5393	0.4455	0.4178	0.5010	0.5252	0.5897	0.4949	0.5129	0.4268	0.4777	0.5446	0.5985	0.4178	0.5985	0.5062	0.0238
Volume (m^3)		0.00059	0.00046	0.00039	0.00051	0.00054	0.00061	0.00054	0.00055	0.00039	0.00052	0.00053	0.00062	0.00039	0.00062	0.00052	0.00003
Density (kg/m^3)		914.068	968.551	1071.368	982.288	972.593	963.562	916.481	932.606	1094.274	918.718	1027.610	968.393	914.068	1094.274	977.543	24.177
Antebrachium l prox-dist(m)	segmented*	0.2200	0.2080	0.2050	0.2020	0.2272	0.2280	0.1920	0.2180	0.2000	0.2000	0.2381	0.2320	0.1920	0.2381	0.2142	0.0061
	3D	0.2114	0.1964	0.2117	0.2018	0.2223	0.2200	0.1931	0.2245	0.2124	0.1951	0.2304	0.2261	0.1931	0.2304	0.2121	0.0053
Olecranon-	intact	0.2340	0.1860	0.2120	0.2190	0.2030	0.2430	0.2430	0.1860	0.2090	0.2190	0.2030	0.2430	0.1860	0.2430	0.2167	0.0085
Radiale-	intact	0.1950	0.1640	0.2070	0.1980	0.1900	0.2230	0.1980	0.1630	0.2060	0.1980	0.1900	0.2270	0.1630	0.2270	0.1966	0.0079
Elbow c (m)	segmented*	0.2420	0.2620	0.2380	0.2750	0.2500	0.2500	0.2400	0.2540	0.2310	0.2750	0.2500	0.2520	0.2310	0.2750	0.2516	0.0056
Mid c (m)	segmented*	0.1850	0.1750	0.1750	0.1800	0.1800	0.1930	0.1900	0.2000	0.1700	0.1750	0.1750	0.1970	0.1700	0.2000	0.1829	0.0040
Elbow b (m)	intact*	0.0510	0.0690	0.0500	0.0530	0.0620	0.0540	0.0500	0.0670	0.0500	0.0530	0.0620	0.0560	0.0500	0.0690	0.0564	0.0028
	segmented	0.0530	0.0650	0.0520	0.0540	0.0496	0.0540	0.0500	0.0650	0.0520	0.0530	0.0527	0.0560	0.0496	0.0650	0.0547	0.0021
	brach	0.0527	0.0600	0.0510	0.0530	0.0496	0.0510	0.0521	0.0630	0.0505	0.0527	0.0465	0.0530	0.0465	0.0630	0.0529	0.0018
$I_{int/ext}$ ($kg*m^2$)		0.00111	0.00048	0.00081	0.00123	0.00108	0.00120	0.00122	0.00092	0.00044	0.00132	0.00075	0.00122	0.00044	0.00132	0.00098	0.00012
$I_{abd/add}$ ($kg*m^2$)		0.00297	0.00398	0.00330	0.00293	0.00274	0.00327	0.00247	0.00456	0.00313	0.00252	0.00322	0.00413	0.00247	0.00456	0.00327	0.00026
$I_{flx/ext}$ ($kg*m^2$)		0.00304	0.00208	0.00236	0.00294	0.00288	0.00296	0.00203	0.00331	0.00254	0.00211	0.00275	0.00324	0.00203	0.00331	0.00269	0.00018

		Paired Samples Test								Paired Sample Correlations	
		Paired Differences									
					95% Confidence Interval of the						
		Mean	Std. Deviation	Std. Error Mean	Lower	Upper	t	df	Sig. (2-tailed)	Correlation	Sig.
Pair 1	Antebrachium_l_proxdist_m_s - Antebrachium_l_proxdist_m_3d	.0021	.0074	.0021	-.0026	.0068	.975	11	.351	.869	.000

Within-Subjects Factors			Mauchly's Test of Sphericity[a]							
Elbow_breadth	Dependent Variable								Epsilon[b]	
1	Elbow_b_m_i		Within Subjects Effect	Mauchly's W	Approx. Chi-Square	df	Sig.	Greenhouse-Geisser	Huynh-Feldt	Lower-bound
2	Elbow_b_m_s		Elbow_breadth	.326	11.198	2	.004	.597	.629	.500
3	Brachium_b		Tests the null hypothesis that the error covariance matrix of the orthonormalized							
			a. Design: Intercept							
			b. May be used to adjust the degrees of freedom for the averaged tests of significance.							

Tests of Within-Subjects Effects

Source		Type III Sum of Squares	df	Mean Square	F	Sig.
Elbow_breadth	Sphericity Assumed	7.322E-05	2	3.7E-05	3.630	.043
	Greenhouse-Geisser	7.322E-05	1.195	6.1E-05	3.630	.073
	Huynh-Feldt	7.322E-05	1.259	5.8E-05	3.630	.070
	Lower-bound	7.322E-05	1.000	7.3E-05	3.630	.083
Error(Elbow_breadth)	Sphericity Assumed	.000	22	1.0E-05		
	Greenhouse-Geisser	.000	13.145	1.7E-05		
	Huynh-Feldt	.000	13.844	1.6E-05		
	Lower-bound	.000	11.000	2.0E-05		

Left Brachium/Upper Arm											
Subject/Parameter		1	2	3	4	5	6	Min	Max	Mean	SE Mean
Mass (kg)		0.7337	0.7550	1.1442	1.0729	1.0969	0.7791	0.7337	1.1442	0.9303	0.0788
Volume (m^3)		0.000770	0.000770	0.001150	0.001110	0.001220	0.000845	0.0008	0.0012	0.000978	0.0001
Density (kg/m^3)		952.8571	980.4762	994.9275	966.6066	899.1257	922.0118	899.1257	994.9275	952.6675	14.7875
Prox-Dist l (m)	3D*	0.1538	0.1715	0.1814	0.1639	0.1746	0.1462	0.1462	0.1814	0.1652	0.0054
	segmented	0.1473	0.1720	0.1701	0.1669	0.1789	0.1500	0.1473	0.1789	0.1642	0.0052
Acromion-radiale l (m)	segmented*	0.1660	0.1840	0.2009	0.2053	0.1874	0.1640	0.1640	0.2053	0.1846	0.0070
	intact	0.1650	0.2090	0.1620	0.1830	0.1750	0.1970	0.1620	0.2090	0.1818	0.0075
Humerus-radiale l (m)	segmented*	0.1489	0.1440	0.1716	0.1692	0.1468	0.1470	0.1440	0.1716	0.1546	0.0051
	intact	0.1450	0.2000	0.1700	0.1610	0.1630	0.1670	0.1450	0.2000	0.1677	0.0074
Axillary c (m)	segmented*	0.3900	0.4150	0.4280	0.3450	0.4200	0.4230	0.3450	0.4280	0.4035	0.0129
Mid-brachium c (m)	segmented*	0.3200	0.3100	0.3120	0.2700	0.3000	0.3550	0.2700	0.3550	0.3112	0.0113
$I_{int/ext}$ (kg*m^2)		0.00290	0.00130	0.00378	0.00409	0.00353	0.00271	0.0013	0.0041	0.00305	0.0004
$I_{abd/add}$ (kg*m^2)		0.00377	0.00768	0.00750	0.00483	0.00573	0.00699	0.0038	0.0077	0.00608	0.0006
$I_{flx/ext}$ (kg*m^2)		0.00363	0.00313	0.00467	0.00575	0.00565	0.00369	0.0031	0.0057	0.00442	0.0005

		Paired Differences								Paired Sample Correlations	
					95% Confidence Interval of the Difference						
		Mean	Std. Deviation	Std. Error Mean	Lower	Upper	t	df	Sig. (2-tailed)	Correlation	Sig.
Pair 1	prox_dist_l_s - prox_dist_l_3D	-.001043	.006408	.002616	-.007768	.005682	-.399	5	.707	.879	.021
Pair 2	Acromion_radiale_l_i - Acromion_radiale_l_s	-.002767	.027689	.011304	-.031824	.026291	-.245	5	.816	-.211	.688
Pair 3	Hum_rad_l_i - Hum_rad_l_s	.013083	.023901	.009758	-.012000	.038166	1.341	5	.238	-.206	.696

Right Brachium/Upper Arm											
Subject/Parameter		1	2	3	4	5	6	Min	Max	Mean	SE Mean
Mass (kg)		0.6844	0.6312	0.9477	1.1068	0.7000	0.9086	0.6312	1.1068	0.8298	0.0762
Volume (m^3)		0.00069	0.00064	0.00095	0.00116	0.00065	0.00094	0.00064	0.00116	0.00084	0.00009
Density (kg/m^3)		991.836	986.198	997.544	954.138	1076.923	969.691	954.138	1076.923	996.055	17.425
Prox-dist jt ctr l (m)	segmented*	0.1485	0.1630	0.1672	0.1636	0.1564	0.1560	0.1485	0.1672	0.1591	0.0028
	3D	0.1665	0.1627	0.1829	0.1640	0.1608	0.1470	0.1470	0.1829	0.1640	0.0047
Acromion-radiale l (m)	segmented*	0.1720	0.1800	0.1993	0.2058	0.1830	0.1750	0.1720	0.2058	0.1859	0.0056
	intact	0.1650	0.2070	0.1600	0.1830	0.1750	0.1970	0.1600	0.2070	0.1812	0.0075
Humerus-radiale l (m)	segmented*	0.1480	0.1480	0.1700	0.1690	0.1460	0.1560	0.1460	0.1700	0.1562	0.0044
	intact	0.1450	0.2080	0.1720	0.1610	0.1630	0.1670	0.1450	0.2080	0.1693	0.0086
Axillary c (m)	segmented*	0.3900	0.3850	0.4000	0.3730	0.4000	0.4000	0.3730	0.4000	0.3913	0.0045
Mid-brachium c (m)	segmented*	0.3200	0.3200	0.3100	0.2700	0.3100	0.3480	0.2700	0.3480	0.3130	0.0103
$I_{int/ext}$ ($kg*m^2$)		0.00267	0.00168	0.00285	0.00494	0.00271	0.00267	0.00168	0.00494	0.00292	0.00044
$I_{abd/add}$ ($kg*m^2$)		0.00316	0.00189	0.00419	0.00783	0.00363	0.00457	0.00189	0.00783	0.00421	0.00082
$I_{flx/ext}$ ($kg*m^2$)		0.00307	0.00216	0.00406	0.00888	0.00420	0.00354	0.00216	0.00888	0.00432	0.00096

		Paired Differences								Paired Sample Correlations	
					95% Confidence Interval of the Difference						
		Mean	Std. Deviation	Std. Error Mean	Lower	Upper	t	df	Sig. (2-tailed)	Correlation	Sig.
Pair 1	prox_dist_l_s - prox_dist_l_3D	.004881	.010283	.004198	-.005910	.015673	1.163	5	.297	.466	.351
Pair 2	Acromion_radiale_l_i - Acromion_radiale_l_s	-.004683	.025529	.010422	-.031475	.022108	-.449	5	.672	-.264	.613
Pair 3	Hum_rad_l_i - Hum_rad_l_s	.013160	.024691	.010080	-.012751	.039071	1.306	5	.249	-.108	.839

Combined		Left Brachium						Right Brachium									
Subject/Parameter		1	2	3	4	5	6	1	2	3	4	5	6	Min	Max	$\bar{x}$	$\sigma\bar{x}$
Mass (kg)		0.7337	0.7550	1.1442	1.0729	1.0969	0.7791	0.6844	0.6312	0.9477	1.1068	0.7000	0.9086	0.6312	1.1442	0.8800	0.0769
Volume (m^3)		0.00077	0.00077	0.00115	0.00111	0.00122	0.00085	0.00069	0.00064	0.00095	0.00116	0.00065	0.00094	0.00064	0.00122	0.00091	0.00009
Density (kg/m^3)		952.857	980.476	994.928	966.607	899.126	922.012	991.836	986.198	997.544	954.138	1076.923	969.691	899.126	1076.923	974.361	17.972
Prox-Dist l (m)	3D*	0.1538	0.1715	0.1814	0.1639	0.1746	0.1462	0.1665	0.1627	0.1829	0.1640	0.1608	0.1470	0.1462	0.1829	0.1646	0.0048
	segmented	0.1473	0.1720	0.1701	0.1669	0.1789	0.1500	0.1485	0.1630	0.1672	0.1636	0.1564	0.1560	0.1473	0.1789	0.1617	0.0041
Acromion-radiale l (m)	segmented*	0.1660	0.1840	0.2009	0.2053	0.1874	0.1640	0.1720	0.1800	0.1993	0.2058	0.1830	0.1750	0.1640	0.2058	0.1852	0.0060
	intact	0.1650	0.2090	0.1620	0.1830	0.1750	0.1970	0.1650	0.2070	0.1600	0.1830	0.1750	0.1970	0.1600	0.2090	0.1815	0.0071
Humerus-radiale l (m)	segmented*	0.1489	0.1440	0.1716	0.1692	0.1468	0.1470	0.1480	0.1480	0.1700	0.1690	0.1460	0.1560	0.1440	0.1716	0.1554	0.0045
	intact	0.1450	0.2000	0.1700	0.1610	0.1630	0.1670	0.1450	0.2080	0.1720	0.1610	0.1630	0.1670	0.1450	0.2080	0.1685	0.0076
Axillary c (m)	segmented*	0.3900	0.4150	0.4280	0.3450	0.4200	0.4230	0.3900	0.3850	0.4000	0.3730	0.4000	0.4000	0.3450	0.4280	0.3974	0.0096
Mid-brachium c (m)	segmented*	0.3200	0.3100	0.3120	0.2700	0.3000	0.3550	0.3200	0.3200	0.3100	0.2700	0.3100	0.3480	0.2700	0.3550	0.3121	0.0103
$I_{int/ext}$ (kg*m^2)		0.00290	0.00130	0.00378	0.00409	0.00353	0.00271	0.00267	0.00168	0.00285	0.00494	0.00271	0.00267	0.00130	0.00494	0.00299	0.00041
$I_{abd/add}$ (kg*m^2)		0.00377	0.00768	0.00750	0.00483	0.00573	0.00699	0.00316	0.00189	0.00419	0.00783	0.00363	0.00457	0.00189	0.00783	0.00515	0.00081
$I_{flx/ext}$ (kg*m^2)		0.00363	0.00313	0.00467	0.00575	0.00565	0.00369	0.00307	0.00216	0.00406	0.00888	0.00420	0.00354	0.00216	0.00888	0.00437	0.00072

		Paired Differences							Sig. (2-tailed)	Paired Sample Correlations	
		Mean	Std. Deviation	Error Mean	Interval of the Lower	Upper	t	df		Correlation	Sig.
Pair 1	Prox_Dist_l_3d - Prox_Dist_l_s	.002962	.008411	.002428	-.002382	.008306	1.220	11	.248	.717	.009
Pair 2	Acromion_radiale_l_s - Acromion_radiale_l_i	.003725	.025411	.007336	-.012421	.019871	.508	11	.622	-.234	.464
Pair 3	Humerus_radiale_l_s - Humerus_radiale_l_i	-.013122	.023168	.006688	-.027842	.001599	-1.962	11	.076	-.151	.641

Left Pes/Hindpaw											
Subject/Parameter		1	2	3	4	5	6	Min	Max	Mean	SE Mean
Mass (kg)		0.2923	0.3206	0.2771	0.2797	0.3127	0.3389	0.2771	0.3389	0.3036	0.0100
Volume (m^3)		0.00030	0.00033	0.00026	0.00026	0.00029	0.00034	0.00026	0.00034	0.00030	0.00001
Density (kg/m^3)		987.250	971.515	1065.897	1075.769	1078.276	988.144	971.515	1078.276	1027.809	20.563
Proxt jt ctr-tip of met III l (m)	segmented	0.2047	0.2048	0.1838	0.2018	0.2099	0.1980	0.1838	0.2099	0.2005	0.0037
Heel-tip of met III l (m)	segmented*	0.2305	0.2490	0.2390	0.2280	0.2370	0.2400	0.2280	0.2490	0.2373	0.0031
	3D	0.2352	0.2500	0.2392	0.2279	0.2365	0.2398	0.2279	0.2500	0.2381	0.0029
Heel-mtpj III l (m)	segmented	0.1650	0.1700	0.1583	0.1566	0.1620	0.1680	0.1566	0.1700	0.1633	0.0022
Pes (paw only) l (m)	segmented	0.0876	0.0780	0.0700	0.0782	0.0847	0.0730	0.0700	0.0876	0.0786	0.0027
tarsus/metatarsus l (m)	intact	0.1650	0.1690	0.1500	0.1520	0.1520	0.1690	0.1500	0.1690	0.1595	0.0037
Ankle c (m)	segmented	0.1965	0.2150	0.2020	0.1830	0.2020	0.2020	0.1830	0.2150	0.2001	0.0042
Mid-pes c (m)	intact	0.1320	0.1350	0.1170	0.1230	0.1300	0.1350	0.1170	0.1350	0.1287	0.0030
Pes c (m)	segmented	0.1600	0.1550	0.1410	0.1560	0.1490	0.1650	0.1410	0.1650	0.1543	0.0034
Ankle b (m)	intact	0.0420	0.0430	0.0410	0.0437	0.0407	0.0450	0.0407	0.0450	0.0426	0.0007
Pes b (m)	segmented	0.0576	0.0530	0.0515	0.0540	0.0510	0.0550	0.0510	0.0576	0.0537	0.0010
	intact	0.0560	0.0560	0.0500	0.0480	0.0500	0.0560	0.0480	0.0560	0.0527	0.0015
tarsus/metatarsus b (m)	intact	0.0390	0.0370	0.0380	0.0370	0.0410	0.0430	0.0370	0.0430	0.0392	0.0010
Pes d (m)	intact	0.0380	0.0420	0.0420	0.0420	0.0450	0.0460	0.0380	0.0460	0.0425	0.0011
tarsus/metatarsus d (m)	intact	0.0420	0.0430	0.0400	0.0380	0.0430	0.0440	0.0380	0.0440	0.0417	0.0009
$I_{int/ext}$ ($kg*m^2$)		0.00161	0.00220	0.00223	0.00150	0.00174	0.00167	0.0015	0.0022	0.00182	0.0001
$I_{abd/add}$ ($kg*m^2$)		0.00087	0.00062	0.00086	0.00100	0.00085	0.00079	0.0006	0.0010	0.00083	0.0001
$I_{flx/ext}$ ($kg*m^2$)		0.00160	0.00196	0.00174	0.00159	0.00176	0.00184	0.0016	0.0020	0.00175	0.0001

		Paired Differences								Paired Sample Correlations	
		Mean	Std. Deviation	Std. Error Mean	95% Confidence Interval of the		t	df	Sig. (2-tailed)	Correlation	Sig.
					Lower	Upper					
Pair 1	Heel_tip_of_pIII_l_3d - Heel_tip_of_pIII_l_cut	.00085	.00196	.00080	-.00121	.00291	1.064	5	.336	.965	.002

Right Pes/Hindpaw											
Subject/Parameter		1	2	3	4	5	6	Min	Max	Mean	SE Mean
Mass (kg)		0.2990	0.3230	0.2766	0.2808	0.3035	0.3343	0.2766	0.3343	0.3029	0.0093
Volume (m^3)		0.00031	0.00033	0.00026	0.00028	0.00031	0.00034	0.00026	0.00034	0.00030	0.00001
Density (kg/m^3)		980.328	978.788	1063.846	1002.857	979.140	974.636	974.636	1063.846	996.599	14.060
Proxt jt ctr-tip of met III l (m)	segmented*	0.2040	0.2048	0.1838	0.2008	0.2090	0.2020	0.1838	0.2090	0.2007	0.0036
Heel-tip of met III l (m)	segmented*	0.2351	0.2460	0.2261	0.2330	0.2467	0.2400	0.2261	0.2467	0.2378	0.0033
	3D	0.2377	0.2453	0.2345	0.2346	0.2383	0.2399	0.2345	0.2453	0.2384	0.0016
Heel-mtpj III l (m)	segmented*	0.1680	0.1750	0.1583	0.1688	0.1620	0.1630	0.1583	0.1750	0.1659	0.0024
Pes (paw only) l (m)	segmented*	0.0610	0.0800	0.0552	0.0653	0.0576	0.0650	0.0552	0.0800	0.0640	0.0036
tarsus/metatarsus l (m)	intact	0.1680	0.1750	0.1583	0.1688	0.1620	0.1630	0.1583	0.1750	0.1659	0.0024
Ankle c (m)	segmented	0.1980	0.2140	0.2010	0.1845	0.2020	0.2040	0.1845	0.2140	0.2006	0.0039
Mid-pes c (m)	intact	0.1330	0.1350	0.1170	0.1250	0.1310	0.1330	0.1170	0.1350	0.1290	0.0028
Pes c (m)	segmented	0.1680	0.1530	0.1410	0.1580	0.1490	0.1650	0.1410	0.1680	0.1557	0.0041
Ankle b (m)	intact	0.0420	0.0420	0.0410	0.0439	0.0407	0.0440	0.0407	0.0440	0.0423	0.0006
Pes b (m)	segmented*	0.0540	0.0530	0.0530	0.0550	0.0520	0.0540	0.0520	0.0550	0.0535	0.0004
	intact	0.0555	0.0570	0.0500	0.0500	0.0500	0.0560	0.0500	0.0570	0.0531	0.0014
tarsus/metatarsus b (m)	intact	0.0400	0.0380	0.0370	0.0350	0.0410	0.0440	0.0350	0.0440	0.0392	0.0013
Pes d (m)	intact	0.0420	0.0420	0.0419	0.0420	0.0420	0.0430	0.0419	0.0430	0.0422	0.0002
tarsus/metatarsus d (m)	intact	0.0420	0.0430	0.0340	0.0370	0.0430	0.0420	0.0340	0.0430	0.0402	0.0015
$I_{int/ext}$ (kg*m^2)		0.00135	0.00232	0.00219	0.00149	0.00207	0.00190	0.0013	0.0023	0.00189	0.0002
$I_{abd/add}$ (kg*m^2)		0.00093	0.00061	0.00078	0.00120	0.00097	0.00087	0.0006	0.0012	0.00089	0.0001
$I_{flx/ext}$ (kg*m^2)		0.00157	0.00183	0.00186	0.00160	0.00172	0.00182	0.0016	0.0019	0.00173	0.0001

		Paired Differences								Paired Sample Correlations	
					95% Confidence Interval of the Difference						
		Mean	Std. Deviation	Std. Error Mean	Lower	Upper	t	df	Sig. (2-tailed)	Correlation	Sig.
Pair 1	Heel_tip_of_met_III_l_3d - Heel_tip_of_met_III_l_cut	.00057	.00547	.00223	-.00517	.00630	.253	5	.810	.780	.067
Pair 2	Pes_b_i - Pes_b_s	-.00042	.00344	.00140	-.00403	.00319	-.297	5	.779	.126	.812

Combined		Left Pes						Right Pes						Min	Max	x̄	σx̄
Subject/Parameter		1	2	3	4	5	6	1	2	3	4	5	6				
Mass (kg)		0.2923	0.3206	0.2771	0.2797	0.3127	0.3389	0.2990	0.3230	0.2766	0.2808	0.3035	0.3343	0.2766	0.3343	0.3029	0.0093
Volume (m³)		0.00030	0.00033	0.00026	0.00026	0.00029	0.00034	0.00031	0.00033	0.00026	0.00028	0.00031	0.00034	0.00026	0.00034	0.00030	0.00001
Density (kg/m³)		987.250	971.515	1065.897	1075.769	1078.276	988.144	980.328	978.788	1063.846	1002.857	979.140	974.636	974.636	1063.846	996.599	14.060
Proxt jt ctr-tip of met III l (m)	segmented	0.2047	0.2048	0.1838	0.2018	0.2099	0.1980	0.2040	0.2048	0.1838	0.2008	0.2090	0.2020	0.1838	0.2090	0.2007	0.0036
Heel-tip of met III l (m)	segmented*	0.2305	0.2490	0.2390	0.2280	0.2370	0.2400	0.2351	0.2460	0.2261	0.2330	0.2467	0.2400	0.2261	0.2467	0.2378	0.0033
	3D	0.2352	0.2500	0.2392	0.2279	0.2365	0.2398	0.2377	0.2453	0.2345	0.2346	0.2383	0.2399	0.2345	0.2453	0.2384	0.0016
Heel-mtpj III l (m)	segmented	0.1650	0.1700	0.1583	0.1566	0.1620	0.1680	0.1680	0.1750	0.1583	0.1688	0.1620	0.1630	0.1583	0.1750	0.1659	0.0024
Pes (paw only) l (m)	segmented	0.0876	0.0780	0.0700	0.0782	0.0847	0.0730	0.0610	0.0800	0.0552	0.0653	0.0576	0.0650	0.0552	0.0800	0.0640	0.0036
tarsus/metatarsus l (m)	intact	0.1650	0.1690	0.1500	0.1520	0.1520	0.1690	0.1680	0.1750	0.1583	0.1688	0.1620	0.1630	0.1583	0.1750	0.1659	0.0024
Ankle c (m)	segmented	0.1965	0.2150	0.2020	0.1830	0.2020	0.2020	0.1980	0.2140	0.2010	0.1845	0.2020	0.2040	0.1845	0.2140	0.2006	0.0039
Mid-pes c (m)	intact	0.1320	0.1350	0.1170	0.1230	0.1300	0.1350	0.1330	0.1350	0.1170	0.1250	0.1310	0.1330	0.1170	0.1350	0.1290	0.0028
Pes c (m)	segmented	0.1600	0.1550	0.1410	0.1560	0.1490	0.1650	0.1680	0.1530	0.1410	0.1580	0.1490	0.1650	0.1410	0.1680	0.1557	0.0041
Ankle b (m)	intact	0.0420	0.0430	0.0410	0.0437	0.0407	0.0450	0.0420	0.0420	0.0410	0.0439	0.0407	0.0440	0.0407	0.0440	0.0423	0.0006
Pes b (m)	segmented	0.0576	0.0530	0.0515	0.0540	0.0510	0.0550	0.0540	0.0530	0.0530	0.0550	0.0520	0.0540	0.0520	0.0550	0.0535	0.0004
	intact	0.0560	0.0560	0.0500	0.0480	0.0500	0.0560	0.0555	0.0570	0.0500	0.0500	0.0500	0.0560	0.0500	0.0570	0.0531	0.0014
tarsus/metatarsus b (m)	intact	0.0390	0.0370	0.0380	0.0370	0.0410	0.0430	0.0400	0.0380	0.0370	0.0350	0.0410	0.0440	0.0350	0.0440	0.0392	0.0013
Pes d (m)	intact	0.0380	0.0420	0.0420	0.0420	0.0450	0.0460	0.0420	0.0420	0.0419	0.0420	0.0420	0.0430	0.0419	0.0430	0.0422	0.0002
tarsus/metatarsus d (m)	intact	0.0420	0.0430	0.0400	0.0380	0.0430	0.0440	0.0420	0.0430	0.0340	0.0370	0.0430	0.0420	0.0340	0.0430	0.0402	0.0015
$I_{int/ext}$ (kg*m²)		0.00161	0.00220	0.00223	0.00150	0.00174	0.00167	0.00135	0.00232	0.00219	0.00149	0.00207	0.00190	0.00135	0.00232	0.00189	0.00016
$I_{abd/add}$ (kg*m²)		0.00087	0.00062	0.00086	0.00100	0.00085	0.00079	0.00093	0.00061	0.00078	0.00120	0.00097	0.00087	0.00061	0.00120	0.00089	0.00008
$I_{flx/ext}$ (kg*m²)		0.00160	0.00196	0.00174	0.00159	0.00176	0.00184	0.00157	0.00183	0.00186	0.00160	0.00172	0.00182	0.00157	0.00186	0.00173	0.00005

		Paired Differences								Paired Sample Correlations	
					95% Confidence Interval of the Difference						
		Mean	Std. Deviation	Std. Error Mean	Lower	Upper	t	df	Sig. (2-tailed)	Correlation	Sig.
Pair 1	Heel_tip_of_met_III_l_s - Heel_tip_of_met_III_l_i	-.000708	.003918	.001131	-.003197	.001781	-.626	11	.544	.854	.000
Pair 2	Pes_b_s - Pes_b_i	.000717	.003103	.000896	-.001255	.002688	.800	11	.441	.427	.166

Left Crus/Calf											
Subject/Parameter		1	2	3	4	5	6	Min	Max	Mean	SE Mean
Mass (kg)		0.4929	0.6618	0.4546	0.4722	0.6152	0.5410	0.4546	0.6618	0.5396	0.0339
Volume (m^3)		0.00050	0.00068	0.00043	0.00051	0.00058	0.00057	0.00043	0.00068	0.00054	0.00004
Density (kg/m^3)		985.8667	973.1863	1069.7255	925.8824	1060.6322	945.8625	925.8824	1069.7255	993.5259	24.2415
Prox-dist jt ctr l (m)	3d	0.2042	0.2220	0.2047	0.1975	0.2057	0.2106	0.1975	0.2220	0.2075	0.0034
	segmented	0.1910	0.2280	0.1810	0.2042	0.1910	0.2230	0.1810	0.2280	0.2030	0.0077
Tibiale med-sphyrion (m)	intact	0.2150	0.2370	0.2230	0.1970	0.2167	0.2230	0.1970	0.2370	0.2186	0.0054
stifle (knee) c (m)	segmented*	0.3000	0.3350	0.3175	0.2800	0.3200	0.3200	0.2800	0.3350	0.3121	0.0079
	intact	0.3200	0.3450	0.3320	0.2760	0.3000	0.3300	0.2760	0.3450	0.3172	0.0103
calf c (m)	segmented*	0.2610	0.2350	0.1870	0.2400	0.2250	0.2500	0.1870	0.2610	0.2330	0.0105
	intact	0.2230	0.2400	0.1800	0.2350	0.1695	0.2280	0.1695	0.2400	0.2126	0.0123
stifle (knee) b (m)	intact*	0.0560	0.0530	0.0560	0.0671	0.0400	0.0590	0.0400	0.0671	0.0552	0.0036
$I_{int/ext}$ ($kg*m^2$)		0.00141	0.00192	0.00164	0.00126	0.00152	0.00178	0.00126	0.00192	0.00159	0.00010
$I_{abd/add}$ ($kg*m^2$)		0.00078	0.00386	0.00222	0.00081	0.00203	0.00255	0.00078	0.00386	0.00204	0.00047
$I_{flx/ext}$ ($kg*m^2$)		0.00215	0.00330	0.00261	0.00216	0.00259	0.00255	0.00215	0.00330	0.00256	0.00017

		Paired Differences								Paired Sample Correlations	
		Mean	Std. Deviation	Std. Error Mean	95% Confidence Interval of the Difference		t	df	Sig. (2-tailed)	Correlation	Sig.
					Lower	Upper					
Pair 1	Prox_dist_jt_ctr_1_s - Prox_dist_jt_ctr_1_3d	-.004418	.014646	.005979	-.019788	.010952	-.739	5	.493	.681	.136
Pair 2	stifle_knee_c_s - stifle_knee_c_i	-.005083	.014637	.005976	-.020444	.010277	-.851	5	.434	.814	.049
Pair 3	calf_c_s - calf_c_i	.020417	.022831	.009321	-.003543	.044376	2.190	5	.080	.675	.141

Right Crus/Calf											
Subject/Parameter		1	2	3	4	5	6	Min	Max	Mean	SE Mean
Mass (kg)		0.5756	0.5921	0.4509	0.6403	0.5775	0.5152	0.4509	0.6403	0.5586	0.0270
Volume (m^3)		0.000630	0.000620	0.000410	0.000570	0.000550	0.000505	0.0004	0.0006	0.000548	0.0000
Density (kg/m^3)		913.6508	955.0538	1099.8374	1123.3333	1049.9394	1020.1980	913.6508	1123.3333	1027.0021	33.2577
Prox-dist jt ctr l (m)	3d	0.2093	0.2168	0.1908	0.2077	0.2081	0.2106	0.1908	0.2168	0.2072	0.0035
	segmented	0.1860	0.2310	0.1890	0.1840	0.2038	0.2200	0.1840	0.2310	0.2023	0.0080
Tibiale med-sphyrion (m)	intact	0.2100	0.2380	0.2200	0.1930	0.2102	0.2190	0.1930	0.2380	0.2150	0.0061
stifle (knee) c (m)	segmented*	0.3150	0.3300	0.3160	0.2900	0.3240	0.3200	0.2900	0.3300	0.3158	0.0056
	intact	0.3450	0.3370	0.3320	0.2870	0.3000	0.3300	0.2870	0.3450	0.3218	0.0094
calf c (m)	segmented*	0.2850	0.2620	0.2110	0.2200	0.2130	0.2430	0.2110	0.2850	0.2390	0.0122
	intact	0.2200	0.2400	0.1800	0.2170	0.1695	0.2280	0.1695	0.2400	0.2091	0.0114
stifle (knee) b (m)	intact*	0.0580	0.0530	0.0540	0.0703	0.0400	0.0590	0.0400	0.0703	0.0557	0.0040
$I_{int/ext}$ ($kg*m^2$)		0.00174	0.00103	0.00147	0.00239	0.00142	0.00124	0.00103	0.00239	0.00155	0.00019
$I_{abd/add}$ ($kg*m^2$)		0.00307	0.00244	0.00240	0.00370	0.00280	0.00272	0.00240	0.00370	0.00285	0.00020
$I_{flx/ext}$ ($kg*m^2$)		0.00290	0.00233	0.00242	0.00349	0.00286	0.00279	0.00233	0.00349	0.00280	0.00017

		Paired Differences							Sig. (2-tailed)	Paired Sample Correlations	
		Mean	Std. Deviation	Std. Error Mean	95% Confidence Interval of the Difference		t	df		Correlation	Sig.
					Lower	Upper					
Pair 1	Prox_dist_jt_ctr_l_c - Prox_dist_jt_ctr_l_3d	.001734	.023042	.009407	-.022448	.025915	.184	5	.861	.485	.330
Pair 2	stifle_knee_c_c - stifle_knee_c_i	-.006000	.018298	.007470	-.025202	.013202	-.803	5	.458	.602	.206
Pair 3	calf_c_c - calf_c_i	.029917	.022028	.008993	.006799	.053034	3.327	5	.021	.712	.112

Subject/Parameter		1	2	3	4	5	6	1	2	3	4	5	6	Min	Max	$\bar{x}$	$\sigma\bar{x}$
	Combined					Left Crus						Right Crus					
Mass (kg)		0.4929	0.6618	0.4546	0.4722	0.6152	0.5410	0.5756	0.5921	0.4509	0.6403	0.5775	0.5152	0.4509	0.6403	0.5586	0.0270
Volume (m³)		0.00050	0.00068	0.00043	0.00051	0.00058	0.00057	0.00063	0.00062	0.00041	0.00057	0.00055	0.00051	0.00041	0.00063	0.00055	0.00003
Density (kg/m³)		985.8667	973.1863	1069.7255	925.8824	1060.6322	945.8625	913.6508	955.0538	1099.8374	1123.3333	1049.9394	1020.1980	913.6508	1123.3333	1027.0021	33.2577
Prox-dist jt ctr l (m)	3d	0.2042	0.2220	0.2047	0.1975	0.2057	0.2106	0.2093	0.2168	0.1908	0.2077	0.2081	0.2106	0.1908	0.2168	0.2072	0.0035
	segmented	0.1910	0.2280	0.1810	0.2042	0.1910	0.2230	0.1860	0.2310	0.1890	0.1840	0.2038	0.2200	0.1840	0.2310	0.2023	0.0080
Tibiale med-sphyrion (m)	intact	0.2150	0.2370	0.2230	0.1970	0.2167	0.2230	0.2100	0.2380	0.2200	0.1930	0.2102	0.2190	0.1930	0.2380	0.2150	0.0061
stifle (knee) c (m)	segmented*	0.3000	0.3350	0.3175	0.2800	0.3200	0.3200	0.3150	0.3300	0.3160	0.2900	0.3240	0.3200	0.2900	0.3300	0.3158	0.0056
	intact	0.3200	0.3450	0.3320	0.2760	0.3000	0.3300	0.3450	0.3370	0.3320	0.2870	0.3000	0.3300	0.2870	0.3450	0.3218	0.0094
calf c (m)	segmented*	0.2610	0.2350	0.1870	0.2400	0.2250	0.2500	0.2850	0.2620	0.2110	0.2200	0.2130	0.2430	0.2110	0.2850	0.2390	0.0122
	intact	0.2230	0.2400	0.1800	0.2350	0.1695	0.2280	0.2200	0.2400	0.1800	0.2170	0.1695	0.2280	0.1695	0.2400	0.2091	0.0114
stifle (knee) b (m)	intact*	0.0560	0.0530	0.0560	0.0671	0.0400	0.0590	0.0580	0.0530	0.0540	0.0703	0.0400	0.0590	0.0400	0.0703	0.0557	0.0040
$I_{int/ext}$ (kg*m²)		0.00141	0.00192	0.00164	0.00126	0.00152	0.00178	0.00174	0.00103	0.00147	0.00239	0.00142	0.00124	0.00103	0.00239	0.00155	0.00019
$I_{abd/add}$ (kg*m²)		0.00078	0.00386	0.00222	0.00081	0.00203	0.00255	0.00307	0.00244	0.00240	0.00370	0.00280	0.00272	0.00240	0.00370	0.00285	0.00020
$I_{flx/ext}$ (kg*m²)		0.00215	0.00330	0.00261	0.00216	0.00259	0.00255	0.00290	0.00233	0.00242	0.00349	0.00286	0.00279	0.00233	0.00349	0.00280	0.00017

		Paired Differences								Paired Sample Correlations	
		Mean	Std. Deviation	Std. Error Mean	95% Confidence Interval of the Difference Lower	Upper	t	df	Sig. (2-tailed)	Correlation	Sig.
Pair 1	Prox_dist_jt_ctr_l_3d - Prox_dist_jt_ctr_l_s	.004675	.014604	.004216	-.004604	.013954	1.109	11	.291	.639	.025
Pair 2	stifle_c_s - stifle_c_i	-.005542	.015805	.004562	-.015584	.004500	-1.215	11	.250	.729	.007
Pair 3	calf_c_s - calf_c_i	.025167	.021957	.006338	.011216	.039117	3.970	11	.002	.676	.016

Left Thigh											
Subject/Parameter		1	2	3	4	5	6	Min	Max	Mean	SE Mean
Mass (kg)		1.5866	1.7060	1.6729	1.2374	2.2624	1.5856	1.2374	2.2624	1.6752	0.1358
Volume (m^3)		0.00178	0.00172	0.00170	0.00135	0.00240	0.00169	0.00135	0.00240	0.00177	0.00014
Density (kg/m^3)		891.3483	991.8605	984.0588	916.5926	942.6667	938.2446	891.3483	991.8605	944.1286	15.7623
Prox-dist jt ctr l (m)	3d*	0.1534	0.1474	0.1745	0.1433	0.1892	0.1673	0.1433	0.1892	0.1625	0.0072
trochanter-fem condyle l (m)	pre	0.1640	0.1610	0.1820	0.1740	0.1940	0.1530	0.1530	0.1940	0.1713	0.0061
Upper thigh c (m)	pre	0.4520	0.4350	0.4330	0.4600	0.4590	0.4480	0.4330	0.4600	0.4478	0.0047
Mid thigh c (m)	pre	0.3990	0.4050	0.3800	0.3750	0.4400	0.4300	0.3750	0.4400	0.4048	0.0107
$I_{int/ext}$ (kg*m^2)		0.00816	0.01156	0.01169	0.00919	0.00998	0.01089	0.0082	0.0117	0.01025	0.0006
$I_{abd/add}$ (kg*m^2)		0.00729	0.00911	0.00923	0.00642	0.01098	0.00792	0.0064	0.0110	0.00849	0.0007
$I_{flx/ext}$ (kg*m^2)		0.00849	0.01040	0.01215	0.00757	0.01382	0.01145	0.0076	0.0138	0.01065	0.0010
Right Thigh											
Subject/Parameter		1	2	3	4	5	6	Min	Max	Mean	SE Mean
Mass (kg)		1.7151	1.7412	1.7644	0.9204	1.9907	1.5726	0.9204	1.9907	1.6174	0.1498
Volume (m^3)		0.00186	0.00177	0.00179	0.00100	0.00240	0.00172	0.00100	0.00240	0.00176	0.00018
Density (kg/m^3)		922.0968	983.7100	985.6797	920.4333	829.4722	914.3023	829.4722	985.6797	925.9491	23.3757
Prox-dist jt ctr l (m)	3d*	0.1411	0.1665	0.1773	0.1396	0.1874	0.1522	0.1396	0.1874	0.1607	0.0080
trochanter-fem condyle l (m)	pre	0.1650	0.1570	0.1810	0.1820	0.1900	0.1530	0.1530	0.1900	0.1713	0.0062
Upper thigh c (m)	segmented	0.4900	0.4600	0.4670	0.5000	0.4500	0.4780	0.4500	0.5000	0.4742	0.0077
Mid thigh c (m)	segmented	0.4150	0.4360	0.4250	0.3900	0.4200	0.4250	0.3900	0.4360	0.4185	0.0064
$I_{int/ext}$ (kg*m^2)		0.00962	0.01075	0.00937	0.00637	0.01320	0.01106	0.0064	0.0132	0.01006	0.0009
$I_{abd/add}$ (kg*m^2)		0.00703	0.01167	0.00787	0.00330	0.01079	0.00719	0.0033	0.0117	0.00797	0.0012
$I_{flx/ext}$ (kg*m^2)		0.01051	0.01149	0.01119	0.00647	0.01547	0.01081	0.0065	0.0155	0.01099	0.0012

Combined		Left Thigh						Right Thigh									
Subject/Parameter		1	2	3	4	5	6	1	2	3	4	5	6	Min	Max	$\bar{x}$	$\sigma\bar{x}$
Mass (kg)		1.5866	1.7060	1.6729	1.2374	2.2624	1.5856	1.7151	1.7412	1.7644	0.9204	1.9907	1.5726	0.9204	1.9907	1.6174	0.1498
Volume (m^3)		0.00178	0.00172	0.00170	0.00135	0.00240	0.00169	0.00186	0.00177	0.00179	0.00100	0.00240	0.00172	0.00100	0.00240	0.00176	0.00018
Density (kg/m^3)		891.35	991.86	984.06	916.59	942.67	938.24	922.10	983.71	985.68	920.43	829.47	914.30	829.47	985.68	925.95	23.38
Prox-dist jt ctr l (m)	3d*	0.1534	0.1474	0.1745	0.1433	0.1892	0.1673	0.1411	0.1665	0.1773	0.1396	0.1874	0.1522	0.1396	0.1874	0.1607	0.0080
(m)	pre	0.1640	0.1610	0.1820	0.1740	0.1940	0.1530	0.1650	0.1570	0.1810	0.1820	0.1900	0.1530	0.1530	0.1900	0.1713	0.0062
Upper thigh c (m)	pre	0.4520	0.4350	0.4330	0.4600	0.4590	0.4480	0.4900	0.4600	0.4670	0.5000	0.4500	0.4780	0.4500	0.5000	0.4742	0.0077
Mid thigh c (m)	pre	0.3990	0.4050	0.3800	0.3750	0.4400	0.4300	0.4150	0.4360	0.4250	0.3900	0.4200	0.4250	0.3900	0.4360	0.4185	0.0064
$I_{int/ext}$ ($kg*m^2$)		0.00816	0.01156	0.01169	0.00919	0.00998	0.01089	0.00962	0.01075	0.00937	0.00637	0.01320	0.01106	0.00637	0.01320	0.01006	0.00092
$I_{abd/add}$ ($kg*m^2$)		0.00729	0.00911	0.00923	0.00642	0.01098	0.00792	0.00703	0.01167	0.00787	0.00330	0.01079	0.00719	0.00330	0.01167	0.00797	0.00122
$I_{flx/ext}$ ($kg*m^2$)		0.00849	0.01040	0.01215	0.00757	0.01382	0.01145	0.01051	0.01149	0.01119	0.00647	0.01547	0.01081	0.00647	0.01547	0.01099	0.00117

Subject/Parameter		1	2	3	4	5	6	Min	Max	$\overline{x}$	$\sigma\overline{x}$
					Head						
Mass (kg)		2.9984	3.0248	2.4267	2.5282	2.8680	3.1056	2.4267	3.1056	2.8253	0.1151
Volume (m^3)		0.00298	0.00315	0.00224	0.00258	0.00300	0.00299	0.00224	0.00315	0.00282	0.00014
Density (kg/m^3)		1006.1857	960.2540	1083.3482	979.9354	956.0000	1039.3686	956.0000	1083.3482	1004.1820	20.2883
Head jt ctr-tip of nose l (m)	3d	0.2550	0.2454	0.2317	0.2514	0.2456	0.2457	0.2317	0.2550	0.2458	0.0032
Nasion-prosthion l (m)	intact	0.1080	0.1130	0.1130	0.1170	0.1092	0.1060	0.1060	0.1170	0.1110	0.0016
Inion-prosthion l (m)	intact	0.2660	0.2710	0.2540	0.2730	0.2520	0.2760	0.2520	0.2760	0.2653	0.0041
Inion -nasion l (m)	intact	0.1580	0.1580	0.1410	0.1560	0.1428	0.1700	0.1410	0.1700	0.1543	0.0044
Head base c (m)	segmented	0.5300	0.4870	0.4820	0.5000	0.4700	0.5150	0.4700	0.5300	0.4973	0.0091
Cranial c (m)	intact	0.5120	0.5220	0.5000	0.5020	0.4780	0.5300	0.4780	0.5300	0.5073	0.0075
Nose @ nasion c (m)	segmented	0.3200	0.3560	0.2900	0.3040	0.3250	0.3540	0.2900	0.3560	0.3248	0.0108
Base of nose @ incisors c (m	segmented	0.2600	0.2850	0.2350	0.2600	0.2300	0.2660	0.2300	0.2850	0.2560	0.0083
Mid-head c (m)	segmented	0.4900	0.5070	0.4800	0.4600	0.5000	0.5350	0.4600	0.5350	0.4953	0.0104
Biorbital b (m)	intact	0.1175	0.1290	0.1200	0.1090	0.1180	0.1220	0.1090	0.1290	0.1193	0.0027
Bizygomatic b (m)	3d	0.1393	0.1310	0.1368	0.1670	0.1420	0.1838	0.1310	0.1838	0.1500	0.0085
	intact	0.1350	0.1460	0.1340	0.1350	0.1430	0.1500	0.1340	0.1500	0.1405	0.0028
Bieurional b (m)	intact	0.1020	0.1400	0.1200	0.1220	0.1200	0.1120	0.1020	0.1400	0.1193	0.0051
Bigonial b (m)	intact	0.1225	0.1030	0.1420	0.1420	0.1030	0.1300	0.1030	0.1420	0.1238	0.0072
Viscerocranial b	intact	0.0640	0.0700	0.0560	0.0630	0.0800	0.0780	0.0560	0.0800	0.0685	0.0038
$I_{int/ext}$ (kg*m^2)		0.02497	0.02563	0.02744	0.02323	0.02527	0.02567	0.0232	0.0274	0.02537	0.0006
$I_{abd/add}$ (kg*m^2)		0.01778	0.02476	0.01864	0.01313	0.01857	0.02208	0.0131	0.0248	0.01916	0.0016
$I_{flx/ext}$ (kg*m^2)		0.02246	0.02788	0.02558	0.02160	0.02448	0.02716	0.0216	0.0279	0.02486	0.0010

		Paired Differences								Paired Sample Correlations	
		Mean	Std. Deviation	Std. Error Mean	95% Confidence Interval of the		t	df	Sig. (2-tailed)	Correlation	Sig.
					Lower	Upper					
Pair 1	Bizygomatic_b_3d - Bizygomatic_b_i	.009483	.019384	.007913	-.010859	.029825	1.198	5	.284	.354	.492

Neck											
Subject/Parameter		1	2	3	4	5	6	Min	Max	$\bar{x}$	$\sigma\bar{x}$
Mass (kg)		3.2741	2.4491	1.8877	2.0112	1.8783	2.9746	1.8783	3.2741	2.4125	0.2437
Volume (m^3)		0.00368	0.00249	0.00182	0.00195	0.00224	0.00309	0.00182	0.00368	0.00255	0.00029
Density (kg/m^3)		889.6920	983.5877	1037.1795	1031.4017	838.5268	962.3423	838.5268	1037.1795	957.1217	32.2831
Caud-cran jt ctr l (m)	segmented	0.1860	0.1790	0.1390	0.1450	0.1370	0.1880	0.1370	0.1880	0.1623	0.0100
	3d	0.1863	0.1795	0.1386	0.1217	0.1395	0.1795	0.1217	0.1863	0.1575	0.0112
C7-Axis spinous proc l (m)	intact	0.1960	0.1850	0.1350	0.1810	0.2050	0.2170	0.1350	0.2170	0.1865	0.0116
caudal end @ shoulders c (m)	segmented	0.5020	0.5120	0.4920	0.4950	0.5100	0.4800	0.4800	0.5120	0.4985	0.0049
mid c (m)	segmented	0.4850	0.4700	0.4680	0.4690	0.4760	0.4790	0.4680	0.4850	0.4745	0.0027
	intact	0.4600	0.5300	0.4800	0.4830	0.4840	0.4900	0.4600	0.5300	0.4878	0.0094
cranial end @ axis c (m)	segmented	0.4600	0.4450	0.4580	0.4550	0.4610	0.4750	0.4450	0.4750	0.4590	0.0040
neck b (m)	intact	0.1170	0.1300	0.1300	0.1580	0.1260	0.1440	0.1170	0.1580	0.1342	0.0059
neck d (m)	intact	0.1760	0.1570	0.1600	0.1580	0.1430	0.1440	0.1430	0.1760	0.1563	0.0049
$I_{int/ext}$ (kg*m^2)		0.01637	0.02131	0.01348	0.01046	0.01329	0.01812	0.0105	0.0213	0.0155	0.0016
$I_{abd/add}$ (kg*m^2)		0.01642	0.01997	0.01692	0.01263	0.01313	0.01709	0.0126	0.0200	0.01603	0.0011
$I_{flx/ext}$ (kg*m^2)		0.01792	0.01921	0.01284	0.00908	0.00846	0.01813	0.0085	0.0192	0.01428	0.0020

		Paired Differences								Paired Sample Correlations	
		Mean	Std. Deviation	Std. Error Mean	Lower	Upper	t	df	Sig. (2-tailed)	Correlation	Sig.
					Confidence Interval of the						
Pair 1	Caud_cran_jt_ctr_l_c - Caud_cran_jt_ctr_l_i	.00479	.00982	.00401	-.00552	.01510	1.195	5	.286	.935	.006
Pair 2	mid_c_c - mid_c_i	-.01333	.02714	.01108	-.04182	.01515	-1.203	5	.283	-.517	.293

Abdomen												
Subject/Parameter		1	2	3	4	5	6	Min	Max	$\overline{x}$	$\sigma\overline{x}$
Mass (kg)		8.0680	6.5230	9.3417	11.6930	8.5243	9.4683	6.5230	11.6930	8.9364	0.7022
Volume (m^3)		0.00850	0.00694	0.00950	0.01225	0.00880	0.00959	0.0069	0.0123	0.009263	0.0007
Density (kg/m^3)		949.1765	940.5912	983.3333	954.5306	968.6742	987.0044	940.5912	987.0044	963.8850	7.7074
LT13/L1-L7S1 segment ctr l (m)	3d	0.3209	0.3433	0.3734	0.4096	0.3970	0.3686	0.3209	0.4096	0.3688	0.0134
LT13/L1-L7S1 spin proc l (m)	segmented	0.2950	0.3250	0.3990	0.4040	0.4110	0.3760	0.2950	0.4110	0.3683	0.0194
mid-abdominal c (m)	segmented	0.7700	0.6050	0.7500	0.7990	0.7150	0.7100	0.6050	0.7990	0.7248	0.0276
waist (omphalion) c (m)	intact	0.7470	0.5700	0.6980	0.7910	0.7030	0.6780	0.5700	0.7910	0.6978	0.0305
	segmented	0.6450	0.5750	0.6000	0.6000	0.5900	0.6580	0.5750	0.6580	0.6113	0.0133
waist (@ crease) c (m)	intact	0.5880	0.5670	0.4950	0.6600	0.6400	0.6480	0.4950	0.6600	0.5997	0.0257
	segmented	0.5200	0.5350	0.5180	0.6280	0.5100	0.6400	0.5100	0.6400	0.5585	0.0242
bitrochanteric b (m)	segmented	0.1400	0.1490	0.0950	0.1380	0.1161	0.1490	0.0950	0.1490	0.1312	0.0087
iliac b (m)	segmented	0.1820	0.1600	0.1176	0.2000	0.1530	0.2100	0.1176	0.2100	0.1704	0.0139
waist (base of ribs) b (m)	segmented	0.1830	0.1960	0.1630	0.1860	0.2016	0.1970	0.1630	0.2016	0.1878	0.0057
waist (omphalion) b (m)	intact	0.1820	0.1300	0.1900	0.2580	0.1820	0.2390	0.1300	0.2580	0.1968	0.0187
waist (@ crease) b (m)	intact	0.1480	0.1400	0.1310	0.2220	0.1860	0.2280	0.1310	0.2280	0.1758	0.0173
waist (omphalion) d (m)	intact	0.2570	0.2080	0.2260	0.2760	0.2300	0.2220	0.2080	0.2760	0.2365	0.0103
waist (@ crease) d (m)	intact	0.2140	0.2060	0.1610	0.2020	0.1670	0.2170	0.1610	0.2170	0.1945	0.0099
$I_{int/ext}$ (kg*m^2)		0.09975	0.15095	0.16399	0.03997	0.10360	0.14055	0.0400	0.1640	0.11647	0.0186
$I_{abd/add}$ (kg*m^2)		0.06429	0.04554	0.06586	0.12109	0.06369	0.08204	0.0455	0.1211	0.07375	0.0106
$I_{flx/ext}$ (kg*m^2)		0.10863	0.08512	0.16634	0.23378	0.12677	0.15399	0.0851	0.2338	0.14577	0.0213

		Paired Differences			95% Confidence Interval of the					Paired Sample Correlations	
		Mean	Std. Deviation	Std. Error Mean	Lower	Upper	t	df	Sig. (2-tailed)	Correlation	Sig.
Pair 1	LT13/L1-L7S1 spin proc l (m) - LT13/L1-L7S1 segment ctr l (m)	-.00410	.02040	.00771	-.02296	.01477	-0.531	6	.614	.960	.001
Pair 2	waist_omphalion_c_c - waist_omphalion_c_i	-.08650	.07041	.02875	-.16039	-.01261	-3.009	5	.030	.345	.503
Pair 3	waist_crease_c_c - waist_crease_c_i	-.04117	.05291	.02160	-.09669	.01436	-1.906	5	.115	.626	.184

Subject/Parameter		Thorax									
		1	2	3	4	5	6	Min	Max	$\overline{x}$	$\sigma\overline{x}$
Mass (kg)		14.738	13.815	14.071	15.302	14.166	12.097	12.097	15.302	14.031	0.444
Volume (m^3)		0.01520	0.01491	0.01040	0.01665	0.01060	0.01215	0.01040	0.01665	0.01332	0.0011
Density (kg/m^3)		969.621	926.786	1352.981	919.039	1336.384	995.501	919.039	1352.981	1083.385	83.444
C7T1-T13/L1 jt ctrs l (m)	3d	0.3650	0.3585	0.3679	0.4171	0.3921	0.3241	0.3241	0.4171	0.3708	0.0129
Central long axis of segment l (m)	segmented	0.3930	0.3430	0.3684	0.3920	0.3920	0.3240	0.3240	0.3930	0.3687	0.0120
C7T1-T13/L1 spin proc l (m)	segmented	0.3350	0.2900	0.3060	0.3650	0.3675	0.3400	0.2900	0.3675	0.3339	0.0127
T13/L1 - suprasternale l (m)	intact	0.2530	0.3130	0.3240	0.3280	0.3490	0.2460	0.2460	0.3490	0.3022	0.0173
Tip of xyphoid c (m)	segmented	0.7900	0.7070	0.7700	0.8150	0.7550	0.7500	0.7070	0.8150	0.7645	0.0151
	intact	0.7900	0.7860	0.7250	0.7890	0.8000	0.7700	0.7250	0.8000	0.7767	0.0111
mid thorax c (m)	segmented	0.7800	0.7820	0.7200	0.7400	0.7180	0.7600	0.7180	0.7820	0.7500	0.0116
	intact	0.8000	0.7800	0.7620	0.7450	0.7300	0.7640	0.7300	0.8000	0.7635	0.0101
largest c (m)	segmented	0.8100	0.7730	0.6900	0.7300	0.7300	0.7650	0.6900	0.8100	0.7497	0.0171
base of neck c (m)	segmented	0.6400	0.6650	0.5600	0.5500	0.5800	0.4050	0.4050	0.6650	0.5667	0.0373
base of ribs b (m)	segmented	0.2080	0.1960	0.2280	0.2360	0.2090	0.1960	0.1960	0.2360	0.2122	0.0068
mid segment b (m)	segmented	0.2000	0.2040	0.1820	0.1850	0.1673	0.2030	0.1673	0.2040	0.1902	0.0060
	intact	0.2040	0.2000	0.1750	0.2360	0.2050	0.1940	0.1750	0.2360	0.2023	0.0081
biacromial b (m)	intact	0.2140	0.2100	0.1540	0.1500	0.2110	0.2140	0.1500	0.2140	0.1922	0.0127
neck b (m)	segmented	0.1700	0.1920	0.1733	0.1340	0.1550	0.1540	0.1340	0.1920	0.1631	0.0081
chest d (m)	intact	0.2860	0.2770	0.2610	0.3030	0.2500	0.2600	0.2500	0.3030	0.2728	0.0080
$I_{int/ext}$ ($kg*m^2$)		0.30309	0.26957	0.27646	0.32327	0.30302	0.21162	0.21162	0.32327	0.28117	0.01605
$I_{abd/add}$ ($kg*m^2$)		0.14312	0.12838	0.13048	0.14594	0.13843	0.12403	0.12403	0.14594	0.13506	0.00357
$I_{flx/ext}$ ($kg*m^2$)		0.30544	0.27192	0.26520	0.33025	0.30929	0.21296	0.21296	0.33025	0.28251	0.01710

		Paired Differences			Confidence Interval of the					Paired Sample Correlations	
		Mean	Std. Deviation	Std. Error Mean	Lower	Upper	t	df	Sig. (2-tailed)	Correlation	Sig.
Pair 1	xyphoidproc_c_s - xyphoidproc_c_i	-.01217	.04578	.01869	-.06021	.03588	-.651	5	.544	.003	.995
Pair 2	mid_thorax_c_s - mid_thorax_c_i	-.01350	.01587	.00648	-.03016	.00316	-2.084	5	.092	.831	.040
Pair 3	mid_segment_b_s - mid_segment_b_i	-.01212	.02570	.01049	-.03909	.01486	-1.155	5	.300	-.093	.861

Tail											
Subject/Parameter		1	2	3	4	5	6	Min	Max	$\bar{x}$	$\sigma\bar{x}$
Mass (kg)		0.2920	0.2555	0.2299	0.3741	0.2912	0.3339	0.2299	0.3741	0.2961	0.0213
Volume (m^3)		0.000380	0.000330	0.000220	0.000540	0.000270	0.000331	0.0002	0.0005	0.000345	0.0000
Density (kg/m^3)		768.3333	774.2424	1045.0000	692.7778	1078.5185	1008.8620	692.7778	1078.5185	894.6223	68.4747
Sacrum to tip of tail l (m)	3d	0.4293	0.4577	0.4266	0.4313	0.4190	0.4653	0.4190	0.4653	0.4382	0.0076
	intact	0.4310	0.4600	0.4440	0.4310	0.4200	0.4100	0.4100	0.4600	0.4327	0.0072
Caudal vert 1 to tip of tail (m)	segmented	0.4270	0.4570	0.4300	0.4150	0.3956	0.4830	0.3956	0.4830	0.4346	0.0127
Base of tail at sacrum c (m)	segmented	0.1500	0.1480	0.1340	0.1580	0.1420	0.1600	0.1340	0.1600	0.1487	0.0040
Base of tail at caudal vert 1 c (m)	segmented	0.1350	0.1290	0.1310	0.1480	0.1590	0.1640	0.1290	0.1640	0.1443	0.0061
Mid tail c (m)	segmented	0.1000	0.0860	0.0800	0.0980	0.0940	0.0990	0.0800	0.1000	0.0928	0.0033
	intact	0.1280	0.1080	0.0800	0.1000	0.1190	0.0950	0.0800	0.1280	0.1050	0.0070
Mid tail b (m)	intact	0.0355	0.0410	0.0260	0.0420	0.0340	0.0640	0.0260	0.0640	0.0404	0.0053
$I_{int/ext}$ ($kg*m^2$)		0.00079	0.00044	0.00046	0.00134	0.00085	0.00104	0.00044	0.00134	0.00082	0.00014
$I_{abd/add}$ ($kg*m^2$)		0.00575	0.00569	0.00505	0.00682	0.00525	0.00786	0.00505	0.00786	0.00607	0.00044
$I_{flx/ext}$ ($kg*m^2$)		0.00460	0.00592	0.00442	0.00400	0.00380	0.00636	0.00380	0.00636	0.00485	0.00043

		Paired Differences								Paired Sample Correlations	
					95% Confidence Interval of the						
		Mean	Std. Deviation	Std. Error Mean	Lower	Upper	t	df	Sig. (2-tailed)	Correlation	Sig.
Pair 1	Sacrum_to_tailend_l_3d - Sacrum_to_tailend_l_i	.00552	.02523	.01030	-.02095	.03200	.536	5	.615	.035	.948
Pair 2	Sacrum_to_tailtip_l_3d-Caudal_vert1_to_tailtip	.00359	.01461	.00597	-.01175	.01893	.602	5	.574	.949	.004
Pair 3	Midtail_c_s-Midtail_c_i	-.01217	.01432	.00584	-.02719	.00286	-2.082	5	.092	.564	.244

APPENDIX F: RESULTS OF GEOMETRIC CORRELATIONS FOR ESTIMATING SEGMENT MASS USING WHOLE BODY MASS AND VOLUME DERIVED FROM MORPHOMETRIC DIMENSIONS

Manus (Forefoot)									
Mass/Volume	Left (n=6)	Adjusted Corr	Right (n=6)	Adjusted Corr	L + R (n=12)	Adjusted Corr	Shape	Dimension1	Dimension2	Length
Volume 1	0.938	0.894	0.916	0.855	0.909	0.888	Frustum	Wrist	2nd-5th mcpj	3D
Volume 2	0.944	0.904	0.952	0.919	0.934	0.919	Frustum	Wrist	2nd-5th mcpj	Measured
Volume 3	0.567	-	0.645	0.160	0.598	0.463	Cylinder	COM		3D
Volume 4	0.976	0.960	0.979	0.965	**0.944**	**0.931**	Cylinder	Wrist		3D
Volume 5	0.901	0.828	0.864	0.760	0.869	0.837	Cylinder	2nd-5th		3D
Volume 6	0.688	0.351	0.679	0.319	0.614	0.489	Cylinder	COM		Measured
Volume 7	0.958	0.929	0.989	0.982	0.953	0.943	Cylinder	Wrist		Measured
Volume 8	0.905	0.836	0.901	0.828	0.892	0.866	Cylinder	2nd-5th		Measured
Volume 9	0.952	0.919	0.957	0.928	0.929	0.913	Cylinder	Wrist Ave		Ave 3D+measured

Antebrachium									
Mass/ Volume	Left (n=6)	Adjusted Corr	Right (n=6)	Adjusted Corr	L + R (n=12)	Adjusted Corr	Shape	Dimension1	Dimension2	Length
Volume 1	0.689	0.353	0.736	0.486	0.706	0.623	Frustum	Elbow	Wrist	3D
Volume 2	0.748	0.516	0.828	0.690	0.728	0.653	Frustum	Elbow	Wrist	Measured
Volume 9	0.727	0.462	0.803	0.000	0.725	0.648	Frustum	Elbow	Wrist	Combined ave
Volume 3	0.915	0.853	0.842	0.718	0.855	0.820	Cylinder	Forearm		3D
Volume 4	0.373	-	0.571	-	0.450	0.161	Cylinder	Elbow		3D
Volume 5	0.985	0.974	0.972	0.952	0.965	0.957	Cylinder	Wrist		3D
Volume 6	0.975	0.959	0.944	0.904	0.941	0.927	Cylinder	Forearm		Measured
Volume 7	0.469	-	0.699	0.385	0.523	0.335	Cylinder	Elbow		Measured
Volume 8	0.993	0.988	0.975	0.958	0.937	0.922	Cylinder	Wrist		Measured
Volume10	0.952	0.918	0.905	0.836	0.905	0.883	Cylinder	Forearm		Combined ave
Volume11	0.952	0.918	0.905	0.836	0.905	0.883	Cylinder	Elbow		Combined ave
Volume12	0.993	0.988	0.978	0.963	**0.955**	**0.945**	Cylinder	Wrist		Combined ave
Volume13	0.964	0.939	0.932	0.883	0.923	0.906	Cylinder	Wristave		Combined ave

Brachium									
Mass/ Volume	Left (n=6)	Adjusted Corr	Right (n=6)	Adjusted Corr	L + R (n=12)	Adjusted Corr	Shape	Dimension1	Dimension2	Length
Volume 1	0.976	0.961	0.663	0.258	0.805	0.754	Frustum	Axillary	Elbow	3D jt ctr to jt ctr
Volume 2	0.664	0.261	0.840	0.714	0.882	0.853	Frustum	Axillary	Elbow	Acromion/Radiale
Volume 3	0.664	0.261	0.989	0.982	0.904	0.882	Frustum	Axillary	Elbow	Humerus/Radiale
Volume 4	0.889	0.806	0.834	0.702	**0.843**	**0.804**	Frustum	Axillary	Elbow	Prox-Dist
Volume 5	0.909	0.842	0.881	0.792	0.898	0.874	Frustum	Axillary	Elbow	jt ctr to jt ctr ave
Volume 6	0.856	0.745	0.675	0.305	0.743	0.672	Frustum	Triceps	Elbow	3D jt ctr to jt ctr
Volume 7	0.708	0.410	0.866	0.763	0.699	0.613	Frustum	Triceps	Elbow	Acromion/Radiale
Volume 8	0.708	0.410	0.857	0.746	0.570	0.418	Frustum	Triceps	Elbow	Humerus/Radiale
Volume 9	0.533	-	0.746	0.512	0.654	0.548	Frustum	Triceps	Elbow	Prox-Dist
Volume 10	0.508	-	0.848	0.729	0.698	0.611	Frustum	Triceps	Elbow	jt ctr to jt ctr ave
Volume 11	0.448	-	0.637	0.102	0.519	0.327	Cylinder	Triceps		3D jt ctr to jt ctr
Volume 12	0.582	-	0.665	0.265	0.614	0.488	Cylinder	Elbow		3D jt ctr to jt ctr
Volume 13	0.906	0.838	0.641	0.131	0.748	0.680	Cylinder	Axillary		3D jt ctr to jt ctr
Volume 14	0.61	-	0.691	0.36015	0.53	0.34759	Cylinder	Triceps		Acromion/Radiale
Volume 15	0.46	-	0.719	0.4427	0.613	0.48682	Cylinder	Elbow		Acromion/Radiale
Volume 16	0.62	-	0.772	0.57208	0.848	0.81048	Cylinder	Axillary		Acromion/Radiale
Volume 17	0.61	-	0.702	0.39437	0.519	0.32696	Cylinder	Triceps		Humerus/Radiale
Volume 18	0.46	-	0.785	0.6011	0.616	0.49196	Cylinder	Elbow		Humerus/Radiale
Volume 19	0.62	-	0.841	0.71481	0.803	0.75195	Cylinder	Axillary		Humerus/Radiale
Volume 20	0.45	-	0.659	0.23838	0.524	0.33737	Cylinder	Triceps		Prox-Dist
Volume 21	0.53	-	0.697	0.37751	0.615	0.48961	Cylinder	Elbow		Prox-Dist

Brachium, cont'd									
Mass/ Volume	Left (n=6)	Adjusted Corr	Right (n=6)	Adjusted Corr	L + R (n=12)	Adjusted Corr	Shape	Dimension1	Dimension2	Length
Volume 22	0.88	0.7883	0.751	0.52197	0.812	0.76405	Cylinder	Axillary		Prox-Dist
Volume 23	0.52	-	0.665	0.26603	0.521	0.33093	Cylinder	Triceps		jt ctr to jt ctr ave
Volume 24	0.47	-	0.719	0.4407	0.62	0.49788	Cylinder	Elbow		jt ctr to jt ctr ave
Volume 25	0.81	0.6446	0.741	0.49967	0.822	0.7769	Cylinder	Axillary		jt ctr to jt ctr ave

Pes									
Mass/ Volume	Left (n=6)	Adjusted Corr	Right (n=6)	Adjusted Corr	L + R (n=12)	Adjusted Corr	Shape	Dimension1	Dimension2	Length
Volume 1	0.611	-	0.837	0.708	0.689	0.598	Cylinder	Ankle		3D
Volume 2	0.860	0.753	0.852	0.738	0.830	0.787	Cylinder	COM		3D
Volume 3	0.866	0.764	0.884	0.798	0.867	0.835	Cylinder	midlength		3D
Volume 4	0.817	0.667	0.845	0.724	0.816	0.769	Cylinder	paw @ mt pad		3D
Volume 5	0.682	0.330	0.821	0.676	0.746	0.677	Cylinder	Ankle		Prox jt ctr - pad tip
Volume 6	0.857	0.747	0.857	0.747	0.845	0.807	Cylinder	COM		Prox jt ctr - pad tip
Volume 7	0.830	0.694	0.870	0.772	0.848	0.810	Cylinder	midlength		Prox jt ctr - pad tip
Volume 8	0.832	0.697	0.871	0.773	0.843	0.804	Cylinder	paw @ mt pad		Prox jt ctr - pad tip
Volume 9	0.627	-	0.798	0.628	0.695	0.607	Cylinder	Ankle		Heel - pad tip
Volume 10	0.872	0.775	0.866	0.765	0.842	0.803	Cylinder	COM		Heel - pad tip
Volume 11	0.892	0.812	0.882	0.793	0.874	0.843	Cylinder	midlength		Heel - pad tip
Volume 12	0.840	0.714	0.886	0.801	0.846	0.808	Cylinder	paw @ mt pad		Heel - pad tip
Volume 13	0.832	0.699	0.669	0.280	0.676	0.580	Cylinder	Ankle		Heel - mtpj
Volume 14	0.872	0.775	0.784	0.597	0.802	0.751	Cylinder	COM		Heel - mtpj
Volume 15	0.866	0.765	0.826	0.685	0.838	0.798	Cylinder	midlength		Heel - mtpj
Volume 16	0.821	0.676	0.805	0.644	0.798	0.745	Cylinder	paw @ mt pad		Heel - mtpj
Volume 17	0.944	0.905	0.836	0.705	0.863	0.829	Pyramid	Foot Breadth	Foot Depth	3D
Volume 18	0.988	0.980	0.934	0.887	0.956	0.946	Pyramid	Foot Breadth	Foot Depth	Prox jt ctr - pad tip
Volume 19	0.928	0.876	0.964	0.940	0.905	0.883	Pyramid	Foot Breadth	Foot Depth	Heel - pad tip
Volume 20	0.966	0.943	0.683	0.332	0.829	0.786	Pyramid	Foot Breadth	Foot Depth	Heel - mtpj

Crus									
Mass/ Volume	Left (n=6)	Adjusted Corr	Right (n=6)	Adjusted Corr	L + R (n=12)	Adjusted Corr	Shape	Dimension1	Dimension2	Length
Volume 1	0.932	0.883	0.723	0.451	0.792	0.738	Frustum	Knee C_s	Ankle C_s	3D jt ctr to jt ctr
Volume 2	0.806	0.645	0.619	-	0.515	0.319	Frustum	Knee C_s	Ankle C_s	Prox-Dist
Volume 3	0.810	0.653	0.496	-	0.576	0.429	Frustum	Knee C_s	Ankle C_s	tibiale med to sphyrion
Volume 4	0.875	0.781	0.681	0.325	0.690	0.600	Frustum	Knee C_s	Ankle C_s	Average p-d
Volume 5	0.749	0.517	0.473	-	0.327	-	Frustum	Knee C_i	Ankle C_i	3D jt ctr to jt ctr
Volume 6	0.633	0.035	0.496	-	0.265	-	Frustum	Knee C_i	Ankle C_i	Prox-Dist
Volume 7	0.905	0.835	0.446	-	0.249	-	Frustum	Knee C_i	Ankle C_i	tibiale med to sphyrion
Volume 8	0.620	-	0.492	-	0.321	-	Frustum	Knee C_i	Ankle C_i	Average p-d
Volume 9	0.687	0.346	0.585	-	0.201	-	Frustum	Knee b	Ankle B	3D jt ctr to jt ctr
Volume 10	0.633	0.044	0.545	-	0.170	-	Frustum	Knee b	Ankle B	Prox-Dist
Volume 11	0.717	0.435	0.510	-	0.169	-	Frustum	Knee b	Ankle B	tibiale med to sphyrion
Volume 12	0.653	0.209	0.565	-	0.183	-	Frustum	Knee b	Ankle B	Average p-d
Volume 13	0.829	0.692	0.636	0.091	0.655	0.549	Frustum	Ave knee c	Ankle C_s	3D jt ctr to jt ctr
Volume 14	0.715	0.430	0.608	-	0.431	0.066	Frustum	Ave knee c	Ankle C_s	3D jt ctr to jt ctr
Volume 15	0.622	-	0.407	-	0.262	-	Frustum	Ave knee c	Ankle C_s	3D jt ctr to jt ctr
Volume 16	0.734	0.482	0.651	0.197	0.598	0.464	Frustum	Ave knee c	Ankle C_s	Prox-Dist
Volume 17	0.999	0.998	0.796	0.625	**0.808**	**0.759**	Cylinder	Ank c_s		3D jt ctr to jt ctr
Volume 18	0.682	0.331	0.606	-	0.312	-	Cylinder	Mid c_s		3D jt ctr to jt ctr
Volume 19	0.873	0.776	0.678	0.314	0.762	0.698	Cylinder	Knee c_s		3D jt ctr to jt ctr
Volume 20	0.621	-	0.504	-	0.487	0.261	Cylinder	Ave knee c		3D jt ctr to jt ctr
Volume 21	0.888	0.806	0.834	0.703	0.785	0.728	Cylinder	Ank c_i		3D jt ctr to jt ctr
Volume 22	0.627	-	0.692	0.364	0.308	-	Cylinder	Mid c_i		3D jt ctr to jt ctr

Crus, cont'd										
Mass/ Volume	Left (n=6)	Adjusted Corr	Right (n=6)	Adjusted Corr	L + R (n=12)	Adjusted Corr	Shape	Dimension1	Dimension2	Length
Volume 23	0.84	0.71146	0.41	-	0.19	-	Cylinder	Knee c_i		3D jt ctr to jt ctr
Volume 24	0.8	0.62622	0.66	0.25202	0.471	0.22005	Cylinder	Ank c-post		Prox-Dist
Volume 25	0.69	0.34535	0.66	0.22366	0.272	-	Cylinder	Mid c-post		Prox-Dist
Volume 26	0.81	0.64323	0.59	-	0.531	0.34968	Cylinder	Knee c-post		Prox-Dist
Volume 27	0.67	0.2993	0.52	-	0.376	-	Cylinder	Ave knee c		Prox-Dist
Volume 28	0.74	0.49106	0.68	0.31136	0.424	-	Cylinder	Ank c_i		Prox-Dist
Volume 29	0.64	0.07826	0.68	0.32974	0.261	-	Cylinder	Mid c_i		Prox-Dist
Volume 30	0.62	-	0.41	-	0.182	-	Cylinder	Knee c_i		Prox-Dist
Volume 31	0.93	0.88609	0.66	0.24468	0.602	0.46924	Cylinder	Ank c-post		tibiale med to sphyrion
Volume 32	0.67	0.30225	0.58	-	0.246	-	Cylinder	Mid c-post		tibiale med to sphyrion
Volume 33	0.76	0.54906	0.43	-	0.528	0.34425	Cylinder	Knee c-post		tibiale med to sphyrion
Volume 34	0.77	0.56515	0.46	-	0.164	-	Cylinder	Ave knee c		tibiale med to sphyrion
Volume 35	0.96	0.92974	0.81	0.65637	0.657	0.55311	Cylinder	Ank c_i		tibiale med to sphyrion
Volume 36	0.63	-	0.67	0.26516	0.249	-	Cylinder	Mid c_i		tibiale med to sphyrion
Volume 37	0.92	0.8648	0.48	-	0.291	-	Cylinder	Knee c_i		tibiale med to sphyrion
Volume 38	0.87	0.77647	0.74	0.48648	0.653	0.54693	Cylinder	Ank c-post		Average p-d
Volume 39	0.69	0.34171	0.63	-	0.293	-	Cylinder	Mid c-post		Average p-d
Volume 40	0.86	0.75318	0.65	0.16752	0.69	0.59933	Cylinder	Knee c-post		Average p-d
Volume 41	0.66	0.23957	0.53	-	0.482	0.24871	Cylinder	Ave knee c		Average p-d
Volume 42	0.77	0.57178	0.76	0.55309	0.603	0.47114	Cylinder	Ank c_i		Average p-d
Volume 43	0.63	-	0.69	0.35189	0.284	-	Cylinder	Mid c_i		Average p-d

Crus, cont'd									
Mass/ Volume	Left (n=6)	Adjusted Corr	Right (n=6)	Adjusted Corr	L + R (n=12)	Adjusted Corr	Shape	Dimension1	Dimension2	Length
Volume 44	0.66	0.23797	0.41	-	0.189	-	Cylinder	Knee c_i		Average p-d
Volume 45	0.72	0.44158	0.46	-	0.164	-	Cylinder	Knee b		3D jt ctr to jt ctr
Volume 46	0.63	-	0.69	0.3393	0.383	-	Cylinder	Ank b		3D jt ctr to jt ctr
Volume 47	0.66	0.24502	0.45	-	0.171	-	Cylinder	Knee b		Prox-Dist
Volume 48	0.65	0.18303	0.64	0.10437	0.3	-	Cylinder	Ank b		Prox-Dist
Volume 49	0.75	0.50856	0.42	-	0.209	-	Cylinder	Knee b		tibiale med to sphyrion
Volume 50	0.62	-	0.65	0.16924	0.277	-	Cylinder	Ank b		tibiale med to sphyrion
Volume 51	0.69	0.34176	0.45	-	0.165	-	Cylinder	Knee b		Average p-d
Volume 52	0.64	0.13524	0.66	0.24572	0.34	-	Cylinder	Ank b		Average p-d

Thigh									
Mass/ Volume	Left n=6	Adjusted Corr	Right n=6	Adjusted Corr	L & R (n=12)	Adjusted Corr	Shape	Dimension1	Dimension2	Length
Volume 1	0.914	0.852	0.834	0.702	0.769	0.708	Frustum	Up. Thigh Circ_s	Knee Circ_s	Length (from 3D measures)
Volume 2	0.849	0.731	0.653	0.212	0.387	-	Frustum	Up. Thigh Circ_s	Knee Circ_s	Length (prox-dist)
Volume 3	0.929	0.878	0.781	0.591	0.743	0.673	Frustum	Up. Thigh Circ_s	Knee Circ_s	Length cut (troch-femcondyle)
Volume 4	0.923	0.868	0.763	0.551	0.261	-	Frustum	Up. Thigh Circ_s	Knee Circ_s	Length int (troch-femcondyle)
Volume 5	0.838	0.709	0.820	0.674	0.808	0.759	Frustum	Up. Thigh Circ _i	Knee Circ _i	Length (from 3D measures)
Volume 6	0.823	0.679	0.678	0.314	0.248	-	Frustum	Up. Thigh Circ _i	Knee Circ _i	Length (prox-dist)
Volume 7	0.922	0.865	0.754	0.531	0.700	0.613	Frustum	Up. Thigh Circ _i	Knee Circ _i	Length cut (troch-femcondyle)
Volume 8	0.874	0.779	0.657	0.229	0.078	-	Cylinder	Up. Thigh Circ _i	Knee Circ _i	Length int (troch-femcondyle)
Volume 9	0.881	0.791	0.871	0.773	**0.873**	**0.842**	Cylinder	Knee circ		Length (from 3D measures)
Volume 10	0.886	0.802	0.865	0.762	0.863	0.830	Cylinder	Mid thigh circ		Length (from 3D measures)
Volume 11	0.932	0.884	0.870	0.771	0.458	0.184	Cylinder	Upper thigh circ		Length (from 3D measures)
Volume 12	0.841	0.715	0.768	0.562	0.687	0.595	Cylinder	Knee circ		Length (prox-dist)
Volume 13	0.784	0.598	0.732	0.476	0.544	0.374	Cylinder	Mid thigh circ		Length (prox-dist)
Volume 14	0.853	0.740	0.732	0.476	0.474	0.228	Cylinder	Upper thigh circ		Length (prox-dist)
Volume 15	0.941	0.900	0.817	0.667	0.830	0.787	Cylinder	Knee circ		Length cut (troch-femcondyle)
Volume 16	0.917	0.857	0.808	0.650	0.773	0.713	Cylinder	Mid thigh circ		Length cut (troch-femcondyle)
Volume 17	0.913	0.850	0.727	0.463	0.495	0.278	Cylinder	Upper thigh circ		Length cut (troch-femcondyle)
Volume 18	0.896	0.820	0.900	0.827	0.811	0.763	Cylinder	Knee circ		Length int (troch-femcondyle)
Volume 19	0.972	0.954	0.844	0.722	0.737	0.664	Cylinder	Mid thigh circ		Length int (troch-femcondyle)
Volume 20	0.926	0.873	0.664	0.262	0.201	-	Cylinder	Upper thigh circ		Length int (troch-femcondyle)

Head						
Mass/Volume	Corr	Adjusted Corr	Shape	Dimension1	Dimension2	Length
Volume 1	0.756	0.535	Frustum	Head Base Circ	End of nose @ incisors	3D jt ctr to nose
Volume 2	0.690	0.357	Frustum	Knee Circ_s	Ankle Circ_s	Inion to Prosthion
Volume 3	0.768	0.563	Ellipse	Head base circ		3D jt ctr to nose
Volume 4	0.928	0.876	Ellipse	Head mid circ		3D jt ctr to nose
Volume 5	0.622	-	Ellipse	3D Head width		3D jt ctr to nose
Volume 6	**0.931**	**0.882**	Ellipse	Biorbital breadth		3D jt ctr to nose
Volume 7	0.707	0.409	Ellipse	Head base circ		Inion to Prosthion
Volume 8	0.830	0.694	Ellipse	Head mid circ		Inion to Prosthion
Volume 9	0.592	-	Ellipse	3D Head width		Inion to Prosthion
Volume 10	0.735	0.484	Ellipse	Biorbital breadth		Inion to Prosthion
Volume 11	0.690	0.356	Sphere			Inion to Glabella
Volume 12	0.833	0.700	Sphere			Inion to Glabella

Neck						
Mass/Volume	Corr	Adjusted Corr	Shape	Dimension1	Dimension2	Length
Volume 1	0.534	-	Frustum	Circ @ Shoulders	Circ @Neck	Prox-Dist_3d
Volume 2	0.970	0.950	Frustum	Circ @ Shoulders	Circ @Neck	Prox-Dist_s
Volume 3	0.640	0.128	Cylinder	Mid Circ		Prox-Dist_3d
Volume 4	**0.985**	**0.976**	Cylinder	Mid Circ		Prox-Dist_s

Abdomen						
Mass/Volume	Corr	Adjusted Corr	Shape	Dimension1	Dimension2	Length
Volume 1	0.987	0.979	Frustum	Circ cranial end	Circ hips	Prox-Dist_3d
Volume 2	**0.987**	**0.978**	Frustum	Circ cranial end	Circ hips	Prox-Dist_i
Volume 3	0.937	0.893	Cylinder	Circ cranial end		Prox-Dist_3d
Volume 4	0.903	0.832	Cylinder	Circ omphilion		Prox-Dist_3d
Volume 5	0.94	0.90072	Cylinder	Circ hips		Prox-Dist_3d
Volume 6	0.93	0.88114	Cylinder	Circ cranial end		Prox-Dist_i
Volume 7	0.93	0.87186	Cylinder	Circ omphilion		Prox-Dist_i
Volume 8	0.96	0.93098	Cylinder	Circ hips		Prox-Dist_i

Thorax						
Mass/Volume	Corr	Adjusted Corr	Shape	Dimension1	Dimension2	Length
Volume 1	**0.994**	**0.989**	Frustum	Circ base of ribs	Circ base of neck	Prox-Dist_3d
Volume 2	0.957	0.927	Frustum	Circ base of ribs	Circ base of neck	Prox-Dist_i
Volume 3	0.897	0.822	Frustum	Circ base of ribs	Circ base of neck	T1 to T13
Volume 4	0.954	0.922	Cylinder	Circ base of ribs	Circ base of neck	Prox-Dist_3d
Volume 5	0.830	0.693	Cylinder	Circ mid segment		Prox-Dist_3d
Volume 6	0.702	0.392	Cylinder	Circ @sternum (widest)		Prox-Dist_3d
Volume 7	0.975	0.957	Cylinder	Circ base of neck		Prox-Dist_3d
Volume 8	0.890	0.809	Cylinder	Circ base of ribs		Prox-Dist_i
Volume 9	0.774	0.577	Cylinder	Circ mid segment		Prox-Dist_i
Volume 10	0.652	0.206	Cylinder	Circ @sternum (widest)		Prox-Dist_i
Volume 11	0.956	0.925	Cylinder	Circ base of neck		Prox-Dist_i
Volume 12	0.681	0.327	Cylinder	Circ base of ribs		T1 to T13

Tail						
Mass/Volume	Corr	Adjusted Corr	Shape	Dimension1	Dimension2	Length
Volume 1	**0.980**	**0.966**	Cone	Circ base of tail		Prox-Dist_3d
Volume 2	0.871	0.773	Cone	Circ @ caudal vertebra		Prox-Dist_3d
Volume 3	0.962	0.937	Cone	Circ base of tail		Prox-Dist_i
Volume 4	0.877	0.784	Cone	Circ @ caudal vertebra		Prox-Dist_i

APPENDIX G: RESULTS OF GEOMETRIC CORRELATIONS FOR
ESTIMATING SEGMENT MASS MOMENT OF INERTIA USING WHOLE
BODY MASS AND SPECIFIC MORPHOMETRIC DIMENSIONS

Numbers highlighted in yellow are significant at P<.05, those highlighted in grey are
significant at p<.1. Red text indicates the model used in for the regression equation. Adjusted
r was used for multiple regression analysis using body mass and geometric model. Simple r
the geometric model is used by itself.

Manus	Axis	Left		Right		Both	
		simple r	multi r	simple r	multi r	simple r	multi r
Cyl_meas_Wrist C	x	.442	.977	.623	.866	.310	.604
	y	.820	.871	.747	.849	.005	.213
	z	.924	.953	.878	.968	.811	.213
Cyl_meas_Mid C	x	.695	.891	.059	.872	.382	.671
	y	.844	.942	.741	.863	.078	.143
	z	.936	.991	.799	.958	.777	.143
Cyl_meas_Paw C	x	.623	.988	.559	.932	.100	.604
	y	.899	.969	.768	.865	.056	.167
	z	.963	.990	.873	.977	.814	.167
Frustum_meas	x	.588	.995	.604	.914	.165	.603
	y	.925	.986	.765	.868	.047	.172
	z	.972	.989	.871	.980	.823	.172
Cyl_3d_Wrist C	x	.442	.977	.623	.866	.287	.706
	y	.848	.965	.889	.890	.003	.229
	z	.901	.938	.927	.951	.904	.229
Cyl_3d_Mid C	x	.695	.891	.059	.872	.187	.709
	y	.851	.957	.909	.911	.004	.190
	z	.892	.917	.890	.944	.881	.190
Cyl_3d_Paw C	x	.623	.988	.559	.932	.122	.705
	y	.888	.963	.904	.907	.021	.226
	z	.913	.925	.926	.958	.906	.226
Frustum_3d	x	.588	.995	.604	.914	.175	.705
	y	.903	.960	.903	.908	.029	.226
	z	.916	.921	.928	.963	.907	.226

Antebrachium	Axis	Left		Right		Both		
		simple r	multi r	simple r	multi r	simple r	multi r	adjst'd r
Cyl_Wrist C	x	.652	.934	.400	.912	.146	.733	.769
	y	.794	.970	.558	.939	.642	.680	.655
	z	.671	.920	.858	.859	.758	.778	.739
Cyl_Mid C	x	.662	.934	.425	.913	.159	.735	.771
	y	.804	.971	.579	.941	.662	.698	.677
	z	.932	.984	.704	.991	.758	.876	.942
Cyl_Elb C	x	.691	.926	.374	.919			
	y	.832	.965	.529	.946			
	z	.353	.863	.661	.662			
Frustum	x	.701	.922	.362	.921	.123	.743	.784
	y	.843	.963	.516	.948	.622	.679	.666
	z	.429	.843	.723	.731	.450	.532	.551
Cyl_3d_Wrist C	x	.848	.964	.609	.899	.154	.734	
	y	.789	.893	.751	.929	.704	.729	
	z	.671	.920	.858	.859	.757	.777	
Cyl__3D_Mid C	x	.850	.963	.640	.902	.169	.815	
	y	.794	.894	.777	.933	.759	.776	
	z	.932	.984	.704	.991	.498	.696	
Cyl_3D_Elb C	x	.886	.961	.585	.909			
	y	.820	.887	.728	.939			
	z	.353	.863	.661	.662			
Frustum_3D	x	.895	.958	.573	.913	.147	.829	
	y	.832	.887	.715	.943	.743	.778	
	z	.429	.843	.723	.731	.602	.668	

Brachium	Axis	Left		Right		Both		
		simple r	multi r	simple r	multi r	simple r	multi r	adjst'd r
Frustum_PtoD	x	.314	.951	.710	.962	.413	.951	.940
	y	.449	.952	.754	.939	.446	.882	.853
	z	.620	.793	.739	.856	.708	.718	.639
Frustum_acro_l	x	.688	.912	.877	.971	.784	.942	.929
	y	.801	.922	.900	.953	.813	.901	.877
	z	.620	.793	.739	.856	.708	.718	.639
Frustum_hum_l	x	.819	.968	.826	.961	.823	.961	.952
	y	.609	.807	.786	.908	.691	.837	.796
	z	.620	.793	.739	.856	.708	.718	.639
Cyl_AxC_Acrl	x	.690	.901	.877	.973	.783	.938	.923
	y	.805	.912	.903	.957	.812	.896	.871
	z	.576	.761	.181	.867	.477	.548	.380

Pes	Axis	Left		Right		Both		
		simple r	multi r	simple r	multi r	simple r	multi r	adjst'd r
Pyramid_P2D	x	.880	.991	.654	.996	.014	.936	.922
	y	.846	.905	.726	.849	.082	.829	.786
	z	.846	.953	.836	.836	.070	.792	.737
Pyramid_heel2tip	x	.881	.967	.504	.998	.311	.961	.952
	y	.905	.992	.445	.786	.046	.830	.787
	z	.165	.953	.836	.836	.070	.792	.737
Pyramid_heel2mtpj	x	.681	.977	.540	.989	.523	.946	.934
	y	.811	.909	.757	.880	.473	.844	.805
	z	.301	.953	.836	.836	.070	.792	.737
Pyramid_3d	x	.613	.990	.823	.994	.387	.971	.965
	y	.835	.992	.794	.836	.117	.830	.787
	z	.317	.953	.836	.836	.070	.792	.737
Cyl_p2d3d_c	x	.258	.977	.555	.989	.420	.904	.881
	y	.326	.899	.753	.864	.527	.796	.743
	z	.852	.967	.881	.950	.842	.930	.914
Cyl_p2d3d_ank	x	.920	.962	.823	.995	.795	.941	.928
	y	.873	.902	.598	.777	.751	.829	.786
	z	.613	.886	.858	.990	.667	.760	.695
Cyl_p2d_c	x	.296	.980	.563	.989	.436	.934	.918
	y	.367	.900	.764	.869	.547	.845	.807
	z	.852	.967	.881	.950	.855	.945	.933
Cyl_p2d_ank	x	.904	.966	.771	.995	.817	.934	.919
	y	.843	.902	.534	.785	.737	.829	.786
	z	.693	.808	.696	.765	.684	.772	.712
Cyl_heel2tip_c	x	.261	.977	.560	.989	.465	.934	.918
	y	.319	.900	.756	.866	.545	.845	.806
	z	.852	.967	.881	.950	.855	.945	.933
Cyl_p2d_ank	x	.918	.962	.776	.996	.772	.942	.929
	y	.882	.906	.563	.776	.738	.829	.786
	z	.693	.808	.696	.765	.684	.772	.712
Cyl_heel2mtpj_c	x	.265	.977	.550	.989	.464	.933	.918
	y	.334	.899	.760	.868	.562	.847	.809
	z	.852	.967	.881	.950	.855	.945	.933
Cyl_heel2mtpj_ank	x	.921	.963	.836	.995	.787	.938	.924
	y	.869	.901	.590	.788	.720	.830	.787
	z	.693	.808	.696	.765	.684	.772	.712

Crus	Axis	Left		Right			Both	
		simple r	multi r	simple r	multi r	adjst'd r	simple r	multi r
cyl_p2d_ankc	x	.830	.927	.620	.970	.950	.505	.580
	y	.833	.920	.606	.996	.993	.620	.622
	z	.860	.950	.973	.982	.970	.281	.289
cyl_tib2sphyr_ankc	x	.872	.914	.889	.935	.889	.136	.729
	y	.843	.926	.933	.950	.915	.162	.606
	z	.860	.950	.973	.982	.970	.281	.289
cyl_p2d_kneec	x	.877	.934	.589	.956	.925	.562	.613
	y	.868	.923	.587	.986	.977	.646	.653
	z	.846	.952	.165	.948	.912	.076	.338
cyl_tib2_kneec	x	.880	.905	.881	.905	.836	.180	.619
	y	.846	.905	.905	.943	.902	.124	.492
	z	.846	.952	.165	.948	.912	.077	.338
Frustum_hum_l							.582	.620
							.659	.678
							.164	.340

Neck	Axis			
		simple r	multi r	adjst'd r
frustum	x	.149	.943	.903
	y	.913	.960	.933
	z	.825	.993	.988
cylinder	x	.731	.902	.830
	y	.796	.973	.954
	z	.601	.985	.974
cylinder	x	.689	.919	.860
	y	.808	.967	.945
	z	.639	.990	.983

Head	Axis			
		simple r	multi r	adjst'd r
ypse l_p2d_bior	x	.993	.995	.992
	y	.740	.912	.849
	z	.906	.908	.841

Thigh	Axis	Left		Right		Both		
		simple r	multi r	simple r	multi r	simple r	multi r	adjst'd r
cyl_p2d_kneec	x	.772	.915	.661	.926	.672	.883	.855
	y	.888	.986	.833	.869	.848	.911	.890
	z	.710	.742	.977	.977	.745	.751	.683
cyl_p2d_uppcpre	x	.597	.920	.324	.918	.400	.869	.837
	y	.718	.982	.595	.815	.639	.881	.852
	z	.780	.784	.748	.803	.756	.771	.710
cyl_p2d_uppcpost	x	.636	.903	.395	.912	.456	.852	.816
	y	.763	.972	.667	.830	.673	.856	.821
	z	.929	.953	.810	.855	.826	.831	.788
cyl_p2d_midc_pre	x	.681	.904	.613	.929	.605	.889	.862
	y	.811	.978	.835	.890	.806	.914	.894
	z	.301	.718	.317	.762	.030	.643	.531
cyl_p2d_midc_post	x	.785	.907	.662	.921	.683	.878	.849
	y	.904	.982	.830	.863	.851	.903	.880
	z	.729	.729	.848	.863	.688	.688	.597
cyl_trch/fem_kneec	x	.532	.955	.236	.915	.025	.817	.770
	y	.446	.818	.107	.754	.256	.756	.690
	z	.710	.742	.977	.977	.746	.752	.685
cyl_trch/fem_uppc	x	.304	.959	.531	.890	.255	.778	.719
	y	.236	.805	.219	.632	.025	.679	.584
	z	.780	.784	.748	.803	.756	.771	.710
cyl_trch/fem_midc	x	.341	.950	.533	.882	.228	.768	.706
	y	.267	.798	.204	.642	.001	.665	.563
	z	.929	.953	.810	.855	.826	.831	.788
frustum_l_p2d	x	.456	.991	.315	.931	.036	.844	.806
	y	.402	.869	.062	.804	.215	.806	.756
	z	.301	.718	.317	.762	.032	.638	.524
frustum_l_trch/fem	x	.549	.947	.237	.909	.027	.807	.757
	y	.459	.809	.108	.746	.257	.746	.676
	z	.729	.729	.848	.863	.686	.686	.594

Abdomen	Axis	simple r	multi r	adjst'd r
frustum_jt ctr	x	.919	.925	.872
	y	.874	.886	.801
	z	.612	.894	.817
frustum_spin proc	x	.919	.925	.872
	y	.787	.873	.777
	z	.338	.919	.860
cylinder_jt ctr@ribs	x	.779	.862	.757
	y	.882	.884	.798
	z	.696	.889	.806
cylinder_jt ctr @ mid	x	.467	.858	.749
	y	.853	.873	.778
	z	.645	.887	.803
cylinder_jt ctr @ waist	x	.863	.978	.964
	y	.867	.891	.810
	z	.638	.885	.799
cylinder_spin proc@ribs	x	.779	.862	.757
	y	.828	.876	.783
	z	.452	.911	.846
cylinder_spin proc@mid	x	.467	.858	.749
	y	.782	.871	.774
	z	.367	.908	.842
cylinder_spin proc@waist	x	.863	.978	.964
	y	.811	.890	.808

Thorax	Axis	simple r	multi r	adjst'd r
frustum_jt ctr	x	.803	.980	.967
	y	.900	.918	.860
	z	.899	.926	.873
frustum_sgmtctr	x	.803	.980	.967
	y	.892	.903	.832
	z	.908	.930	.880
cylinder_jtctr_T13L1	x	.826	.858	.749
	y	.680	.777	.583
	z	.872	.910	.845
cylinder_jtctr @ mid	x	.251	.859	.750
	y	.621	.778	.585
	z	.888	.928	.877
cylinder_jtctr @ T1C7	x	.395	.909	.843
	y	.477	.784	.599
	z	.806	.920	.863
cylinder_sgmtctr_T13L1	x	.826	.858	.749
	y	.483	.863	.758
	z	.812	.890	.808
cylinder_sgmtctr @ mid	x	.251	.859	.750
	y	.380	.893	.814
	z	.815	.899	.825
cylinder_sgmtctr @ T1C7	x	.395	.909	.843
	y	.240	.869	.770
	z	.719	.899	.826

Tail	Axis	simple r	multi r	adjst'd r
cone_sacr l_sacr c	x	.955	.983	.972
	y	.717	.988	.980
	z	.901	.974	.956
cone_sacr l_ caudv c	x	.960	.987	.978
	y	.715	.988	.979
	z	.770	.925	.871
cone_sacr l_mid c	x	.955	.984	.973
	y	.722	.988	.980
	z	.866	.917	.858
cone_caud l_sacr c	x	.816	.947	.910
	y	.876	.986	.976
	z	.901	.974	.956
cone_caud l_ caudv c	x	.819	.949	.913
	y	.875	.986	.976
	z	.770	.925	.871
cone_caud l_mid c	x	.813	.946	.908
	y	.878	.985	.976
	z	.866	.917	.858

APPENDIX H: CORRELATION RESULTS - SEGMENT MASS TO BODY MASS

Segment	Side	R	R²	StErrofEst(kg)
Manus	Left	.005	.000	.02659
	Right	.201	.041	.02989
	Both	.110	.012	.02544
Antebrachium	Left	.331	.110	.06653
	Right	.162	.026	.06477
	Both	.094	.009	.06075
Brachium	Left	.447	.200	.19298
	Right	.637	.405	.16100
	Both	.519	.269	.16900
Pes	Left	.527	.278	.02335
	Right	.574	.329	.02082
	Both	.549	.302	.01979
Crus	Left	.620	.384	.07297
	Right	.404	.163	.06773
	Both	.163	.027	.07486
Thigh	Left	.359	.129	.34712
	Right	.649	.422	.31203
	Both	.000	.000	.35194
Thorax		.561	.315	1.00693
Abdomen		.845	.715	1.02745
Head		.454	.207	.28073
Neck		.170	.029	.65759
Tail		.736	.542	.03944

Note: yellow indicates significant at $p<.05$;

grey indicates significant at $p<.10$

APPENDIX I: CORRELATION RESULTS - SEGMENT MOI TO BODY MASS

Left and Right Limbs Separate						Left and Right Limbs Combined				
Segment	Rotation Axis	R	R^2	StErrof Est		Segment	Rotation Axis	R	R^2	StErrof Est
LManus	i/e (x)	.652	.425	.0001		Manus	i/e (x)	.603	.364	.0002
LManus	f/e (y)	.728	.530	.0003		Manus	f/e (y)	.121	.015	.0004
LManus	ab/ad (z)	.759	.576	.0002		Manus	ab/ad (z)	.716	.512	.0002
RManus	i/e (x)	.849	.721	.0001		Abr	ab/ad (x)	.702	.493	.0004
RManus	f/e (y)	.836	.699	.0002		Abr	f/e (y)	.166	.028	.0004
RManus	ab/ad (z)	.930	.866	.0002		Abr	i/e (z)	.514	.265	.0002
LAbr	ab/ad (x)	.829	.688	.0003		Br	ab/ad (x)	.874	.764	.0005
LAbr	f/e (y)	.764	.583	.0003		Br	f/e (y)	.780	.608	.0012
LAbr	i/e (z)	.829	.688	.0002		Br	i/e (z)	.131	.017	.0021
RAbr	ab/ad (x)	.835	.697	.0005		Pes	ab/ad (x)	.933	.871	.0001
RAbr	f/e (y)	.778	.606	.0004		Pes	f/e (y)	.829	.688	.0001
RAbr	i/e (z)	.451	.203	.0003		Pes	i/e (z)	.771	.594	.0002
LBr	ab/ad (x)	.828	.686	.0006		Crus	ab/ad (x)	.306	.094	.0009
LBr	f/e (y)	.746	.557	.0008		Crus	f/e (y)	.015	.000	.0004
LBr	i/e (z)	.742	.551	.0012		Crus	i/e (z)	.284	.081	.0004
RBr	ab/ad (x)	.922	.850	.0005		Thigh	ab/ad (x)	.671	.450	.0018
RBr	f/e (y)	.868	.753	.0013		Thigh	f/e (y)	.459	.211	.0023
RBr	i/e (z)	.855	.731	.0012		Thigh	i/e (z)	.596	.355	.0015
LPes	ab/ad (x)	.959	.920	.0000		Body				
LPes	f/e (y)	.896	.803	.0001		Segment	Rotation Axis	R	R2	StErrof Est
LPes	i/e (z)	.797	.636	.0002						
RPes	ab/ad (x)	.988	.977	.0000		Thx	ab/ad (x)	.793	.630	.0059
RPes	f/e (y)	.760	.577	.0001		Thx	f/e (y)	.609	.371	.0371
RPes	i/e (z)	.765	.585	.0003		Thx	i/e (z)	.584	.341	.0357
LCrus	ab/ad (x)	.904	.817	.0006		Abd	ab/ad (x)	.858	.736	.0149
LCrus	f/e (y)	.892	.796	.0002		Abd	f/e (y)	.777	.604	.0368
LCrus	i/e (z)	.948	.899	.0001		Abd	i/e (z)	.885	.783	.0237
RCrus	ab/ad (x)	.905	.819	.0002		Hd	ab/ad (x)	.955	.912	.0013
RCrus	f/e (y)	.942	.887	.0002		Hd	f/e (y)	.900	.810	.0012
RCrus	i/e (z)	.936	.876	.0002		Hd	i/e (z)	.683	.466	.0011
LThigh	ab/ad (x)	.499	.249	.0016		Neck	ab/ad (x)	.899	.808	.0013
LThigh	f/e (y)	.436	.190	.0023		Neck	f/e (y)	.676	.456	.0040
LThigh	i/e (z)	.712	.508	.0011		Neck	i/e (z)	.864	.747	.0022
RThigh	ab/ad (x)	.816	.666	.0019		Tail	ab/ad (x)	.246	.061	.0012
RThigh	f/e (y)	.484	.234	.0028		Tail	f/e (y)	.668	.447	.0009
RThigh	i/e (z)	.552	.305	.0021		Tail	i/e (z)	.837	.700	.0002
Note:	yellow =	significance at p<.05;			grey =	significance at p<.10				

APPENDIX J: VICON BODYLANGUAGE CODE FOR CALCULATING JOINT

CENTRES

```
* GaitLab 2.0 BodyBuilder model*}
{* For use with Gaitlab Marker and Parameter File *}
{*========================================================*}
{* Macro for Cross Product *}

MACRO CrossProduct ( First, Second, Result )
       Result = { First(2)*Second(3)-First(3)*Second(2),
       First(3)*Second(1)-First(1)*Second(3),
       First(1)*Second(2)-First(2)*Second(1)}
ENDMACRO


{*========================================================*}


{* Macro for Dot Product *}

MACRO DotProduct (One,Two,DotProd)
       DotProd = (1(One)*1(Two)+2(One)*2(Two)+3(One)*3(Two))
ENDMACRO



{*========================================================*}



{*Joint Centre Estimations – Hind Limb*}
{*========================*}

{*Pelvis*}
       Vpel = (LCDIS-RCDIS)/(ABS(LCDIS-RCDIS))
OneA = RCDIS-SACRUM
TwoA = LCDIS-SACRUM
CrossProduct( OneA, TwoA, UpA)

       Wpel = UpA/(ABS(UpA))

CrossProduct( Vpel, Wpel, Upel)

       Upel = Upel

RHJC = RHIP + 0.0*$CDISBreadth*Upel + 0.531*$CDISBreadth*Vpel -
0.0*$CDISBreadth*Wpel
LHJC = LHIP + 0.0*$CDISBreadth*Upel - 0.531*$CDISBreadth*Vpel -
0.0*$CDISBreadth*Wpel
```

{*STIFLE*}
    VRCRUS = (RANK-RSTIFLE)/(ABS(RANK-RSTIFLE))
    VLCRUS = (LANK-LSTIFLE)/(ABS(LANK-LSTIFLE))

One = RCWAND-RSTIFLE
Two = RANK-RSTIFLE
Three = LCWAND-LSTIFLE
Four = LANK-LSTIFLE
CrossProduct(One, Two, Up)
CrossProduct(Three, Four, Down)

    WRCRUS = Up/(ABS(Up))
    WLCRUS = Down/(Abs(Down))

CrossProduct(WRCRUS, VRCRUS, URCRUS)
CrossProduct(VLCRUS, WLCRUS, ULCRUS)

    URCRUS = URCRUS
    ULCRUS = ULCRUS

RKJC = RSTIFLE + 0.5*($MarkerDiameter + $RightSTIFLEDiam)*URCRUS
LKJC = LSTIFLE - 0.5*($MarkerDiameter + $LeftSTIFLEDiam)*ULCRUS

[Oosterlinck et al.]
    URPES = (RMTPJ-RHEEL)/(ABS(RMTPJ-RHEEL))
    ULPES = (LMTPJ-LHEEL)/(ABS(LMTPJ-LHEEL))

One1 = RMTPJ-RANK
Two1 = RHEEL-RANK
Three1 = LMTPJ-LANK
Four1 = LHEEL-LANK

CrossProduct(One1, Two1, Up1)
CrossProduct (Three1, Four1, Down1)

    WRPES = Up1/(ABS(Up1))
    WLPES = Down1/(ABS(Down1))

CrossProduct(WRPES, URPES, VRPES)
CrossProduct(WLPES, ULPES, VLPES)

    VLPES = VLPES
    VRPES = VRPES

RAJC = RANK + 0.0*$RightPESLength*URPES + 0.0*$RightAnkleHeight*VRPES + 0.5*$RightAnkleWidth*WRPES
LAJC = LANK + 0.0*$LeftPESLength*ULPES + 0.0*$LeftAnkleHeight*VLPES - 0.5*$LeftAnkleWidth*WLPES

RMTPJP = RANK + 0.0*$RightPESLength*URPES + 0.5*$RightAnkleHeight*VRPES - 0.0*$RightPESBreadth*WRPES
LMTPJP = LANK + 0.0*$LeftPESLength*ULPES + 0.5*$LeftAnkleHeight*VLPES + 0.0*$LeftPESBreadth*WLPES

OUTPUT (RHJC,LHJC,RKJC,LKJC,RAJC,LAJC,RMTPJP,LMTPJP)

{*Joint Centre Estimations - Forelimb*}
{*========================*}

{*Shoulder*}
        Vshj = (LACJ-RACJ)/(ABS(LACJ-RACJ))
OneA = RACJ-C7
TwoA = LACJ-C7
CrossProduct(OneA, TwoA, UpA)

        Ushj = UpA/(ABS(UpA))

CrossProduct(VShj, UShj, WShj)

        Wshj = WShj

RSHJC = RACJ + 0.0*$ShoulderBreadth*UShj + 0.344*$ShoulderBreadth*VShj - 0.0*$ShoulderBreadth*WShj
LSHJC = LACJ + 0.0*$ShoulderBreadth*UShj - 0.344*$ShoulderBreadth*VShj - 0.0*$ShoulderBreadth*WShj

{*Elbow*}
        VRAntebrach = (RLATWRIST-RELBOW)/(ABS(RLATWRIST-RELBOW))
        VLAntebrach = (LLATWRIST-LELBOW)/(ABS(LLATWRIST-LELBOW))

One = RLATWRIST-RELBOW
Two = RMEDWRIST-RELBOW
Three = LLATWRIST-LELBOW
Four = LMEDWRIST-LELBOW
CrossProduct(One, Two, Up)
CrossProduct(Three, Four, Down)

WRAntebrach = Up/(ABS(Up))
WLAntebrach = Down/(Abs(Down))

CrossProduct(WRAntebrach, VRAntebrach, URAntebrach)
CrossProduct(VLAntebrach, WLAntebrach, ULAntebrach)

URAntebrach = URAntebrach
ULAntebrach = ULAntebrach

REJC = RELBOW + 0.5*($MarkerDiameter + $RightELBOWDiam)*URAntebrach
LEJC = LELBOW - 0.5*($MarkerDiameter + $LeftELBOWDiam)*ULAntebrach

{*Wrist*}

WRMANUS = (RMEDWRIST-RLATWRIST)/(ABS(RMEDWRIST-RLATWRIST))
WLMANUS = (LMEDWRIST-LLATWRIST)/(ABS(LMEDWRIST-LLATWRIST))

LMIDWRIST=(LLATWRIST+LMEDWRIST)/2
RMIDWRIST=(RLATWRIST+RMEDWRIST)/2

VRMANUS = (RMIDWRIST-RMCPJ)/(ABS(RMEDWRIST-RMCPJ))
VLMANUS = (LMIDWRIST-LMCPJ)/(ABS(LMEDWRIST-LMCPJ))

CrossProduct(WRMANUS, VRMANUS, URMANUS)
CrossProduct(VLMANUS, WLMANUS, ULMANUS)

ULMANUS = ULMANUS
URMANUS = URMANUS

RWJC = RLATWRIST + 0.0*$RightWRISTWidth*URMANUS +
0.0*$RightWRISTWidth*VRMANUS + 0.5*$RightWRISTWidth*WRMANUS
LWJC = LLATWRIST + 0.0*$LeftWRISTWidth*ULMANUS +
0.0*$LeftWRISTWidth*VLMANUS + 0.5*$LeftWRISTWidth*WLMANUS

RMCPJP= RMCPJ - 0.5*$RightMANUSDepth*URMANUS
LMCPJP = LMCPJ - 0.5*$LeftMANUSDepth*ULMANUS

OUTPUT (RSHJC,LSHJC,REJC,LEJC,RMCPJP,LMCPJP,
,RMIDWRIST,LMIDWRIST)

APPENDIX K: VICON BODYLANGUAGE CODE FOR CALCULATING

FLEXION/EXTENSION ANGLES FROM JOINT CENTRES

```
MACRO DotProduct (One,Two,Three,DotProd)
Seg1=One-Two
Seg2=Three-Two
Mag1=DIST(One,Two)
Mag2=DIST(Two,Three)
DotProd = (1(Seg1)*1(Seg2)+2(Seg1)*2(Seg2)+3(Seg1)*3(Seg2))/(Mag1*Mag2)
ENDMACRO

{*Hind Leg Flexion/Extension Angles*}
{*--------------------------------*}

PelF = (LCDIS+RCDIS)/2
PelO = (PelF+SACRUM)/2
Pelvis = [PelO,LCDIS-RCDIS,PelF-SACRUM,yzx]

DotProduct(PelO,LHJC,LKJC,LeftHip)
LHA1=45-ASIN(LeftHip)
OUTPUT(LHA1)
LeftHipAngle=<LHA1,0,0>
OUTPUT(LeftHipAngle)

DotProduct(PelO,RHJC,RKJC,RightHip)
RHA1=45-ASIN(RightHip)
OUTPUT(RHA1)
RightHipAngle=<RHA1,0,0>
OUTPUT(RightHipAngle)

DotProduct(LHJC,LKJC,LAJC,LeftStifle)
LKA1=90-ASIN(LeftStifle)
OUTPUT(LKA1)
LeftStifleAngle=<LKA1,0,0>
OUTPUT(LeftStifleAngle)

DotProduct(RHJC,RKJC,RAJC,RightStifle)
RKA1=90-ASIN(RightStifle)
OUTPUT(RKA1)
RightStifleAngle=<RKA1,0,0>
OUTPUT(RightStifleAngle)

DotProduct(LKJC,LAJC,LMTPJ,LeftAnkle)
LAA1=90-ASIN(LeftAnkle)
```

249

OUTPUT(LAA1)
LeftAnkleAngle=<LAA1,0,0>
OUTPUT(LeftAnkleAngle)

DotProduct(RKJC,RAJC,RMTPJ,RightAnkle)
RAA1=90-ASIN(RightAnkle)
OUTPUT(RAA1)
RightAnkleAngle=<RAA1,0,0>
OUTPUT(RightAnkleAngle)

{*Fore Leg Flexion/Extension Angles*}
{*--------------------------------*}

DotProduct(C7,LSHJC,LEJC,LeftShoulder)
LSHA1=90-ASIN(LeftShoulder)
OUTPUT(LSHA1)
LeftShoulderAngle4=<LSHA1,0,0>
OUTPUT(LeftShoulderAngle4)

DotProduct(C7,RSHJC,REJC,RightShoulder)
RSHA1=90-ASIN(RightShoulder)
OUTPUT(RSHA1)
RightShoulderAngle4=<RSHA1,0,0>
OUTPUT(RightShoulderAngle4)

DotProduct(LSHJC,LEJC,LMIDWRIST,LeftElbow)
LEA1=90-ASIN(LeftElbow)
OUTPUT(LEA1)
LeftElbowAngle=<LEA1,0,0>
OUTPUT(LeftElbowAngle)

DotProduct(RSHJC,REJC,RMIDWRIST,RightElbow)
REA1=90-ASIN(RightElbow)
OUTPUT(REA1)
RightElbowAngle=<REA1,0,0>
OUTPUT(RightElbowAngle)

DotProduct(LEJC,LMIDWRIST,LMCPJP,LeftWrist)
LWA1=-90-ASIN(LeftWrist)
OUTPUT(LWA1)
LeftWristAngle=<LWA1,0,0>
OUTPUT(LeftWristAngle)

DotProduct(REJC,RMIDWRIST,RMCPJP,RightWrist)

RWA1=-90-ASIN(RightWrist)
OUTPUT(RWA1)
RightWristAngle=<RWA1,0,0>
OUTPUT(RightWristAngle)

REFERENCES

Ackland TR, Blanksby BA and Bloomfield J (1988). Inertial characteristics of adolescent male body segments. *Journal of Biomechanics*; **21**: 319-327.

ACVS. (2015). Canine Hip Dysplasia. *Small Animal Topics* Retrieved February 16, 2015, from https://www.acvs.org/small-animal/canine-hip-dysplasia.

ACVS. (2015). Cranial Cruciate Ligament Disease. *Small Animal Health Topics* Retrieved February 17, 2015, from https://www.acvs.org/small-animal/cranial-cruciate-ligament-disease.

Agostinho FS, Rahal SC, Miqueleto NSML, Verdugo MR, Inamassu LR and El-Warrak AO (2011). Kinematic analysis of Labrador Retrievers and Rottweilers trotting on a treadmill. *Veterinary and Comparative Orthopaedics and Traumatology*; **24**(3): 185-191.

Alexander EJ and Andriacchi TP (2001). Correcting for deformation in skin-based marker systems. *Journal of Biomechanics*; **34**(3): 355-361.

Alexander JW (1992). The Pathogenesis of Canine Hip Dysplasia. *Veterinary Clinics of North America: Small Animal Practice*; **22**(3): 503-511.

Allen K, Decamp CE, Braden TD and Bahns M (1994). Kinematic gait analysis of the trot in healthy mixed breed dogs. *Veterinary and Comparative Orthopaedics and Traumatology*; **7**(4): 148-153.

Alpak H, Mutus R and Onar V (2004). Correlation analysis of the skull and long bone measurements of the dog. *Annals of Anatomy-Anatomischer Anzeiger*; **186**(4): 323-330.

American Kennel Club. (2015). AKC Glossary. Retrieved Sept 20, 2015, from http://www.akc.org/about/glossary/.

Amit T, Gomberg BR, Milgram J and Shahar R (2009). Segmental inertial properties in dogs determined by magnetic resonance imaging. *Veterinary Journal*; **182**(1): 94-99.

Animal Critical Care Group (2005). *Centre for Canine Performance and Health: A canine performance and health initiative*. S. Raschke. Vancouver, BC Canada, British Columbia Institute of Technology.

Asher L, Diesel G, Summers JF, McGreevy PD and Collins LM (2009). Inherited defects in pedigree dogs. Part 1: Disorders related to breed standards. *The Veterinary Journal*; **182**(3): 402-411.

Averill DR, Jr. (1973). Degenerative myelopathy in the aging German Shepherd dog: clinical and pathologic findings. *J Am Vet Med Assoc*; **162**(12): 1045-1051.

Awano T, Johnson GS, Wade CM, Katz ML, Johnson GC, Taylor JF, Perloski M, Biagi T, Baranowska I, Long S, March PA, Olby NJ, Shelton GD, Khan S, O'Brien DP, Lindblad-Toh K and Coates JR (2009). Genome-wide association analysis reveals a SOD1 mutation in canine degenerative myelopathy that resembles amyotrophic lateral sclerosis. *Proceedings of the National Academy of Sciences*; **106**(8): 2794-2799.

Back W, Barneveld A, Vanweeren PR and Vandenbogert AJ (1993). Kinematic gait analysis in equine carpal lameness. *Acta Anatomica*; **146**(2-3): 86-89.

Baker R (2006). Gait analysis methods in rehabilitation. *Journal of NeuroEngineering and Rehabilitation*; **3**(1): 1-10.

Barclay KB and Haines DM (1994). Immunohistochemical evidence for immunoglobulin and complement deposition in spinal cord lesions in degenerative myelopathy in German shepherd dogs. *Canadian Journal of Veterinary Research*; **58**(1): 20.

Barrey E (1999). Methods, Applications and Limitations of Gait Analysis in Horses. *The Veterinary Journal*; **157**(1): 7-22.

Barter JT (1957). *Estimation of the mass of body segments*, Wright Air Development Center, Air Research and Development Command, United States Air Force, Wright-Patterson Air Force Base, Ohio.

Becker K. (2012, April 16, 2012). If Your Dog's Gait is Changing, Check for Elbow Dysplasia. *Healthy Pets* Retrieved Feb 17, 2015, from http://healthypets.mercola. com/sites/healthypets/archive/2012/04/16/canine-elbow-dysplasia.aspx.

Behnke AR, Feen BG and Welham WC (1995). The specific gravity of healthy men. Body weight divided by volume as an index of obesity. *Obesity Research*; **3**(3): 295-300.

Bennett RL, DeCamp CE, Flo GL, Hauptman JG and Stajich M (1996). Kinematic gait analysis in dogs with hip displasia. *American Journal of Veterinary Research*; **57**(7): 966-971.

Bernstein N (1967). *The coordination and regulation of movement*. London, Pergamon Press.

Bernstein N, Salzgeber O, Pavlenko P and Gurvich N (1936). Determination of location of the centers of gravity and mass of the limbs of the living human body. *All-Union Institute of Experimental Medicine, Moscow*.

Boece H, Bellenden J, Mylne R and Pierpont Morgan L (1536). *The history and croniklis of Scotland* Scotland. (Scots.)

Borelli GA (1681). *De motu animalium, puos posthumum* Rome.

Bouisset S and Pertuzon E (1968). Experimental determination of the moment of inertia of limb segments. *Biomechanics I*: 106-109.

Brand RA (1989). Can Biomechanics Contribute to Clinical Orthopaedic Assessments? *The Iowa Orthopaedic Journal*; **9**: 61-64.

Braune W and Fischer O (1889). *The center of gravity of the human body as related to the german infantrymen*. Leipzig, National Technical Information Services.

Brehm H, Loeffler K and Komeyli H (1985). Skull shape in the dog. *Anat. Histol. Embryol*; **14**: 324-331.

Brooks CB and Jacobs AM (1975). The gamma mass scanning technique for inertial anthropometric measurement. *Medicine and Science in Sports*; **7**: 290-294.

Buchner HHF, ObermÜLler S and Scheidl M (2000). Body centre of mass movement in the sound horse. *The Veterinary Journal*; **160**(3): 225-234.

Buchner HHF, ObermÜLler S and Scheidl M (2001). Body centre of mass movement in the lame horse. *Equine Veterinary Journal*; **33**(S33): 122-127.

Buchner HHF, Savelberg H, Schamhardt HC and Barneveld A (1996). Head and trunk movement adaptations in horses with experimentally induced fore- or hindlimb lameness. *Equine Veterinary Journal*; **28**(1): 71-76.

Buchner HHF, Savelberg H, Schamhardt HC and Barneveld A (1997). Inertial properties of Dutch Warmblood horses. *Journal of Biomechanics*; **30**(6): 653-658.

Buczek FL, Rainbow MJ, Cooney KM, Walker MR and Sanders JO (2010). Implications of using hierarchical and six degree-of-freedom models for normal gait analyses. *Gait & Posture*; **31**(1): 57-63.

Cappozzo A (1983). Considerations on clinical gait evaluation. *Journal of Biomechanics*; **16**(4): 302.

Cappozzo A, Della Croce U, Leardini A and Chiari L (2005). Human movement analysis using stereophotogrammetry: Part 1: theoretical background. *Gait & Posture*; **21**(2): 186-196.

CGD Network. (2009). Degenerative Myelopathy - Disease Basics. Retrieved Feb 18, 2015, from http://www.caninegeneticdiseases.net/DM/basicDM.htm.

Chandler RF, Clauser CE, McConville JT, Reynolds HM and Young JW (1975). *Investigation of the inertial properties of the human body*. Springfield, Va, National Technical Information Service.

Cheng C-K, Chen H-H, Chen C-S, Lee C-L and Chen C-Y (2000). Segment inertial properties of Chinese adults determined from magnetic resonance imaging. *Clinical Biomechanics*; **15**(8): 559-566.

Clarys J and Marfell-Jones M (1986). Anatomical segmentation in humans and the prediction of segmental masses from intra-segmental anthropometry. *Human Biology*: 771-782.

Clauser CE, McConville JT and Young JW (1969). *Weight, volume, and center of mass of segments of the human body*. Springfield, Va.

Clayton HM, Lanovaz JL, Schamhardt HC, Willemen MA and Colborne GR (1998). Net joint moments and powers in the equine forelimb during the stance phase of the trot. *Equine Veterinary Journal*; **30**(5): 384-389.

Clayton HM and Schamhardt HC (2000). *Equine Locomotion* Amsterdam, Elsevier.

Clements DN, Owen MR, Carmichael S and Reid SW (2005). Kinematic analysis of the gait of 10 labrador retrievers during treadmill locomotion. *The Veterinary record*; **156**(15): 478-481.

Clemmons RM (1992). Degenerative Myelopathy. *Veterinary Clinics of North America: Small Animal Practice*; **22**(4): 965-971.

Coates JR, March PA, Oglesbee M, Ruaux CG, Olby NJ, Berghaus RD, O'Brien DP, Keating JH, Johnson GS and Williams DA (2007). Clinical characterization of a familial degenerative myelopathy in Pembroke Welsh Corgi dogs. *Journal of Veterinary Internal Medicine*; **21**(6): 1323-1331.

Coates JR and Wininger FA (2010). Canine Degenerative Myelopathy. *Veterinary Clinics of North America-Small Animal Practice*; **40**(5): 929-+.

Colborne GR (2004). Gait analysis: technology looking for a place to happen? *Veterinary Journal*; **168**(2): 112-113.

Colborne GR (2007). Bringing canine biomechanics research out of the dark ages. *Veterinary Journal*; **173**(3): 469-470.

Colborne GR, Innes JF, Comerford EJ, Owen MR and Fuller CJ (2005). Distribution of power across the hind limb joints in Labrador Retrievers and Greyhounds. *American Journal of Veterinary Research*; **66**(9): 1563-1571.

Contini R, Drillis RJ and Bluestein M (1963). Determination of body segment parameters. *Human Factors*; **5**(5): 493-504.

Cook CR and Cook JL (2009). Diagnostic imaging of canine elbow dysplasia: a review. *Veterinary Surgery*; **38**(2): 144-153.

Crompton RH, Li Y, Alexander RMN, Wang W and Gunther MM (1996). Segment inertial properties of primates: New techniques for laboratory and field studies of locomotion. *American Journal of Physical Anthropology*; **99**(4): 547-570.

Damavandi M, Barbier F, Leboucher J, Farahpour N and Allard P (2009). Effect of the calculation methods on body moment of inertia estimations in

individuals of different morphology. *Medical Engineering & Physics*; **31**(7): 880-886.

Davis RB (1997). Reflections on clinical gait analysis. *Journal of Electromyography and Kinesiology*; **7**(4): 251-257.

de Leva P (1996). Adjustments to Zatsiorsky-Seluyanov's segment inertia parameters. *Journal of Biomechanics*; **29**(9): 1223-1230.

DeCamp CE (1997). Kinetic and kinematic gait analysis and the assessment of lameness in the dog. *Veterinary Clinics of North America-Small Animal Practice*; **27**(4): 825-&.

DeCamp CE, Riggs CM, Olivier B, Hauptman JG, Hottinger HA and Soutas-Little RW (1996). Kinematic evaluation of gait in dogs with cranial cruciate ligament rupture. *American Journal of Veterinary Research*; **57**(1): 120-126.

Decamp CE, Soutaslittle RW, Hauptman J, Olivier B, Braden T and Walton A (1993). Kinematic gait analysis of the trot in healthy greyhounds. *American Journal of Veterinary Research*; **54**(4): 627-634.

DeLuca PA, Davis Iii RB, Õunpuu S, Rose S and Sirkin R (1997). Alterations in surgical decision making in patients with cerebral palsy based on three-dimensional gait analysis. *Journal of Pediatric Orthopaedics*; **17**(5): 608-614.

DeLuca PA, Õunpuu S, Davis RB and Walsh JHP (1998). Effect of hamstring and Psoas lengthening on pelvic tilt in patients with spastic diplegic cerebral palsy. *Journal of Pediatric Orthopaedics*; **18**(6): 712-718.

Dempster WT (1955). *Space requirements of the seated operator. Geometrical, kinematic, and mechanical aspects of the body with special reference to the limbs. U S A F Wright Air Development Center Tech Dept*. Dayton, OH, Wright Patterson Air Force Base.

Diss CE (2001). The reliability of kinetic and kinematic variables used to analyse normal running gait. *Gait & Posture*; **14**(2): 98-103.

Dogan S, Manley PA, Vanderby R, Kohles SS, Hartman LM and McBeath AA (1991). Canine intersegmental hip joint forces and moments before and after cemented total hip replacement. *Journal of Biomechanics*; **24**(6): 397-407.

Dowling JJ, Durkin JL and Andrews DM (2006). The uncertainty of the pendulum method for the determination of the moment of inertia. *Medical Engineering & Physics*; **28**(8): 837-841.

Drillis R and Contini R (1966). *Body segment parameters*. New York, New York University, School of Engineering and Science, Research Division.

Drillis R, Contini R and Bluestein M (1964). Body segment parameters: a survey of measurement techniques. *Artificial limbs*; **8**: 44-66.

Du Bois-Reymond R (1900). Die Grenzen der Unterstutzungflache beim Stehen. *Archiv Anat Physiol*; **23**: 562-564.

Dumas R, Cheze L and Verriest JP (2007). Adjustments to McConville et al. and Young et al. body segment inertial parameters. *Journal of Biomechanics*; **40**(3): 543-553.

Durkin JL and Dowling JJ (2003). Analysis of body segment parameter differences between four human populations and the estimation errors of four popular mathematical models. *Journal of Biomechanical Engineering-Transactions of the Asme*; **125**(4): 515-522.

Durkin JL and Dowling JJ (2006). Body segment parameter estimation of the human lower leg using an elliptical model with validation from DEXA. *Annals of Biomedical Engineering*; **34**(9): 1483-1493.

Dyce KM, Sack WO and Wensing CJG (2009). *Textbook of veterinary anatomy*, Elsevier Health Sciences.

Evans HE and De Lahunta A (2013). *Miller's Anatomy of the Dog*, Elsevier Health Sciences.

Fechner H, Johnston P, Sharp N, Montague P, Griffiths I, Wang X, Olby N, Looman A, Poller W and Flegel T (2002). Molecular genetic and expression analysis of alpha-tocopherol transfer protein mRNA in German shepherd dogs with degenerative myelopathy. *Berliner Und Munchener Tierarztliche Wochenschrift*; **116**(1-2): 31-36.

Fischer O (1906). *Theoretical fundamentals for a mechanics of living bodies with special applications to mass as well as to some processes of motion in machines*. Berlin, B.G Teubner.

Foss K, da Costa RC and Moore S (2013a). Three-Dimensional Kinematic Gait Analysis of Doberman Pinschers with and without Cervical Spondylomyelopathy. *Journal of Veterinary Internal Medicine*; **27**(1): 112-119.

Foss K, da Costa RC, Rajala-Schultz PJ and Allen MJ (2013b). Force Plate Gait Analysis in Doberman Pinschers with and without Cervical Spondylomyelopathy. *Journal of Veterinary Internal Medicine*; **27**(1): 106-111.

Fredricson I and Drevemo S (1971). A new method of investigating equine locomotion. *Equine Veterinary Journal*; **3**(4): 137-140.

Fries CL and Remedios AM (1995). The pathogenesis and diagnosis of canine hip dysplasia: a review. *The Canadian Veterinary Journal*; **36**(8): 494-502.

Gage JR, Deluca PA and Renshaw TS (1995). Gait analysis: Principles and applications: Emphasis on its use in cerebral palsy. *Journal of Bone and Joint Surgery - Series A*; **77**(10): 1607-1623.

Gage JR and Novacheck TF (2001). An update on the treatment of gait problems in cerebral palsy. *Journal of Pediatric Orthopaedics Part B*; **10**(4): 265-274.

Geary JE and Kingsbury HB (1975). *The dynamics of the equine foreleg*, Department of Mechanical and Aerospace Engineering, University of Delaware.

Gerhardt JJ and Ripstein J (1990). *Measuring and Recording of Joint Motion : Instrumentation and Techniques* Toronto, Hogrefe and Huber.

German Culture. (2012, 2012). German Shepherd - The Ultimate Service Dog. *German Culture* Retrieved January 20, 2015, from http://www.germanculture. com.ua/library/weekly/german_shepherds.htm.

Gillette RL and Angle TC (2008). Recent developments in canine locomotor analysis: A review. *Veterinary Journal*; **178**(2): 165-176.

Gillette RL and Zebas CJ (1999). A two-dimensional analysis of limb symmetry in the trot of Labrador retrievers. *Journal of the American Animal Hospital Association*; **35**(6): 515-520.

Ginja MMD, Silvestre AM, Gonzalo-Orden JM and Ferreira AJA (2010). Diagnosis, genetic control and preventive management of canine hip dysplasia: A review. *The Veterinary Journal*; **184**(3): 269-276.

Goff L, Van Weeren PR, Jeffcott L, Condie P and McGowan C (2010). Quantification of equine sacral and iliac motion during gait: a comparison between motion capture with skin-mounted and bone-fixated sensors. *Equine veterinary journal. Supplement*(38): 468-474.

Goff LM, Jeffcott LB, Jasiewicz J and McGowan CM (2008). Structural and biomechanical aspects of equine sacroiliac joint function and their relationship to clinical disease. *Veterinary Journal*; **176**(3): 281-293.

Griffin TM, Kram R, Wickler SJ and Hoyt DF (2004). Biomechanical and energetic determinants of the walk-trot transition in horses. *Journal of Experimental Biology*; **207**(24): 4215-4223.

Gustås P, Johnston C and Drevemo S (2006). Ground reaction force and hoof deceleration patterns on two different surfaces at the trot. *Equine and Comparative Exercise Physiology, 2006, Vol.3(4), pp.209-216*; **3**(4).

Hanavan E P J (1964). *A mathematical model of the human body*. Dayton, OH, NTIS No AD 608463.

Harasen G (2002). Diagnosing rupture of the cranial cruciate ligament. *The Canadian Veterinary Journal*; **43**(6): 475-476.

Harless E (1858). *Textbook of plastic anatomy. Part III* Munich. (German)

Harless E (1860). Die statischen momente der menschlichen gliedmassen. *Abhandl, Match.-Physikal. El. Koenig.* (in German). Bayr, Akad. d. Wissensch; **8**.

Harless E (1860). The static moments of the component masses of the human body. *Trans. Of the Math-Phys., Royal Bavarian Acad. Of Sci., 8 (1): 69-70, 1860.(Unpublished English Translation, FTD-TT-61-295, Wright-Patterson AFB, Ohio.)*.

Harrison SM, Whitton RC, Kawcak CE, Stover SM and Pandy MG (2010). Relationship between muscle forces, joint loading and utilization of elastic strain energy in equine locomotion. *Journal of Experimental Biology*; **213**(23): 3998-4009.

Hatze H (1980). A mathematical model for the computational determination of parameter values of Anthropomorphic segments. *Journal of Biomechanics*; **13**(10): 833-843.

Hay JG (1973). The center of gravity of the human body. *Kinesiology III*: 20-44.

Helms G, Behrens BA, Stolorz M, Wefstaedt P and Nolte I (2009). Multi-body simulation of a canine hind limb: model development, experimental validation and calculation of ground reaction forces. *Biomedical Engineering Online*; **8**.

Hicks DA and Millis DL (2014). Kinetic and kinematic evaluation of compensatory movements of the head, pelvis and thoracolumbar spine associated with asymmetric weight bearing of the pelvic limbs in trotting dogs. *Veterinary and Comparative Orthopaedics and Traumatology*; **27**(6): 453-460.

Hinrichs RN (1985). Regression equations to predict segmental moments of inertia from anthropometric measurements: An extension of the data of Chandler et al. (1975). *Journal of Biomechanics*; **18**(8): 621-624.

Hottinger HA, DeCamp CE, Olivier B, Hauptman JG and Soutas-Little RW (1996). Noninvasive kinematic analysis of the walk of healthy large-breed dogs. *American Journal of Veterinary Research*; **57**(3): 381-388.

Hower RO (1970). Advances in freeze-dry preservation of biological specimens. *Curator*; **13**: 135-152.

Huang H and Suarez FR (1983). Evaluation of cross-sectional geometry and mass density distributions of humans and laboratory animals using computerized tomography. *Journal of Biomechanics*; **16**(10): 821-832.

Ivanitzkiy MF (1956). *Human Anatomy* (3rd). Moscow. (Russian)

Jeffcott LB, Rossdale PD, Freestone J, Frank CJ and Towers-Clark PF (1982). An assessment of wastage in Thoroughbred racing from conception to four years of age. *Equine Veterinary Journal*; **14**: 185-198.

Jensen RK (1989). Changes in segment inertia proportions between 4 and 20 years. *Journal of Biomechanics*; **22**(6): 529-536.

Jensen RK (1993). Human morphology: its role in the mechanics of movement. *Journal of Biomechanics*; **26**: 81-94.

Johnson JM and Johnson AL (1993). Cranial Cruciate Ligament Rupture: Pathogenesis, Diagnosis, and Postoperative Rehabilitation. *Veterinary Clinics of North America: Small Animal Practice*; **23**(4): 717-733.

Kathmann I, Cizinauskas S, Doherr M, Steffen F and Jaggy A (2006). Daily controlled physiotherapy increases survival time in dogs with suspected degenerative myelopathy. *Journal of Veterinary Internal Medicine*; **20**(4): 927-932.

Keegan KG (2007). Evidence-based lameness detection and quantification. *Veterinary Clinics of North America-Equine Practice*; **23**(2): 403-+.

Keegan KG, Wilson DA, Wilson DJ, Smith B, Gaughan EM, Pleasant RS, Lillich JD, Kramer J, Howard RD, Bacon-Miller C, Davis EG, May KA, Cheramie HS, Valentino WL and van Harreveld PD (1998). Evaluation of mild lameness in horses trotting on a treadmill by clinicians and interns or residents and correlation of their assessments with kinematic gait analysis. *American Journal of Veterinary Research*; **59**(11): 1370-1377.

Kirberger RM and Fourie SL (1998) Elbow dysplasia in the dog : pathophysiology, diagnosis and control : review article; **69**, p.43-54.

Krüger W (1941). Über das Verhalten des Schwerpunktes bei der normalen Fortbewegung des Pferdes. *Tierärztliche Rundschau*; **47**: 147-151.

Kubo K, Sakai T, Sakuraoka H and Ishii K (1992). Segmental body weight, volume and mass center in Thoroughbred horses. *Jpn J Equine Sci*; **3**: 149-155.

Lanovaz JL, Clayton HM, Colborne GR and Schamhardt HC (1999). Forelimb kinematics and net joint moments during the swing phase of the trot. *Equine veterinary journal. Supplement*(30): 235-239.

Le SN, Lee MK and Fang AC (2009). Non-linear Image-Based Regression of Body Segment Parameters. *13th International Conference on Biomedical Engineering, Vols 1-3* (in. C. T. Lim and J. C. H. Goh; **23:** 2038-2042.

Lee WLM (2014). *A History of Police in England*.

Lephart SA (1984). Measuring the iniertial properties of cadaver segments. *Journal of Biomechanics*; **17**(7): 537-543.

Leslie M. (2001). The Man Who Stopped Time. *Stanford Alumni* Retrieved May 30, 2015, from https://alumni.stanford.edu/get/page/magazine/article/?article_id= 39117.

Martin P, Cheze L, Pourcelot P, Desquilbet L, Duray L and Chateau H (2016). Effect of the rider position during rising trot on the horse's biomechanics (back and trunk kinematics and pressure under the saddle). *Journal of Biomechanics*; **49**(7): 1027-1033.

Martin PE, Mungiole M, Marzke MW and Longhill JM (1989). The use of magnetic resonance imaging for measuring segment inertial properties. *Journal of Biomechanics*; **22**(4): 367-&.

Maynard V, Bakheit AMO, Oldham J and Freeman J (2003). Intra-rater and inter-rater reliability of gait measurements with CODA mpx30 motion analysis system. *Gait & Posture*; **17**(1): 59-67.

McConville JT and Clauser CE (1976). Anthropometric assessment of the mass distribution characteristics of the living human body. *Ergonomics*; **19**(3): 384-384.

McConville JT and US Air Force AMRL (1981). *Anthropometric relationships of body and body segment moments of inertia* Wright-Patterson Air Force Base, Ohio : Washington, D.C. : Springfield, Va., US Air Force Aerospace Medical Research Laboratory, Aerospace Medical Division, Air Force Systems Command.

McKinon W, Hartford C, Di Zio L, van Schalkwyk J, Veliotes D, Hofmeyr A and Rogers G (2004). The agreement between reaction-board measurements and kinematic estimation of adult male human whole body centre of mass location during running. *Physiological Measurement*; **25**(6): 1339.

Merkens HW and Schamhardt HC (1988). Evaluation of equine locomotion during different degrees of experimentally induced lameness. I: Lameness model and quantification of ground reaction force patterns of the limbs. *Equine veterinary journal. Supplement*(6): 99-106.

Michelsen J (2013). Canine elbow dysplasia: aetiopathogenesis and current treatment recommendations. *The Veterinary Journal*; **196**(1): 12-19.

Miqueleto NSML, Rahal SC, Agostinho FS, Siqueira EGM, Araujo FAP and El-Warrak AO (2013). Kinematic analysis in healthy and hip-dysplastic German Shepherd dogs. *Veterinary Journal*; **195**(2): 210-215.

Monaghan K, Delahunt E and Caulfield B (2007). Increasing the number of gait trial recordings maximises intra-rater reliability of the CODA motion analysis system. *Gait & Posture*; **25**(2): 303-315.

Moore J (2010). General biomechanics: The horse as a biological machine. *Journal of Equine Veterinary Science*; **30**(7): 379-383.

Mungiole M and Martin PE (1990). Estimatng segment inertial proerties - Comparison of magnetic-resonance-imaging with existing methods. *Journal of Biomechanics*; **23**(10): 1039-1046.

Nauwelaerts S, Allen WA, Lane JM and Clayton HM (2011). Inertial properties of equine limb segments. *Journal of Anatomy*; **218**(5): 500-509.

Nielsen C, Stover SM, Schulz KS, Hubbard M and Hawkins DA (2003). Two-dimensional link-segment model of the forelimb of dogs at a walk. *American Journal of Veterinary Research*; **64**(5): 609-617.

Nigg B (1994). Inertial properties of the human or animal body. *Biomechanics of the musculoskeletal system*: 337-364.

Nomenclature ICoGVA (2005). *Nomina Anatomica Veterinaria*. Knoxville, TN, World Association Veterinary Anatomists; **5:** 166.

Nova Scotia German Shepherd Dog Club. (2014, 2014). The German Shepherd Dog - Breed History.   Retrieved January 20, 2015, from http://www.nsgsdc.com/breedhistory.shtml.

Nunamaker DM and Blauner PD (1985). Normal and abnormal gait. *Textbook of small animal orthopaedics* (in**:** 1083-1095.

Oberg E (1992). *Machinery's Handbook 24th Edition, A Reference Book for the Mechanical Engineer, Designer* New York, Industrial Press Inc.

Onar V (1999). A morphometric study on the skull of the German shepherd dog (Alsatian). *Anatomia Histologia Embryologia-Journal of Veterinary Medicine Series C-Zentralblatt Fur Veterinarmedizin Reihe C*; **28**(4): 253-256.

Onar V and Gunes H (2003). On the variability of skull shape in German shepherd (Alsatian) puppies. *Anatomical Record Part a-Discoveries in Molecular Cellular and Evolutionary Biology*; **272A**(1): 460-466.

Onar V, Mutuş R and Kahvecioğlu K (1997). Morphometric analysis of the foramen magnum in German Shepherd dogs (Alsatians). *Annals of Anatomy-Anatomischer Anzeiger*; **179**(6): 563-568.

Oosterlinck M, Pille F, Huppes T, Gasthuys F and Back W (2010). Comparison of pressure plate and force plate gait kinetics in sound Warmbloods at walk and trot. *Veterinary Journal*; **186**(3): 347-351.

Õunpuu S, Bell KJ, Davis Iii RB and DeLuca PA (1996). An evaluation of the posterior leaf spring orthosis using joint kinematics and kinetics. *Journal of Pediatric Orthopaedics*; **16**(3): 378-384.

Õunpuu S, Davis RB and DeLuca PA (1996). Joint kinetics: Methods, interpretation and treatment decision-making in children with cerebral palsy and myelomeningocele. *Gait and Posture*; **4**(1): 62-78.

Ounpuu S, Gage JR and Davis RB (1991). Three-dimensional lower extremity joint kinetics in normal pediatric gait. *Journal of Pediatric Orthopaedics*; **11**(3): 341-349.

Owen M, Richards J, Clements D, Drew S, Bennett D and Carmichael S (2004). Kinematics of the elbow and stifle joints in greyhounds during treadmill trotting–An investigation of familiarisation. *Vet Comp Orthop Traumatol*; **17**(3): 141.

Page A, Candelas P, Belmar F and De Rosario H (2007). Analysis of 3D rigid-body motion using photogrammetry: A simple model based on a mechanical analogy. *American Journal of Physics*; **75**(1): 56-61.

Paul JP (1994). Gait analysis in lower limb amputees. *Journal of Rehabilitation Sciences*; **7**(SUPPL.): 38-42.

Pearsall DJ and Reid JG (1994). The study of human body segment parameters in biomechanics - An historical review and current status report. *Sports Medicine*; **18**(2): 126-140.

Pearsall DJ, Reid JG and Livingston LA (1996). Segmental inertial parameters of the human trunk as determined from computed tomography. *Annals of Biomedical Engineering*; **24**(2): 198-210.

Perry J, Burnfield JM and Cabico LM (1992). *Gait analysis: normal and pathological function* Thorofare, NJ, Slack Incorporated.

Pfau T, de Rivaz AG, Brighton S and Weller R (2011). Kinetics of jump landing in agility dogs. *Veterinary Journal*; **190**(2): 278-283.

Pierson WR (1963). A photogrammetric technique for the estimation of surface area and volume. *Annals of the New York Academy of Sciences*; **110**(1): 109-112.

Piovesan D, Pierobon A, DiZio P and Lackner JR (2011). Comparative analysis of methods for estimating arm segment parameters and joint torques from inverse dynamics. *Journal of Biomechanical Engineering*; **133**(3): 031003.

Plaga JA, Albery C, Boehmer M, Goodyear C and Thomas G (2005). *Design and Development of Anthropometrically Correct Head Forms for Joint Strike Fighter Ejection Seat Testing*, DTIC Document.

Plagenhoef S (1979). Dynamics of human and animal motion. *Environment, behaviour, and morphology: dynamic interactions in primates. New York: Gustav Fisher. p*: 95-118.

Powers PNR and Harrison AJ (1999). Models for biomechanical analysis of jumping horses. *Journal of Equine Veterinary Science*; **19**(12): 799-806.

Poy NSJ, DeCamp CE, Bennett RL and Hauptman JG (2000). Additional kinematic variables to describe differences in the trot between clinically normal dogs and dogs with hip displasia. *American Journal of Veterinary Research*; **61**(8): 974-978.

Ragetly CA, Griffon DJ, Hsu MKI, Klump LM and Hsiao-Wecksler ET (2012). Kinetic and kinematic analysis of the right hind limb during trotting on a treadmill in Labrador Retrievers presumed predisposed or not predisposed to cranial cruciate ligament disease. *American Journal of Veterinary Research*; **73**(8): 1171-1177.

Ragetly CA, Griffon DJ, Thomas JE, Mostafa AA, Schaeffer DJ, Pijanowski GJ and Hsiao-Wecksler ET (2008). Noninvasive determination of body segment

parameters of the hind limb in Labrador Retrievers with and without cranial cruciate ligament disease. *American Journal of Veterinary Research*; **69**(9): 1188-1196.

Raichlen DA (2005). Ontogeny of limb mass distribution in infant baboons (Papio cynocephalus). *Journal of Human Evolution*; **49**: 452-467.

RCMP Police Dog Services. (2008, July 24, 2008). Police Dog Services Quick Facts. Retrieved January 20, 2015, from http://www.rcmp-grc.gc.ca/fs-fd/dog-chien-eng.htm.

Reid JG and Jensen RK (1990). Human Body Segment Inertia Parameters: A Survey and Status Report. *Exercise and Sport Sciences Reviews*; **18**(1): 225-242.

Reuss-Lamky H (2012). Canine Elbow Dysplasia. *The Veterinary Technician*; **33**(7): E1-E6.

Reynolds HM (1974). *Measurement of the Inertial Properties of the Segmented Savannah Baboon*. PhD, Southern Methodist University.

Reynolds HM, Clauser CE, Mcconville J, Chandler R and Young JW (1975). *Mass distribution properties of the male cadaver*, SAE Technical Paper.

Riggs CM, DeCamp CE, Soutas-Little RW, Braden TD and Richter MA (1993). Effects of subject velocity on force plate-measured ground reaction forces in Greyhounds at the trot. *American Journal of Veterinary Research*; **54**(9): 1523-1526.

Robilliard JJ, Pfau T and Wilson AM (2007). Gait characterisation and classification in horses. *Journal of Experimental Biology*; **210**(2): 187-197.

Rodrigue D and Gagnon M (1983). The evaluation of forearm density with axial tomography. *Journal of Biomechanics*; **16**(11): 907-913.

Schaefer SL, DeCamp CE, Hauptman JG and Walton A (1998). Kinematic gait analysis of hind limb symmetry in dogs at the trot. *American Journal of Veterinary Research*; **59**(6): 680-685.

Schoonaert K, D'Aout K and Aerts P (2007). Morphometrics and inertial properties in the body segments of chimpanzees (Pan troglodytes). *Journal of Anatomy*; **210**(5): 518-531.

Seder JA and Vickery CE (2003). Temporal and kinematic gait variables of thoroughbred racehorses at or near racing speeds. *Journal of Equine Veterinary Science*; **23**(5): S82-S112.

Shahar R and Banks-Sills L (2004). A quasi-static three-dimensional, mathematical, three-body segment model of the canine knee. *Journal of Biomechanics*; **37**(12): 1849-1859.

Silva GC, Brennecke AS, Gaiad TP, Brolio MP, Oliveira VC, Neto AA, Martins DS and Ambrósio CE (2014). Kinematic gait analyses in healthy Golden Retrievers. *Pesq. Vet. Bras*; **34**(12): 1263-1268.

Simoens P, Poels P and Lauwers H (1994). Morphometric analysis of the foramen magnum in Pekingese dogs. *American Journal of Veterinary Research*; **55**(1): 34-39.

Simon SR (2004). Quantification of human motion: gait analysis - benefits and limitations to its application to clinical problems. *Journal of Biomechanics*; **37**(12): 1869-1880.

Sloane CF (1955). Dogs in War, Police Work and on Patrol. *Journal of Criminal Law and Criminology*; **46**(3): 385-395.

Sprigings E and Leach D (1986). Standardized technique for determining the centre of gravity of body and limb segments of horses. *Equine Veterinary Journal*; **18**: 43-49.

Strasser T, Peham C and Bockstahler BA (2014). A comparison of ground reaction forces during level and cross-slope walking in Labrador Retrievers. *BMC Veterinary Research, 2014, Vol.10(1)*; **10**(1).

Sutherland DH (1978). Gait analysis in cerebral palsy. *Developmental Medicine and Child Neurology*; **20**(6): 807-813.

Sutherland DH (2002). The evolution of clinical gait analysis: Part II Kinematics. *Gait & Posture*; **16**(2): 159-179.

Sutherland DH (2005). The evolution of clinical gait analysis part III - kinetics and energy assessment. *Gait & Posture*; **21**(4): 447-461.

Sutherland DH, Schottstaedt ER, Larsen LJ, Ashley RK, Callander JN and James PM (1969). Clinical and electromyographic study of seven spastic children with internal rotation gait. *Journal of Bone and Joint Surgery - Series A*; **51**(6): 1070-1082.

Swindle MM, Makin A, Herron AJ, Clubb FJ and Frazier KS (2012). Swine as Models in Biomedical Research and Toxicology Testing. *Veterinary Pathology Online*; **49**(2): 344-356.

Tanner JM (1951). Current advances in the study of physique. Photogrammetric anthropometry and an androgyny scale. *The Lancet*; **257**(6654): 574-579.

Thorup VM, Tøgersen FA, Jørgensen B and Jensen BR (2007). Joint axes of rotation and body segment parameters of pig limbs. *Acta Veterinaria Scandinavica*; **49**(1).

Tian W, Cong Q and Menon C (2011). Investigation on Walking and Pacing Stability of German Shepherd Dog for Different Locomotion Speeds. *Journal of Bionic Engineering*; **8**(1): 18-24.

Torres BT, Moens NMM, Al-Nadaf S, Reynolds LR, Fu Y-C and Budsberg SC (2013). Comparison of overground and treadmill-based gaits of dogs. *American Journal of Veterinary Research*; **74**(4): 535-541.

Trostel CT, McLaughlin RM and Pool RR (2003a). Canine elbow dysplasia: anatomy and pathogenesis. *Compendium on Continuing Education for the Practicing Veterinarian*; **25**(10): 754-762.

Trostel CT, McLaughlin RM and Pool RR (2003b). Canine elbow dysplasia: incidence, diagnosis, treatment, and prognosis. *Compendium on Continuing Education for the Practicing Veterinarian*; **25**(10): 763-773.

Unt VE, Evans J, Reed SR, Pfau T and Weller R (2010). Variation in frontal plane joint angles in horses. *Equine Veterinary Journal*; **42**: 444-450.

van den Bogert AJ (1989). *Computer Simulation of Locomotion in the Horse: Met Een Samenvatting in Het Nederlands*, Rijksuniversiteit te Utrecht.

van den Bogert AJ, Schamhardt HC and Crowe A (1989). Simulation of quadrupedal locomotion using a rigid body model. *Journal of Biomechanics*; **22**(1): 33-41.

van Weeren PR, van den Bogert AJ and Barneveld A (1992). Correction models for skin displacement in equine kinematics gait analysis. *Journal of Equine Veterinary Science, 1992, Vol.12(3), pp.178-192*; **12**(3).

Vaughn CL, Davis BL and O'Connor JC (1999). *Dynamics of Human Gait (Second Edition)* Cape Town, South Africa, Kiboho Publishers.

Veeger HEJ, Yu B, An KN and Rozendal RH (1997). Parameters for modeling the upper extremity. *Journal of Biomechanics*; **30**(6): 647-652.

Vilensky JA (1979). Masses, centers-of-gravity, and moments-of-inertia of the body segments of the rhesus monkey (Macaca mulatta). *American Journal of Physical Anthropology*; **50**(1): 57-65.

Wahl JM, Herbst SM, Clark LA, Tsai KL and Murphy KE (2008). A review of hereditary diseases of the German shepherd dog. *Journal of Veterinary Behavior: Clinical Applications and Research*; **3**(6): 255-265.

Weber W and Weber EF (1836). *Mechanik der menschlichen Gehwerkzeuge: eine anatomisch-physiologische Untersuchung*, Dietrich.

Weinbach A (1938). Contour maps, center of gravity, moment of inertia and surface area of the human body. *Human Biology*; **10**(3): 356-371.

Weishaupt MA, Wiestner T, Hogg HP, Jordan P and Auer JA (2004). Compensatory load redistribution of horses with induced weightbearing hindlimb lameness trotting on a treadmill. *Equine Veterinary Journal*; **36**(8): 727-733.

Weishaupt MA, Wiestner T, von Peinen K, Waldern N, Roepstorff L, Van Weeren R, Meyer H and Johnston C (2006). Effect of head and neck position on vertical ground reaction forces and interlimb coordination in the dressage horse ridden at walk and trot on a treadmill. *Equine Veterinary Journal*; **38**(S36): 387-392.

Wells JP and DeMenthon DF (1987). Measurement of body segment mass, center of gravity, and determination of moments of inertia by double pendulum in Lemur fulvus. *American Journal of Primatology*; **12**(3): 299-308.

Wennerstrand J, Alvarez CBG, Meulenbelt R, Johnston C, van Weeren PR, Roethlisberger-Holm K and Drevemo S (2009). Spinal kinematics in horses with induced back pain. *Veterinary and Comparative Orthopaedics and Traumatology*; **22**(6): 448-454.

Wentink GH (1978). Biokinetical analysis of the movements of the pelvic limb of the horse and the role of the muscles in the walk and the trot. *Anatomy and Embryology*; **152**: 261-272.

Wentink GH (1979). Dynamics of the hind limb at walk in the horse and dog. *Anatomy and Embryology*; **155**(2): 179-190.

Whitsett Jr CE (1962). *Some dynamic response characteristics of weightless man*, DTIC Document.

Whittle MW (1996). Clinical gait analysis: A review. *Human Movement Science*; **15**(3): 369-387.

Wicke J and Dumas GA (2014). A new geometric-based model to accurately estimate arm and leg inertial estimates. *Journal of Biomechanics*; **47**(8): 1869-1875.

Wicke J, Dumas GA and Costigan PA (2009). A comparison between a new model and current models for estimating trunk segment inertial parameters. *Journal of Biomechanics*; **42**(1): 55-60.

Wild T (1954). Simplified volume measurement with the polar planimeter. *Surveying and Mapping*; **14**(2): 218-220.

Williams D, Prymak C and Baughan J (1985). *Tocopherol (vitamin E) status in canine degenerative myelopathy*. American College of Veterinary Internal Medicine 3rd Annual Meeting San Diego, CA.

Winstandley WC, Wittman TJ and Eifert MC (1968). *Special equipment for measurement of mechanical dynamic properties of emergency escape systems*, Wright-Patterson Air Force Base, Ohio.

Winter DA (1976). The locomotion laboratory as a clinical assessment system. *Medical Progress through Technology*; **4**(3): 95-106.

Winter DA (1981). Use of kinetic analyses in the diagnostics of pathological gait. *Physiotherapy Canada*; **33**(4): 209-214.

Winter DA (1990). *Biomechanics and Motor Control of Human Movement, Second Edition* (2nd). Toronto, CA, John Wiley and Sons, Inc.

Winter DA (1993). Knowledge base for diagnostic gait assessments. *Medical Progress through Technology*; **19**(2): 61-81.

Winter DA and Robertson DGE (1978). Joit torque and energy patterns in normal gait. *Biological Cybernetics*; **29**(3): 137-142.

Winter DA and Sienko SE (1988). Biomechanics of below-knee amputee gait. *Journal of Biomechanics*; **21**(5): 361-367.

Yeadon MR and Morlock M (1989). The appropriate use of regression equations for the estimation of segmental inertia parameters. *Journal of Biomechanics*; **22**(6-7): 683-689.

Yildiz B, Serbest A, Yilmaz O and Kirbiyik H (1993). The comparison of the head measures of Turkish and German shepherd dog breeds. *J Fac Vet Med Univ Uludag*; **1**: 35-39.

Young JW, Chandler RF, Snow CC, Robinette KM, Zehner GF and Lofberg MS (1983). *Anthropometrics and mass distribution characteristics of the adult female*. Oklahoma City, National Highway Traffic Safety Administration.

Zatsiorsky VM and Seluyanov V (1985). Estimation of the mass and inertial characteristics of the human body by means of the best predictive regression equations. *BiomechanicsIX-B* (in. D. A. Winter, R. W. Norman, R. P. Wells, K. C. Hayes and A. E. Patla. Champaign, IL, Human Kinetics**:** 233-239.

Zatsiorsky VM and Seluyanov VN (1983). The mass and inertia characteristics of the main segments of the human body. *Biomechanics VIII-B*; **56**(2): 1152-1159.

Zeiler GE, van der Zwan H and Oosthuizen MC (2013). Genetic testing of canine degenerative myelopathy in the South African Boxer dog population. *Journal of the South African Veterinary Association*; **84**(1): 1-5.